AGSO JOURNAL
OF AUSTRALIAN GEOLOGY & GEOPHYSICS

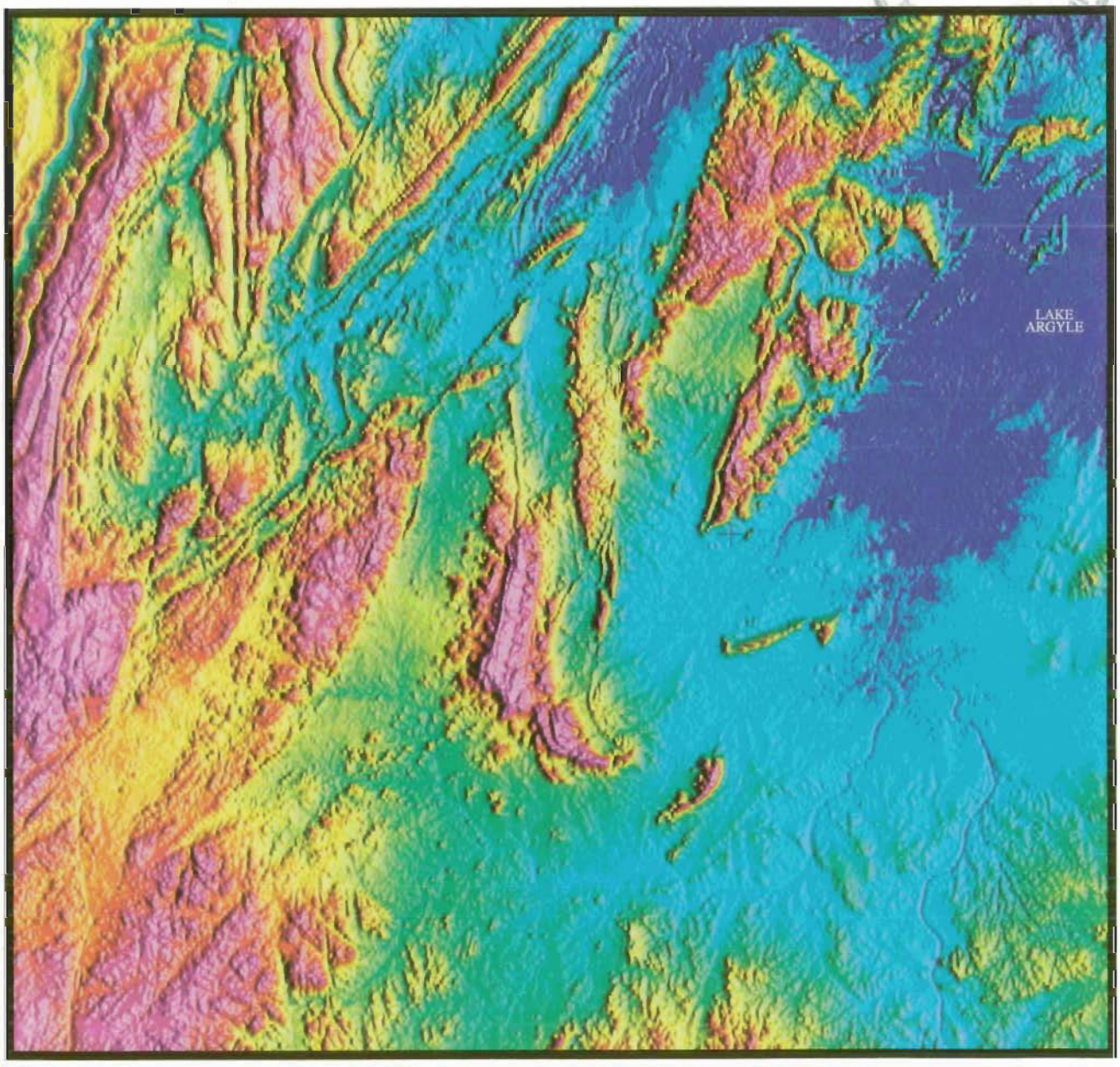

VOLUME 15, NUMBER 4
1994

AGSO Journal of Australian Geology & Geophysics

Editor: Karl H. Wolf, Corporate Publications, Australian Geological Survey Organisation

Policy

The *AGSO Journal of Australian Geology & Geophysics* is a quarterly journal of geoscientific research results relating to the program and interests of the Australian Geological Survey Organisation (AGSO). It complements other earth science journals by focusing on Australia, and includes papers covering the broader Australasian and SW Pacific region.

The *Journal*'s target audience is the world-wide geoscientific community, catering for the interests of the resource, exploration and environmental industries, as well as those of researchers in universities and State and Federal agencies.

The Editorial Board is responsible for the scientific policies and standards of the *Journal*, which will publish papers on fundamental research, applied research and review topics. Contributions are invited from anyone. Scientific excellence and relevance to the broad aims of AGSO are the main criteria for acceptance of manuscripts for publication. Peer review and editorial and production standards are similar to those of leading international journals.

Guide for contributors

Submission of a paper to the *Journal* implies that the paper is original and unpublished, and is not being considered for publication elsewhere. Papers published in the *AGSO Journal of Australian Geology & Geophysics* become Commonwealth copyright. Authors are responsible for obtaining permission to reproduce any material, especially a figure, that has been published previously.

All submissions will be peer-reviewed. Submissions by AGSO authors will normally be reviewed by non-AGSO referees; those by non-AGSO authors, by at least one AGSO referee.

When your paper has been accepted you will be asked to supply a copy on an IBM-compatible diskette. Do not send this until it is requested.

Submission of manuscripts

- Three copies of the complete manuscript should be sent to the Editor.
- Your manuscript should be double-spaced, with margins of at least 25 mm, on one side only of A4 paper, with all pages numbered. Single-spaced copies are not suitable for refereeing or editing and will not be accepted.
- Use a straightforward print-out in Times or Courier font. Do not use desktop publishing software to prepare your manuscript.
- Photocopies of draft figures are acceptable when the manuscript is first submitted, as long as they are clear enough for the reviewers. Final versions of figures must be supplied when the final version of the manuscript is accepted for publication.
- Photographs should be supplied as glossy prints.

Style

Contributions should be written in English, and spelling should follow the latest edition of *The Macquarie Dictionary*. Refer to a recent issue of the *Journal* for further guidance on general style. But note that a revised style for references is being introduced with these instructions. Heading hierarchy should be indicated in the margin by ringed capital letters; A for main headings, B for second level headings, etc.

Abstract and key words

An abstract is required at the beginning of the manuscript. It should provide an informative summary of the main results and conclusions contained in the manuscript. It should not exceed 300 words. (An abstract is not adequate if it states that certain work was done, but fails to summarise the outcomes.) Up to 10 key words or short phrases should be supplied to assist indexing of your paper.

References

The Journal does not cite 'in prep' references. References 'in press' are acceptable only if the journal and issue can be supplied. References to unpublished data, if necessary, should be quoted as personal communications, giving the affiliation of the person being quoted and the date of communication. References should be cited in the text by author(s) and year in the normal Harvard style. For example: 'Ernest (1976, p. 312) showed that ..' or as described by earlier workers (Zagreb 1931; Ernest 1976; Melway & Murray 1977; Melway et al. 1978). References should be listed at the end of the text, in alphabetical order and in the style shown below. Please note that all journal titles are spelt out in full.

Continued inside back cover

AGSO JOURNAL

OF AUSTRALIAN GEOLOGY & GEOPHYSICS

VOLUME 15, NUMBER 4, 1994

CONTENTS

ISSN 1320–1271

Subscriptions to the AGSO Journal are available through the Australian Geological Survey Organisation (GPO Box 378, Canberra ACT 2601; tel. 06 249 9642, fax 06 249 9982).

Other matters concerning the Journal should be sent to the Editor, AGSO Journal

Editor, AGSO Journal: Dr. Karl H. Wolf
Cover design and figures prepared by AGSO Cartographic Services Unit unless otherwise indicated
Prepared for publication by Lin Kay

Printed in Australia by National Capital Printing Fyshwick, A.C.T. 2609

AUSTRALIAN GOVERNMENT PUBLISHING SERVICE CANBERRA 1995

Month of issue, March 1995

Front-cover illustration:

Digital Elevation Model (low, blue–high, magenta) pixel image map of the Lissadell 1:250 000 Sheet of the East Kimberley region, Western Australia. The basic height data used to produce this image were acquired on east–west lines flown 100 m above ground level and spaced 400 m apart. The satellite Global Positioning System (GPS) provided both the height and the navigation data. Range data were recorded by two GPS receivers, one located in the aircraft and the other at a known location on the ground.

The two data sets were later combined and processed to increase the final accuracy of the horizontal positioning data by a factor of at least 10. Final elevation data were then produced by correcting for the height of the aircraft above the ground (radio-altimeter data), the geoid-ellipsoid separation (N value), and the height difference between the radio-altimeter and GPS antennas.

The final profile data, which represent height of the ground surface relative to the geoid, were gridded to a cell-size of 90 m, using minimum curvature; the image produced from the grid was artificially illuminated from the east.

This pixel image map is a product of the Airborne Group, Geophysical Observatories and Mapping Program, AGSO, and may by purchased from the AGSO Sales Centre. Digital data can be ordered through Duncan Souter of Geophysical Mapping AGSO, GPO Box 378, Canberra, ACT 2601 (tel 06–2499223; fax 06–2499986)

AGSO Journal of Australian Geology & Geophysics, 15(4), 395–407

Whole-rock regional oxygen-isotope depletion patterns as a guide to epithermal gold exploration in north Queensland

G.R. Ewers,[1] D.E. Mackenzie,[1] B.I. Cruikshank,[1] & A.S. Andrew[2]

The recognition of regional oxygen-isotope depletion patterns in high-level igneous rocks provides a means to discriminate areas potentially prospective for low sulphidation (adularia–sericite type) epithermal gold mineralisation. The coincidence of an extensive regional oxygen-isotope depletion pattern over most of the northern Drummond Basin with a recently discovered epithermal district is consistent with a similar association for younger, world-class epithermal districts in the United States. Reconnaissance whole-rock oxygen-isotope data for Permo-Carboniferous volcanic rocks in the northern Coen Inlier indicate an area of isotopic depletion that correlates with regional stream-sediment geochemical anomalies normally associated with epithermal deposits. The data suggest that the northern Coen Inlier is a region of high epithermal potential worthy of more systematic exploration. In contrast, extensive exploration within and around the Featherbed Cauldron Complex has failed to define any significant epithermal mineralisation. Whole-rock oxygen-isotope values are predominantly near normal, and isotopic depletion is confined largely to the Late Carboniferous volcanic rocks in the southern areas of the complex, particularly along caldera margins where major structures provided pathways for fluid circulation. The data are consistent with earlier observations that the Late Carboniferous sequence is more closely associated with hydrothermal activity than the Early Permian volcanics, and that meteoric fluids were focussed through these major structures, at least during the waning stages of igneous activity.

Introduction

Oxygen-isotope data from unaltered primary igneous rocks are typically restricted to a narrow range, between about +5.5 and +10 per mil (Taylor 1974a), relative to standard mean ocean water (SMOW), although more recent data suggest that the upper limit may be as high as +14 per mil (Sheppard 1986). These data provide a reference against which the effects of processes that drastically alter the $\delta^{18}O$ values of igneous rocks can be assessed.

Over the past 30 years, there has been a growing recognition that on a regional scale $\delta^{18}O$ values for some volcanic and plutonic rocks are substantially below the lower limit for 'normal' igneous rocks. Low-^{18}O igneous rocks have been recognised in the western Cascades (Taylor 1971), the Skaergaard intrusion (Taylor & Forester 1979), Iceland (Muehlenbachs et al. 1974), Au–Ag mineralised areas in western Nevada (Taylor 1973), the Scottish Hebrides (Taylor & Forester 1971), the San Juan volcanic field in Colorado (Taylor 1974b; Larson & Taylor 1986), the Yellowstone volcanic field (Hildreth et al. 1984), and the Lebombo Monocline in southern Africa (Harris & Erlank 1992). Depletion in whole-rock $\delta^{18}O$ values by 5 to 10 per mil can be explained only through low-^{18}O meteoric fluids interacting with rocks either at high temperatures at the subsolidus stage, or through magmas assimilating hydrothermally altered low-^{18}O wall rocks or exchanging directly with low-^{18}O fluids. Other fluids (e.g. magmatic or metamorphic) are more ^{18}O-enriched and will either increase or only slightly decrease 'normal' igneous values. Low-temperature meteoric water interaction cannot produce whole-rock ^{18}O depletion, because the constituent mineral-water fractionation curves predict ^{18}O enrichment rather than depletion (Friedman & O'Neil 1977). This is confirmed by the $\delta^{18}O$ values of rocks affected by low-temperature alteration (Gregory & Taylor 1981).

O'Neil & Silberman (1974) first reported a coincidence between areas of igneous whole-rock ^{18}O depletion and epithermal districts. Tertiary epithermal gold deposits in the USA, including major producers such as Round Mountain, the Comstock Lode, and Goldfield, are associated with igneous rocks that have undergone regional oxygen-isotope depletion (see Table 3, Ewers et al. 1994). However, the application of regional ^{18}O depletion patterns as a tool to discriminate areas prospective for epithermal mineralisation is not apparent from the literature, even though an association between epithermal mineralisation and regional ^{18}O depletion should be anticipated. Low-sulphidation epithermal systems almost invariably involve meteoric water, and hydrothermal systems dominated by meteoric water could be expected in subaerial volcanic terranes during the waning stages of igneous activity. Virtually all of the areas where regional ^{18}O depletion has been reported in the literature are Tertiary or younger.

The discovery of extensive epithermal gold mineralisation in the northern part of the late Palaeozoic Drummond Basin, north Queensland, (with economic deposits at Pajingo and Wirralie and numerous prospects) was followed by the recognition of ^{18}O depletion of the associated volcanic rocks over at least 1500 km^2 (Ewers et al. 1991, 1994). This prompted the Australian Geological Survey Organisation (AGSO) to collect and compile oxygen-isotope data for Palaeozoic igneous rocks in north Queensland, to assess whether depletion patterns can be used as a tool to discriminate areas with epithermal gold potential.

This paper documents reconnaissance whole-rock oxygen-isotope data recently obtained for Permo-Carboniferous volcanic rocks from the Featherbed Cauldron Complex and the northern Coen Inlier–Torres Strait region. These results are discussed in terms of the epithermal potential for these two areas against the background of results from the northern Drummond Basin. The work was carried out as part of the North Queensland National Geoscience Mapping Accord (NGMA) Project, the main participants being AGSO and the Geological Survey of Queensland (GSQ).

Analytical methods

Samples were prepared for oxygen-isotope analysis following the methods outlined by Clayton & Mayeda (1963), and Taylor & Epstein (1962), using BrF_5 as the oxidising reagent. Oxygen-isotope compositions were measured with a Micromass 602D mass spectrometer (Featherbed samples) and a Finnigan MAT 252 mass spectrometer

[1] Australian Geological Survey Organisation, GPO Box 378, Canberra, ACT 2601

[2] CSIRO Division of Petroleum Resources, PO Box 136, North Ryde, NSW 2111

(Cape York Peninsula samples). $\delta^{18}O$ values generally have a reproducibility of 0.2 per mil, and are reported relative to standard mean ocean water (SMOW). A single isotopic analysis was obtained for most samples and duplicate analyses were made at random. Sample analyses were monitored by the analysis of standard NBS-28 (+9.6 per mil) and a secondary standard WAC (Western Australian chert, +20.0 per mil).

Oxygen-isotope depletion in igneous rocks

Mechanisms

Some volcanic and plutonic rocks are known or suspected to have been derived from low-^{18}O magmas (e.g. Muehlenbachs et al. 1974; Hildreth et al. 1984; Harris & Erlank 1992), but the mechanism of ^{18}O depletion remains controversial. Two main hypotheses have been put forward: direct interaction of meteoric water with a magma (Friedman et al. 1974; Hildreth et al. 1984); or magmatic assimilation of wall rocks previously depleted in ^{18}O by interaction with meteoric water (Taylor 1986, 1987; Grunder 1987; Bacon et al. 1989).

Compelling arguments against the incorporation of meteoric water into a magma have been put forward, based on the large quantities necessary to produce significant depletion of whole-rock $\delta^{18}O$ values. Granitic magmas emplaced at shallow levels in the Earth's crust can dissolve at most 2 to 3 weight per cent water (Burnham 1967) and, even if this water is entirely of meteoric origin, it is insufficient to lower the $\delta^{18}O$ of a magma significantly (Grunder 1987). ^{18}O depletion in a magma could be caused by assimilation of wall rocks already low in $\delta^{18}O$ as a result of exchange with meteoric water in a hydrothermal system. However, large-scale assimilation would require large volumes of pre-existing hydrothermally altered rocks to be present (particularly if the low ^{18}O magmas were intruded over a wide area), and the assimilation process would probably be inefficient, thereby further increasing the required volume of low ^{18}O rock (Cartwright & Valley 1991). Furthermore, the incorporation of large amounts of wall rock will rapidly cause crystallisation and if the magmas involved are close to their cotectics, it would be impossible to effectively assimilate much material.

In general, regional ^{18}O depletion of igneous rocks has been explained more readily by, and appears to be more consistent with, large-scale interaction between meteoric water and cooling igneous rocks. Volcanic rocks emplaced at the Earth's surface are more porous and permeable than intrusive rocks. They have a primary porosity, owing to their partly fragmental and bedded nature, and a greater susceptibility to fracturing than intrusive rocks. Therefore, they could be expected to interact and exchange isotopically with heated meteoric water to a greater degree than associated intrusive rocks. Oxygen-isotope data from the northern Drummond Basin and elsewhere are consistent with this interpretation (Ewers et al. 1994; Taylor 1974a). Isotopic depletion in some intrusive rocks could result locally from interaction with high-temperature meteoric water along faults and fractures.

Mineralogical evidence of hydrothermal alteration (and, therefore, isotopic exchange) may be minor or absent if hydrothermal interaction occurs at high temperatures or, in the case of low-^{18}O magmas, the minerals directly crystallise from the melt. For example, Hemley & Jones (1964) demonstrated that, in the presence of quartz, the stability fields for K-feldspar, sericite, kaolinite, and pyrophyllite are a function of temperature and fluid chemistry (specifically the K^+/H^+ cation ratio). At high temperatures and high K^+/H^+ ratios, K-feldspar will be the stable phase. Taylor (1971, 1974a) observed that igneous rocks abnormally low in $\delta^{18}O$ may have characteristic mineralogical and isotopic features. For example, feldspars are commonly depleted in $\delta^{18}O$ to a greater degree than other coexisting minerals and typically have a turbid appearance, and the primary igneous ferromagnesian minerals are partly or completely altered, particularly to chlorite and epidote, such that OH-bearing minerals have abnormally low δD values.

Northern Drummond Basin

The potential for significant epithermal gold mineralisation in the northern part of the Drummond Basin was not recognised until the discovery of the Pajingo deposit in 1984 (Porter 1988). Since that time, the region has become an important target for gold exploration in north Queensland, with further discoveries at Wirralie and Yandan and numerous prospects being recognised (Fig. 1). Low $\delta^{18}O$ values for host rocks to Au–Bi and Ag–Pb mineralisation in the Ukalunda and nearby Sunbeam deposits (Fig. 1) led Golding & Wilson (1984) to conclude that meteoric fluids were involved and to suggest an epithermal origin for these deposits.

The regional extent of ^{18}O depletion away from mineralisation in the Drummond Basin was not recognised until recently (Ewers et al. 1991, 1994). Whole-rock oxygen-isotope data for relatively fresh volcanic rocks from the northern Drummond Basin have a mean value of +0.7±4.9 per mil (range of values from –8.2 to +10.4 per mil). The intrusive rocks range from granites to gabbros and have a narrower range in isotopic composition (+1.3 to +8.8, mean +5.8±2.3 per mil). The results indicate that Late Devonian to Early Carboniferous volcanic rocks in the Drummond Basin sequence and those extruded during the Late Carboniferous were consistently depleted in $\delta^{18}O$. Pyroclastic rocks and lavas were equally depleted and, although some intrusive rocks have abnormally low $\delta^{18}O$ values, the majority are near normal. The areal extent of this ^{18}O-depleted region (at least 1500 km^2) has not been fully delineated, but coincides closely with the present outcrop distribution of volcanic and intrusive rocks.

Coincidence of regionally extensive whole-rock oxygen-isotope depletion with areas of epithermal mineralisation observed in the northern Drummond Basin is similar to that observed in Tertiary epithermal districts in the USA (Ewers et al. 1994).

Featherbed Cauldron Complex

Oxygen-isotope data have been collected from the Featherbed Cauldron Complex in north Queensland because it does not appear to be deeply eroded, and unpublished regional oxygen-isotope data suggested that there was depletion over an area of at least 30 km^2 along the southern margin of the complex (Fig. 2). The architecture of this complex has been preserved to a much greater extent than the volcanic suite of similar age in the northern Drummond Basin, and has been mapped in great detail in recent years (Mackenzie 1993), thereby providing a coherent geological framework and a comprehensive suite of material for analysis.

Regional geological and structural setting

The Featherbed Cauldron Complex (Mackenzie 1993) is the largest, best-exposed coherent accumulation of felsic volcanic and associated rocks in northern Queensland. The complex is a composite of three or more Late Carboniferous subsidence structures, associated remnants of outflow sheets, and a Late Carboniferous–Early Permian subsidence structure, overprinted by a fault- and ring dyke-bounded composite of three Early Permian calderas. The complex overlies and intrudes a thick, Siluro-Devonian sedimentary flysch sequence and minor igneous rocks near the western margin of the Hodgkinson Fold Belt, and is mostly confined to a volcano-tectonic depression, which covers about 3000 km^2.

The Featherbed Cauldron Complex lies immediately east of, and is elongated parallel to the Palmerville Fault and other major northwest-trending, subparallel faults in the Hodgkinson Fold Belt. Some of the northwest-trending faults cut the complex. The Palmerville Fault is the bounding fault which forms the western margin to the tightly folded sedimentary sequence in the Hodgkinson Fold Belt, and the structural evolution of the complex appears to have been persistently influenced by the tectonic development along the margin of the fold belt.

The extrusive rocks of the complex can be divided into two main groups: Late Carboniferous I-type rhyolitic to andesitic ignimbrites and minor andesite lava; and Early Permian A-type rhyolitic ignimbrite with minor rhyolitic lava. The Late Carboniferous volcanics (belonging mainly to the Tennyson Caldera and Boonmoo Cauldron sequences) crop out in the southeastern, southern, and southwestern parts of the complex and are associated with coeval dioritic (and rare gabbroic) to granitic intrusive rocks. The major part of the complex to the north and northwest is Early Permian (it consists primarily of the Wakara, Djungan, and Featherbed Caldera sequences), and has been intruded by a peripheral ring dyke of porphyritic microgranite and by resurgent-type plutons of porphyritic microgranite and microgranodiorite.

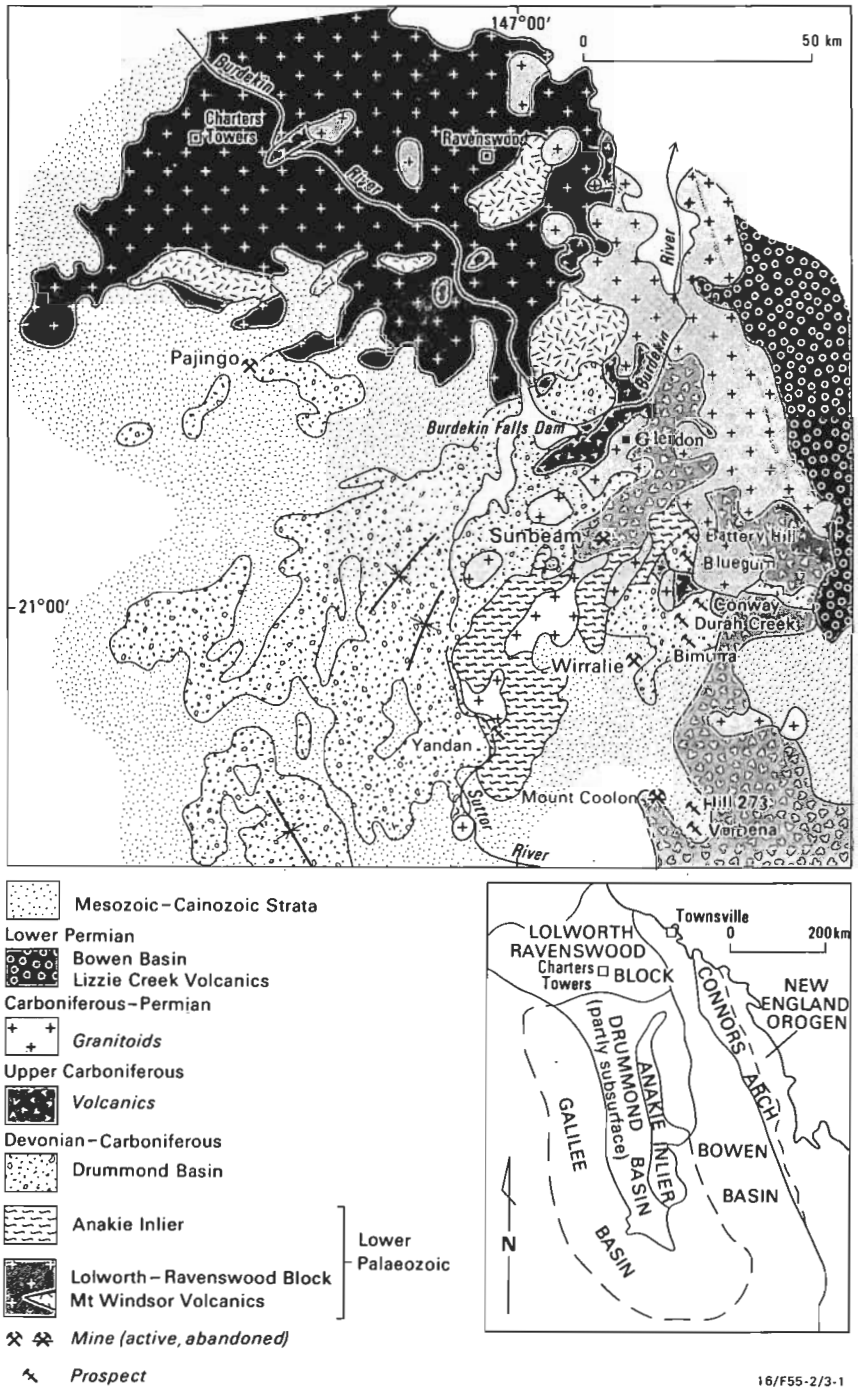

Figure 1. Simplified geological setting of the northern Drummond Basin (modified from McPhie et al. 1990)

Isotopic results

Oxygen-isotope data for 57 whole-rock samples from the Featherbed Cauldron Complex, together with brief descriptions of each rock analysed, their localities in terms of the Australian Map Grid (AMG) coordinates, and alteration features are summarised in Table 1 (Early Permian sequence) and Table 2 (Late Carboniferous sequence). Samples were selected to provide broad coverage and a complete cross-section of the outcrop area of the complex.

The distribution of $\delta^{18}O$ values in relation to the geology and outcrop of the Featherbed Cauldron Complex is shown in Figure 2, and Figures 3A and 3B illustrate the $\delta^{18}O$ values for the Early Permian and Late Carboniferous volcanic sequences, respectively.

The Early Permian rocks have $\delta^{18}O$ values mostly typical of whole-rock igneous values and show little evidence of large-scale interaction with meteoric fluids at high temperature (Fig. 3A). Several samples are slightly depleted in $\delta^{18}O$, and one sample is markedly enriched; but, in general, there are no significant distinctions between

volcanic subgroups. The ^{18}O-enriched sample is a moderately crystal-poor and partly devitrified vitrophyre (Table 1), and clearly the product of low-temperature alteration (e.g. weathering), which mineral-water fractionation curves predict would lead to ^{18}O enrichment rather than depletion (Friedman & O'Neil 1977). It is possible, and in some instances probable, that late, low-temperature alteration processes increased the $\delta^{18}O$ values of otherwise ^{18}O-depleted rocks; however, sample material for isotopic analysis was selected carefully to minimise these effects.

The Late Carboniferous rocks have a similar but much broader spread in $\delta^{18}O$ values, with ten samples yielding values below +5 per mil (Fig. 3B). As with the Permian volcanic rocks, there are no significant differences between the Late Carboniferous volcanic subgroups, but there is clear evidence of high-temperature meteoric water interaction during the earlier phase of igneous activity in the development of the Featherbed Cauldron Complex.

Turbidity in feldspars (both plagioclase and K-feldspar) for both the Early Permian and Late Carboniferous sequences varies from absent to extreme. In general, the Late Carboniferous rocks contain more turbid feldspar than the Early Permian rocks, consistent with a greater degree of hydrothermal interaction during the earlier phase of igneous activity. The isotopically depleted rocks contain turbid feldspar; however, there appears to be no direct correlation between the degree of whole-rock depletion and the extent of feldspar turbidity.

Figure 2 indicates that ^{18}O depletion is confined to the southern areas of the Featherbed Cauldron Complex, and confirms the association of isotopic depletion with Late Carboniferous volcanic rocks. The depleted areas are mostly aligned along caldera margins (particularly where they are intersected by major cross-cutting faults). The major faults and deep fracturing around the caldera margins provided excellent pathways for fluid circulation. Initially, hydrothermal systems may have been dominated by either magmatic or meteoric fluids. However, even if magmatic fluids were dominant, the regional oxygen-isotope data indicate that meteoric water became dominant

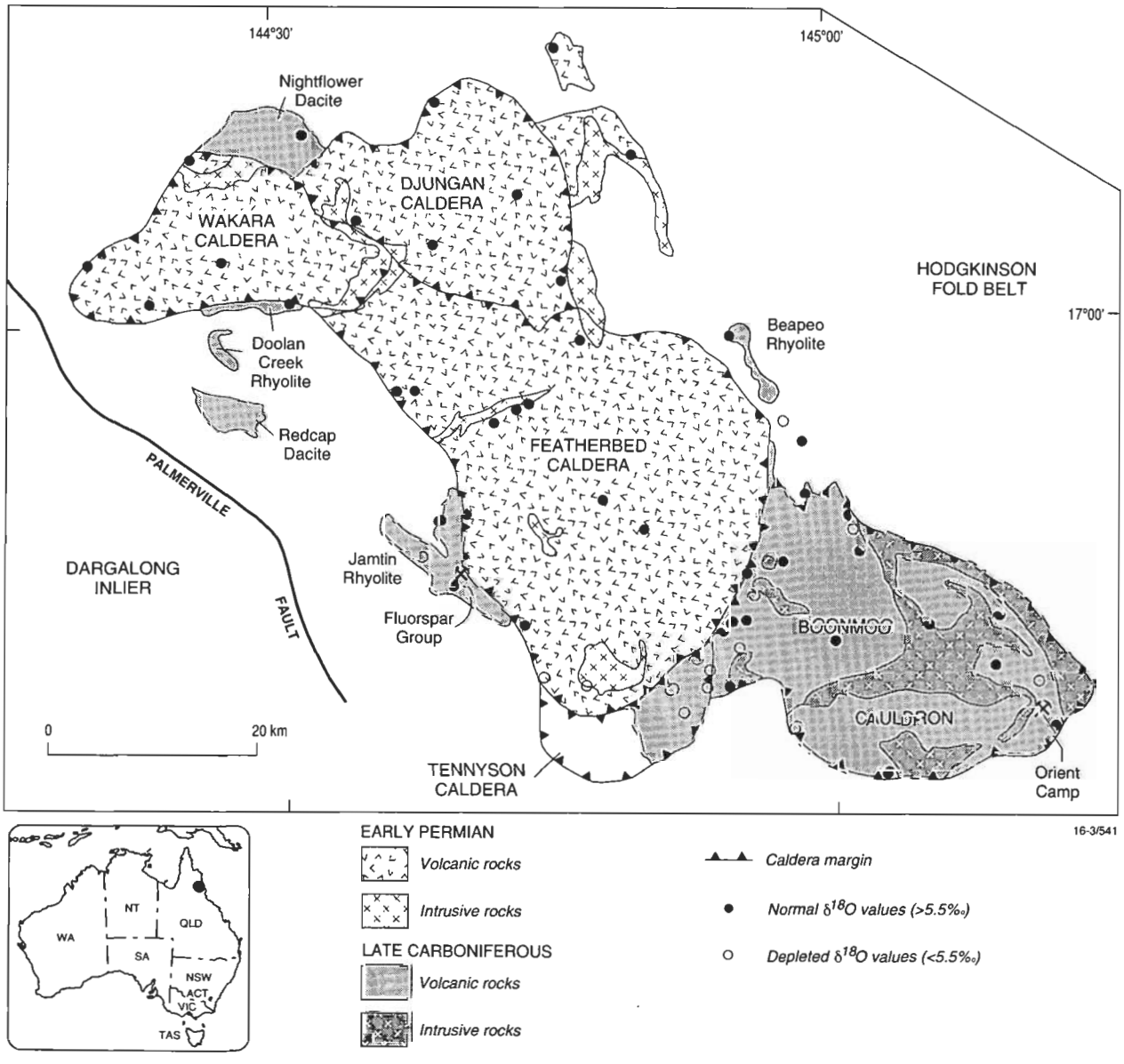

Figure 2. Distribution of $\delta^{18}O$ values in relation to the Featherbed Cauldron Complex (modified from Mackenzie et al. 1993)

Table 1. $\delta^{18}O$ values for the Early Permian Featherbed Cauldron Complex

AGSO No.	*Rock type*	*Unit*	*AMG coords*	$\delta^{18}O_{SMOW}$
8630 0895	Rhyodacitic lava	Ticklehim Rhyolite, WCS	7764-248337	+8.4
Intensely welded, crystal-rich & finely recrystallised; slight alteration to chlorite, sericite & vermiculite, plagioclase very slightly turbid, K-feldspar moderately to very turbid, slight weathering				
8730 3023	Rhyolitic ignimbrite	Ticklehim Rhyolite, WCS	7764-305273	+9.4
Intensely welded,crystal-rich, & finely recrystallised; slight alteration to sericite, chlorite, biotite(?), feldspar slightly turbid & later weathering/alteration to vermiculite				
8630 0938	Rhyodacitic ignimbrite	Unnamed, WCS	7764-267219	+11.2
Crystal-rich; slight alteration to chlorite, sericite, & calcite with slight weathering to iron oxides & clay, feldspar is clear				
8630 0924	Rhyolitic ignimbrite	Gavin Rhyolite, WCS	7764-174245	+7.2
Crystal-rich & lithic-poor; ferruginous with moderate alteration to chlorite & sericite, feldspar slightly turbid				
8630 0947	Rhyolitic ignimbrite	Gavin Rhyolite,	WCS64-376213	+11.3
Poorly to moderately welded, moderately crystal-rich, lithic-poor; moderate alteration to hematite, sericite & chlorite, K-feldspar slightly turbid & plagioclase slightly to moderately turbid				
8630 0848	Rhyolitic ignimbrite	Lumma Rhyolite, DCS	7864-570298	+10.0
Densely welded, crystal-rich & finely recrystallised;slight alteration to chlorite & sericite & slight weathering to clay & iron oxides, feldspar slightly turbid				
8630 0755	Rhyolitic ignimbrite	Scrufflem Rhyolite, DCS	7864-509405	+9.4
Intensely welded, crystal-rich & slightly recrystallised; slight alteration to chlorite, biotite(?), & iron oxides, feldspar clear				
8630 0850	Rhyolitic ignimbrite	Unnamed, DCS	7864-424286	+9.3
Densely welded, lithic-poor & crystal-rich, slightly recrystallised; alteration to chlorite, sericite, calcite & clays, feldspar slightly turbid				
8630 0870	Rhyolitic ignimbrite	Aroonbeta Rhyolite, DCS	7864-505260	+8.6
Crystal-rich & moderately lithic-rich; slight alteration to chlorite & calcite, feldspar slightly to moderately turbid				
8630 0884	Rhyolitic ignimbrite	Lightning Ck Rhyolite, DCS	7864-611205	+10.5
Intensely welded, crystal-rich & lithic-poor, devitrified & recrystallised; moderate alteration to chlorite, calcite & iron oxides, feldspar very slightly turbid				
8330 0277	Rhyolitic ignimbrite	Arringunna Rhyolite, FCS	7863-713993	+8.2
Crystal-rich; ferruginous with slight alteration to chlorite, & sericite, feldspar slightly turbid				
8330 0266	Rhyolitic ignimbrite	Arringunna Rhyolite, FCS	7863-653014	+10.6
Crystal-rich; slight alteration to chlorite, sericite, clay(?), & calcite, K-feldspar slightly turbid and plagioclase moderately turbid				
8330 0068	Rhyolitic ignimbrite	Arringunna Rhyolite, FCS	7863-636151	+7.7
Crystal-rich; slight alteration of ferromagnesian minerals to chlorite & clay(?), K-feldspar very slightly turbid and plagioclase moderately turbid				
8330 0165	Rhyolitic ignimbrite	Arringunna Rhyolite, FCS	7863-621095	+9.6
Very crystal-rich; very slightly altered to chlorite, & sericite(?), feldspar clear to very slightly turbid				
8330 0152	Rhyolitic ignimbrite	Combella Rhyolite, FCS	7863-562084	+10.6
Moderately crystal-rich, devitrified & recrystallised; alteration of biotite to opaque phases, feldspar slightly to moderately turbid				
8330 0161	Rhyolitic ignimbrite	Combella Rhyolite, FCS	7863-614086	+17.2
Moderately crystal-poor & partially devitrified vitrophyre, feldspar clear				
8330 0101	Rhyolitic ignimbrite	Fisherman Rhyolite, FCS	7863-485109	+8.8
Moderately crystal-rich with slightly recrystallised groundmass; moderate alteration to sericite, chlorite, opaque phases, & calcite with ferromagnesian minerals replaced by calcite & opaque oxides; K-feldspar very slightly turbid & plagioclase slightly to moderately turbid				
8330 0104	Rhyolitic ignimbrite	Fisherman Rhyolite, FCS	7863-455105	+5.7
Crystal & lithic-poor; intensely brecciated; very altered with fluorite, calcite, chlorite, & sericite, feldspar extremely turbid				
8330 0240	Rhyolitic ignimbrite	Fisherman Rhyolite, FCS	7863-518008	+8.1
Crystal-poor; slightly to moderately altered to calcite, sericite, & chlorite with slight weathering to form hematite, feldspar slightly turbid				
8330 0299	Rhyolitic ignimbrite	Fisherman Rhyolite, FCS	7863-832963	+6.1
Flow laminated, crystal-poor; moderate alteration to chlorite, & calcite with slight weathering(?) producing clay (vermiculite?) alteration, feldspar very turbid				
8330 0389	Rhyolitic ignimbrite	Fisherman Rhyolite, FCS	7863-575887	+6.5
Poorly to moderately welded, moderately crystal-rich; sericitic alteration, feldspar very turbid				
8330 0472	Rhyolitic ignimbrite	Fisherman Rhyolite, FCS	7863-598830	+3.4
Crystal-poor, devitrified & recrystallised; alteration to sericite, chlorite, & clay(?), feldspar extremely turbid				

AGSO No.	*Rock type*	*Unit*	*AMG coords*	$\delta^{18}O_{SMOW}$
8630 0802	Rhyolite	Controversy Hill Rhyolite, unassigned	7864-679384	+10.4
Intensely welded, moderately recrystallised & phenocryst-poor; moderately altered to chlorite, biotite(?), & calcite, feldspar slightly turbid				
8730 0979	Rhyolitic ignimbrite	Breccia Ck Rhyolite, unassigned	7864-600442	+11.7
Poorly welded, lithic & crystal-poor, devitrified & recrystallised; slight to moderate alteration to sericite, feldspar slightly turbid				
8330 0463	Monzogranite	St Helena Monzogranite, intrusive	7863-652835	+3.7
Strongly porphyritic; slightly to moderately altered to sericite, chlorite, & calcite, K-feldspar slightly turbid & plagioclase moderately turbid				

WCS = Wakara Caldera sequence
DCS = Djungan Caldera sequence
FCS = Featherbed Caldera sequence

Table 2. $\delta^{18}O$ values for the Late Carboniferous Featherbed Cauldron Complex

AGSO No.	*Rock type*	*Unit*	*AMG coords*	$\delta^{18}O_{SMOW}$
8330 0228	Rhyolitic ignimbrite	Jamtin Rhyolite, unassigned	7863-494996	+8.7
Crystal-rich; very slightly altered to chlorite, sericite, & calcite, feldspar slightly to moderately turbid				
8330 0329	Rhyolitic ignimbrite	Jamtin Rhyolite, unassigned	7863-485953	+5.0
Crystal-poor with extensive recrystallisation; slight alteration to sericite, chlorite, muscovite, andalusite(?), & calcite, feldspar slightly to moderately turbid				
8330 0352	Rhyolitic ignimbrite	Jamtin Rhyolite, unassigned	7863-499922	+8.0
Moderately crystal-poor to crystal-rich; slight alteration to sericite, chlorite, calcite, epidote(?), & prehnite, feldspar moderately turbid				
8330 0436	Rhyolitic ignimbrite	Lappa Rhyolite, TCS	7863-726833	+1.6
Moderately to intensely welded, crystal-rich to very crystal-rich; moderate alteration to sericite, chlorite, clay, iron oxides, & calcite, feldspar moderately to very turbid				
8230 0202	Rhyodacitic ignimbrite	Dalnotter Dacite, TCS	7863-734795	+2.8
Very crystal-rich & lithic-poor; moderate alteration to sericite, chlorite, & calcite, feldspar (especially K-feldspar) very turbid				
8230 0137	Rhyolitic ignimbrite	Rock Hole Rhyolite, BCS	7863-805945	+8.4
Moderately crystal-rich; slight to moderate alteration to sericite, chlorite & calcite, feldspar moderately to very turbid				
8230 0156	Andesite	Verdure Andesite, BCS	7863-797903	+6.1
Crystal-rich; slight alteration to chlorite, sericite, opaque phases, titanite, anatase, epidote, & calcite, feldspar moderately to very turbid				
8230 0155	Dacitic-andesitic ignimbrite	Adder Dacite, BCS	7863-801906	+6.2
Crystal-rich, intensely recrystallised & hornfelsed; slight to moderate alteration to sericite, chlorite, epidote & calcite, feldspar moderately to very turbid				
8230 0175	Dacitic ignimbrite	Adder Dacite, BCS	7863-790882	+1.4
Moderately crystal-rich & recrystallised; slight alteration to sericite, chlorite, epidote, calcite, & prehnite(?), feldspar moderately to very turbid				
8330 0441	Dacitic-andesitic ignimbrite	Adder Dacite, BCS	7863-762841	+3.8
Crystal-rich, partially recrystallised with strong alteration (metasomatism?) to biotite, chlorite, hornblende(?), sericite, epidote, & calcite, feldspar moderately to very turbid				
8230 0034	Rhyolitic ignimbrite	Hopscotch Rhyolite, BCS	7963-905899	+8.1
Moderately welded, crystal-rich; primary augite, hornblende, & biotite; very altered to sericite & chlorite, plagioclase slightly to moderately turbid & K-feldspar very turbid				
8230 0186	Rhyolitic ignimbrite	Hopscotch Rhyolite, BCS	7863-762849	+0.3
Crystal-rich; alteration to biotite, chlorite, sericite, anatase, epidote, & calcite, feldspar slightly turbid				
8330 0540	Rhyolitic ignimbrite	Hopscotch Rhyolite, BCS	7963-885976	+5.0
Moderately crystal-poor to crystal-rich; very altered to chlorite, epidote, sericite, & calcite(?), feldspar moderately to very turbid				
8230 0003	Rhyolite	Muirson Rhyolite, BCS	7963-921954	+5.7
Moderately porphyritic; very altered with sericite, prehnite(?), anatase/brookite, & quartz, feldspar altered to sericite, quartz, & calcite				
8330 0284	Rhyolitic ignimbrite	Muirson Rhyolite, BCS	7863-847019	+6.7
Crystal-rich, deformed & recrystallised; moderate alteration to chlorite, sericite, & calcite; intensely fractured with veinlets of quartz, calcite, sericite, feldspar very turbid				

AGSO No.	*Rock type*	*Unit*	*AMG coords*	$\delta^{18}O_{SMOW}$
8330 0535	Rhyolitic ignimbrite	Muirson Rhyolite, BCS	7963-878998	+6.9
Moderately crystal-rich; very altered to sericite, muscovite, chlorite, calcite, prehnite(?) & epidote(?), feldspar very to extremely turbid				
8230 0041	Rhyolitic ignimbrite	Eureka Rhyolite, BCS	7963-984887	+8.2
Intensely welded, moderately crystal-rich, & partially recrystallised;primary hornblende & biotite; slight to moderate alteration to sericite, chlorite, hematite, & "leucoxene" (anatase/brookite), feldspar moderately to very turbid				
8430 0634	Rhyolitic ignimbrite	Eureka Rhyolite, BCS	7963-078852	+5.2
Moderately crystal-rich; slight alteration to chlorite, sericite & calcite, K-feldspar slightly turbid & plagioclase clear to slightly turbid				
8230 0008	Rhyolitic ignimbrite	Bluewater Rhyolite, BCS	7963-053911	+6.3
Poor to moderately welded, moderately crystal-rich; primary augite(?), hornblende, biotite; slightly to moderately altered to chlorite, sericite & epidote, K-feldspar slightly turbid				
8230 0054	Rhyodacitic-rhyolitic ignimbrite	Bluewater Rhyolite, BCS	7963-844783	+3.3
Intensely welded, crystal-rich with finely recrystallised groundmass; primary augite, hornblende, & biotite; moderate alteration to sericite, chlorite, biotite(?), hematite, tremolite-actinolite, plagioclase slightly turbid & K-feldspar moderately turbid				
8230 0060	Rhyodacitic-rhyolitic ignimbrite	Orient Rhyolite, BCS	7963-079795	+6.5
Intensely welded, moderately crystal-rich; primary hornblende & biotite; moderate to strong alteration to sericite, chlorite, calcite, & iron oxides, K-feldspar slightly turbid				
8230 0070	Rhyolitic ignimbrite	Bedlog Rhyolite, BCS	7963-943726	+7.4
Moderately welded, moderately crystal-rich & very lithic-poor; moderate alteration to sericite, chlorite, calcite, & anatase/brookite				
8430 0666	Rhyodacitic ignimbrite	Redcap Dacite, unassigned	7763-267095	+8.7
Moderately crystal poor				
8430 0569	Rhyolitic ignimbrite	Beapeo Rhyolite, unassigned	7863-834105	+3.8
Moderately crystal-rich; moderate alteration to sericite, calcite, chlorite, & iron oxides, feldspar very to extremely turbid				
8230 0088	Rhyodacitic ignimbrite	Doolan Ck Rhyolite,unassigned	7863-785172	+9.0
Crystal rich; slight alteration of biotite to chlorite + opaque phases, K-feldspar very turbid & mottled & plagioclase slightly turbid				
8630 0771	Rhyodacitic-dacitic ignimbrite	Nightflower Dacite, unassigned	7864-364361	+8.6
Crystal-rich & lithic-poor; very altered to sericite, chlorite, & calcite, feldspar very to extremely turbid				
8430 0568	Biotite leucogranite	James Ck Granite, intrusive	7863-838087	+9.0
Complete alteration of biotite to chloritoid & calcite & strong alteration of plagioclase cores to muscovite & calcite, feldspar slightly to moderately turbid				
8430 0579	Leuco-monzogranite	Bamford Granite, intrusive	7863-806909	+8.8
Slight to moderate alteration of plagioclase to sericite & calcite & slight alteration of biotite, feldspar slightly to moderately turbid				
8430 0612	Leuco-monzogranite	Bamford Granite, intrusive	7863-793845	+7.8
Very altered to fine sericite, plagioclase very turbid & K-feldspar slightly turbid				
8130 0717	Dacite-rhyodacite	Cottell Rhyolite, intrusive	7863-760852	-1.0
Porphyritic dyke; alteration of ferromagnesian minerals & feldspar to chlorite, hematite, sericite, prehnite(?), epidote, & calcite, feldspar extremely turbid				
8430 0632	Microgranite	Halpin Granite, intrusive	7963-049870	+6.5
Strongly porphyritic; very altered to sericite, epidote, chlorite, & calcite, feldspar extremely turbid				
8430 0580	Granodiorite	Borneo Granite, intrusive	7863-808917	+3.9
Sparsely porphyritic; slight alteration to sericite, chlorite, iron oxides, calcite, & epidote, feldspar slightly to moderately turbid				

TCS = Tennyson Caldera sequence
BCS = Boonmoo Cauldron sequence

in the waning stages of Late Carboniferous magmatism, exploited the major structures, and caused regional isotopic depletion, particularly adjacent to those structures.

Implications for epithermal Au mineralisation

The Late Carboniferous volcanic rocks of the Featherbed Cauldron Complex appear to be more prospective for mineralisation than the Early Permian A-type rocks, because of their initial composition and range of fractionation. Mackenzie (1987) concluded that these rocks are less voluminous, but were probably more hydrous than the A-type rocks, and appear to have had a much greater capacity to produce and/or interact with hydrothermal fluids. The oxygen-isotope data outlined above support these observations. Extensive Sn, W, Cu, Pb, Ag, and minor Au mineralisation are associated with the Late Carboniferous volcanics, particularly in the southeast. By contrast, the Early Permian volcanics are associated with sparse Au, U, W, base-metal, and Sn mineralisation, even

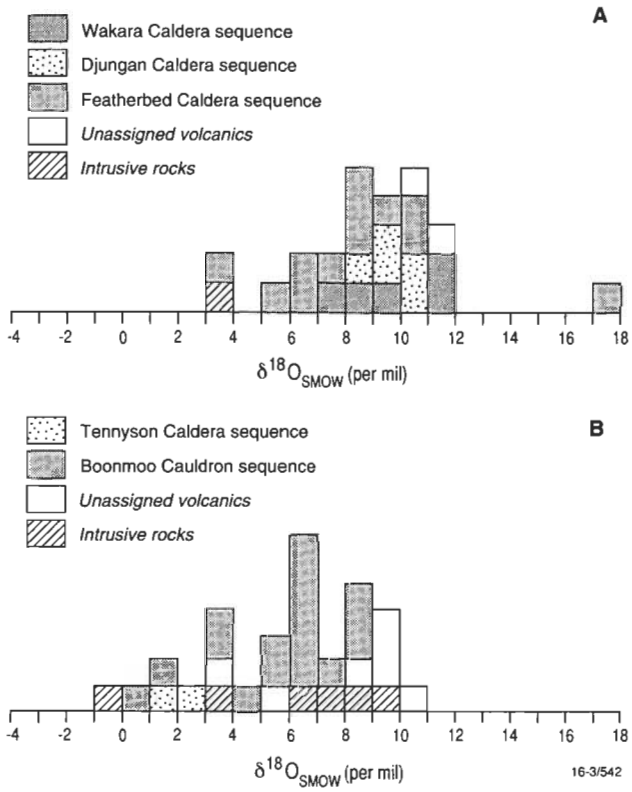

Figure 3. Whole-rock $\delta^{18}O$ values for the Featherbed Cauldron Complex. A—Early Permian sequence. B—Late Carboniferous sequence. Unaltered primary whole-rock igneous $\delta^{18}O$ values are typically greater than +5.5 per mil.

though they are believed to have been emplaced at shallower levels (perhaps 2 km or less) than the I-type magmas.

Examination of exploration data for the complex indicates that no epithermal mineralisation is known from the region. It has been suggested that the Fluorspar Group of workings (Au) and the Orient Camp workings (which produced Pb and Ag, but no Au) could have some epithermal character; however, the evidence (particularly for the Orient Camp workings) is not compelling. It appears that the Late Carboniferous volcanics may be eroded more deeply (perhaps up to 1–2 km) than the Early Permian volcanics. If this is the case, then any epithermal systems produced by the Late Carboniferous igneous activity are likely to have been removed by subsequent erosion, particularly around the eastern margins of the complex, where erosion has been greatest. It is possible that the northwestern areas of Late Carboniferous volcanism could have given rise to epithermal mineralisation, now preserved beneath a blanket of later Permian A-type volcanism, before significant erosion of the Carboniferous sequence took place. However, it is likely that any buried mineralised systems would be difficult to detect with current exploration techniques.

Cape York Peninsula

Regional geological and structural setting

Cape York Peninsula consists of a basement of Proterozoic metamorphic and Palaeozoic granitic rocks (the Coen and Yambo Inliers) overlain and flanked by gently dipping Mesozoic and Cainozoic sedimentary sequences of the Carpentaria, Laura, and Karumba Basins. The dominant structural trend is northerly, and the inliers, igneous belts, and sedimentary basins are elongated in this general direction.

The Coen Inlier is intruded by numerous Siluro-Devonian granites of the Cape York Peninsula Batholith and, in its northern part, is overlain and intruded by Permo-Carboniferous granites and volcanic rocks interbedded with fluviatile and lacustrine sedimentary sequences (Fig. 4A). The Permo-Carboniferous volcanic rocks have been divided into the Janet Ranges Volcanics, Kangaroo Volcanics, and Cape Grenville Volcanics, consisting predominantly of rhyolitic welded tuff, and lesser rhyolite, breccia, agglomerate, rhyodacitic and dacitic welded tuff, andesite and metabasalt (Willmott et al. 1973). The volcanic rocks have been intruded by, and appear to be coeval with, the Weymouth Granite, Wolverton Adamellite, and Twin Humps Adamellite. The regional geophysical data (principally aeromagnetic data) suggest that these Permo-Carboniferous intrusive and extrusive rocks extend northward toward Cape York beneath the Mesozoic and Cainozoic cover (Wellman 1992).

Permo-Carboniferous igneous activity is also evident in the Cape York–Oriomo Inlier in the Torres Strait region. The Torres Strait Volcanics crop out on the mainland at Cape York and throughout many of the islands (Fig. 4B). They consist mainly of rhyolitic welded tuff and have been subdivided into four members on the basis of different eruptive centres—the Eborac Ignimbrite, Endeavour Strait Ignimbrite, Goods Island Ignimbrite and Muralug Ignimbrite. Other rock types are also present (e.g. lavas and volcanic breccias). The volcanic rocks, which vary from rhyolitic to andesitic, have been intruded by the Late Carboniferous Badu Granite, and therefore must be younger.

Isotopic results

Fifteen volcanic rock samples were analysed, comprising rhyolitic to andesitic tuffs and lavas from the Permo-Carboniferous Janet Ranges, Kangaroo River, and Cape Grenville Volcanics in the northern Coen Inlier and the Carboniferous(?) Torres Strait Volcanics (Table 3). The sampling relied heavily on limited reconnaissance material collected by BMR/AGSO during the late 1960s and the current NGMA North Queensland project. Sampling was biased towards volcanic rocks, because past experience in the northern Drummond Basin has shown that these rocks are more consistently and intensely ^{18}O-depleted than the associated intrusive rocks.

The isotopic data indicate that, although several samples from the Torres Strait region are ^{18}O-depleted (Fig. 4B), the majority have near-normal whole-rock igneous values (Table 3). By contrast, most samples from the northern Coen Inlier have low $\delta^{18}O$ values, ranging from +1.3 to –2.7 per mil, and give rise to a zone of consistent ^{18}O depletion that is not a function of volcanic stratigraphy or rock type (Table 3, Figs 4A & 5). Feldspars have a clear to extremely turbid appearance, but there is a poor correlation between the degree of ^{18}O depletion and the appearance of feldspar crystals.

Implications for epithermal Au mineralisation

The high-level igneous environment of Torres Strait and the northern Coen Inlier consists of volcanic rocks intruded by coeval felsic intrusives, which have been only partly unroofed by erosion. Such an environment should

be highly prospective for epithermal mineralisation, but limited geoscientific investigation and exploration have led to a poor understanding of the area's mineral potential. Miezitis & Bain (1991) drew attention to the high potential for gold in the Cape York–Oriomo and Coen Inliers, based on known gold mineralisation (e.g. in the Hamilton, Coen, and Wenlock gold fields and at Horn Island) and perceived similarities to the regional geology of the northeast Queensland felsic volcanic province (Georgetown–Townsville area).

A regional stream-sediment survey (one sample per 10–15 km^2) was carried out by AGSO in 1990 over the Coen Inlier north of 14°S. Part of the results of that survey are shown in Figure 6 for Au and a multielement index of those pathfinder elements characteristic of epithermal gold deposits (Ag, As, Au, Sb, and Tl; Hg was not analysed). This index is the sum of standardised values for the five elements, and was calculated according to the equation:

$$\text{Index} = \sum_{e=1}^{e=5} \left[X_e - \overline{X}_e \right] / S_e$$

where X_e is the element value for a sample, $\overline{X}_e$ is the population mean for that element and S_e is its standard deviation. High Au values (Fig. 6) relate to known Au mineralisation at Iron Range and Wenlock. However, the multielement index indicates a highly anomalous region immediately south of Temple Bay that is broadly coincident with the area of regional ^{18}O depletion. No stable isotope data are available for an area about 80 km due south, near Mount Carter and Jack's Knob (Fig. 4), where moderately high multielement values occur. This area broadly corresponds with the southernmost outcrop of the Permo-Carboniferous Weymouth Granite. The results of an examination of enhanced Landsat Thematic Mapper imagery in the region south of Temple Bay for evidence of clay and silica alteration normally associated with epithermal systems were inconclusive, largely owing to the masking effects of vegetation.

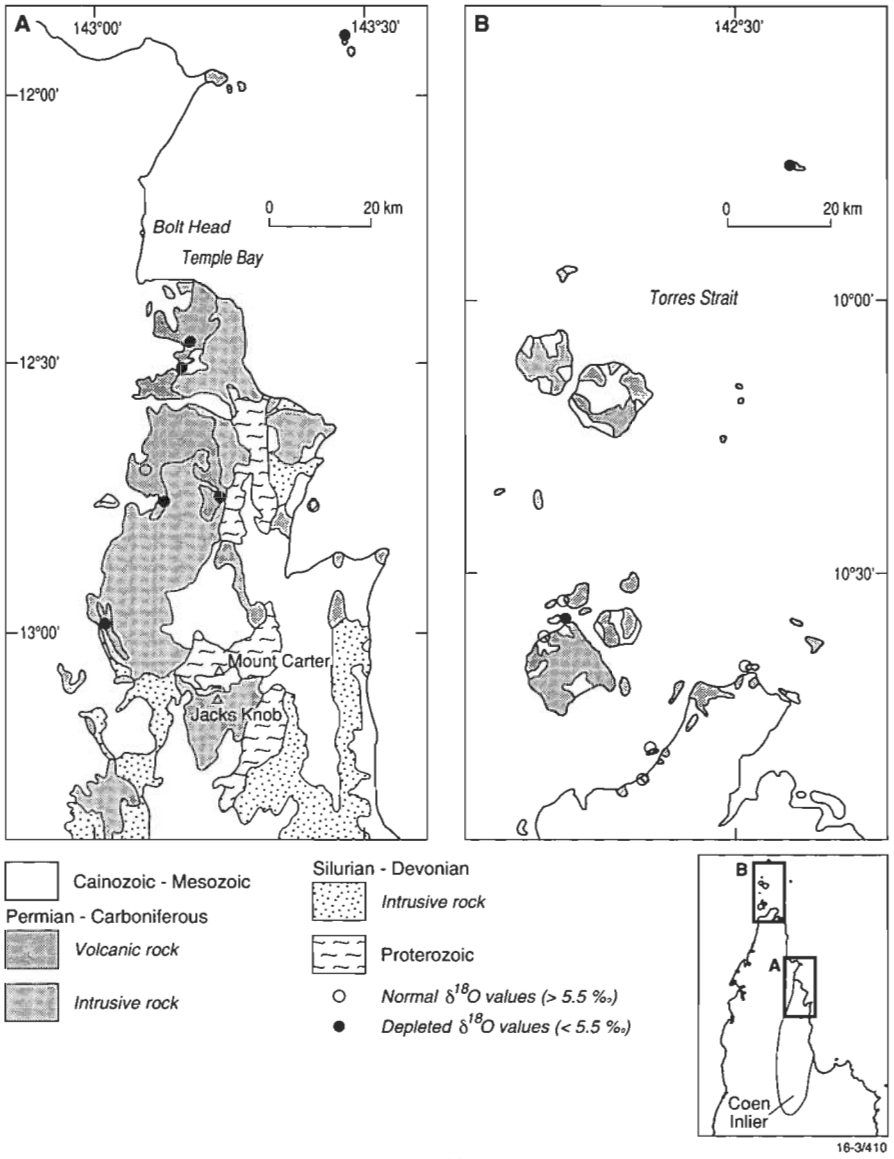

Figure 4. Simplified geology and measured $\delta^{18}O$ values for volcanic rocks in the northern Coen Inlier (A) and Torres Strait region (B), Cape York Peninsula (from Ewers & Cruikshank 1993).

A compilation of previous mineral exploration activity (Culpeper et al. 1992) reveals that parts of the ^{18}O-depleted area in the Coen Inlier have been covered for short periods since 1951 by Authorities to Prospect and Exploration Permits for Cu, U, Au, Sn and W. Notable among these were three Authorities (AP 3815M, AP 4329M, and AP 5019M) held between 1984 and 1988 over parts of the Kangaroo River Volcanics in the Temple Bay area. Although these Authorities were relinquished, companies working there at that time believed they were dealing with epithermal mineralisation (Culpeper et al. 1992). They established from rock-chip and stream-sediment sampling that anomalous Hg, As, Sb, and Au (elements typically concentrated in epithermal deposits) were present. Most attention was focussed on prospects

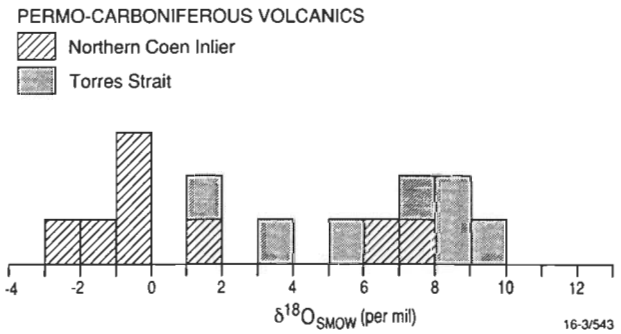

Figure 5. Whole-rock $\delta^{18}O$ values for Cape York Peninsula. Unaltered primary whole-rock igneous $\delta^{18}O$ values are typically greater than +5.5 per mil.

Table 3. $\delta^{18}O$ values for Permo-Carboniferous volcanics from Cape York Peninsula.

AGSO No.	*Rock type*	*Unit*	*AMG coords*	$\delta^{18}O_{SMOW}$
6748 0315	Rhyolitic tuff	Cape Grenville Volcanics, Coen Inlier	7574-688828	0.0
Densely welded with aligned flattened pumice lapilli & sparse plagioclase crystals set in a brownish-purple groundmass; complete alteration of glass & moderate alteration of plagioclase to quartz, sericite, chlorite, epidote & hematite; feldspar very turbid				
6748 0330	Dacitic tuff	Janet Range Volcanics, Coen Inlier	7572-365165	-0.8
Densely welded & massive; complete alteration of glass & moderate to strong alteration of plagioclase to quartz, sericite, chlorite, epidote & iron oxides				
6848 0147	Rhyolitic tuff	Janet Range Volcanics, Coen Inlier	7572-277942	+7.2
Densely welded with aligned flattened pumice lapilli & sparse feldspar & quartz crystals set in a black groundmass; complete alteration of glass & slight to moderate alteration of feldspar to quartz, sericite, chlorite, epidote, calcite, & hematite; feldspar slightly turbid				
9083 6116	Rhyodacite	undivided volcanics, Coen Inlier	7572-179631	-0.3
Grey fine-grained rhyolite with rare feldspar phenocrysts in a groundmass of quartz, feldspar, hornblende, & minor opaque phases; slight alteration to sericite & chlorite; feldspar slightly to moderately turbid				
9083 6153	Rhyolitic tuff	Janet Range Volcanics, Coen Inlier	7572-399892	-1.1
Grey, crystal-poor & lithic-rich welded tuff containing flattened pumice lapilli; slight to moderate sericite, calcite, & lesser chlorite, epidote alteration				
9083 6158	Rhyolite	Janet Range Volcanics, Coen Inlier	7572-303895	+1.3
Light grey, moderately porphyritic rhyolite with quartz & feldspar phenocrysts in a similar fine-grained groundmass which includes hornblende; slight sericite, calcite, & chlorite alteration; feldspar very to extremely turbid				
6748 0377	Andesite	Kangaroo River Volcanics, Coen Inlier	7573-360220	-2.7
Abundantly porphyritic augite(?) andesite; complete alteration of pyroxene & moderate alteration of plagioclase to chlorite, sericite, epidote, opaque phases, calcite, & titanite; plagioclase slightly to moderately turbid				
6848 0142	Rhyolitic tuff	undivided volcanics, Coen Inlier	7572-605882	+6.5
Moderately crystal-poor & lithic-rich in a dark grey devitrified groundmass; complete alteration of ferromagnesian minerals & slight alteration of feldspar to chlorite, sericite, calcite; feldspar moderately turbid				
6848 0046	Dacitic tuff	Goods Island Ignimbrite, Torres St.	7376-293318	+7.1
Welded & crystal-rich dacitic tuff containing plagioclase, hornblende & quartz crystals & lithic fragments; slight to moderate alteration to chlorite & sericite & minor epidote, titanite, & iron oxides; feldspar clear				
6848 0137	Rhyodacitic tuff	Goods Island Ignimbrite, Torres St.	7376-299281	+3.6
Welded & crystal-rich tuff containing feldspar, hornblende & quartz crystals; moderate alteration of feldspars & hornblende to chlorite, sericite, epidote, titanite, & iron oxides; feldspar moderately to very turbid				
6848 0075	Andesite	Endeavour Strait Ignimbrite, Torres St.	7376-438941	+8.7
Hornblende-bearing andesite with pilotaxitic plagioclase growths, opaque phases (magnetite? & hematite) & minor pyroxene; slight chlorite & sericite alteration; plagioclase very slightly turbid				
6848 0135	Rhyolitic tuff	Endeavour Strait Ignimbrite, Torres St.	7376-480008	+5.5
Welded & crystal-rich tuff containing feldspar & quartz crystals in an aphanitic groundmass; slight to moderate alteration to sericite, chlorite, calcite, & iron oxides; feldspar moderately to very turbid				
6848 0140	Rhyolitic tuff	Eborac Ignimbrite, Torres St.	7476-676186	+9.6
Welded & crystal-rich tuff containing feldspar & quartz crystals with minor opaque phases in an aphanitic (originally glassy?) groundmass; slight alteration of feldspar to sericite, & epidote; feldspar slightly turbid				
6848 0136	Rhyolitic tuff	Muralug Ignimbrite, Torres St.	7376-261252	+8.5
Densely welded & crystal-poor (quartz, feldspar, & lesser hornblende crystals) with aligned flattened pumice lapilli set in a brown-grey groundmass; devitrified with moderate alteration of hornblende & feldspar to sericite, chlorite, calcite, & hematite; feldspar moderately turbid				
6848 0180	Rhyolitic tuff	undivided volcanics, Torres St.	7478-786189	+1.2
Welded crystal-poor & lithic-poor dark grey tuff with abundant devitrified glass shards & pumice fragments in the groundmass; slight to moderate alteration of feldspar to sericite, calcite, & chlorite; feldspar very turbid				

around the margins of Temple Bay (Bolt Head, Lake Anomaly and Glennie Inlet prospects). However, the regional oxygen-isotope and stream-sediment geochemical data suggest that the area with epithermal potential may be larger, and that a more systematic and thorough evaluation could be warranted.

Conclusions

Stable-isotope data have demonstrated conclusively that hydrothermal fluids derived from meteoric waters have played a dominant role in the genesis of low-sulphidation (adularia–sericite type) epithermal gold deposits (e.g. O'Neil et al. 1973; Taylor 1973; O'Neil & Silberman 1974; Bethke & Rye 1979; Criss & Taylor 1983). Characteristically, the host rocks to these deposits are ^{18}O depleted as a result of isotopic exchange with meteoric fluids (Field & Fifarek 1985).

An extensive regional oxygen-isotope depletion pattern over most of the northern Drummond Basin and its coincidence with epithermal mineralisation is consistent

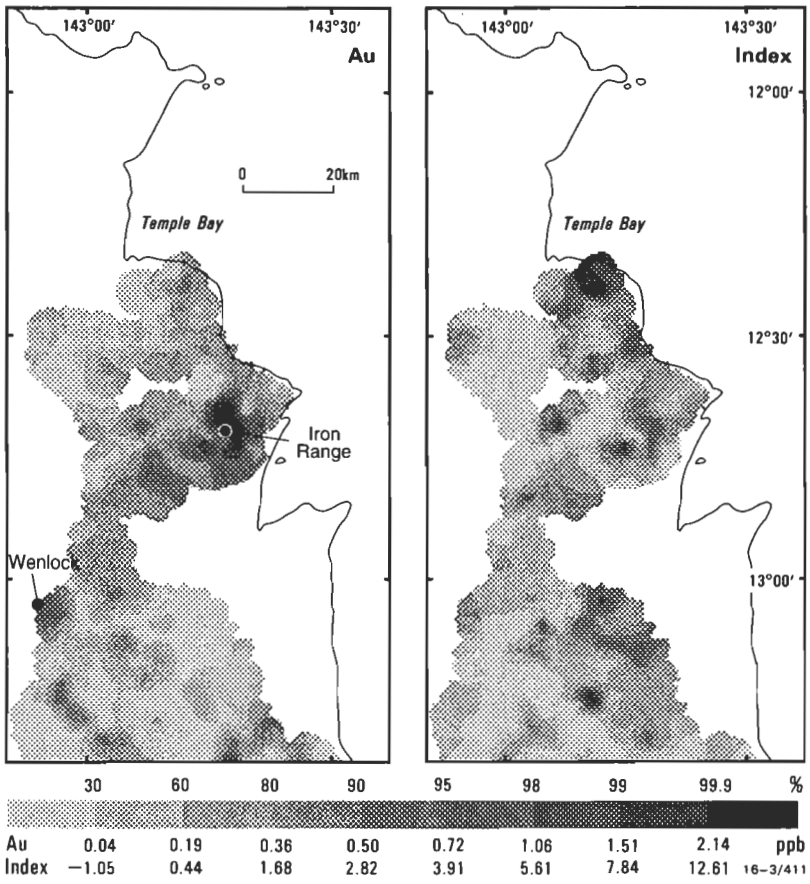

Figure 6. Geochemical images of Au and a multielement index derived from Ag, As, Au, Sb, and Tl. The randomly spaced element or index values were interpolated to a square grid and imaged as shown (from Ewers & Cruikshank 1993).

with a similar association for younger, world-class epithermal districts in the United States (Ewers et al. 1994). This relationship is not surprising, since hydrothermal systems involving meteoric fluids are likely in volcanic environments during the waning stages of igneous activity (Field and Fifarek 1985). Oxygen-isotope depletion patterns provide a potentialy useful exploration tool that could target areas that are prospective for low sulphidation epithermal mineralisation.

Reconnaissance whole-rock oxygen-isotope data for Permo-Carboniferous volcanics in the northern Coen Inlier indicate an area of isotopic depletion that coincides with regional stream-sediment anomalies normally associated with epithermal deposits. This area is concluded to be an excellent target for epithermal mineralisation that warrants more systematic and detailed exploration. By contrast, extensive exploration in and around the Featherbed Cauldron Complex has not defined any significant epithermal mineralisation. Whole-rock oxygen-isotope values are predominantly near normal, and isotopic depletion is confined largely to Late Carboniferous volcanic rocks in southern areas of the complex, particularly along caldera margins where major structures would provide pathways for fluid circulation. The data are consistent with earlier observations that the Late Carboniferous sequence is more closely associated with hydrothermal activity (Mackenzie 1987), and that meteoric fluids have been focussed through these major structures, at least during the waning stages of igneous activity.

The use of regional oxygen-isotope depletion patterns to assess the epithermal potential of areas in north Queensland with late Palaeozoic igneous activity has demonstrated that this association is not simply a Tertiary phenomenon confined to epithermal districts in the USA. Younger terranes are less likely to be eroded or overprinted by later events and, in this sense, regional oxygen-isotope signatures should be more obvious. However, the technique is worth testing elsewhere in geological provinces (possibly much older) that have potential for low-sulphidation epithermal deposits.

Acknowledgments

We thank Taro Macias and Phil Bierwirth (AGSO) for their assistance with Landsat TM imagery in the northern Coen Inlier and Phil Dash (Department of Minerals and Energy, Queensland) for assistance with information on exploration activity in the Featherbed region. Andrew Bryce and Andrew Todd undertook the isotopic analyses at CSIRO. Terry Mernagh and Peter Stuart-Smith provided valuable comments on an earlier draft of the manuscript. The authors also thank David Cooke and Ed Mikucki for their reviews and suggestions to improve the manuscript.

References

Bacon, C.R., Adami, L.H. & Lanphere, M.A., 1989. Direct evidence for the origin of low-^{18}O silicic magmas: quenched samples of a magma chamber's partially-fused granitoid walls, Crater Lake, Oregon. *Earth and Planetary Science Letters*, 96, 199–208.

Bethke, P.M. & Rye, R.O., 1979. Environment of ore deposition in the Creede mining district, San Juan Mountains, Colorado: Part IV. Source of fluids, from oxygen, hydrogen, and carbon isotope studies. *Economic Geology*, 74, 1832–1851.

Burnham, C.W., 1967. Hydrothermal fluids at the magmatic stage. *In* Barnes, H.L. (editor), *Geochemistry of hydrothermal ore deposits.* New York, Holt, Reinhart, and Winston, 34–76.

Cartwright, I. & Valley, J.W., 1991. Low-^{18}O Scourie dike magmas from the Lewisian complex, northwestern Scotland. *Geology*, 19, 578–581.

Clayton, R.N. & Mayeda, T.K., 1963. The use of bromine pentafluoride in the extraction of oxygen from oxides and silicates for isotopic analysis. *Geochimica et Cosmochimica Acta*, 27, 43–52.

Criss, R.E. & Taylor, H.P., Jr., 1983. An $^{18}O/^{16}O$ and D/H study of Tertiary hydrothermal systems in the southern half of the Idaho Batholith. *Geological Society of America Bulletin*, 94, 640–643.

Culpeper, L.G., Denaro, T.J., Willmott, W.F., Whitaker, W.G., Bruvel, F.J., Morwood, D.A. & Shield, C.J., 1992. A review of mineral exploration, Cape York Peninsula, 1969 to 1990. *Queensland Resource Industries Record* 1992/10.

Ewers, G.R. & Cruikshank, B.I., 1993. Epithermal gold potential in the northern Coen Inlier. *AGSO Research Newsletter*, no 18, 1–2.

Ewers, G.R., Mackenzie, D.E., Oversby, B.S. & Wyborn, D., 1991. Regional oxygen-isotope patterns: implications for epithermal gold exploration. *BMR Research Newsletter*, no. 14, 1–2.

Ewers, G.R., Mackenzie, D.E., Wyborn, D., Oversby, B.S., McPhie, J. & Andrew, A.S., 1994. Regional ^{18}O depletions in igneous rocks from the northern Drummond Basin, Queensland, Australia & their implications for epithermal gold mineralisation. *Economic Geology*, 89, 662–673.

Field, C.W. & Fifarek, R.H., 1985. Light stable-isotope systematics in the epithermal environment. *Reviews in Economic Geology*, 2, 99–128.

Friedman, I. & O'Neil, J. R., 1977. Compilation of stable isotope fractionation factors of geochemical interest. *In* Fleischer, M. (editor), Data of geochemistry (sixth edition). *US Geological Survey Professional Paper* 440-KK, KK1–KK12.

Friedman, I., Lipman, P.W., Obradovich, J.D., , Gleason, J.D. & Christiansen, R.L., 1974. Meteoric waters in magmas. *Science*, 184, 1069–1072.

Golding, S.D. & Wilson, A.F., 1984. Stable isotope relationships in epithermal gold deposits, Queensland. Australasian Institute of Mining and Metallurgy Regional Conference Gold - mining, metallurgy, and geology, Perth and Kalgoorlie Branches, October 1984, 1–9.

Gregory, R.T. & Taylor, H.P., Jr., 1981. An oxygen isotope profile in a section of Cretaceous oceanic crust, Samail Ophiolite, Oman: evidence for $\delta^{18}O$ buffering of the oceans by deep (>5km) seawater-hydrothermal circulation at mid-ocean ridges. *Journal of Geophysical Research*, 86, 2737–2755.

Grunder, A.L., 1987. Low-$\delta^{18}O$ silicic volcanic rocks at the Calabozos caldera complex, southern Andes. *Contributions to Mineralogy and Petrology*, 95, 71–81.

Harris, C. & Erlank, A.J., 1992. The production of large-volume, low-$\delta^{18}O$ rhyolites during the rifting of Africa and Antartica: The Lebombo Monocline, southern Africa. *Geochimica et Cosmochimica Acta*, 56, 3561–3570.

Hemley, J.J & Jones, W.R., 1964. Chemical aspects of hydrothermal alteration with emphasis on hydrogen metasomatism. *Economic Geology*, 59, 538–569.

Hildreth, W., Christiansen, R.L. & O'Neil, J.R., 1984. Catastrophic isotopic modification of rhyolitic magma at times of caldera subsidence, Yellowstone Plateau volcanic field. *Journal of Geophysical Research*, 89, 8339–8369.

Larson, P.B. & Taylor, H.P., Jr., 1986. An oxygen isotope study of hydrothermal alteration in the Lake City caldera, San Juan Mountains, Colorado. *Journal of Volcanology and Geothermal Research*, 30, 47–82.

Mackenzie, D.E., 1987. Geology, petrology, and mineralisation of the Permo-Carboniferous Featherbed Volcanics Complex, northeastern Queensland. *Proceedings of Pacific Rim Congress 87, Gold Coast, Queensland 1987*, Australasian Institute of Mining and Metallurgy, Parkville, Australia, 297–301.

Mackenzie, D.E., 1993. Geology of the Featherbed Cauldron Complex, north Queensland: Part 1 - Eruptive rocks and post-volcanic sediments. *Australian Geological Survey Organisation, Record* 1993/82.

Mackenzie, D.E., Bultitude, R.J. & Rienks, I.P., 1993. Geology of the Featherbed Cauldron Complex, Queensland (1:100000-scale geological map). Australian Geological Survey Organisation, Canberra.

McPhie, J., Black, L.P., Law, S.R., Mackenzie, D.E., Oversby, B.S. & Wyborn, D., 1990. Distribution, character and setting of mineralised Palaeozoic volcanic sequences, Burdekin Falls region, northeastern Queensland. *Proceedings of Pacific Rim Congress 90, Gold Coast, Queensland 1990.* Australasian Institute of Mining and Metallurgy, Parkville, Australia, 2, 465–471.

Miezitis, Y. & Bain, J.H.C., 1991. Cape York Peninsula: Comments on mineral potential and availability of data as at January 1990. *Bureau of Mineral Resources, Australia, Record* 1991/74.

Muehlenbachs, K., Anderson, A.T., Jr. & Sigvaldason, G.E., 1974. Low-O^{18} basalts from Iceland. *Geochimica et Cosmochimica Acta*, 38, 577–588.

O'Neil, J.R. & Silberman, M.L., 1974. Stable isotope relations in epithermal Au-Ag deposits. *Economic Geology*, 69, 902–909.

O'Neil, J.R., Silberman, M.L., Fabbi, B.P. & Chesterman, C.W., 1973. Stable isotope and chemical reactions during mineralization in the Bodie mining district, Mono County, California. *Economic Geology*, 68, 765–784.

Porter, R.G., 1988. The Pajingo gold mine. *In* Morrison, G.W. (editor), Bicentennial Gold 88 excursion guidebook: Epithermal and porphyry style gold deposits in north Queensland. *James Cook University of North Queensland, Economic Geology Research Unit Contribution* 29, 23–34.

Sheppard, S.M.F., 1986. Igneous rocks: III. Isotopic case studies of magmatism in Africa, Eurasia and oceanic islands. *In* Valley, J.W., Taylor, H.P.Jr. & O'Neil, J.R. (editors), Reviews in mineralogy. *Mineralogical Society of America*, 16, 319–371.

Taylor, H.P., Jr., 1971. Oxygen isotope evidence for large-scale interaction between meteoric ground waters and Tertiary granodiorite intrusions, western Cascade Range, Oregon. *Journal of Geophysical Research*, 76, 7855–7874.

Taylor, H.P., Jr., 1973. O^{18}/O^{16} evidence for meteoric-hydrothermal alteration and ore deposition in the Tonopah, Comstock Lode, and Goldfield mining districts, Nevada. *Economic Geology*, 68, 747–764.

Taylor, H.P., Jr., 1974a. The application of oxygen and hydrogen isotope studies to problems of hydrothermal alteration and ore deposition. *Economic Geology*, 69, 843–883.

Taylor, H.P., Jr., 1974b. Oxygen and hydrogen isotope evidence for large-scale circulation and interaction between groundwaters and igneous intrusions, with particular reference to the San Juan volcanic field, Colorado. *In* Hofmann, A.W., Giletti, B.J., Yoder, H.S., Jr. & Yund, R.A. (editors), Geochemical transport and kinetics. *Carnegie Institute of Washington Publication* 634, 299–324.

Taylor, H.P., Jr., 1986. Igneous rocks: II. Isotopic case studies of Circumpacific magmatism. *In* Valley, J.W., Taylor, H.P.Jr. & O'Neil, J.R. (editors), *Reviews in mineralogy. Mineralogical Society of America.* 16, 273–317.

Taylor, H.P., Jr., 1987. Comparison of hydrothermal systems in layered gabbros and granites, and the origin of low-^{18}O magmas. *In* Mysen, B.O. (editor), Magmatic processes: physicochemical principles. *Geochemical Society [USA], Special Publication* 1, 337–357.

Taylor, H.P., Jr & Epstein, S., 1962. Relationship between O^{18}/O^{16} ratios in coexisting minerals of igneous and metamorphic rocks. Part I: Principles and experimental

results. *Geological Society of America Bulletin*, 73, 461–480.

Taylor, H.P., Jr. & Forester, R.W., 1971. Low-O^{18} igneous rocks from the intrusive complexes of Skye, Mull, and Ardnamurchan, western Scotland. *Journal of Petrology*, 12, 465–497.

Taylor, H.P., Jr. & Forester, R.W., 1979. An oxygen and hydrogen isotope study of the Skaergaard intrusion and its country rocks: A description of a 55-m.y. old fossil hydrothermal system. *Journal of Petrology*, 20, 355–419

Wellman, P., 1992. A geological interpretation of the regional gravity and magnetic features of north Queensland. *Bureau of Mineral Resources, Australia, Record* 1992/77.

Willmott, W.F., Whitaker, W.G., Palfreyman, W.D. & Trail, D.S., 1973. Igneous and metamorphic rocks of Cape York Peninsula and Torres Strait. *Bureau of Mineral Resources, Australia, Bulletin* 135, 145 pp.

AGSO Journal of Australian Geology & Geophysics, 15(4), 409–412

Relationship between body wave and local magnitudes for Australian earthquakes

Marion Michael-Leiba[1] & Stewart Dennis[1]

For Australian earthquakes with local magnitudes in the range M_L 4.1–6.5, the relationship between M_L and the body-wave magnitude m_b may be predicted by the least squares regression line: $m_b = (0.66 \pm 0.20)(ML - 4.79) + (4.92 \pm 0.04)$. It is based on 15 earthquakes for which there are at least two measurements of M_L and m_b for each event, and an additional 14 for which there was only one measurement of M_L and/or m_b. The more reliable 15 were given four times the weight of the others. A least squares regression line:

$$mb = (0.80 \pm 0.17)(ML - 4.85) + (4.98 \pm 0.04)$$

was obtained from 31 earthquakes, which included these 29, together with the M_L 6.9 Meckering and M_L 7.0 Meeberrie events for which the data were also weighted as less reliable. The local magnitude range used in this regression is M_L 4.1–7.0. We recommend that the first equation be used to estimate m_b from M_L, because the local magnitudes of the two additional earthquakes are dubious and also the linearity of the relationship may not hold at large magnitudes. Body-wave magnitude measurements made on Australian earthquakes at distances of less than 12° may be too high because the attenuation of P waves differs from that in Gutenberg & Richter (1956).

Introduction

Richter (1935) first defined the local magnitude M_L of an earthquake, based on its maximum trace amplitude on a Wood-Anderson seismograph and attenuation of seismic waves in Southern California. Recently, new M_L scales have been derived for parts of Australia, based on a local attenuation function (e.g. Greenhalgh & Parham 1986; Greenhalgh & Singh 1986; Gaull & Gregson 1991; Michael-Leiba & Malafant 1992). These show that, at distances greater than about 100–200 km, attenuation is lower in South Australia, Western Australia and south-eastern Australia than that derived by Richter (1935).

The body-wave magnitude m_b was originally developed by Gutenberg (1945) for teleseisms because it could be used for distant earthquakes at all depths. The following modified formula was published by Gutenberg & Richter (1956):

$$m_b = \log(A/T) + Q(X,h)$$

where A is the maximum half peak-to-peak ground amplitude in micrometres of the P, PP or S wave train, T the corresponding wave period in seconds and Q(X,h) the depth(h)/distance(X) factor. The charts of Q prepared by Gutenberg & Richter (1956) are still in general use today, as recommended by Willmore (1979). During the period 1961–1978, body-wave magnitude was obtained by measuring only the first few cycles of P, and this gave a magnitude which was a mean of 0.7 magnitude units less than the Gutenberg & Richter m_b (McGregor & Ripper 1976). Willmore (1979) recommended reverting to the pre-1961 practice, but this was slow to be adopted at some observatories (Denham 1982).

Gutenberg & Richter (1956) derived the following empirical relationship between M_L and m_b:

$$m_b = 1.7 + 0.8M_L - 0.01M_L2 \quad (1)$$

The linear equation

$$m_b = 1.8 + 0.73M_L,\ 1<M_L<6 \quad (2)$$

approximates this closely (White 1968). At the value 6.4, m_b and M_L are equal (McGregor & Ripper 1976). More recent work has been published by other authors (e.g. Chhabra et al. 1975 for the Himalayas; Gibowicz 1972 for New Zealand; Kiratzi & Papazachos 1984 for Greece).

The aim of our work is to derive a relationship to estimate m_b from M_L for Australian earthquakes using linear regression, as part of a body of work to discriminate between earthquakes and explosions.

Method

Because of the problem mentioned above of the different method of m_b measurement initiated in the 1960s, we excluded USGS body-wave magnitudes during the period 1961–1982.

Except for magnitude M_L 3–5 southwest seismic zone (WA) events for which M_L was measured on the Mundaring Wood-Anderson seismographs, local magnitudes obtained before the new Australian attenuation relationships were in use have been corrected by us to approximate the new M_L values. These are usually around 0.3 less than the published magnitudes, because of the lower attenuation of seismic waves in at least some parts of Australia.

The events and their magnitudes used in our study are shown in Table 1. Events for which M_L or m_b or both were determined by only one measurement are flagged, as they may be less accurate. Because an average of about four M_L measurements was used to determine M_L for the more reliable events, they were given four times the weight of the others. In particular, the local magnitudes for the 1968 Meckering and 1941 Meeberrie earthquakes are unreliable. It would have been very difficult to measure M_L for large or major earthquakes at stations within the distance range for which M_L is defined, because of seismograph saturation problems. Linear regression was used to derive a relationship between M_L and m_b.

Results

The data for the 31 earthquakes in Table 1 along with the least squares regression line are plotted in Figure 1. The predictive form of the equation of the line (with standard errors indicated by ±) is:

$$m_b = (0.80 \pm 0.17)(M_L - 4.85) + (4.98 \pm 0.04) \quad (3)$$

The correlation coefficient r is 0.80 and the standard error of estimate of mb is 0.37.

The more reliable data in Table 1 are shown as solid

[1] Australian Geological Survey Organisation, GPO Box 378, Canberra, ACT 2601

Table 1. Earthquakes used in this study.

Locality	*Date*	*ML*	*mb*	*Quality*
Ravenswood Qld	18-12-1913	5.7 (RIV)	5.8 (RIV)	□
Meeberrie WA	29-04-1941	7.0 (PER)	7.3 (PER)	□
Meckering WA	14-10-1968	6.9 (MUN)	7.4 (RIV)	□
Cadoux, WA	02-06-1979	6.5 (KNA)	5.9 (RIV)	□
Appin NSW	15-11-1981	4.1	4.3 (BMR)	■
Wonnangatta Vic	21-11-1982	5.1	4.8 (BMR)	■
West Wyalong NSW	26-11-1982	4.3	5.4 (BMR)	◆
Cadoux WA	26-01-1983	4.8 (MUN)	5.1 (GS,BMR)	□
Beltana SA	29-12-1983	4.4	5.1 (GS,BMR)	■
Marryat Creek SA	30-03-1986	5.8 (COO)	5.8 (GS)	□
Tennant Creek NT	05-01-1987	4.3	4.4 (GS)	■
Tennant Creek NT	07-01-1987	4.8	5.2 (GS)	□
Tennant Creek NT	08-01-1987	4.5	4.5 (GS)	■
Tennant Creek NT	09-01-1987	4.5	4.1 (GS)	□
Tennant Creek NT	30-01-1987	4.3	4.3 (GS)	□
Nhill Vic	22-12-1987	4.6	4.6 (GS)	■
NE Derby WA	06-02-1988	5.7 (ASPA)	5.2 (GS)	□
Uluru NT	28-05-1989	5.6	5.8 (GS)	■
Newcastle NSW	27-12-1989	5.5 (QIS)	5.4 (GS)	□
Meckering WA	17-01-1990	5.5	5.2 (GS)	■
Lake Eyre SA	08-02-1990	4.6	4.5 (GS)	□
N Port Hedland WA	18-02-1990	4.5	4.3 (GS)	□
Cadoux WA	08-05-1990	4.5	3.9 (GS)	□
Broome WA	17-08-1990	4.2	4.0 (GS)	□
Tennant Creek NT	27-11-1990	5.2	4.8 (GS)	■
Tennant Creek NT	08-07-1991	5.0	5.1 (GS)	■
Cranbrook WA	13-12-1991	4.3	4.4 (GS)	■
N Lake Neale NT	13-06-1992	4.5	5.0 (GS)	■
E Canning Basin WA	15-07-1992	4.8	5.2 (GS)	■
Arnhem Land NT	30-09-1992	5.1	5.4 (GS)	■
Arnhem Land NT	18-12-1993	4.2 (QIS)	4.6 (GS)	□

Quality: ■ ML and mb determined by at least two observations
□ ML and/or mb from only one observation
◆ West Wyalong 1982 earthquake (anomalously high mb)

RIV, PER, MUN, KNA, COO, ASPA, QIS: Code of single station used to determine magnitude.

BMR: Bureau of Mineral Resources
GS: USGS, NEIC

symbols. All the data except for the West Wyalong earthquake fit the regression reasonably well. The m_b for this earthquake appears to be too high probably because the attenuation at distances less than 12 degrees in southeastern Australia differs from that of Gutenberg and Richter (1956) (Denham et al. 1985).

A regression analysis was performed using the 29 pairs of observations, excluding the 1968 Meckering and 1941 Meeberrie earthquakes because of the questionable accuracy of their M_L values and because the relationship may depart significantly from linearity at large magnitudes. The results are plotted in Figure 2. The predictive form of the equation of the least squares line is

$$m_b = (0.66 \pm 0.20)(M_L - 4.79) + (4.92 \pm 0.04) \quad (4)$$

The correlation coefficient r is 0.70 and the standard error of estimate of mb is 0.35, marginally better than for equation (3).

Discussion

Equation (3) was based on 31 observations and M_L in the range 4.1–7.0. Equation (4) was derived from observations only in the range M_L 4.1–6.5 and is based on 29 observations. The standard error of estimate of m_b for

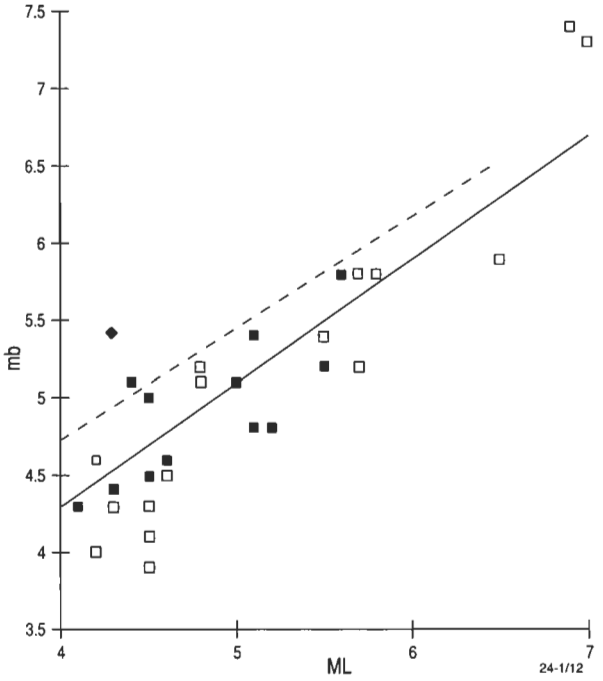

Figure 1. Body wave magnitude m_b as a function of local magnitude M_L for 31 Australian earthquakes. Solid squares represent earthquakes for which there were at least two measurements of each of M_L and m_b; open squares are those for which there was only one measurement of M_L and/or m_b. The diamond represents the 1982 West Wyalong earthquake. The unbroken line is the least squares regression line (equation (3)). The dashed line is represented by equation (2).

(4) is 0.35, marginally lower than the 0.37 for equation (3). The fit of (3) and (4) can be compared visually in Figure 2.

The linear relationships represented by equations (2), (3) and (4) may be compared directly by expressing them all in the same form;

$$m_b = 1.8 + 0.73M_L,\ M_L\ 1.1 - 5.9 \quad (2)$$

$$m_b = 1.1 + 0.80M_L,\ M_L\ 4.1 - 7.0 \quad (5)$$

$$m_b = 1.8 + 0.66M_L,\ M_L\ 4.1 - 6.5 \quad (6)$$

Although all three slopes differ by less than one standard error in equations (3) and (4), Figures 1 and 2 show that equation (2) would overestimate m_b for most of the Australian earthquakes in this study. Equations (4) and (6), (3) and (5) and (2) all appear to underestimate m_b for the magnitude M_L 6.9 Meckering and M_L 7.0 Meeberrie earthquakes. This is probably because the relationship between M_L and m_b is non-linear. Also, it is not possible to obtain a reliable M_L for these events, as the seismic waves saturated all seismographs at distances for which M_L is defined except for the Perth Milne-Shaw seismogram of the Meeberrie earthquake.

Equations (4) and (6) fit the magnitude M_L 6.5 Cadoux earthquake better than (3) and (5). For this reason and its lower standard error for m_b, and because the data on which it is based are more reliable, we recommend using (4) to estimate m_b from M_L for earthquakes with M_L 4.1–6.5.

Data from two small earthquakes in 1994 (Table 2) were omitted entirely from the analysis because of the anomalously high values of m_b from seismograms at distances

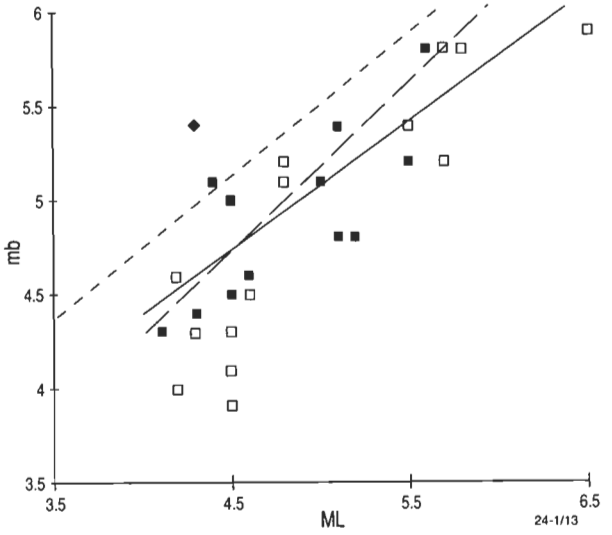

Figure 2. Body wave magnitude m_b as a function of local magnitude M_L for the same data set as in Figure 1, excluding the 1968 Meckering and 1941 Meeberrie earthquakes. The unbroken line is the least squares regression line (equation (4)). The long-dash line is represented by equation (3), and the short-dash line by equation (2).

of 5.4–5.6°. Measurements were of the maximum amplitude (half peak-to-peak) and corresponding period of the first 20–30 s of the P wave train, as recommended by Willmore (1979). The results are consistent with the anomalously high m_b for the West Wyalong earthquake in Table 1 and Figures 1 and 2. When m_b is derived from stations at distances of less than 12°, it is higher than when derived from greater distances, not only for the West Wyalong earthquake, but also for the two others in Table 2 (for which station listings of m_b were published in Denham et al. 1982 and Greenhalgh & Denham 1986). Although these data are few, they indicate that the attenuation of P waves in southeastern Australia at distances of less than 12° may indeed be different from that in the chart of Gutenberg & Richter (1956), as suggested by Denham et al. (1985). The similar result from the small Tennant Creek earthquake in Table 2 may be indicative of different attenuation in other parts of Australia as well, but more measurements are necessary before such a conclusion can be drawn. However, Everingham (1968) remarked that limited evidence from several events suggested that, for shallow Western Australian earthquakes, Gutenberg & Richter's (1956) attenuation was too large. Our observations support his contention. Also, Mizoue (1968) used five reference stations (COL Alaska, TFO Arizona, CAR Venezuela, PMG Papua New Guinea and RAB New Britain) to

Table 2. Body wave magnitudes measured at distances of less than and greater than 12 degrees.

Locality	*Date*	*ML*	*mb (distance < 12°)*	*mb (distance > 12°)*
S. Cobar, NSW	09-07-1994	3.75 (TOO)	4.9 (TOO)	
		3.5 (BFD)	5.0 (BFD)	
Tennant Creek, NT	08-02-1994	3.6 (QIS)	4.8 (QIS)	
Appin, NSW	15-11-1981	4.1	4.4	4.1
W. Wyalong NSW	26-11-1982	4.3	5.6	4.3
Beltana, SA	29-12-1983	4.4	5.6	4.9

TOO, BFD, QIS: magnitudes measured on individual seismographs

investigate the variation with distance of USCGS body-wave magnitudes for shallow earthquakes at epicentral distances of less than 30° in 1965–67. He found that for all stations except TFO the magnitude was up to 1.75 units higher in the distance range 5–13° than that measured at distances of 20–30°. Our findings are similar to his.

Conclusions

The following relations have been derived for earthquakes in Australia:

$$m_b = 0.80(M_L - 4.85) + 5.0, \quad M_L = 4.1 - 7.0 \qquad (3)$$

$$m_b = 0.66(M_L - 4.79) + 4.9, \quad M_L = 4.1 - 6.5 \qquad (4)$$

As the relationship may not be linear for very large magnitudes and equation (3) is derived from less reliable data, we recommend using equation (4) to estimate m_b from M_L in the range 4.1–6.5.

It appears that m_b measurements made on Australian earthquakes at distances of less than 12° may be too high because of the attenuation of P waves differing from that in the chart of Gutenberg & Richter (1956).

Acknowledgments

We thank Kevin McCue, David Denham, Brian Gaull, Stewart Greenhalgh, David Jepsen, Warwick Smith and Spiro Spiliopoulos for critically reading the manuscript and suggesting improvements. We are grateful to Phil McFadden for advice on the statistics. Ed Paull collaborated in redetermining M_L for the 1979 Cadoux earthquake from his original measurements using the Gaull & Gregson (1991) attenuation function—we thank him for his help.

References

Chhabra, M.P., Ghouhan, R.K.S., Srirastava, H.N. & Chandhury, H.M., 1975. The relationship between the body wave and the local magnitudes for Himalayan earthquakes. *Annali di geofisica*, 28, 381–391.

Denham, D., 1982. A review of magnitude scales and some problems in the Australian region. *In* Denham, D. (compiler) Proceedings of the Workshop on Australian Earthquake Magnitude Scales. *Bureau of Mineral Resources, Australia, Record* 1982/29, 1–9.

Denham, D., Bock, G. & Smith, R.S., 1982. The Appin (New South Wales) earthquake of 15 November 1981. *BMR Journal of Australian Geology & Geophysics*, 7(3), 219–223.

Denham, D., Jones, T. & Weekes, J., 1985. The 1982 Wyalong earthquakes (NSW) and recent crustal deformation. *BMR Journal of Australian Geology & Geophysics*, 9, 255–260.

Everingham, I.B., 1968. Seismicity of Western Australia. *Bureau of Mineral Resources, Australia, Report* 132, 44 pp.

Gaull, B.A. & Gregson, P.J., 1991. A new local magnitude scale for Western Australian earthquakes. *Australian Journal of Earth Sciences*, 38, 251–260.

Gibowicz, S.J., 1972. The relationship between teleseismic body-wave magnitude *m* and local magnitude M_L from New Zealand earthquakes. *Bulletin of the Seismological Society of America*, 62, 1–11.

Greenhalgh, S.A. & Denham, D., 1986. The Beltana South Australian earthquake of 29 December 1983 and aftershocks. *Australian Journal of Earth Sciences*, 33, 401–411.

Greenhalgh, S.A. & Parham, R.T., 1986. The Richter earthquake magnitude scale in South Australia. *Australian Journal of Earth Sciences*, 33, 519–528.

Greenhalgh, S.A. & Singh, R., 1986. A revised magnitude scale for South Australian earthquakes. *Bulletin of the Seismological Society of America*, 76, 757–769.

Gutenberg, B., 1945. Amplitudes of P, PP, and S and magnitude of shallow earthquakes. *Bulletin of the Seismological Society of America*, 35, 57–69.

Gutenberg, B. & Richter, C.F. 1956. Magnitude and energy of earthquakes. *Annali di geofisica* 9, 1–15.

Kiratzi, A.A. & Papazachos, B.C., 1984. Magnitude scales for earthquakes in Greece. *Bulletin of the Seismological Society of America*, 74(3), 969–985.

McGregor, P.M. & Ripper, I.D., 1976. Notes on earthquake magnitude scales. *Bureau of Mineral Resources, Australia, Record* 1976/56, 22 pp.

Michael-Leiba, M. & Malafant, K., 1992. A new local magnitude scale for southeastern Australia. *BMR Journal of Australian Geology & Geophysics*, 13, 201–205.

Mizoue, M., 1968. Earthquake magnitude determination in relation to regional variations of P wave amplitudes. Part 1. *Bulletin of the Earthquake Research Institute*, 46, 457–484.

Richter, C.F., 1935. An instrumental earthquake magnitude scale. *Bulletin of the Seismological Society of America*, 25(1), 1–32.

White, R.E., 1968. A local magnitude scale for South Australian earthquakes. *Bulletin of the Seismological Society of America*, 58, 1041–1057.

Willmore, P.L. (editor), 1979. Manual of Seismological Observatory Practice. *World Data Centre A for Solid Earth Geophysics, Report* SE-20.

AGSO Journal of Australian Geology & Geophysics, 15(4), 413–420

Devonian–Carboniferous stratigraphy of Quail 1, Carnarvon Basin, Western Australia: regional implications for geohistory and hydrocarbon prospectivity

Robert S. Nicoll[1] & John D. Gorter[2]

The recovery of conodonts from cores in the onshore Carnarvon Basin petroleum exploration well Quail 1 has lead to a revision of the subsurface Devonian–Carboniferous stratigraphic interpretation in the basin. The Moogooree Limestone is absent in the well; instead, a major unconformity, representing a hiatus of at least 12 million years—the entire Tournaisian Series—separates the Frasnian Gneudna Formation and the Visean Yindagindy Formation. A significant part of the Late Devonian Famennian Stage may also be missing. This suggests that the Wandagee–Yanrey Ridge may be as old as Late Devonian. The Quail Formation is here recognised as a lateral equivalent of the outcropping Harris Sandstone, as originally defined. The Austin Formation is recognised as the base of the Lyons Group. Evaluation of conodont thermal maturation data indicates a former high heat flow in the southern and central parts of the basin, and suggests that some of the Early to Middle Palaeozoic section is overmature for hydrocarbons. The high heat flow may have been related to Jurassic volcanism, represented by the alkali picrites of the Wandagee Province.

Introduction

The onshore Carnarvon Basin of Western Australia (Fig. 1) is predominantly a Palaeozoic basin with Late Cambrian to Permian sediments (Hocking et al. 1987; Gorter et al. 1994). A thin Mesozoic cover expands offshore to form the economically dominant part of this hydrocarbon-rich basin (Hocking 1988). Early studies based on outcrop investigations (Condon 1965, 1967, 1968) and more recent investigations integrating outcrop and subsurface data (Hocking et al. 1987) have suggested that Late Devonian through Permian sedimentation was essentially continuous, except for short breaks in the Carboniferous (Early Tournaisian and Namurian) and Permian (Early Artinskian). New palaeontological studies now demonstrate that in part of the basin, on and near the Wandagee–Yanrey Ridge, the Tournaisian break may be more pronounced and probably extends down into the Late Devonian (Famennian).

Previous interpretations of the Devonian–Carboniferous stratigraphy (Fig. 2) in the onshore Carnarvon Basin petroleum exploration well Quail 1 (Pearson 1964; Hocking et al. 1987; Bentley 1988) suggested a major unconformity between the Munabia Sandstone and the Moogooree Limestone, and also between the Quail Formation and the Harris Sandstone/Lyons Group. Bentley (1988) also suggested that the Quail Formation rests unconformably on the Moogooree Formation in part of the basin.

New conodont information from Quail 1 indicates that the Gneudna Formation and a thin (31 m) sandstone unit, probably the Munabia Sandstone, are overlain by the Yindagindy Formation, rather than the Moogooree Limestone, which rests unconformably on the sandstone. Thus, in this well, the Quail Formation demonstrably rests on the Yindagindy Formation. Miospores recovered in the interval 2146–2562 m in Kybra 1 (Purcell & Ingram 1988) suggest a similar stratigraphic relationship with the Quail Formation overlying Yindagindy Formation. However, in outcrop, the Yindagindy Formation is overlain by the Harris Sandstone (Condon 1965). This study thus raises the possibility that the Quail Formation is laterally equivalent to the Harris Sandstone *sensu* Condon (1965, 1967), as both units rest conformably on the Yindagindy Formation. Recognition of the magnitude of the Early Carboniferous unconformity and the changed stratigraphic relationships have a significant effect on the interpretation of Carnarvon Basin geohistory.

1 Australian Geological Survey Organisation, GPO Box 378, Canberra, ACT 2601

2 Hardy Petroleum Ltd, PO Box 1265, West Perth, WA 6872

Conodont faunas, miospores and age determination

Conodont faunas were recovered from two of three cores in Quail 1, examined for conodonts and other phosphatic fossils (Table 1). Five conodont elements were recovered from core 14 (2637.2–2638.41 m) and twenty-eight from core 15 (2793.6–2796.34 m). Core 13 (2468.9–2470.73 m) contained no conodonts or other age diagnostic fauna. Miospore data are available for cores 12, 15 and 16 (Powis 1985).

Core 14 (Fig. 3) contains a very limited fauna with elements of *Cavusgnathus unicornis* and *Hindeodus cristulus*. In North America (Collinson et al. 1971), both species appear in the upper part of the St Louis Limestone (Visean V3b) and range upward to the top of the Chester Series (Namurian A–E2). In England (Higgins & Varker 1982), *C. unicornis* is found in the Holkerian *Cavusgnathus* Zone, where it is equated with the V2b–V3a. The maximum age range of core 14 could be V2b–E2. However, core 12 (2231.4–2232 m) is dated as Visean V3a–V3c (see below) and this would most probably limit the age of core 14 to the interval Visean V2b–V3b (Fig. 3).

Core 15 (Fig. 4) contains elements of *Icriodus subterminus* and *Polygnathus xylus xylus*. These species, along with *Ozarkodina brevis* and *Ancyrodella* sp., are found in the lower part of the Gneudna Formation in outcrop (Seddon 1969; Nicoll unpublished AGSO collections). *P. xylus xylus* and *O. brevis* range in age from the *Polygnathus varcus* to Early *Palmatolepis hassi* Zone, and *I. subterminus* from the *Klapperina disparilis* Zone to the *Palmatolepis jamieae* Zone. *Ancyrodella* is confined to the Frasnian (Ziegler & Sandberg 1990). These species indicate an age range of the Gneudna Formation from the Late Givetian (*Klapperina disparilis* Zone to the Frasnian, at least as young as the *Palmatolepis hassi* Zone. The restriction of *P. xylus xylus* to only the lower half of the type section of the Gneudna Formation (Seddon 1969) indicates that the unit probably extends through much of the Frasnian. *I subterminus* and *P. xylus xylus* in core 15 indicate that this sample was probably from

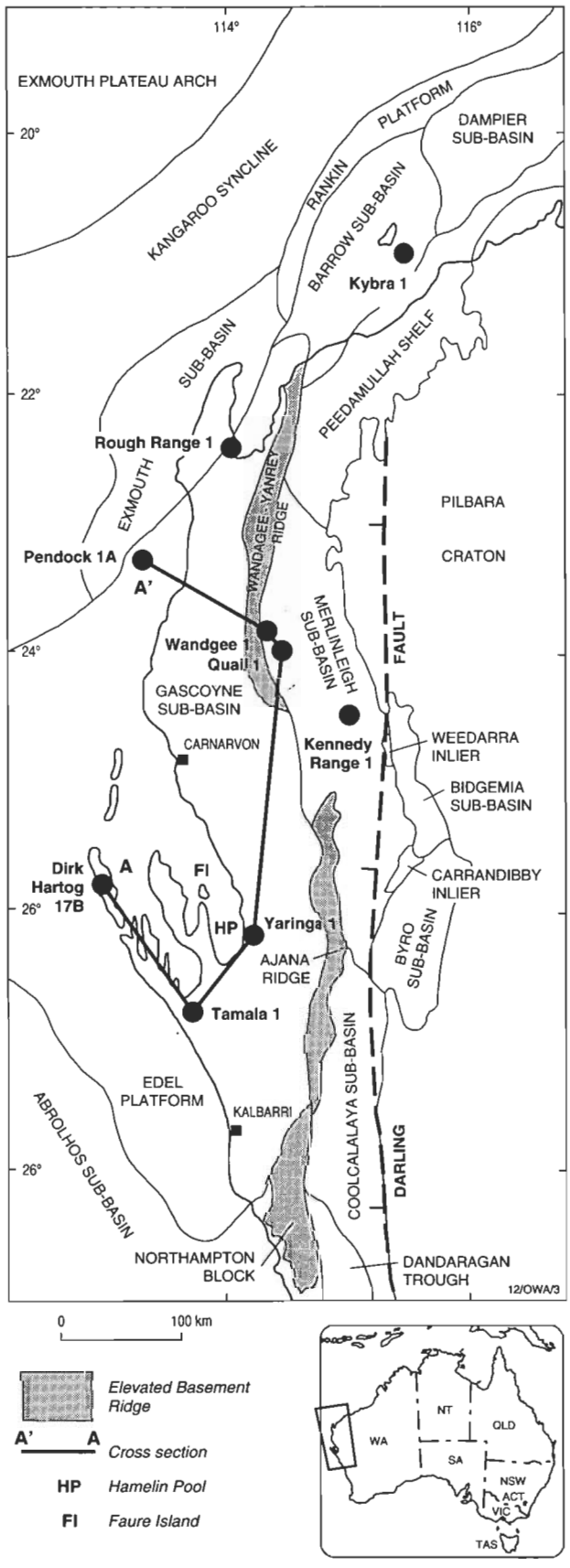

Figure 1. Locality map, showing the Carnarvon Basin and principal structural sub-divisions, position of wells referred to in text and the location of the Wandagee Province (after Hocking et al. 1987). The line of section of wells illustrated in Figure 6 is indicated.

the upper part of the lower half of the Gneudna Formation.

Palynological examination of cores 11 to 16 by Powis (1985) resulted in dateable material from only cores 12, 15 and 16. The sample from core 12 (2231.4–2232.0 m) had a low-yield microflora containing *Grandispora maculosa*, which dates it as belonging to the *G. maculosa* Assemblage and indicates an age range of Visean V3b–V3c (P.J. Jones, AGSO, personal communication, 1994). Cores 15 and 16 yielded acritarchs of Devonian or probable Devonian age (Powis 1985), supporting the age indicated by the conodonts in core 15.

Stratigraphic revision and correlation

Analysis of the conodonts (cores 14 and 15) and microflora (core 12) allows a reinterpretation of the regional stratigraphy of the interval 2100–3121 m in Quail 1 (Fig. 2). The type section of the Quail Formation (2100–2453 m) is here equated with the Harris Sandstone (see following discussion), a unit defined in outcrop (Condon 1967) 50 km east of Quail 1. In the well, this unit is dated by Powis (1985) and Helby (personal communication in Roberts 1985) as belonging to the *Grandispora maculosa* Assemblage.

The carbonate interval 2453–2710 m, previously identified as Moogooree Limestone (Hocking et al. 1987; Bentley 1988), is now recognised as Yindagindy Formation. The conodont fauna of the outcropping Yindagindy Formation (unpublished AGSO data) contains a limited fauna of *Clydagnathus cavusformis*, *Hindeodus cristulus* and *Patrognathus* sp. Based principally on the range of *H. cristulus*, the age of this fauna is from the early Visean (V1a or V1b) to Late Namurian (E2). *Cavusgnathus unicornis* and *H. cristulus* in core 14 somewhat restrict the age range, but confirm the correlation of the outcrop and subsurface sections. In the Carnarvon Basin, *H. cristulus* is confined to the Yindagindy Formation and does not occur in the underlying Moogooree Limestone. The *G. maculosa* flora in the overlying Quail Sandstone constrains the age of the Yindagindy Formation to Visean V2b–V3a.

The thin sandstone at 2710–2741 m has not been dated and could be assigned to any of a number of Devonian or Carboniferous units. It most probably represents the Munabia Sandstone, which overlies the Gneudna Formation. It could also belong to the Williambury Formation, which underlies the Yindagindy Formation, but Hocking et al. (1987) interpreted this unit as an alluvial fan and it probably has only limited areal distribution.

The interval 2741–3082 m is occupied by the Gneudna Formation, and can be correlated to the outcrop by the conodonts recovered from core 15. These place core 15 in the upper-middle part of the Gneudna Formation (Fig. 4). The Nannyarra Sandstone is probably restricted to 3082–3121 m. The stratigraphy of the interval 3121 to 3580 m (T.D.) is discussed by Gorter et al. (1994).

In Kybra 1 well, the interval 2146.5–2170 m, identified as the Quail Formation (Bentley 1988), is correlated with the Harris Sandstone. Purcell & Ingram (1988) found no miospores from this interval, but recovered miospores of the *Grandispora maculosa* Assemblage from a sample at 2170 m and miospores of the *Anapiculatisporites largus* Assemblage from 2192–2562 m. These assemblages indicate that the interval 2170–2562 m. is Visean in age

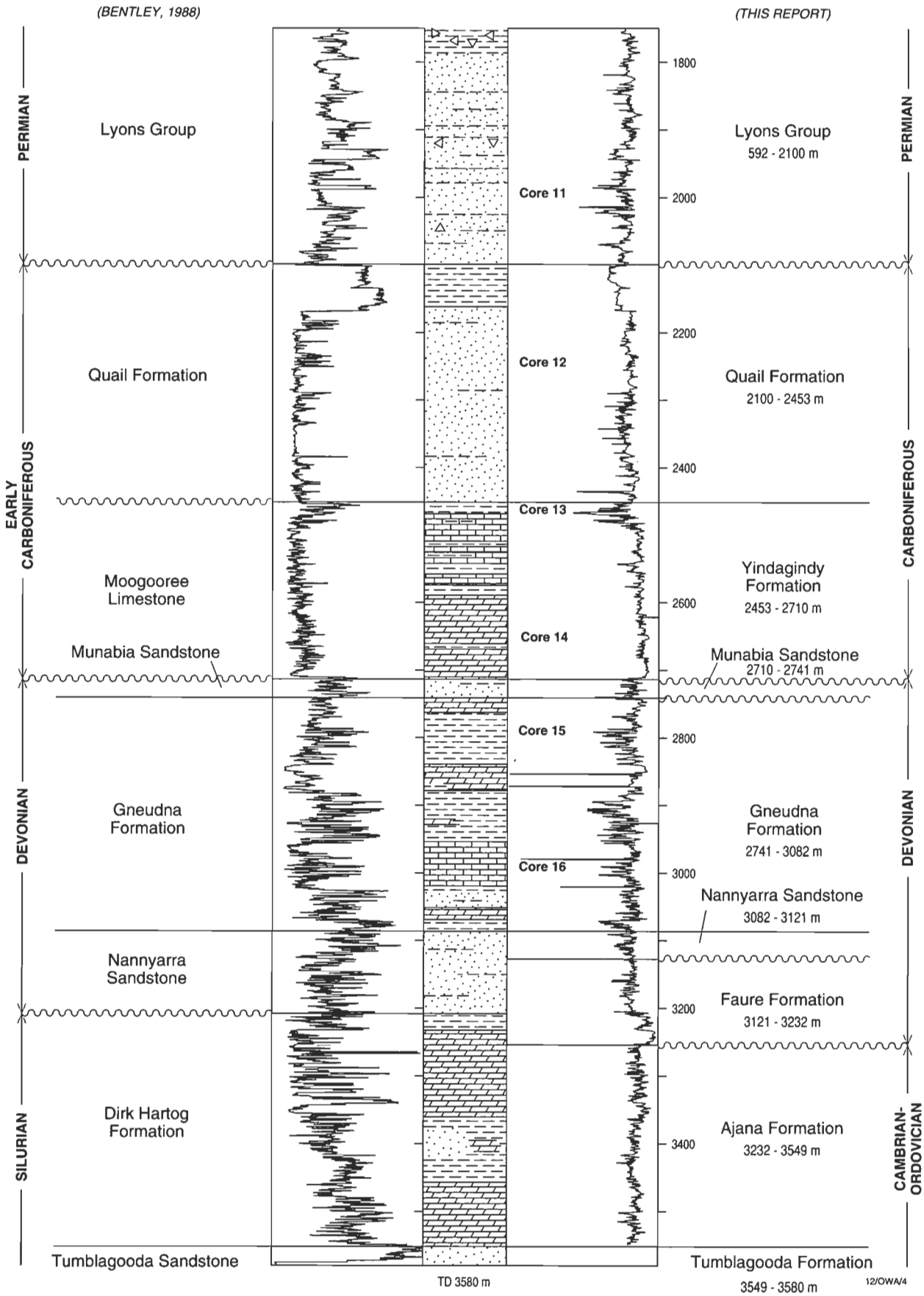

Figure 2. Part of the Quail 1 well log, showing the interpretation of Bentley (1988) and modifications suggested in this report. Lower part of the interpretation based on Gorter et al. (1994).

and thus represents the Yindagindy Formation rather than the Moogooree Formation, which is Tournasian. This well, therefore, indicates that the top of the Yindagindy Formation (2170 m) is as young as the *G. maculosa* Assemblage, an age also reported by Powis (1985) in Quail 1, core 12 (2231.4–2232.0 m), from the Quail Formation.

Table 1. Palaeontological determinations for samples from Quail 1, Kybra 1 and Wandagee (WAPET) corehole 1. Palynological determinations from Quail 1 after Powis (1985). Miospore determinations from Kybra 1 after Purcell & Ingram (1988).

Quail 1

Core 12: 7319–7321 ft (2231–2232 m)

Conodont sample: not sampled.

Palynology sample: 7319–7321 ft; *G. maculosa*

Core 13: 8098–8104 ft (2468.90–2470.73 m)

Conodont sample: 8098–8104 ft; 0 elements

Other fauna: ? phosphatic shell fragments

Palynology sample: 8102–8104 ft; essentially barren

Core 14: 8650–8654 ft (2637.20–2638.41 m)

Conodont sample: 8650–8654 ft; 5 elements; **CAI 4**

Cavusgnathus unicornis (1)

Hindeodus cristulus (2)

S element fragments (2)

Other fauna: pyritised scolecodonts

Palynology sample: 8652–8654; essentially barren

Core 15: 9163–9172 ft (2793.60–2796.34 m)

Conodont sample: 9163–9172 ft; 27 elements; **CAI 4**

Icriodus subterminus (4)

Polygnathus xylus xylus (11)

Other fauna: pyritised bivalves and ostracods, fish scales

Palynology sample: 9169–9172 ft; acritarchs (Devonian)

Core 16: 9741–9751 ft

Conodont sample: not sampled

Palynology sample: acritarchs (?Devonian)

Kybra 1 (from Purcell & Ingram, 1988; based on cuttings samples)

2170 m

Palynology: *Grandispora maculosa* Assemblage

2192–2542 m

Palynology: *Anapiculatisporites largus* Assemblage

WAPET Wandagee core hole

1600–1615 ft (182.9–187.5 m)

Other fauna: ostracods, bivalves & brachiopods, fish

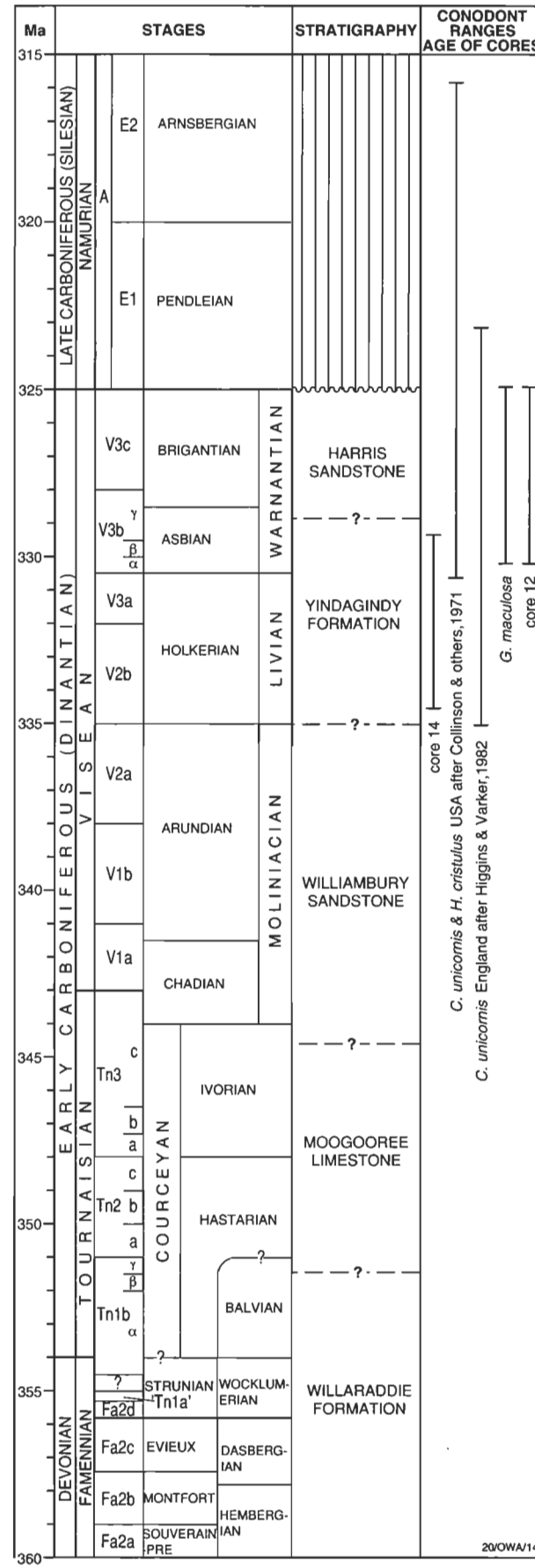

Figure 3. Comparative age ranges of conodonts from core 14 of Quail 1, outcrop sections, North America (after Collinson et al. 1971) and England (after Higgins & Varker 1982). The estimated age ranges of Carboniferous stratigraphic units in the Carnarvon Basin are also shown.

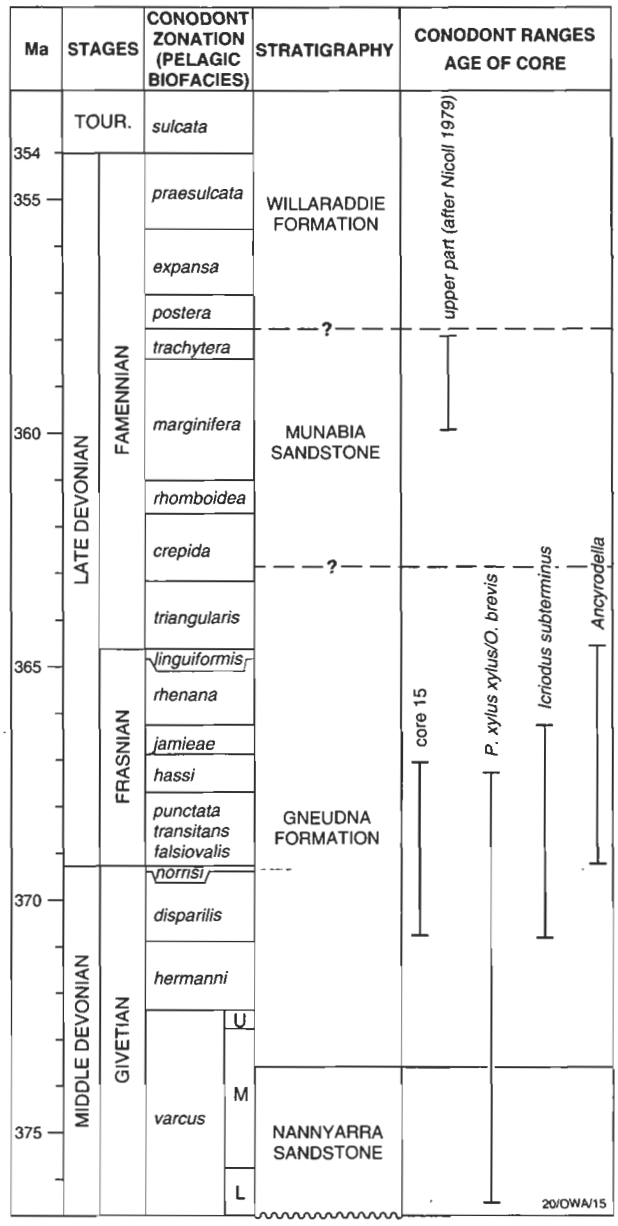

Figure 4. Comparative ranges of conodonts from core 15 of Quail 1 and outcrop sections, and the age of the Gneudna Formation and Munabia Sandstone (after Nicoll 1979). The estimated age ranges of Devonian units in the Carnarvon Basin are also shown.

Structural history

This revised stratigraphy of Quail 1 and Kybra 1 wells has regional structural and geohistory implications (Fig. 5). In Quail 1, the apparent absence of the Moogooree Limestone and the Willaraddie and Williambury Formations, along with the greater part of the Munabia Sandstone, indicates an extended period of uplift and erosion in the Late Devonian and Early Carboniferous in an area corresponding with the Wandagee–Yanrey Ridge. Condon (1968) indicated that the Wandagee–Yanrey Ridge was a positive feature as early as the Devonian, but Hocking et al. (1987) have suggested that it did not start forming until the Triassic, when it developed in association with structuring that was part of the breakup margin rift tectonics. The new age control in Quail 1 well, conodont thermal maturation data (see below), and previous data interpreted along the ridge by Hocking et al. (1987) now suggest that the ridge was a positive feature throughout the Middle to Late Palaeozoic and that it was only occasionally covered by moderately deep sea water.

Harris Sandstone–Quail Formation relationship

Correlation of the subsurface Quail Formation with outcrop of the Harris Sandstone relies on demonstrating lateral continuity or age equivalence of the units. The age of the Harris Sandstone is critical to the correlation, because the existing seismic sections do not allow definitive tracing of the Quail Formation to the outcrop. Unfortunately, the only fossils reported from the Harris Sandstone (*sensu* Condon 1967) are plants. White (1957,

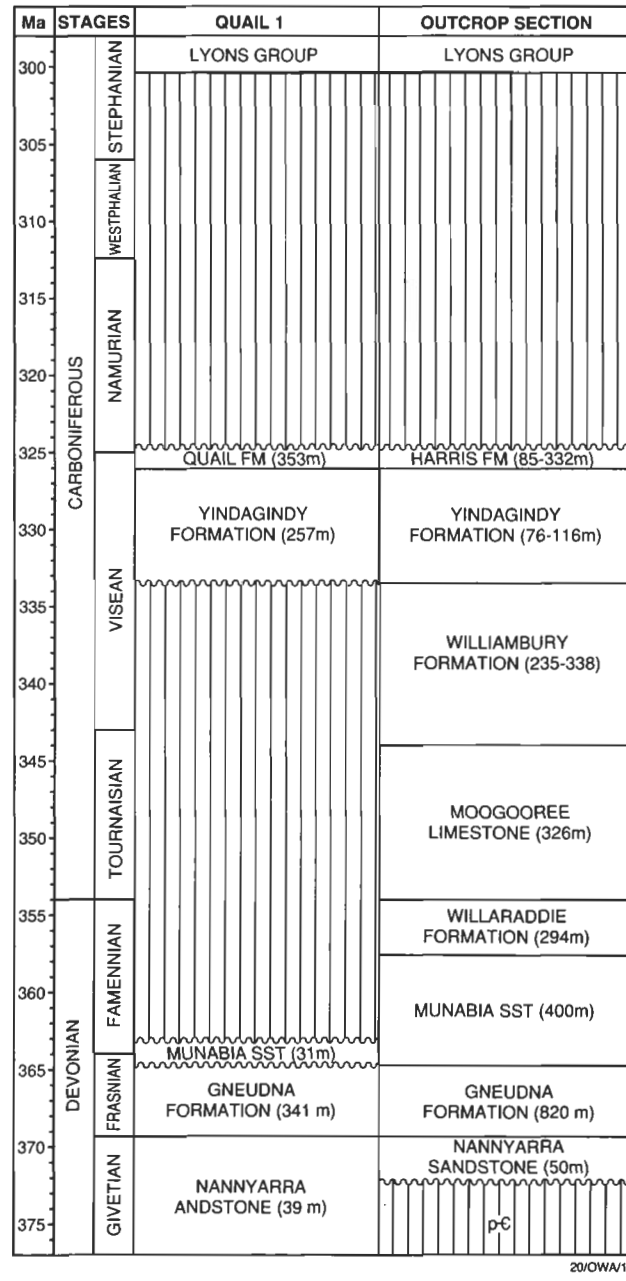

Figure 5. Age relationships of Devonian and Carboniferous stratigraphic units in the outcrop on the eastern margin of the Carnarvon Basin and from Quail 1. Modified from Hocking et al. (1987) and Bentley (1988).

1959) identified specimens from near the base of the Harris Sandstone as *Lycopodiopsis pedroanus* and ascribed them a Lower Permian age. White & Condon (1959) applied the name *Lepidodendron* to other specimens from additional localities and regarded their age as Devonian–Permian. Condon (1967), emphasising the Permian age determinations by White (1957, 1959), associated the Harris Sandstone with the Lyons Group. However, John Rigby (Queensland University of Technology, personal communication, 1994) has indicated that the genus *Lepidodendron* has not been confirmed from the southern hemisphere and that none of the fossils from the Harris Sandstone are well enough preserved to be identified to generic level. He further noted that lepidodendroid plants are thought to be confined to subtropical or tropical environments and are unlikely to have been able to have grown in the proximity of glacial climatic conditions. If correct, this environmental control indicates it is unlikely the Harris Sandstone is associated with glacial conditions of the Late Carboniferous or Early Permian. No definitive age can be assigned to the Harris Sandstone, except that it is younger than the Visean Yindagindy Formation and older than the Austin Formation of the Lyons Group, which is of Asselian to Sakmarian age (Dickins & Thomas 1959; Archbold 1993).

Stratigraphic and lithological relationships tend to indicate correlation of the Quail Formation and the Harris Sandstone, and in a detailed study of the Yindagindy Formation–Harris Sandstone relationship, Read et al. (1973) concluded the two units were disconformable, but the discordance between the two amounted to only a few of metres. In contrast, the relationship of the Austin Formation, the basal unit of the Lyons Group (Condon, 1967), was described as an angular unconformity (Read et al., 1973). Condon (1965) made similar observations on the Yindagindy–Harris relationship, but later placed the major regional unconformity between the Yindagindy Formation and the Harris Sandstone (Condon, 1967).

Condon (1967) and Read et al. (1973) differentiated the Harris Sandstone from the overlying Austin Formation lithologically, but Condon (1967) suggested that the Harris Sandstone was laterally gradational with the Austin Formation. However, exposures of these units are poor and contacts difficult to interpret. Hocking et al. (1987) did observe striated surfaces and cobbles or boulders that may be of glacial origin in the lower part of the Harris Sandstone (*sensu* Condon, 1967) and, on the basis of this, included the Austin Formation within the broader concept of the Harris Sandstone (Hocking 1985; Hocking et al. 1987).

We conclude that the Asselian–Sakmarian Austin Formation, as defined by Condon (1967), and not the Harris Sandstone, is the lowest unit of the Lyons Group and represents the onset of extensive marine glacial sedimentation in the Carnarvon Basin. This means that the Harris Sandstone, as originally defined by Condon (1965, 1967) and interpreted by Read et al. (1973), is probably no younger than Visean or Namurian, and that the ages of the Harris Sandstone and Quail Formation, of the subsurface, probably overlap. For this reason we have equated the units, but cannot recommend abandoning the term Quail Formation until physical continuity or age equivalence is conclusively documented.

The depositional break between a Late Visean Harris Sandstone/Quail Formation and the Sakmarian Austin Formation indicates a time gap of approximately 25 million years (Peter J. Jones, AGSO, personal communication, 1994). The relationship is substantiated by the pronounced unconformity between the Lyons Group and a wide suite of older units.

Thermal maturation

Conodont faunas from Quail 1, cores 14 and 15 (Table 1), have a colour alteration index (CAI) of 4, which indicates exposure to a temperature of 190–300°C (Epstein et al. 1977), well into the overmature hydrocarbon zone. This contrasts with CAI values of 1 from all outcrop samples of the Gneudna Formation, Moogooree Limestone and Yindagindy Formation (unpublished AGSO data). However, it is on the same gradient (Fig. 6) as wells like Dirk Hartog 17B, Tamala 1, and Wandagee 1 (Gorter et al. 1994). Only the CAI 2 value at 2190 m in Pendock 1A suggests a more moderate thermal gradient.

The comparatively high CAI value of 4 obtained at 2600–2800 m in Quail 1 can be explained in two ways: either the regional thermal gradient in the central and southern part of the Carnarvon Basin was significantly higher than that of the northwestern part of the basin, or a considerable thickness of Permian or Mesozoic sediments has been stripped from this area. Nicoll & Foster (1994, fig. 6) summarised the range of conodont CAI ranges from the northwestern Australian margin, showing that a CAI value of 4 at a depth of 3000 m could be produced with the same geothermal gradient as recorded in the Broome Arch area of the Canning Basin. However, the same CAI value could also be the product of a much lower thermal gradient and burial to a depth of 5000 m, which is the composite thickness suggested by Hocking et al. (1987) for the Permian rocks in the vicinity of Kennedy Range 1. The evidence suggests there is no significantly thicker Permian section in the immediate vicinity of Quail 1 or over the nearby Wandagee–Yanrey Ridge. However, the Permian section is at least 1500 m thicker in the vicinity of Wandagee Hill, some 13 km NNW of Quail 1 (Hocking et al. 1987).

Alternatively, an elevated thermal gradient could be related to the Late Jurassic alkali-picrite intrusives of the Wandagee Province (Jaques et al. 1986) in the vicinity of Quail 1. Data from the Canning Basin (Nicoll 1981) indicate that individual small intrusives had a negligible thermal impact, except very close to them. However, Nicoll & Gorter (1984b) have associated a hot thermal trend on the Lennard Shelf close to the Miocene lamproites of the West Kimberley Province (Jaques et al. 1986). Thus, with depth, a measurable regional thermal imprint appears to be associated with such volcanic fields. The intrusive complex would thus have produced a limited area of high thermal impact centred on the zone of surface extrusion.

The conodonts and other phosphatic fossils recovered from Wandagee 1 (Gorter et al. 1994) and WAPET Wandagee No. 1 have CAI values (or equivalents; see Table 1) at gradient with the conodont elements in cores 14 and 15 in Quail 1. They indicate burial of the Devonian rocks on the Wandagee–Yanrey Ridge by no more than 1000 m of additional, post-Carboniferous, sediment. This substantiates the concept of the Wandagee–Yanrey Ridge as a positive structure before the initiation of Permian sedimentation in the basin. Had there been 2500 m of Permian overlying the Wandagee–Yanrey Ridge, the ex-

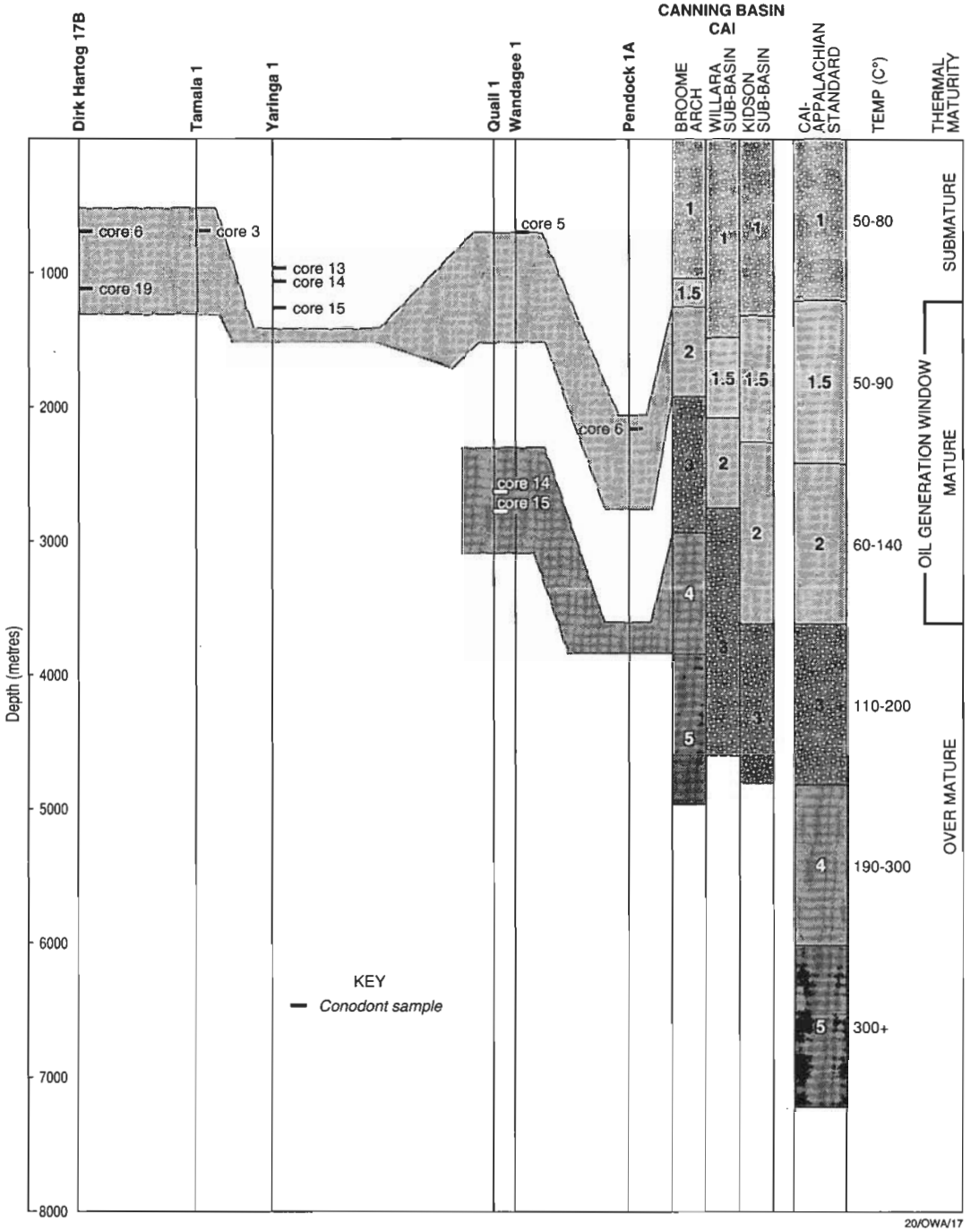

Figure 6. Comparison of CAI values in Dirk Hartog 17B, Tamala 1, Yaringa 1, Quail 1, Wandagee 1 and Pendock 1A compared with wells in the Canning and Bonaparte Basins. Modified from Nicoll & Gorter (1984a, 1984b) and Nicoll & Foster (1994). Line of section located on Figure 1.

pected conodont CAI values in the Wandagee wells would have been similar to the CAI 4 recorded in Quail 1.

While conodont colour alteration (CAI) and miospore thermal alteration (TAI) data (Powis 1985) indicate that both Early and Middle Palaeozoic rocks in the southern and central parts of the onshore Carnarvon Basin have been heated to a level where the Early Palaeozoic sediments are within the oil-generation window or are gas prone, away from the direct influence of Jurassic volcanism, the Devonian (Gneudna Formation) and Carboniferous sedimentary rocks (Moogooree Limestone and Yindagindy Formation) have source potential. This applies especially to units of marine black shales of Middle to Late Devonian age.

Acknowledgments

We thank Peter J. Jones (AGSO) and Roger Hocking (Geological Survey of Western Australia) for critically reading the manuscript and for subsequent discussions. John Rigby (Queensland Institute of Technology) discussed the significance of plant material from the Harris Sandstone.

References

Archbold, N.W., 1993. A zonation of the Permian brachiopod faunas of western Australia. *In* Findlay, R.H., Unrug, R., Banks, M.R. & Veevers, J.J. (editors), Gondwana Eight: assembly, evolution and dispersal. *Proceedings of the eighth Gondwana symposium, Hobart, Tasmania, Australia.* Balkema, Rotterdam. 313–321.

Bentley, J., 1988. The Candace Terrace—a geological perspective. *In* Purcell, P.G. & Purcell, R.R. (editors), *The North West Shelf, Australia.* Proceedings of Petroleum Exploration Society of Australia Symposium, Perth, 1988, 157–171.

Collinson, C., Rexroad, C.B. & Thompson, T.L., 1971. Conodont zonation of the North American Mississippian. *In* Sweet, W.C. & Bergström, S.M. (editors), Symposium on conodont biostratigraphy. *Geological Society of America, Memoir* 127, 353–394.

Condon, M.A., 1965. The geology of the Carnarvon Basin, Western Australia. Pre-Permian stratigraphy. *Bureau of Mineral Resources, Australia, Bulletin* 77, Part 1, 1–84

Condon, M.A., 1967. The geology of the Carnarvon Basin, Western Australia. Permian stratigraphy. *Bureau of Mineral Resources, Australia, Bulletin* 77, Part 2, 1–191.

Condon, M.A., 1968. The geology of the Carnarvon Basin, Western Australia. Post-Permian stratigraphy, structure, economic geology. *Bureau of Mineral Resources, Australia, Bulletin* 77, Part 3, 1–68.

Dickins, J.M. & Thomas, G.A., 1959. The marine fauna of the Lyons Group and the Carrandibby Formation of the Carnarvon Basin, Western Australia. *Bureau of Mineral Resources, Australia, Report* 38, 65–96.

Epstein, A.G., Epstein, J.B. & Harris, L.D., 1977. Conodont color alteration—an index to organic metamorphism. *United States Geological Survey, Professional Paper* 995, 1–27.

Gorter, J.D., Nicoll, R.S. & Foster, C.B., 1994. Lower Palaeozoic facies in the Carnarvon Basin, Western Australia: stratigraphy and hydrocarbon prospectivity. *In* Purcell, P.G. & Purcell, R.R. (editors), *The sedimentary basins of Western Australia.* Proceedings of Petroleum Exploration Society of Australia Symposium, Perth, 1994, 447–470.

Higgins, A.C. & Varker, W.J., 1982. Lower Carboniferous conodont faunas from Ravenstonedale, Cumbria. *Palaeontology*, 25, 145–166.

Hocking, R.M., 1985. Revised stratigraphic nomenclature in the Carnarvon Basin, W.A. *Geological Survey of Western Australia Record* 1985/6.

Hocking, R.M., 1988. Regional geology of the northern Carnarvon Basin. *In* Purcell, P.G. & Purcell, R.R., (editors), *The North West Shelf, Australia.* Proceedings of Petroleum Exploration Society of Australia Symposium, Perth, 1988, 97–114.

Hocking, R.M., Moors, H.T. & Van de Graaff, W.J.E., 1987. Geology of the Carnarvon Basin, Western Australia. *Geological Survey of Western Australia, Bulletin* 133, 1–289.

Jaques, A.L., Lewis, J.D., & Smith, C.B., 1986. The kimberlites and lamproites of Western Australia. *Geological Survey of Western Australia, Bulletin* 132, 268 pp.

Nicoll, R.S., 1979. A Late Devonian age for the Munabia Sandstone, Carnarvon Basin, W.A. Bureau of Mineral Resources, Australia, (Unpublished Professional Opinion 1979/034).

Nicoll, R.S., 1981. Conodont colour alteration adjacent to a volcanic plug, Canning Basin, Western Australia. *BMR Journal of Australian Geology & Geophysics*, 6, 265–267.

Nicoll, R.S. & Gorter, J.D., 1984a. Conodont colour alteration, thermal maturation and the geothermal history of the Canning Basin, Western Australia. *The APEA Journal*, 24 (I), 243–258.

Nicoll, R.S. & Gorter, J.D., 1984b. Interpretation of additional conodont colour alteration data and the thermal maturation and geothermal history of the Canning Basin, Western Australia. *In* Purcell, P.G. (editor), *The Canning Basin, W.A.* Proceedings of Geological Society of Australia / Petroleum Exploration Society of Australia Symposium, Perth. 412–425.

Pearson, G.R., 1964. Quail No. 1 Well Completion Report. West Australian Petroleum Pty Limited. May, 1964. (unpublished)

Powis, G.D., 1985. Palynological report on four wells from the Merlinleigh Sub-basin, Western Australia. Report for ESSO Australia (unpublished)

Purcell, R. & Ingram, B., 1988. Kybra 1, Palynology Report WP01/88. Bond Corporation Pty. Ltd. Petroleum Division. (unpublished)

Read, J.F., Alcock, P.J. & Hoseman, P., 1973. Harris Sandstone – Yindagindy Formation relationships and possible position of Permo-Carboniferous boundary, Carnarvon Basin, Western Australia. *Journal of the Royal Society of Western Australia*, 56, 80–85.

Roberts, J., 1985. Carboniferous sea level changes derived from depositional patterns in Australia. *In* Wagner, R.H., Prins, C.F.W., & Granados, L.F. (editors), *The Carboniferous of the World, II—Australia, Indian Subcontinent, South Africa, South America & North Africa.* IUGS Publication 20, 43–64.

Seddon, G., 1969. Conodont and fish remains from the Gneudna Formation, Carnarvon Basin, Western Australia. *Journal of The Royal Society of Western Australia*, 52, 21–30.

White, M.E., 1957. Lepidodendroid plant remains from near Arthur River woolshed, Carnarvon Basin, W.A. *Bureau of Mineral Resources, Australia, Record* 1957/30, 1–2.

White, M.E., 1959. Botanical report on a Lepidodendroid log from the Harris Sandstone, Carnarvon Basin, Western Australia. *Bureau of Mineral Resources, Australia, Report* 38, 53–54.

White, M.E. & Condon, M.A., 1959. A species of Lepidodendron from the basal Lyons Group Carnarvon Basin, Western Australia. *Bureau of Mineral Resources, Australia, Report* 38, 55–64.

Ziegler, W. & Sandberg, C.A., 1990. The Late Devonian standard conodont zonation. *Courier Forschungsinstitut Senckenberg*, 121, 1–115.

AGSO Journal of Australian Geology & Geophysics, 15(4), 421–444

Cainozoic sedimentary basins in the eastern Arunta Block, Alice Springs region, central Australia

B.R.Senior[1], E.M.Truswell[2], M.Idnurm[2], R.D.Shaw[2] & R.G.Warren[2]

Tertiary sedimentary rocks, in places over 200 m thick, occupy a series of elongate basins within and partly surrounding the Arunta crystalline basement in the Alice Springs region, central Australia. The best-known sedimentary succession is that of the Hale Basin, where four distinctive members constitute the poorly indurated Early Tertiary Hale Formation. The oldest, the Ambalindum Sandstone Member, rests on deeply weathered basement. It is overlain by the Delaney Mudstone Member, olive-green mudstone and siltstone, deposited probably under quiet-water reducing conditions in a series of large lakes. At this time there was low input of terrigenous detritus from the nearby MacDonnell, Strangways and Harts Ranges. In places, these fine-grained sediments grade upwards and laterally into a lignite and oil shale unit, the Ulgnamba Lignite Member, probably reflecting local development of shoals and peripheral swamps. A mid to Late Eocene age is likely for this member. The Ulgnamba Lignite Member or, where it is absent, the Delaney Mudstone Member, passes abruptly upwards into the poorly sorted, coarse-grained Tug Sandstone Member. This unit is likely to have been deposited rapidly on piedmont slopes flanking the margins of the uplands. The abrupt change in sedimentary characteristics suggests either uplift in the nearby ranges or a change in climate, or both. In the Hale Basin and other Cainozoic basins, the uppermost part of the Cainozoic succession, the Waite Formation, generally consists of green and red, silty sandstone, containing ferruginous pisoliths and a few massive chalcedonic calcrete beds. Erosion, possibly in the Oligocene, partly removed the older Cainozoic sediments as well as ferricrete formed at the basin margins, and incorporated some of the detritus in the Waite Formation. Other Tertiary basins overlying the eastern part of the Arunta Block show a broad lithostratigraphic similarity to the Hale Basin. Palynological studies of carbonaceous sedimentary rocks and lignite in the Hale, Bundey and Ayers Rock Basins, combined with palaeomagnetic and stratigraphic data, suggest that sedimentation in these basins took place in two main phases—the first, largely in the Paleogene, may have begun in the Late Cretaceous; the other, in the Neogene, began in the Late Miocene or Early Pliocene after one or more breaks in deposition, which are likely to have occurred in the Oligocene. Although there are large gaps in the sedimentary succession, there are sufficient data to broadly relate the depositional sequence to the pattern of uplift and sagging in the Alice Springs region and, in a general way, equate these movements with tectonism within the Australian Plate. Palaeomagnetic dating, in some cases supported by palynology, has identified two main periods of intense chemical weathering in these central Australian basins. The younger, near the top of the Hale Formation, has a Late Eocene magnetic age. The older is represented by relict weathered profiles developed in the Arunta basement, and may be earliest Tertiary or older. In addition to these two main weathering periods, various oxidised, mottled or silicified rocks in several basins indicate other, lesser periods of interrupted sedimentation and weathering.

Introduction

The distribution and stratigraphy of central Australian Tertiary basins in general have been discussed by Perry et al. (1962), Hays (1967), and Mabbutt (1967), but since then they have received little attention in the geological literature, owing, in part, to their poor outcrop and to strong weathering overprints. Early investigations of specific basins tended to focus on groundwater (e.g. Woolley 1965a, b, 1966; Morton 1965; O'Sullivan 1973a, b; Jacobson et al. 1989; McDonald et al. 1988a, b), but lignite has been investigated in the Hale Basin, vertebrate fossils at Alcoota in the Waite Basin (Woodburne 1967), and uranium in the Ti-Tree Basin (O'Sullivan 1973; Hughes & O'Sullivan 1973).

This study reviews current understanding of Cainozoic sedimentary basins in the eastern part of the Arunta Block, with particular focus on the Hale, Ti-Tree, Waite, Bundey, and Aremra Basins, where stratigraphic drilling was carried out from 1973 to 1986 by the then Bureau of Mineral Resources (BMR; now the Australian Geological Survey Organisation, AGSO). The results provide a framework for reconstruction of the probable Cainozoic depositional, weathering, climatic and tectonic history of central Australia. Although there are still large gaps in our knowledge, the data have wide implications in the context of the palaeogeographic and tectonic evolution of the Australian Plate.

Drilling and reconnaissance geological mapping have shown that the basin sequences have been profoundly altered by weathering, with its associated mineralogical and chemical changes. The sedimentary sequence also contains contemporaneous siliceous and calcareous beds, as well as redeposited or recycled sediments, including former weathered and/or chemically precipitated rock types.

Besides drilling, the main stratigraphic information comes from geological reconnaissance in several Tertiary basins. The Waite Basin (Alcoota 1:250 000 Sheet area) was investigated by Yeates (1971). Parts of the Sixteen Mile, the Burt and the Ti-Tree Basins were drilled in 1973. Both the Aremra Basin (Illogwa Creek 1:250 000 Sheet area) and southwestern part of the Ti-Tree Basin (Alcoota 1:250 000 Sheet area) were investigated by BMR in 1979. The Hale River Basin was also drilled by BMR in 1979. Results from drilling in the Hale Basin by the Northern Territory Geological Survey (NTGS; Clarke, 1975) and by industry in the early 1980s are also incorporated.

Much of this investigation was carried out by B.R. Senior (Senior, 1972; Shaw et al., 1982). A multidisciplinary study of the sedimentation, age and weathering history of Cainozoic epicratonic basins commenced in BMR in 1979. This study included preliminary palaeomagnetic dating of ferruginous weathered profiles and palynological studies of a carbonaceous and lignitic succession from the Hale Basin, as well as further geological studies elsewhere in the region. Palynological work was carried out on lignite and carbonaceous rock types in drill core supplied by the Northern Territory Geological Survey from the Hale Basin east of The Garden homestead, (Truswell & Marchant, 1986). Ferruginised rocks were studied palaeomagnetically to establish the timing of weathering events in the Alice Springs region. This paper summarises the published palynological work, as well as

[1] Senior & Associates Pty Ltd, Geological Consultants, 246 Gundaroo Rd, Bungendore, NSW 2621

[2] Australian Geological Survey Organisation, GPO Box 378, Canberra, ACT 2601.

interim results of the palaeomagnetic work already mentioned. It also attempts to synthesise the findings, up to 1994, of other BMR/AGSO research in the region.

Outline of Cainozoic geology

Tertiary rocks in the Alice Springs region occupy elongate intermontane basins (which, at least in some cases, are fault-controlled) and flanking palaeodrainages and piedmont deposits—some basins appear to have been initiated as early as the Late Cretaceous (Harris & Twidale 1991). In places, the succession is more than 200 m thick, but outcrops are rare and mostly deeply weathered. The Tertiary sequences are mantled by widespread unconsolidated Quaternary sediments, forming the flat or subdued depositional landscapes of the main river systems, including those of the Ti-Tree, Hanson, Plenty, Bundey, Illogwa, and Hale Rivers. Most of the riverine plains are partly bounded by steep, deeply dissected mountain ranges, some merging with lowlands of bedrock dotted with flat-topped residuals.

The Cainozoic sedimentary succession mostly overlies crystalline Proterozoic Arunta basement, but it also overlies parts of the Neoproterozoic to Palaeozoic Amadeus and Georgina Basins (Fig. 1). Much of the Tertiary sedimentary succession has been eroded from the northwestern, central and southeastern parts of the Amadeus Basin.

Evidence presented here suggests that, for the most part, sediment accumulated in two separate pulses, one in the Paleogene and the other in the Neogene. The first partly filled narrow depressions within mountain ranges of the Precambrian crystalline Arunta basement; examples are the Hale, Burt, Mount Wedge, and Whitcherry Basins. Deposition in the second pulse was in palaeodrainage depressions on the northern and eastern flanks of the uplands formed by the basement; depressions preserving this pulse include, for example, the Aremra, Bundey, Ti-Tree, Willowra, Ngalabaldjiri, and Yaloogarie Basins.

On the southernmost flanks of the uplands, which here include part of the Amadeus Basin, the Cainozoic history was very different. Piedmont fans formed on actively steepening slopes were dissected, both during and after deposition, to form a series of mesas (Fig. 1). The most active period of dissection started possibly in the late Pliocene with uplift in the MacDonnell Ranges (Shaw & Wells 1983). Only in the Ayers Rock Basin was deposition more-or-less continual (Jacobson et al. 1989). An idealised overview of how the mapped lithostratigraphic units relate to landforms is given in Figure 2.

The basement complex and the Tertiary sequences appear to have undergone more than one period of intense chemical weathering. According to Senior (1972), a trizonal weathered profile developed in crystalline Arunta rocks. This profile is up to 40 m thick and grades from a lowermost leached zone through an intermediate mottled zone to a ferruginous top. Erosion subsequently stripped the profile from most of the area, some of the detritus being incorporated into sediments accumulating within the intermontane basins. The Tertiary rocks were, in turn, weathered and crusts of silcrete, ferricrete, and thin ferruginous profiles developed in the Yaloogarie Basin (Stewart 1976), Hale Basin (this paper), and in the western Ti-Tree Basin (O'Sullivan 1973). Earlier, Mabbutt (1967) drew attention to the lateral variation from laterite at the centre to silcrete at the margins of the Hale Plain (Hale Basin), attributing this variation to a shallower, less-fluctuating former water table in the axial region, together with possible down-slope migration of iron.

Results from reconnaissance geological work indicate that ferruginous profiles on the Lower to Upper Jurassic Hooray Sandstone, along the northwest margin of the Eromanga Basin in the Illogwa Creek 1:250 000 Sheet area, were ferruginised possibly during the Late Cretaceous and Paleocene. In the Hale Basin and at three places in the Arunta basement rocks, recognition of a mid-Tertiary ferruginisation event is supported by palaeomagnetic work.

Because of the complex weathering history, which altered the mineralogical composition of much exposed rock, and the absence or destruction of fossils, age relations between individual Cainozoic rock units in the Alice Springs region remain uncertain. Nevertheless, some idea of the most likely stratigraphic framework is provided by palaeontological evidence from adjacent areas that appear to have a parallel history.

Palynological work between Ayers Rock and the Olgas suggests that deposition there may have begun as early as the Late Cretaceous, possibly even earlier. Lignites near the base of the 100 m thick succession were dated originally as Paleocene (Twidale & Harris 1977), but a recent reassessment, based on discovery of further diagnostic spore species, suggests that parts of the section are as old as the Maastrichtian Stage of the Late Cretaceous (Harris & Twidale 1991). Harris & Twidale (1991) concluded that there were at least three depositional phases in the area—a Late Cretaceous, a possible mid to Late Paleocene, and a Late Eocene phase.

Palynology indicates that carbonaceous clay in BMR Napperby 1, in a probable arm of the Whitcherry Basin (Fig. 1), is also of Eocene age (Kemp 1976). Carbonaceous sediments in the Ti-Tree Basin were described by Galloway & Kemp (1977) as possibly Miocene, but they could, on more recent data, be as old as Eocene. Vertebrate fossils indicate a Late Miocene or Early Pliocene age for the upper part of the Waite Formation near Alcoota station (Woodburne 1967). The palaeontological evidence, therefore, suggests that most of the sedimentary succession in the eastern Arunta region is Late Cretaceous to Miocene or Pliocene. From the Pliocene to the present day, sedimentation continued intermittently in local depressions.

The sequence of poorly to moderately lithified sedimentary rocks (conglomerate, sandstone, siltstone, mudstone, lignite, oil shale, and calcarenitic chalcedonic limestone) and weathered profiles of Cainozoic age in the Hale Basin northeast of Alice Springs is shown in Table 1. This composite reference section, established from surface mapping and drilling, forms the basis of the regional

Figure 1. Inferred outline of Tertiary basins, showing their relation to the underlying Arunta basement (non-standard projection). The 1:250 000 map sheets are abbreviated as follows: AC—Alcoota, AS—Alice Springs, AY—Ayers Rock, BC—Barrow Creek, BW—Bonney Well, EL—Elkedra, FK—Finke, FR—Frew River, HA—Hale River, HN—Henbury, HE—Hermannsburg, HU—Huckitta, IL—Illogwa Creek, KG—Kulgera, LA—Lake Amadeus, MC—McDills, MD—Mount Doreen, ML—Mount Liebig, MP—Mount Peake, MS—Mount Solitaire, MT—Mount Theo, NA—Napperby, RO—Rodinga.

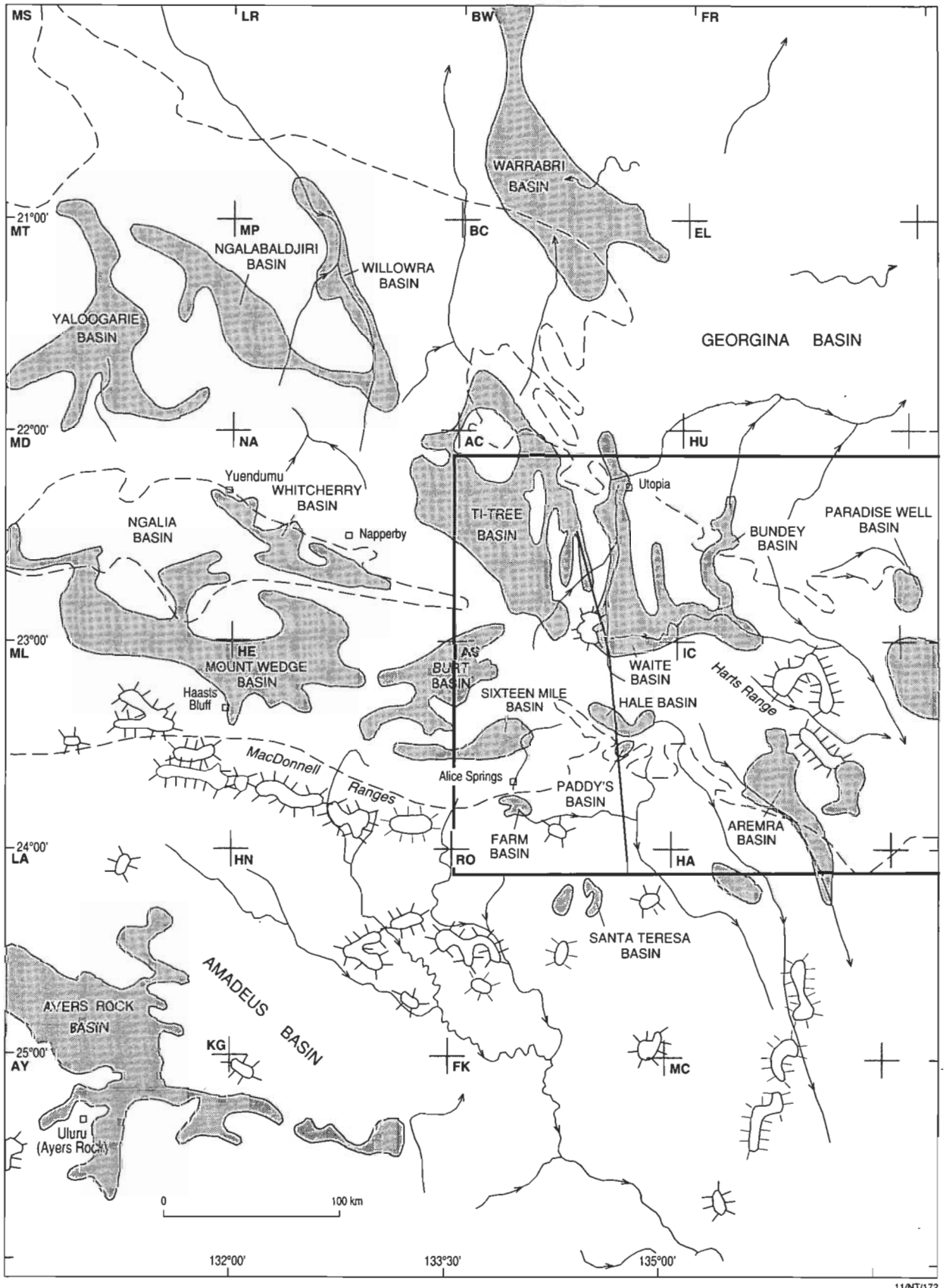
MS
LR
BW
FR
WARRABRI BASIN
21°00'
MT
MP
BC
EL
NGALABALDJIRI BASIN
WILLOWRA BASIN
YALOOGARIE BASIN
GEORGINA BASIN
22°00'
MD
NA
AC
HU
Yuendumu
WHITCHERRY BASIN
Utopia
TI-TREE BASIN
PARADISE WELL BASIN
NGALIA BASIN
Napperby
BUNDEY BASIN
23°00'
ML
HE
AS
IC
MOUNT WEDGE BASIN
BURT BASIN
WAITE BASIN
Harts Range
Haasts Bluff
SIXTEEN MILE BASIN
HALE BASIN
MacDonnell Ranges
Alice Springs
PADDY'S BASIN
AREMRA BASIN
24°00'
LA
HN
RO
FARM BASIN
HA
SANTA TERESA BASIN
AMADEUS BASIN
AYERS ROCK BASIN
KG
25°00'
AY
FK
MC
Uluru (Ayers Rock)
0
100 km
132°00'
133°30'
135°00'
11/NT/172
Tertiary sedimentary basin
Present-day drainage
1:250 000 sheet area
MC
Mesas of dissected Tertiary sedimentary rock
Outline of Precambrian Arunta basement block
Study Area
Cross section in Fig. 2

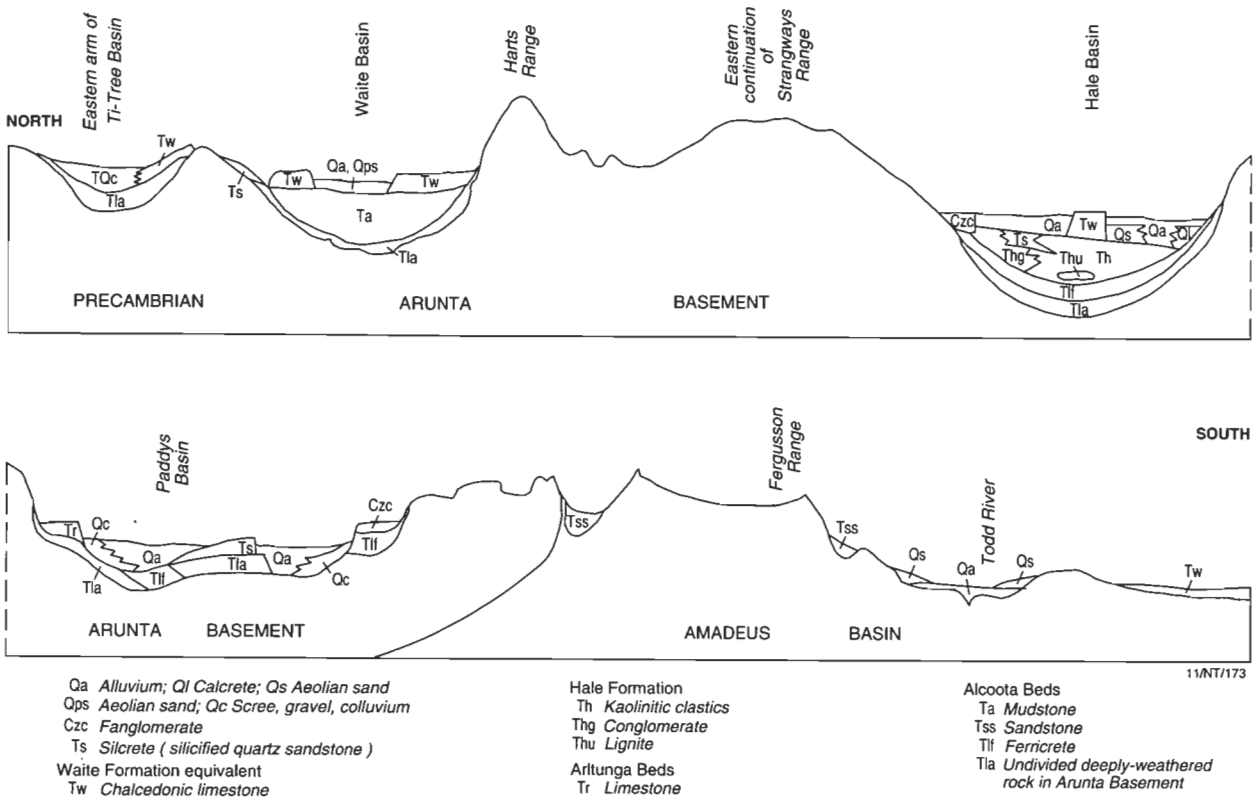

Figure 2. Diagrammatic N–S cross-section of the Hale Basin and regions bordering the eastern MacDonnell Ranges, showing the relationship between the surficial geological units and the topography.

stratigraphic framework described here. It incorporates data from Lloyd (1968), Senior (1972), Shaw & Warren (1975), and Shaw et al. (1979a, b), and the results of more recent studies. The stratigraphic succession and ages of some units, and particularly of weathering events, have been updated in accordance with evidence discussed here.

Hale Basin

This basin lies about 80 km northeast of Alice Springs (Figs 1–3). It underlies the Hale Plain between Claraville and The Garden homesteads, and is one of a number of small, sediment-filled depressions on a deeply weathered surface of Proterozoic and early Palaeozoic rocks. The basin forms a complex arcuate depression about 45 km long and up to 13 km wide. Its southern margin may have been a fault which controlled initial subsidence in the Late Cretaceous or Early Paleocene. The full succession is developed in the more extensive western part of the basin, where the reference succession is located in BMR DDH Alice Springs SH 2; another section has been described from the NTGS DDH 1 (Figs 4 & 5). A thinner sequence is preserved in the east in the Claraville Sub-basin, which is separated from the main basin by a basement ridge. The surrounding basement rocks comprise largely metamorphic rocks and granites of the Arunta Block (Shaw & Wells 1983).

The basin is filled with mainly fluviatile and lacustrine clastics (Clarke 1975; Senior *in* Shaw et al. 1982; Shaw et al. 1984). The spatial and temporal distributions of the deposits have been determined from reconnaissance mapping (Shaw & Langworthy 1984; Shaw et al. 1984), the logging of chip samples left *in situ* by an exploration company (Fig. 5), and stratigraphic drilling by BMR in 1966 and NTGS in 1975 (Figs 3–5 for locations).

Stratigraphy

At the base of the succession, overlying the deeply weathered metamorphics of the basement complex (Tlf of the map units, Table 1; weathering event A in Figure 4), is the Hale Formation (Th) (Stewart et al. 1980a; Shaw et al. 1984), a unit of kaolinitic quartz sandstone, siltstone, and mudstone, which grades into coarser sediments at the basin margins. In the Hale Formation (Fig. 4; Table 1) the succession begins with the Ambalindum Sandstone Member (Thg), argillaceous, poorly sorted sandstone with intercalations of granule and pebble conglomerate. It is about 55 m thick in BMR DDH Alice Springs No. 2. Conformably overlying this unit in the main western part of the basin is the Ulgnamba Lignite Member (Thu), formally defined by Stewart et al. (1980b) as the unit of lignite and carbonaceous shale which is 4 m thick in its type section in BMR DDH Alice Springs SH 2. The lignite also crops out, in a very weathered state, in a mesa 3 km west-northwest of Claraville homestead. Locally, the lignite is accompanied by pockets of oil shale. In the Claraville Sub-basin, an olive-green unit of mudstone and siltstone lies immediately below a discontinuous, carbonaceous clay unit assigned to the Ulgnamba Lignite Member. The olive-green unit is informally referred to as the Delaney Mudstone Member (Thc) and appears to belong to the same episode of deposition as the lignite. Thus, the Ulgnamba Lignite Member is a facies variant of the upper part of the Delaney Mudstone Member.

In the eastern Claraville Sub-basin, the Delaney Mudstone Member rests in places on weathered (yellow) sandstone (weathering event B in Figs 4 & 5), presumed to be the Ambalindum Sandstone Member (Fig. 5). The Delaney Mudstone Member (Thc) occurs as lenses in several of the drill holes penetrating the Hale Plain; it becomes

Table 1. Summary of stratigraphy.

Rock unit	*Lithology*	*Thickness*	*Tectonic events*	*Environment, fossils and age*
Qa	Fine and coarse clay-quartzose sand, silt and minor gravel, lacking a marked soil profile		Possible uplift in the area of the Harts, Strangways and MacDonnell Ranges or rejuvenation due to subsidence within the Lake Eyre Basin	Channels date from latest pluvial period—either Holocene or latest Pleistocene.
Ql	Calcrete; hard calcareous cements within formerly porous sediments			Humid oxidising conditions succeeded by aridity and aeolian activity. Cementation of porous surface sediments and colluvium forming calcareous crusts.
Qs, Qps	Quartzose sand (Qs); with fixed dunes (Qps)		Region tectonically stable	Development of broad sand plains with minor dune fields.
Qc	Colluvium, eluvium, scree			
Qr	Shallow red, oxidised, clayey and sandy oxidised soil ("Red earth"), clayey, oxidised silty-sand			Soil produced by repeated phases of alluviation and burial. Mixed with sheet sands (Qs) suggesting that the unit began forming in the late Pliocene (Litchfield 1969).
Czg	Redistributed ferricrete and quartz gravel	20 m		Transported ferruginous clastics derived from deeply weathered profiles.
Czc	Fanglomerate	20 m	Movement on some faults	Alluvial fan deposits flanking uplands.
Tw Waite Formation and equivalents	Greenish grey siltstone and chalcedonic limestone in type area.	20 m	Region tectonically stable	Argillaceous sediments and chemical precipitates in very quiet lacustrine environments. Age is Late Miocene–Early Pliocene (Woodburne 1967).
Arltunga beds Tr	Arenaceous limestone, silicified limestone, pebbly sandstone	4 m	Probable mild uplift and warping of some fault-bounded blocks	Coarse clastics grading to minor lake sediments. Probably equivalent to Tw (above) or, less likely, Th (below). Preceded by widespread hiatus.
Ts, Tl (overprint of Tlf, Tla)	Silcrete (strongly silicified quartzose sedimentary or felsic igneous rocks), Weathering Event C		Region tectonically stable	Groundwater silica sourced from felsic igneous rocks in regions of restricted drainage (e.g. margin of Hale and Paddys Plain Basins). Late Eocene age for Weathering Event C determined palaeomagnetically.
Hale Formation Th, (Thr, Thu, Thc, Thg)	Kaolinitic quartzose sandstone, siltstone and mudstone, minor conglomerate and lignite	195 m in Sixteen Mile Bore (Nth of Alice Springs)	Probable mild uplift and warping of some fault-bounded blocks	Lakes and swamps succeeded by river sediments grading laterally to coarse, poorly sorted clastics along intermontane margins. Probably equivalent to unit Ta of the Waite and Aremra Basins.
Tug Sandstone Member Thr	Brown sand and minor silt (subsurface)	30 m in NTGS DDH-1		
Ulgnamba Lignite Member, Thu	Grey carbonaceous clay, lignite	10 m in NTGS DDH-1		Marsh or swamp habitat. Lignite is probably mid-Late Eocene (Truswell & Marchant 1986).
Delaney Mudstone Member, Thc	Olive green mudstone and siltstone, locally developed mottled Weathering Event B	Equiv. unit 72 m in BMR Alcoota 20		Weathering Event B
Ambalindum Sandstone Member, Thg	Poorly sorted boulder conglomerate at basin margin in outcrop; Silty sand and sand in subsurface	55 m in DDH BMR Alice SH2		High energy fluviatile deposits
Tlf	Ferricrete (Weathering Event A extensive, Weathering Event C overprint)		See below	See below
Tla	Undivided weathered profile with ferruginous, mottled and leached zones, in places grading down into unweathered rocks. Well developed on coarsely crystalline igneous rocks. Weathering Event A.	±20 m	Region tectonically stable, widespread weathering.	Deep weathering under humid conditions. Seasonal precipitation, and fluctuating water-table, forming a trizonal weathered profile. Palaeomagnetic evidence from the Eromanga Basin suggests a Maastrichtian to Early Eocene weathering event (Idnurm & Senior 1978).

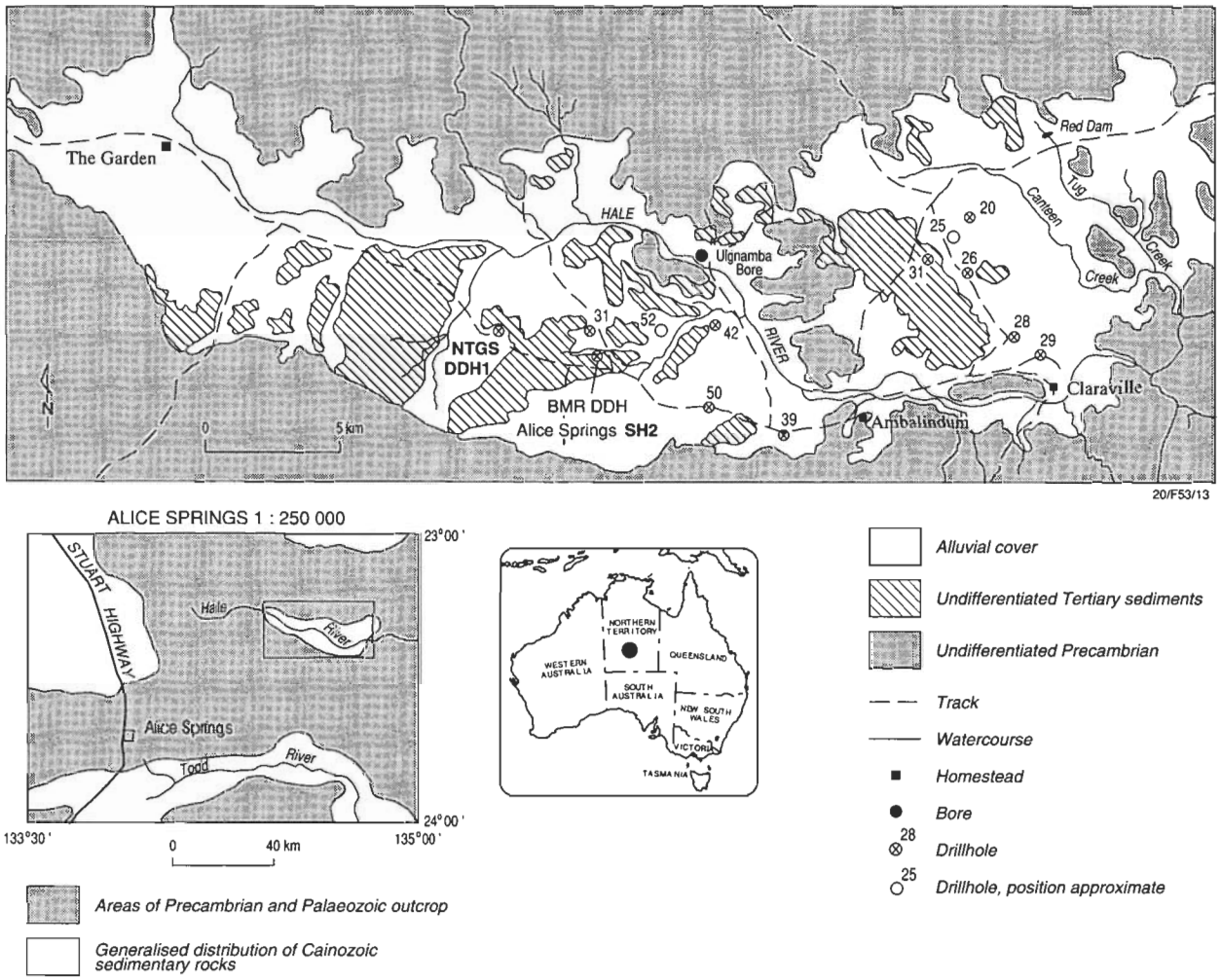

Figure 3. Sketch map of the Hale Basin, showing the location of NTGS DDH1, BMR DDH Alice Springs SH2 and a series of company drill holes.

sandier westwards so that in the region of BMR DDH Alice Springs SH2 it equates with a sandstone above a thin conglomerate (Fig. 5).

Above the lignite, the uppermost part of the Hale Formation has been referred to informally as the 'Arltunga Member', a unit mapped in the Paddys Basin several kilometres to the south. This is a succession of poorly consolidated, fine-grained brown silty sandstone, with minor sandy siltstone, and clay interbeds. There is some confusion about its nomenclature, as the name Arltunga beds has been used for calcarenitic limestones which may be more appropriately grouped with either the Hale Formation (Senior *in* Shaw et al. 1979a) or the overlying Waite Formation equivalents (Shaw & Wells 1983; Shaw et al. 1984). For this reason, it is placed in a new unit, the Tug Sandstone Member (Tht).

The Hale Formation appears to record deposition in a progressively flooding and slowly subsiding basin (Clarke 1975). The basal sandstones reflect a relatively high-energy fluvial environment, whereas the Ulgnamba Lignite Member records a marsh or swamp habitat and the Tug Sandstone Member probably a phase of relatively low-energy fluviolacustrine sedimentation. As noted earlier, such specific palaeoenvironmental interpretations need to be confirmed by more detailed future studies—for example, little information on sedimentary structures is at present available.

Formation of silcrete (Ts) in former porous and permeable quartzose sandstone, presumably by groundwater movements, and another interval of deep weathering (weathering event C in Figs 4 & 5) affected the Tug Sandstone Member and the adjoining basement. This weathering preceded deposition of a fine-grained clastic unit equated with the Waite Formation (Tw). In the surrounding basement, the ferruginous weathering unit, now placed in Tl, had been previously assigned to Tlf (Shaw et al. 1984). The Waite Formation was originally defined in the Waite Basin to the northeast (Shaw et al. 1982), where Woodburne (1967) described a Late Miocene to Early Pliocene vertebrate fossil assemblage.

Age of the Ulgnamba Lignite Member (Thu)

Dating the relatively thin successions in the Cainozoic basins of inland Australia continues to be a major problem. The difficulties of setting up a time framework within these basins were outlined by Truswell & Harris (1982): the sequences are entirely non-marine, and frequently deeply weathered; there are no intercalated volcanics that would allow radiometric dating; and the sequences are for the most part too thin to permit the use of magnetic reversal stratigraphy as a dating tool. In addition, they are remote from key palynological reference sections for Australia, which have been defined in the southeast.

In the Hale River Basin, the Hale Formation is both

underlain and overlain by deeply weathered profiles. The climatic event that produced a trizonal weathered profile in the basement Arunta rocks on which the Cainozoic sequences rest is likely to have occurred in the Late Cretaceous and/or Paleocene, based on a comparison with the chronology of weathered profile development in the Eromanga Basin of southwest Queensland. The second, younger, weathering event, which affected the top of the Hale Formation, was suggested by Senior (in Shaw et al. 1979b) to be Late Oligocene to Early Miocene, on the assumption that this event correlated with the younger of the two weathering events in the Eromanga Basin (see Senior et al. 1978). However, preliminary palaeomagnetic results from the Hale Basin indicate Late Eocene as the most likely age for the weathering (see **Discussion** below), suggesting Late Eocene as the probable younger age limit for the Hale Formation and its included Ulgnamba Lignite Member. The outcropping ferruginised or deeply weathered basement rocks sampled north of the Hale Basin similarly record a Late Eocene age of magnetisation.

Truswell & Marchant (1986) described palynomorphs from the Ulgnamba Lignite Member, at 42.2 m depth in the borehole DDH-1, drilled by the Northern Territory Geological Survey. The assemblage was correlated with the middle *Nothofagidites asperus* Zone of the Gippsland

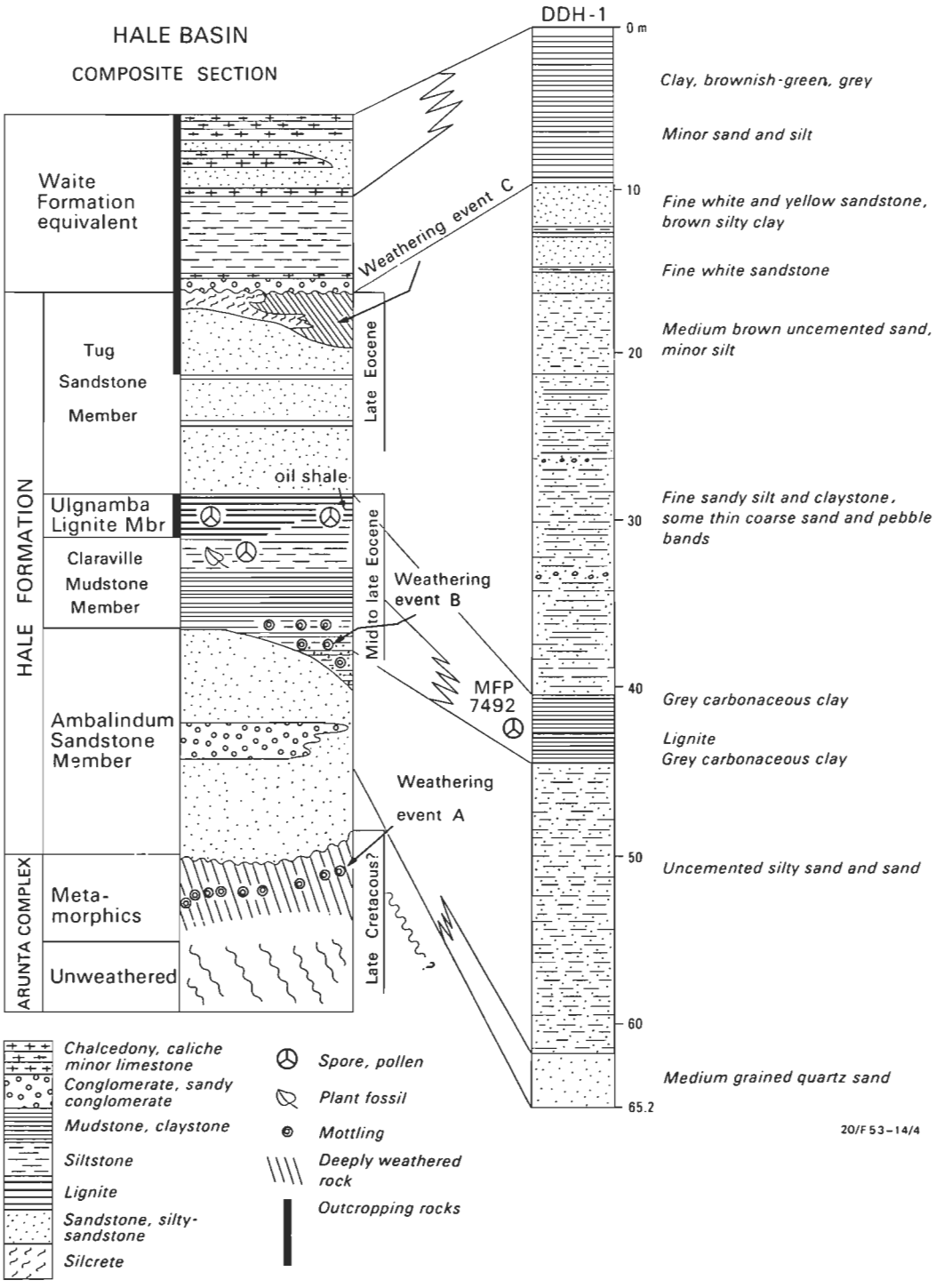

Figure 4. Stratigraphic column for NTGS DDH1, showing correlation with a generalised section of the Hale Basin, which is based in part on the succession intersected in BMR DDH Alice Springs SH2.

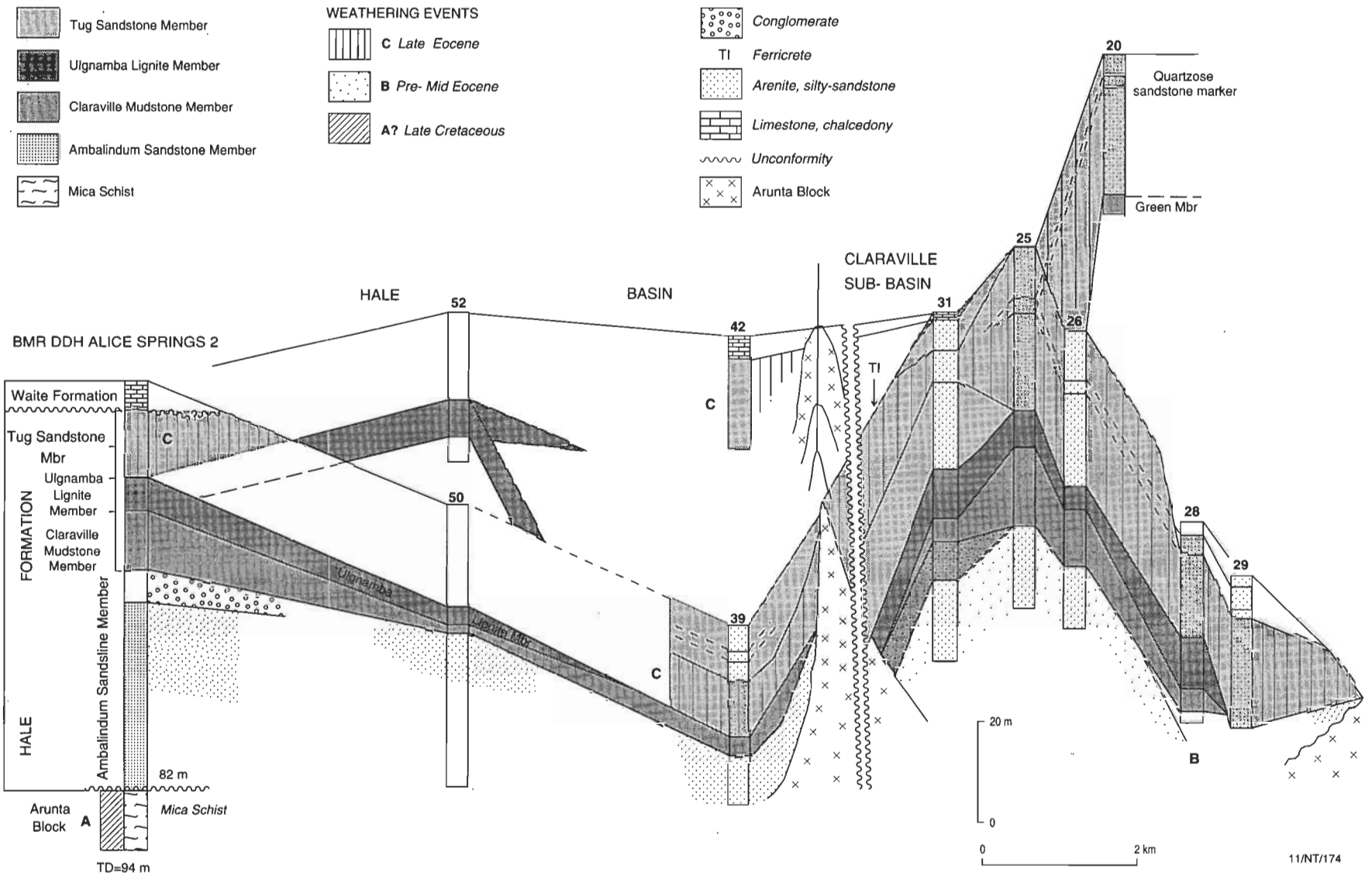

Figure 5. Panel diagram showing members of the Hale Formation and their relationship to weathering events within the eastern part of the Hale Basin and the Claraville Sub-basin; based on selected company scout holes as numbered in Fig. 3. Note, Claraville homestead is located at the eastern (RHS) apex of the diagram (see Fig. 3).

Basin, which, in its type area, spans the Middle to Late Eocene boundary. The correlation rests on relatively small numbers of index species, namely, on the presence of *Nothofagidites falcatus, Santalumidites cainozoicus,* and *Proteacidites confragosus,* so that precise relationships are difficult to determine. Assuming that the time ranges of species are similar in central and southeastern Australia, then a Middle to Late Eocene age is implied, consistent with the palaeomagnetic results.

Ti-Tree Basin

The Ti-Tree Basin lies mainly in the northwestern Alcoota Sheet area, and also overlaps the Napperby and Barrow Creek Sheet areas (Fig. 6), covering possibly as much as 1000 km^2. Exposure of the basin deposits is limited to low, sandy soil-mantled rises, and most of the succession is known only from drill holes and from lithological logs of water bores. The basin is thought to be thickest in the east, where it is crossed by both the Woodforde River and the Stuart Highway, south of the Ti-Tree roadhouse (Fig. 6).

Previous investigations

The groundwater potential of the basin was investigated by Edworthy (1966) and McDonald (1988a, b), and the recharge mechanism and groundwater age have been assessed by Calf et al. (1991). The uranium potential of the basin was examined by O'Sullivan (1973) and Hughes & O'Sullivan (1973).

Distribution and stratigraphy

Hanson River region. This northeasternmost part of the basin, south of the Ti-Tree roadside village has been investigated by industry drilling (O'Sullivan 1973). The succession is shown schematically in Figure 9. Depth to basement in six stratigraphic holes drilled by CRA Exploration Pty Ltd, ranged from 146 to 319 m. Weathered rocks were intersected at the base of the succession in two of the holes. In the deeper holes, up to 130 m of white siltstone and claystone rests on basement and is overlain by lenticular units of lignite and carbonaceous claystone. The carbonaceous units, or where they are absent, the 'white beds', are overlain by greenish-grey siltstone and silty sandstone. These pass, in turn, upwards into their weathered and oxidised equivalents. The uppermost 60 m or so is commonly dominated by reddish-brown sandy siltstone, whereas the lower 60 m or so is, in places, characterised by multicoloured (pale-grey, brownish-grey, white or yellow) siltstone or mudstone, and includes minor coarse sandstone and gritty sandstone layers. In one hole, a second weathered sequence was intersected within a greenish-grey siltstone unit, which lacked carbonaceous intervals. The greenish siltstone unit and the associated carbonaceous lenses were absent in two holes.

The age of this succession is inferred on the basis of correlation with the nearby Whitcherry Basin (Fig. 1). Similar carbonaceous sediments to those in the Ti-Tree Basin were intersected in an arm of the Whitcherry Basin at a depth of 136–139 m in BMR Napperby No. 1 located 13.5 km southwest of Napperby homestead (Fig. 1). These carbonaceous sedimentary rocks contain a Middle to Late Eocene microflora (Kemp 1976). If these correlations are correct, they suggest that the weathered profile at the base of the succession in the northwestern part of the Ti-Tree Basin may be older than Middle Eocene. The second profile, recognised locally in the greenish-grey siltstone, may correlate with weathering event B of the Hale Basin (Fig. 4).

Bushy Park region. In the southwestern part of the Ti-Tree Basin (in the southwestern Alcoota Sheet area), the Cainozoic succession reaches more than 194 m thick, as recorded in BMR SH 2 (Fig. 6). Reduced successions were intersected in other stratigraphic holes, such as BMR Alcoota Nos 2, 18 and 19. In the nearby BMR Alcoota No. 20, a 25 m thick sequence—comprising calcareous siltstone, green claystone, minor granule conglomerate, and rare limestone—was found to overlie silicified sandstone basement at a depth of about 184 m. The overlying 70 m thick olive-green or white mudstone includes 12 m of grey, green and brown siltstone and sandstone in its upper part. Plant fossil fragments were recorded infrequently in this interval. This mudstone is correlated with unit Ta in the Waite Basin (Fig. 7; see below) and with the Delaney Mudstone Member of the Hale Formation in the Hale Basin (Fig. 7; see above). The remaining interval of about 87 m is assigned to TQt (see below) and consists of variously oxidised red and brown silty sandstone, minor siltstone, and pebbly silty sandstone. It is overprinted by ferruginous weathering.

This upper unit, TQt, can be divided in the southeastern Ti-Tree Basin region, into four sub-units (TQt_{1-4}), three of which ($TQt_{1,2,3}$) are represented in Alcoota No. 20. These sub-units (and the correlative units Ta_{4-5}) are as follows:

- The lowest (TQt_1), up to 30–40 m thick, is dominated by siltstone and minor silty sandstone. A similar lutite was intersected in BMR Alcoota 3 in the Waite Basin (see below and Fig. 6). The lower, more silty part of TQt in the southeastern Ti-Tree Basin may correlate with the multicoloured siltstone and, in places, mudstone and coarse angular sandstone lenses, intersected in drill holes in the northwestern part of the Ti-Tree Basin (e.g. hole TT4 in O'Sullivan 1973). TQt_1, the lower part of TQt, may also correlate, in part, with the Waite Formation (see above), as well as Ta_4. The lowest part of this unit in BMR Alcoota 20 includes grey siltstone and white sandstone, lithological types reminiscent of the 'clean' sandstones in Ta_4 in the Aremra Basin (see below).

- The next unit (TQt_2) is commonly sand dominated, and is up to about 25 m thick. It may be multicoloured in places rather than red-brown. It commonly includes high proportions of silt and clay, and rarely includes calcareous elements and conglomeratic intervals with white mica and basement clasts. It may correlate with the multicoloured siltstone and, in places, mudstone, sandstone and coarse angular sandstone, intersected in drill holes in the northwestern part of the Ti-Tree Basin (e.g. hole TT4 in O'Sullivan 1973). This lower part of TQt may also correlate, in part, with the Waite Formation (see above) and the lower part of Ta_5.

- The upper unit (TQt_3) is about 20 m thick and commonly dominated by brown or red-brown, poorly sorted sandstone. It may correlate with the upper unit of reddish sandy siltstone and sandstone of the northwestern part of the basin (O'Sullivan 1973) as well as the upper part of Ta_5 in the Aremra Basin (see below), characterised by red-brown silty sandstone. In BMR Alcoota 20 it has a strong ferruginous overprint.

- Unit TQt consists of calcrete and brown silty sandstone. Chalcedonic cappings and strong ferruginisation, which are characteristic of the Waite Formation (see below and also McDonald 1988a, b) are absent. The lack of these weathering imprints indicates that the upper part of TQt most likely postdates the Waite Formation of the Waite Basin.

Allungra Creek region. Drilling by Northern Territory Power and Water Authority (McDonald 1988a) in this central-northern part of the basin (Fig. 6) delineated an 80 m thick unit of poorly consolidated, oxidised silty sandstone. McDonald considered this to be TQt and interpreted it as a fluviatile deposit. In the deeper part of the basin it grades downwards into grey-green mudrock (Ta_2) of possible lacustrine origin (McDonald 1988a). TQt is not readily subdivided as it shows wide lithological variation within a complex drainage system. The unit is commonly calcareous and, locally, appears to interfinger with chalcedonic, calcarenitic limestone of the Waite Formation type (Tw).

Palaeogeography

The palaeodrainage system within the western Ti-Tree Basin (Hanson Plain of Shaw et al. 1979b; Shaw & Warren 1975) is considered to have formed at about the same time as the 'Waite Surface' (see below) and to have continued to evolve during the Pleistocene and into the early Holocene. TQt may span a stratigraphic interval ranging from the Tug Sandstone Member of the Hale Formation to the Waite Formation (Tw), i.e. from Late Eocene to Late Miocene or younger, and in places possibly through to that of the oxidised alluvial unit Qr. In places, marginal tilting appears to have occurred at some stage, resulting in erosion of Tw before deposition of the last phase of TQt (see McDonald 1988a). The complex drainage system, outlined by calcrete deposits, then shifted slightly to a new location and continued to evolve as a coalescing northerly flowing palaeodrainage system. In the Pleistocene, the depositional basin (the Hanson Plain) became covered by ferruginous 'red earth' soil (Qr), then by aeolian sand, which contains subdued dune landforms. Wet interludes, in this otherwise arid period, produced

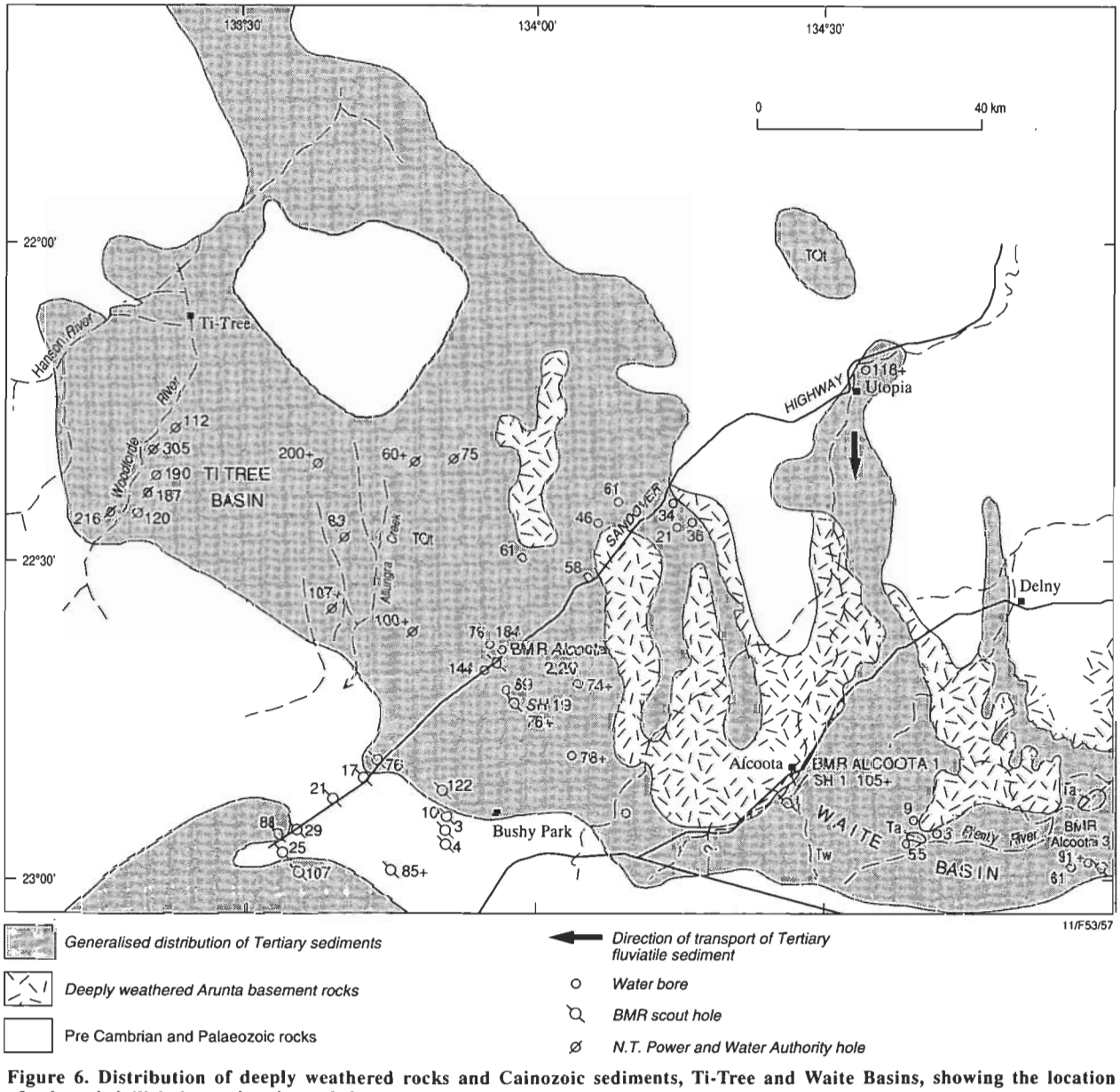

Figure 6. Distribution of deeply weathered rocks and Cainozoic sediments, Ti-Tree and Waite Basins, showing the location of selected drill holes and estimated depths to basement.

north-flowing drainage channels with deposition of alluvium. Since then, these drainage channels have been largely abandoned, to be replaced by the present Hanson drainage system.

Waite Basin

The Waite or Plenty River Basin is an east–west depression north of the Harts Range, covering possibly 1200 km^2 (Figs 1, 6 & 7). It contains up to 180 m of Tertiary lacustrine and fluviatile sedimentary rocks, referred to informally as the Alcoota beds (Ta). These rocks are similar to those in the subsurface at the eastern part of the Ti-Tree Basin, but, to a limited extent, have been uplifted and dissected. The outcropping and dissected sequence in the western part of the Waite Basin belongs to the younger Late Miocene to Early Pliocene Waite Formation (Woodburne 1967).

Uplift within the MacDonnell, Strangways, and Harts Ranges—together with probable subsidence to the north (i.e. northern part of the Alcoota Sheet area)—terminated much of the southeasterly drainage in the western part of the Waite Basin, possibly in the Pliocene. As a result, the Sandover and Bundey River systems developed on new, largely north-dipping, slopes. The eastern part of the Plenty River system continued eastwards in the direction of the earlier river system that deposited the Waite Basin succession.

The Alcoota beds (Ta) (Map units Ta, Waite Formation Tw, and minor TQt) 'Alcoota beds' is an informal name applied to Tertiary units, largely preserved in subcrop in the Alcoota Sheet area. (Only about 15 per cent of the total thickness of Tertiary sedimentary units is exposed.) The Alcoota beds have a composite thickness of about 250 m, as inferred from stratigraphic drill holes, BMR Alcoota SH1, 2 and 3. Of this, the basal mudstone and siltstone sequence (Ta) is represented by less than 5 m of outcrop in the Plenty River valley. The Waite Formation (Tw), a sub-unit of the Alcoota beds, crops out extensively in escarpments around flat-topped landforms in a belt roughly peripheral to the margins of the Waite Basin (Woodburne 1967) in the southeast quadrant of the Alcoota Sheet area.

Near the margins of the Waite Basin, the Waite Formation unconformably overlies a partly truncated weathered profile developed in crystalline rock (Fig. 6). It seems likely that the onset of deposition of the Waite Formation related to former low-lying zones within the Arunta Block, where surface drainage and groundwater conditions were conducive to development and preservation of this profile. Further downwarping of this weathered surface, combined with some erosion and dispersion of weathered materials, replicated the position of the developing Waite Basin. The youngest sediments, originally mapped as TQt and included in the Alcoota beds, are represented at the surface by only a few metres of fine quartz sandstone, chalcedonic calcarenitic limestone, and greenish-grey siltstone (Fig. 6). TQt is restricted to the Ti-Tree Basin (see above) and, hence, is excluded from the Alcoota beds. It correlates in part with the Waite Formation, but includes younger elements and probably also older elements.

The lithology of the Alcoota beds in subcrop differs appreciably from that of the majority of outcrops, but for ease of mapping (see Shaw & Warren 1975) the name 'Alcoota beds' was applied informally to the entire succession. The formally defined Waite Formation (Woodburne 1967) becomes the middle unit within this framework. The lower limit of the Alcoota beds is unknown: the only two drill holes in the basin, BMR Alcoota 2 and 20, failed to reach the basement.

The lithology and possible correlation between units in the Alcoota beds are shown in Figure 7. The coarse-grained sediments in BMR Alcoota No. 3 are thought to be a facies equivalent of the Waite Formation and to have been derived locally from the nearby Harts Range.

These thick Tertiary sediments, discovered during drilling in 1971 in the Alcoota Sheet area, may have potential for hosting uranium. They are derived from nearby crystalline basement, where felsic plutonic source rocks are abundant and include rocks with significant U values. The sediments appear to have been deposited in fluviatile and lacustrine environments and show a variety of red, white and green zones, the result of alternating periods of oxidation and reduction. Such conditions are known to favour uranium precipitation.

Gamma-ray logs were run in BMR Alcoota 2 and in three abandoned water bores on Annitowa station (previously Woodgreen station). Two of the holes indicate small and apparently anomalous zones of relatively high radioactivity. In BMR Alcoota 2 (Fig. 7), the small anomaly, recorded from a sandy conglomerate bed in the interval 90–100 m, may reflect very low concentrations of uranium in groundwater (Senior 1972). The second anomaly, obtained in the bore Woodgreen 1, is 10.5 m thick and, according to the driller's log, lies in a median position between a red micaceous sandstone and a green and grey medium-grained sandstone (fig. 7 in Senior 1972). However, subsequent investigation of the Tertiary sediments in the Ti-Tree Basin in the northwest of the Alcoota 1:250 000 Sheet area revealed only low U contents, the maximum reported being 23 ppm. Here, calcrete assigned to TQt, intersected in shallow bores, was 6–12 m thick, forming an irregular channel-like body, closely linked with basement morphology (cf. O'Sullivan 1973).

Unit Ta

BMR Alcoota SH1 & 2 drill holes penetrated a massive mudstone and siltstone unit below the Waite Formation to a total depth of 194 m (Senior 1972, fig. 5). The upper part of these argillaceous deposits is weathered, mottled and stained by red iron oxide. The red coloration is especially evident in BMR Alcoota SH1. However, in both holes the unit includes a zone of slightly leached white mudstone and siltstone, which in BMR Alcoota SH2 grades into a basal sequence of green and grey, unaltered mudstone. These rocks are almost devoid of bedding except for a few faint laminations. This may reflect deposition in a quiet-water lacustrine environment.

Waite Formation (Tw)

The type section of the Waite Formation is a small mesa on the north side of Waite Creek, 6 km southwest of Alcoota homestead and 15 km northeast of Mud Tank Bore. Only about 440 m of the upper part of the formation crop out; the full thickness is not known.

In outcrop, the Waite Formation consists of interbedded chalcedonic calcarenitic limestone, sandstone, siltstone, and minor sandy conglomerate. Beds of cream or white chalcedonic calcarenitic limestone form the hard resistant

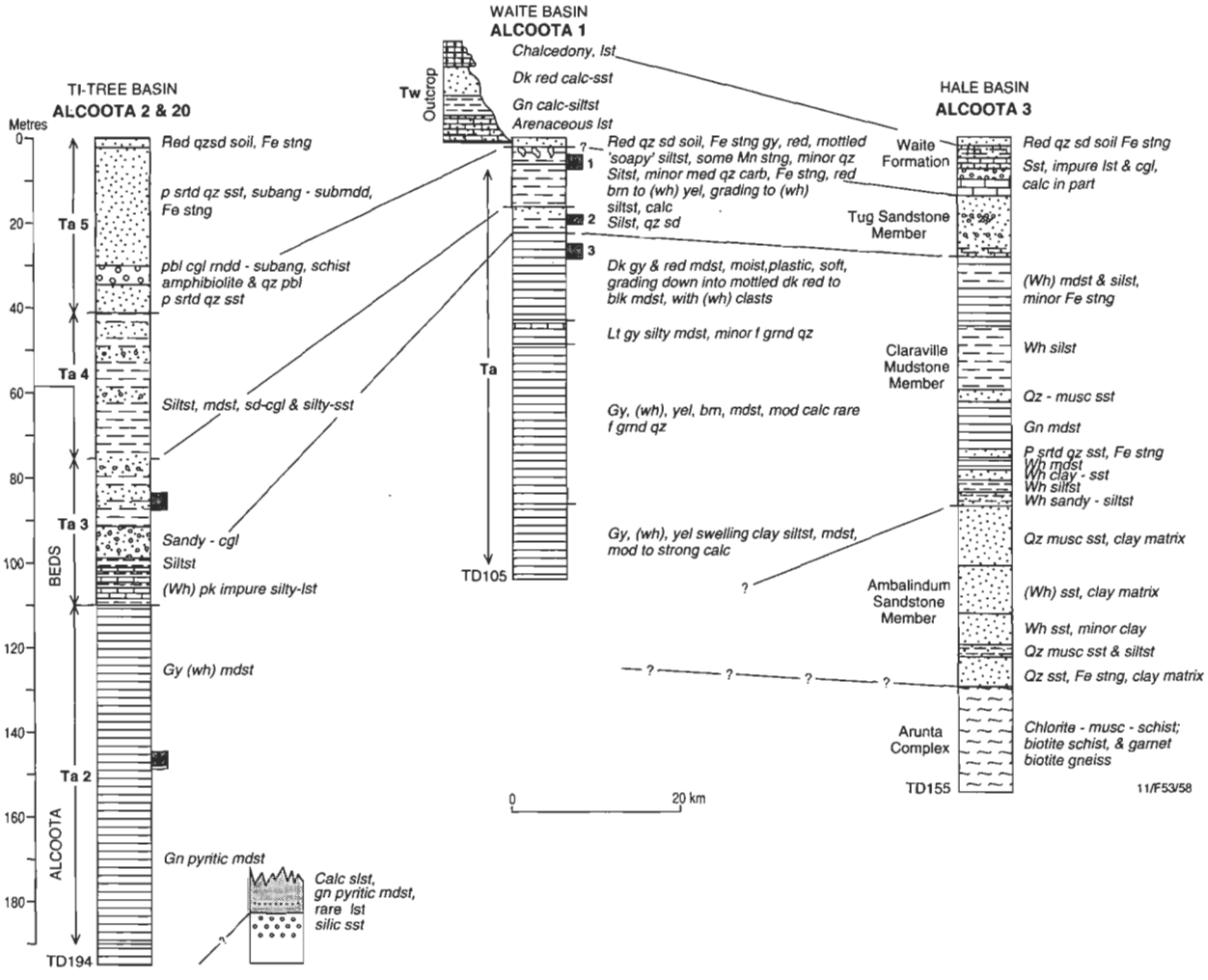

Figure 7. Correlation between drill holes in the Ti-Tree and Waite Basins, and possible correlation with the units of the Hale Basin.

summit caps on many low plateaus and mesas. In places, chalcedonic silica is dominant and there is a lack of clastic detritus, which indicates that they formed by chemical precipitation of silica and are contemporaneous with interbedded clastic deposits of the Waite Formation. Some of the siliceous beds have a sedimentary fabric, owing to penecontemporaneous replacement of calcium by silica. A sample of chalcedonic limestone, analysed by x-ray fluorescence, consisted dominantly of SiO_2 (96.7%) with minor iron oxides (0.77%), CaO (0.35%), and P_2O_5 (0.25%).

In most outcrops, the grain size of clastics in the Waite Formation increases upwards. In the Alcoota Sheet area, Woodburne (1967) attributed this to a change from a lacustrine to a fluviatile environment of deposition. Core from BMR Alcoota SH1 drill hole tends to confirm an initial lacustrine environment, because the subsurface sediments are dominantly argillaceous and include abundant mudstone, siltstone, and claystone. The sedimentary sequence may well equate with deposition within a regressive lake.

Vertebrate fossils in the outcropping lacustrine part of the sequence were described as being of Late Miocene or Early Pliocene age (Woodburne 1967). Subsequently, in an overview of the stratigraphic relationships of Australia's fossil mammal faunas, Woodburne et al. (1985) tentatively placed the Alcoota fauna in the Late Miocene on the basis of evolutionary relationships, equating it with faunas of the Cheltenhamian Stage in southeastern Australia.

The prolific iron staining observed from near the top of BMR Alcoota SH1 ("grey-red mottled 'soapy' siltstone" (Fig. 7): the result of contemporaneous weathering) suggests correlation with weathering event C which affected the Tug Sandstone Member in the Hale Basin. Sediments from cuttings in the interval 102–105 m in BMR Alcoota SH1 (Ta) were palynologically barren.

The distribution of Tertiary sediments (Figs 1 & 6) shows two north-trending extensions of the Waite Basin. On the westernmost extension, at a site 10 km south of Utopia homestead, coarse-grained sediments contain pebble to small boulder-sized clasts. The linear distribution and coarse clastic composition of these deposits, coupled with decrease in grain-size southwards, indicate a northerly source for the detritus. This is the reverse of the present-day drainage direction. If the vertebrate fossils present in the upper part of the Waite Formation are Late Miocene, then the Waite Basin must have been dissected after this date.

Deeply weathered rocks—Ti-Tree and Waite Basins (includes older units Tla and Tlf and younger unit Tl)

In the region surrounding the Ti-Tree and Waite Basins, a well-developed profile is formed in the Arunta igneous and metamorphic basement rocks, and in lacustrine and fluviatile Tertiary sediments referred to as the Alcoota beds (see above; mainly in the Alcoota 1:250 000 Sheet area). Deep chemical weathering has altered the upper 40 m of exposed crystalline rocks, forming a trizonal profile, comprising a lowermost leached zone, an intermediate mottled zone, and a ferruginous upper zone. In subcrop, it underlies some of the Cainozoic sediments, as seen from drill cuttings. In outcrop, only the Waite Formation rests unconformably on the weathered profile developed in Arunta basement rocks.

The trizonal weathered profile has been most extensively studied in the Alcoota Sheet area (Senior 1972), where it is widely preserved. A mid-Tertiary age was initially assigned (Senior 1972) on the assumption, proposed by Woolnough (1927), that such profiles formed during a continent-wide phase of chemical weathering. Subsequent stratigraphic and palaeomagnetic studies of thick, deeply weathered profiles in western Queensland indicated two major weathering episodes (Senior et al. 1978; Senior & Mabbutt 1979). The older of these is either Late Cretaceous or early Tertiary (Morney profile) and the younger is middle Tertiary (Canaway profile). The Canaway profile overprinted the partly eroded Morney profile over extensive areas of the Eromanga and Surat Basins. Within the current study area, palaeomagnetic studies at three sites have identified only a mid-Tertiary, probably Late Eocene, magnetic age of ferruginisation.

Drilling has shown that the Arunta basement rocks underlying the Hale Basin (weathering event A in Fig. 4) and the Aremra Basin are deeply weathered. The probable Middle to Late Eocene Ulgnamba Lignite Member is sandwiched between strongly oxidised rocks, which appear to represent either contemporaneous weathering and/or input of former weathered detritus. It seems possible, therefore, that the Arunta basement profile in these drill holes (equivalent to weathering event A in Figs 4 & 5) may be equivalent, at least in part, to the Morney profile of the Eromanga Basin (i.e. Late Cretaceous and/or Paleocene). From palynological evidence, deposition may have begun in central Australia in the Late Cretaceous, or possibly earlier, implying that the deep weathering of Arunta basement is Cretaceous or older. A third weathering profile (weathering event C in Figs 4 & 5) appears to affect the Tug Sandstone Member exposed at Red Ochre Dam (see map accompanying Shaw et al. 1984).

As noted above, a pilot palaeomagnetic study of weathered profiles indicates a possible Late Eocene magnetic age for outcropping profiles in the Hale Basin area, in agreement with results from the northern margin of the Waite Basin. The estimate is based on 44 samples collected from seven localities (Senior et al. in press). Thermal demagnetisation, using 13–18 steps, gives a palaeomagnetic pole at lat. 113.0° E, long. 65.8° S (radius A_{95} of 95% confidence circle 3.9°), coincident with the Late Eocene pole on the Australian apparent polar wander path (Idnurm 1994). Late Eocene is, therefore, the most likely age, but Early Eocene or Late Oligocene cannot be ruled out with 95% confidence. The confidence circle for the pole does not enclose the pole of the Canaway profile of southwest Queensland, suggesting a possible shift in timing of a single mid-Tertiary weathering event or two separate events, one in each region. (It should also be noted that the confidence circle does not enclose the older Morney profile pole.)

A period of erosion (possibly in the Oligocene, cf. Kamp 1991; see Table 2) removed part of the Eocene and older profiles, and detritus was incorporated into the Waite Formation (see Table 1 and below). In some depressions, such as in the southeastern part of Alcoota 1:250 000 Sheet area (see Senior 1972; fig. 4), an almost complete weathering profile is preserved below the Waite Formation. The trizonal character of this profile implies that it largely corresponds to weathering event A (largely mapped as units Tl, Tla—see Table 1), but that it has been overprinted by weathering event C (mapped as units Tl, Ts). The fact that the deep trizonal profile normally predates the initiation of Tertiary deposition has been established from surface mapping in the Hale Basin. The less-well-developed mottling and ferruginisation of sediments, probably equivalents of the Tug Sandstone Member, immediately underlying the Waite Formation (Fig. 7) are correlated with weathering event C from the Hale Basin.

The leached or clay-rich zone at the base of the exposed profile, developed in Arunta Block rocks, grades from relatively unweathered parent rock upwards into a zone dominated by white kaolinitic clay minerals. It is generally possible to identify the gross lithology of the parent rock in the basal to middle part of this zone. In this zone, textural features of the host rock are preserved, together with quartz veins and remnants of large phenocrysts, such as quartz and muscovite.

The kaolinitic zone grades up into a multicoloured or mottled zone, up to 10 m thick. This zone contains patches stained pink, purple, brown or yellow by iron oxides, contrasting markedly with the white clay-rich matrix. Individual stained patches or mottles vary from small nodules to structureless masses. Iron-oxide staining and enrichment increase upwards through the mottled zone. Kaolinite and quartz are dominant, with subordinate amounts of hematite and goethite (see Senior 1972, table 1). The texture of the parent rock cannot be recognised at the top of the mottled zone, even though there is a tendency for this type of profile to have developed within formerly strongly textured, coarsely crystalline gneissic or granitic rock types.

Overlying the mottled zone is a ferruginous zone up to 8 m thick. This, the most strongly indurated part of the profile, forms prominent vertical escarpments with generally a columnar structure. Goethite and hematite are the dominant iron minerals. The rock is generally fine-grained and massive, except for an irregular mosaic of fine fractures. Numerous vertical and subhorizontal joints give the zone a pronounced columnar structure similar to that developed in some soil profiles as a result of volume changes. In places, the upper 3 or 4 m of the ferruginous zone is reworked by pedogenic processes and consists of a re-cemented layer of fragments and pisolites. The latter are up to 1 cm in diameter and have a simple structure of concentric shells of iron oxides of contrasting colour. This material has locally slumped down vertical fractures into the underlying ferruginous zone, thereby forming 'pipe-like' infillings. Some pisolites are strongly

Table 2. Tentative interpretation of tectonic and palaeogeographic setting.

Period approx.	*Age[1] (Ma) ~ base*	*Units*	*Plate-wide[3,4] tectonism*	*Central Australian tectonism*	*Lat.[4] C. Aust °S, °shift*	*Plate-wide palaeo-geography[2, 7]*	*Suggested central Australian depositional environment*	*Tentative central Australian climate*
Holocene	0.01	Qa, Qs, Ql	Craton stable	Stable	24, 0	Present-day conditions	Present-day drainage and deposition	Present-day dry conditions
Pleistocene–latest Pliocene	~ 2	Qps, Qa, Qs	Craton stable	Stable	24+, 0	Waxing & waning of ice caps	Sand plains, minor dune fields	Dry, sporadic pluvial period
Late Pliocene	~ 3	Qr, TQt_4 Czc, Czg	Localised uplift, ?compressional tectonism	Upward doming of ranges, drainage reversal of Sandover River	24+, 0	Rejuvenation of drainage	Oxidised soil development, sheet sand	Wetter conditions, followed by increasing aridity
Early Pliocene–Late Miocene	~ 3–20	Tw, Tr, TQt_{1-3}, Ta_{4-5}	Craton stable	Switch in sites of sedimentation	25+, –1	Lowering of sea level & expansion of ice cap	Restricted drainage, lakes including salt lakes	Moderate temperatures, seasonal rain
Early Miocene to Oligocene	~ 20–35	Hiatus	Beginning of N Aust. collision[5]	Widespread uplift	≥43, –19	Sea level rise at ~ 20 Ma after episode of widespread weathering (Canaway Profile eq.)	Widespread hiatus	?Drier
Late Eocene	~ 35–45	Tl, Ts	Plate rearranngement. Inversion and wrenching of early structures at plate margins. Uplift of parts of continent	Reduced rates of subsidence, break in sedimentation in Claraville sub-basin	46, –22	Beginning of expansion of Antarctic ice cap and sea level fall	End of widespread deep weathering, especially east of ranges	Uncertain
Late to mid-Eocene	~ 45±	Tht, Ta_3,Tss	Pacific plate rearrangement[6]	Limited upward doming of ranges, minor tilting east of ranges	48, –24	Humid, temperate climate over much of the continent	River sediments, sheet outwash, coelescing piedmonts	Warm, moist
Mid - Eocene	~ 50±	Thu, Thc, Ta_2,Tss	Start of rapid spreading away from Antarctica, end Tasman Sea spreading, start spreading Coral Sea, subsidence in Murray Basin and in Eromanga Basins after break	Renewed localised subsidence after local break	≥50, –26	Moist, increased circulation of warmer seas, presence of lakes, peat swamps and forest	Localised lakes and peat swamps, forest on slopes.	Warm, moist, possibly with dry phases
Early Eocene - Paleocene	~ 55–65	Thg, Ta_1, Tss	Continued spreading between Australia and Antarctica, subsidence in Eromanga Basin	Narrow intermontane basins, rapid local subsidence	54, –30	Main present-day river systems established, major disturbance of ocean currents, negligible ice cap	Coarse river deposits, forest and peat swamps very locally	Warm, moist, possibly with some dry episodes
Earliest (?) Paleocene - Late Cretaceous	~ 70–90	Tlf, Tla	Start of Tasman Sea rifting, and continued spreading between Australia and Antartica	Broad uplift over much of continent, more marked in the Eastern Highlands	58, –34	Subaerial erosion (Morney Profile eq.) of much of Australia and Antartica	Widespread deep weathering (age uncertain)	Warm, moist, possibly seasonal rain

References: 1) Harland & others 1990, 2) BMR Palaeogeographic Group 1990, 3) Etheridge et al. 1991, 4) Veevers et al. 1991, 5) Kamp 1991, 6) Wells 1989, 7) Truswell & Harris 1982.

magnetic, probably due to some near-surface process whereby goethite and hematite are converted to maghemite. The morphology of the ferruginous zone is very similar to that of the upper crust-forming portion of the Canaway profile of western Queensland and may have formed by analogous processes. As previously mentioned, the timing of the weathering events, as determined palaeomagnetically (Idnurm & Senior 1978), indicates that weathering began earlier (Late Eocene) in the Alice Springs region, compared to a Late Oligocene or Early Miocene age for the Canaway profile.

X-ray diffraction and X-ray fluorescence studies (Senior 1972) have shown that the profile developed through *in situ* rock decomposition, liberation of alkali and alkaline earth metals (K, Na, Ca, Mg) as well as leaching of silica, accompanied by concentration of iron and aluminium oxides in addition to hydroxides. In general, iron oxide concentrations increase upwards, reaching 40 per cent or more in the ferruginous zone. The abundances of SiO_2 in the leached and mottled zones are similar, but in the ferruginous zone SiO_2 is markedly reduced.

Bundey Basin

The name 'Bundey Basin' is applied to a sedimentary fill up to 40 m thick, intersected in water bores along the Bundey River in the Huckitta 1:250 000 Sheet area (Fig. 1). These deposits consist of siltstone and claystone with interbedded sandstone and conglomerate beds. Drilling by the Northern Territory Geological Survey in 1982 intersected chalcedonic limestone at shallow depths and most of the rocks in the water bores may be regarded as Waite Formation equivalents or unit TQt (Freeman 1986). However, cored hole NTGS HUC11, on the Huckitta 1:250 000 Sheet Area, intersected partly carbonaceous siltstone, then sandstone and siltstone to a total depth of 127 m. This thickness exceeds that of other Cainozoic sedimentary rocks in the Bundey Creek region. Preliminary palynological determination (Truswell 1987; Freeman 1986) suggested that the carbonaceous siltstone accumulated in the Paleocene. However, the carbonaceous claystone contains many undescribed pollen types, including forms morphologically similar to species that Harris & Twidale (1991) now consider to be Late Cretaceous, described from lignitic sedimentary rocks above the basement between Ayers Rock and the Olgas, and the material from HUC11 could well be just as old.

Aremra Basin

The Aremra Basin, in the southwestern part of the Illogwa Creek 1:250 000 Sheet area (Figs 1 & 8), is known only from the subsurface; it is named after Aremra Creek. The basin appears to extend from just west of Gidyea Bore southwards, for 80 km or more, along the eastern margin to ranges of metamorphic rocks bordering Illogwa Creek. Structurally, it comprises flat-lying beds that occupy a southeast-trending depression centred on the present-day position of Aremra Creek.

The succession in the Aremra Basin, referred to as unit Ta, is similar to that in the Ti-Tree and Waite Basins (Alcoota and Napperby 1:250 000 Sheet areas). Ta rests unconformably on schists and gneisses of the Arunta Block (BMR Illogwa Creek 2), except in the southeast, where it probably rests unconformably on the Hooray Sandstone, a Late Jurassic and Early Cretaceous unit within the Eromanga Basin succession. Ta is overlain, probably conformably, by Waite Formation equivalents (Tw) and by unconsolidated Quaternary deposits.

The oldest lithological components in the basin are claystone and interbedded sandstone. The massive nature of the claystone suggests quiet-water deposition; there is a lack of terrigenous detritus from the nearby ranges. These rocks pass abruptly upwards into poorly sorted clastics deposited as a series of coalescing piedmont fans. The clastics are intensely weathered and contain abundant iron oxide pisoliths. The succession is capped by a thin veneer of chalcedonic calcarenitic limestone (Tw), which is more extensive in the east, where it caps weathered metamorphic rocks. As this basin provides an additional key reference section for Cainozoic stratigraphy in the Alice Springs region, it is described in some detail below. A generalised stratigraphy is given in Figure 9.

Deep-weathering profiles in the Aremra Basin region. (Tl, Tla, Tlf, Illogwa Creek Sheet area)

As mapped, Tl is a composite unit, incorporating several weathering events. These profiles are most extensively developed north and west of the Aremra Basin (Fig. 8). They are best preserved along the interfluve between Huckitta and Atula Creeks, forming scattered exposures in the flatter eastern two-thirds of Illogwa Creek 1:250 000 Sheet area, away from the higher ranges.

The most widespread and probably oldest weathered profile (Tla, Tlf) is up to 30 m thick and trizonal, comprising a lowermost kaolinised zone, an intermediate mottled zone, and a ferruginous top. It is correlated with an identical profile in the Alcoota 1:250 000 Sheet area (see above and Senior 1972), suggesting former continuity between these two regions. Decomposed, soft kaolinitic metamorphics of the Arunta Block, which may have been affected by the same weathering event, were intersected below the unnamed Cainozoic sediments (Ta) in BMR Illogwa Creek 1 and 2. The marked ferruginisation that is widely developed on the Mesozoic Hooray Sandstone is also correlated with this deep weathering profile (Senior in Shaw et al. 1982).

In addition, several younger periods of intensive oxidation leading to weathered profile development are recorded within unit Ta in the Aremra Basin, indicating that intense weathering continued during deposition. Of these profiles, the one associated with the strongest oxidisation (affecting subunit Ta_3, see below) is correlated with Tl. The formerly extensive Tl weathering profiles were buried in the Miocene or Early Pliocene by lacustrine and fluvial sediments of the Waite Formation. The tops of mesas of Waite Formation equivalents (Tw) and the underlying weathered profile, dip gently southwards, diminishing in relief until they become concealed by Quaternary and recent aeolian sands around the northwest edge of the Simpson Desert.

The revision of weathering chronology on rocks sampled for palaeomagnetic study and described above, suggests a Late Eocene date for the main period of ferruginisation.

Unnamed Cainozoic sedimentary rocks and sediments (Ta) (after Senior in Shaw et al. 1982)

These consist of soft, red and green siltstone, claystone, and friable lithic sandstone, with lesser amounts of quartzose sandstone and conglomerate. Carbonaceous

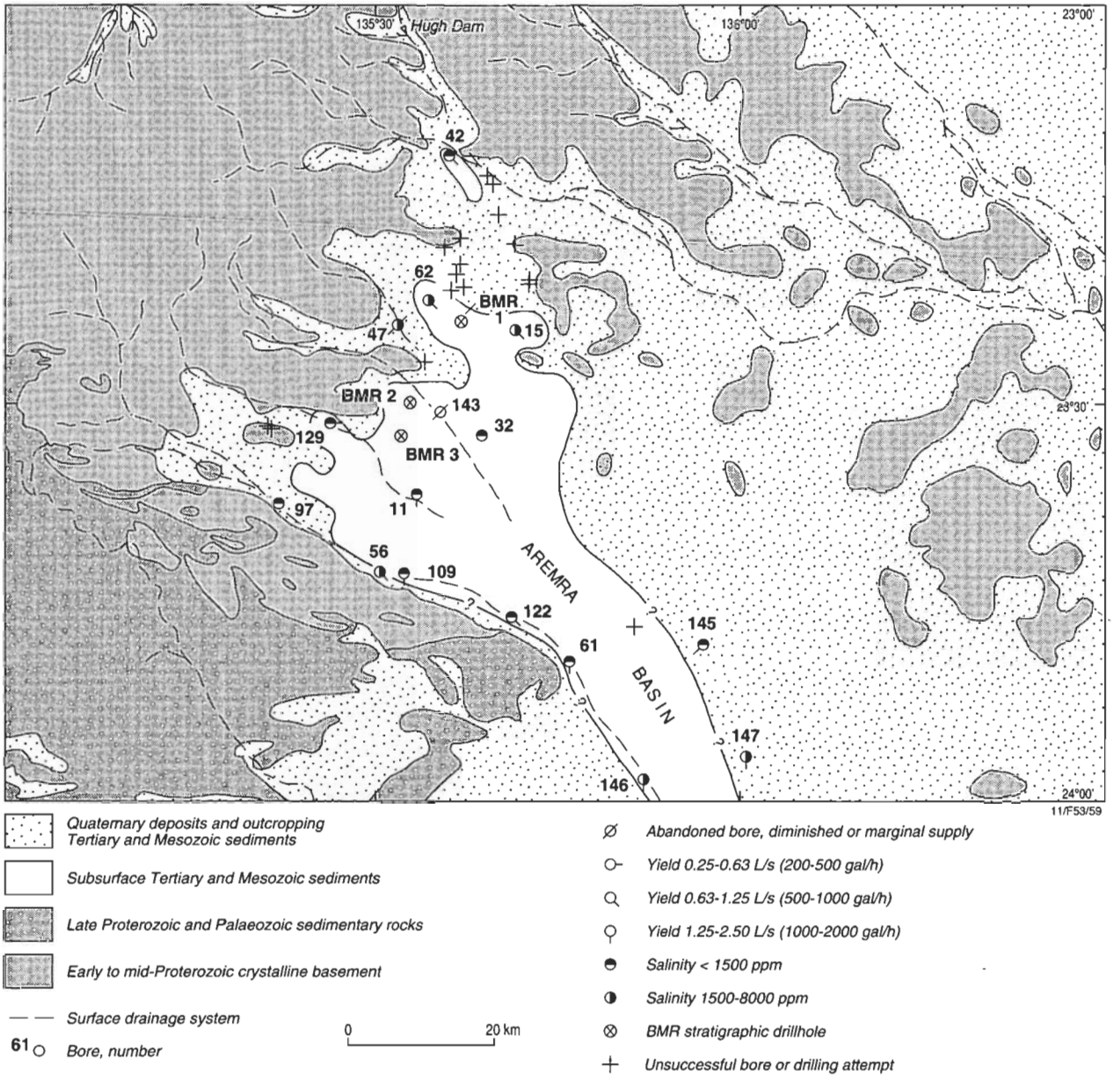

Figure 8. Sketch map of Cainozoic sediments in the Illogwa 1:250 000 Sheet area, showing the approximate outline of the Aremra Basin and details of drilling for groundwater.

matter, gypsum, and ironstone are present locally. Calcareous lenses and pedoliths occur at shallow depths. The unit is up to 250 m thick in drill holes. It grades upwards into either Waite Formation equivalents (Tw) or unconsolidated aeolian and alluvial Quaternary sediments (Qs, Qa, Qr).

The succession is divided into five units on the basis of drilling results from 18 holes by Agip Nucleare (1977, 1979), and cores from three holes by BMR (Fig. 9) and one by the Northern Territory Mines Department. From the base upwards these are:

- Unit 1 (Ta_1) is up to 20 m thick, but commonly much thinner. It consists mainly of iron-oxide-enriched sedimentary rocks, minor silcrete developed in quartz sandstone, and minor white or greenish claystone. The rocks comprise ferruginised red-brown and yellowish claystone interbedded with reddish quartzose sandstone. A lacustrine environment with fluviatile incursions is inferred from the variety of rock types, possibly reflecting a humid climate with dry intervals resulting in oxidation and silicification.

- Unit 2 (Ta_2) is dominated by an olive and green claystone with interbeds of quartzose sandstone and minor red-brown siltstone. Gypsum and carbonaceous fragments are present locally. Ta_2 is up to 144 m thick and grades upwards, through a mottled zone, into unit 3. Lacustrine and pediment distributary fan and plain accumulations are the likely depositional environments. Periods of desiccation resulted in the formation of gypsum. The presence of carbonaceous material and oil shale suggests that vegetation and abundant aquatic organisms were present in marginal swamplands.

- Unit 3 (Ta_3) comprises oxidised red-brown silty and clayey sandstone intercalated with minor layers of quartzose sandstone. These clastics contain fragments of ironstone derived from weathered profiles and rare

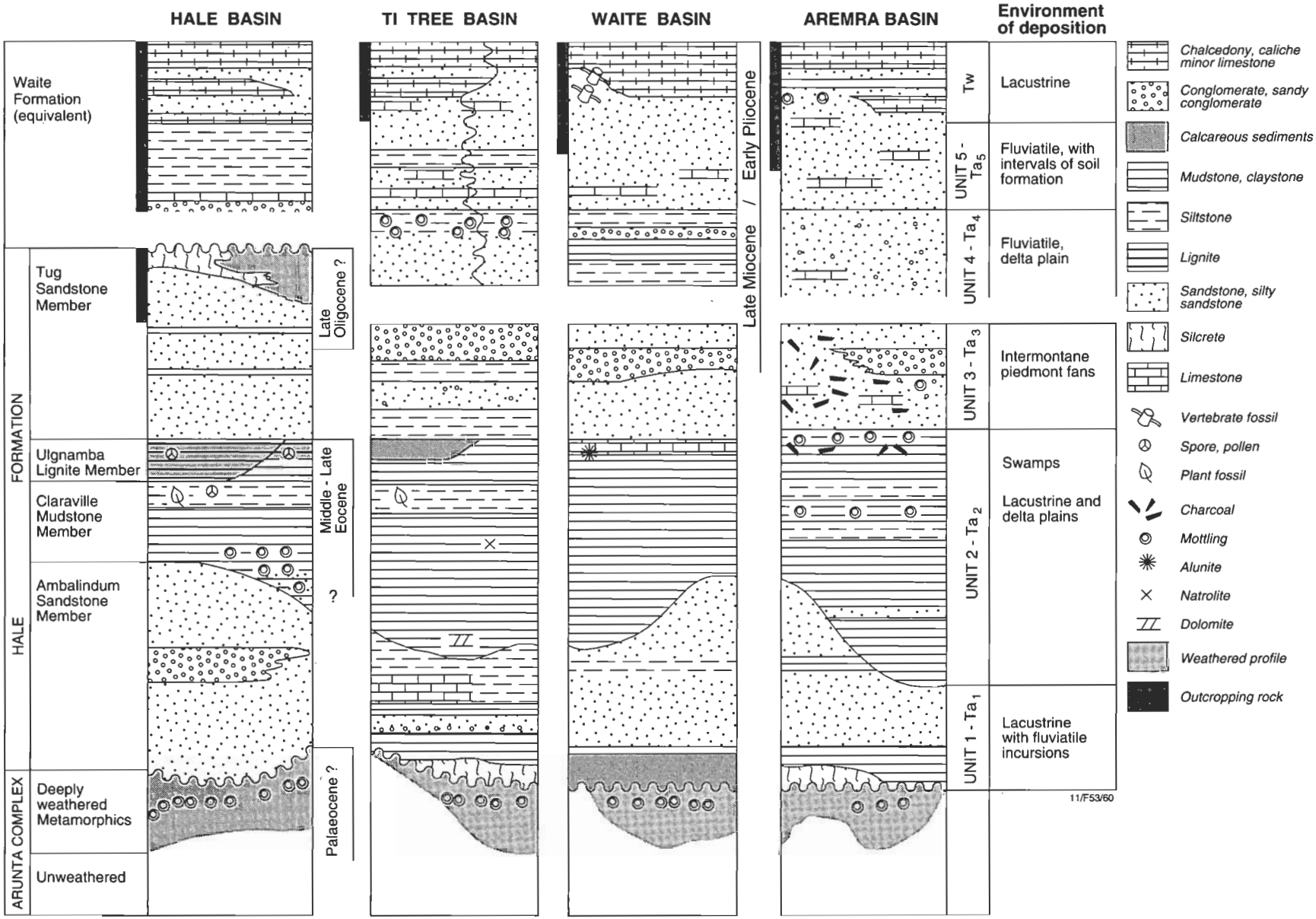

Figure 9. Diagrammatic correlation model for Tertiary units overlying the eastern part of the Arunta Block.

carbonaceous matter. The unit varies in thickness from less than 20 m (IR6 & IR9) to more than 100 m (IR11 & IR12). A prominent coarse quartz sandstone, 10–15 m thick, is widespread, generally at depths of 50–60 m. Rapid filling in intermontane piedmont fans is suggested by the poorly sorted nature of the sedimentary sequence. This would be consistent with an arid climate and sparse vegetation on the Harts, Strangways and MacDonnell Ranges, and rapid erosion in highland source regions. However, such a sedimentary facies would also equate with pluvial conditions in a humid climate. Concurrent tectonic movement is suggested by the tilted peneplain remnants forming concordant summit levels in the western hill country of the Illogwa Creek 1:250 000 Sheet area.

- Unit 4 (Ta_4) is widely distributed and consists of up to about 20 m of medium, coarse, or very coarse quartz–lithic sandstone. The sandstone is generally clean but in places may have a matrix of brown clay. Dominantly fluviatile deposition in a tributary and/or distributary drainage system is inferred by the widespread and generally matrix-free nature of the sandstones. These sediments appear to become increasingly fine-grained towards the axis of the basins, as is indicated by the dominantly fine clastic and lutitic sequence encountered at 10–40 m in BMR DDH 1. Stringers of coarse sandstone and conglomerate indicate periodic fluvial incursions in channel-like watercourses.

- Unit 5 (Ta_5), the uppermost unit, consists of intensely oxidised, red-brown silty sandstone with thin calcareous layers and nodules of probable pedogenic origin. Plant fragments were noted at a depth of 18 m in BMR Illogwa Creek 3. Ta_5 varies in thickness between 4 and 15 m. Lower energy fluviatile conditions are implied by the siltstone–sandstone facies. Lengthy periods of non-deposition, soil formation, and precipitation of calcareous materials are suggested by the oxidised nature of the sediments and the calcareous layers. The intensely oxidised nature of the sediments and precipitation of chalcedony may reflect seasonal rainfall under a dominantly arid climate.

Unit Ta is correlated with deposits, also mapped as Ta, in the Waite Basin and elsewhere (see above). For example, Ta_1 contains a minor silcrete at the base of the succession in the Aremra Basin and may equate with the very resistant silcrete (possibly Late Cretaceous in age) encountered below a thick green claystone–siltstone succession in BMR Alcoota 20 (i.e. in the Ti-Tree Basin, Alcoota Sheet area; Fig. 7; Shaw et al. 1979b). In addition, Ta_1 of the Aremra Basin has equivalents elsewhere in the region. For example, similar green claystones and siltstones lie stratigraphically below Mid–Late Eocene lignite and carbonaceous siltstone in the Hale Basin in the Alice Springs 1:250 000 Sheet area and in the southwestern part of the Ti-Tree Basin in the Alcoota 1:250 000 Sheet area (see above).

An early Tertiary or slightly older age is implied for the onset of deposition of Ta_1 following silcrete formation. The green claystone and siltstone unit (Ta_2) is considered to be Eocene, which is the age inferred for the lithologically similar Delaney Mudstone Member (Thc) below the Mid–Late Eocene lignite in the Hale Basin (see above; Truswell & Marchant 1986). Weathered elements in Ta_3 may correlate with weathering event C in the Hale Basin (Fig. 4), where palaeomagnetic data give Late Eocene as the most likely magnetic age. Although Tw appears to conformably overlie these units (Ta_{1-5}) it is possible they may be equivalent to or, in the case of Ta_5, slightly younger than Tw, as they occupy a stratigraphically lower position in the more depressed part of the basin. Thus, deposition of Ta_4 to Ta_5 may overlap in time with the deposition of the Waite Formation, which is Late Miocene or Early Pliocene.

Waite Formation equivalents (Tw)

The Waite Formation equivalents (Tw) consist of red and green silty sandstone with irregular calcareous nodules, travertine, calcarenitic and some pelletoidal limestone, and massive chalcedony. Up to 35 m of the unit is exposed on the rim of the Aremra Basin in the Illogwa Creek 1:250 000 Sheet area. Drill holes show that this formation grades downwards into unnamed poorly sorted sandstones and mudstones more than 200 m thick (Ta).

Tw forms extensive plateaus, mesas and rounded pinnacle-like hills. Its characteristic pale tones on aerial photographs are due to the presence of pale grey to whitish chalcedony layers, which are prevalent in the upper part of this formation. Upstanding landforms have flat summits and prominent bounding escarpments formed by beds of resistant chalcedony. Summit levels slope gently southwards, reflecting regional down-warping towards the broad Cretaceous and Cainozoic depression of the Lake Eyre Basin.

Beds within the unit are flat-lying. They consist of interbedded, reddish or greenish silty sandstone, sandstone, siltstone, and minor sandy conglomerate. Reworked clasts of ferruginous pisoliths and angular, conglomeratic, ferruginous fragments occur near the base, particularly where the formation overlies the weathered profile in Arunta basement rocks. In some places, chalcedonic layers are interbedded with fine sandstone, siltstone and mudstone lenses. The multiplicity of chalcedonic layers and the lack of clastic detritus indicate that they were formed by the precipitation of silica, possibly in shallow alkaline lakes or within groundwater discharge areas.

The unit is thought to represent an extensive sedimentary succession deposited in rivers and lakes (cf. Woodburne 1967). It overlies deeply weathered Arunta basement rocks in many areas, notably north of the Aremra Basin, north and east of Hugh Dam (Fig. 8). Elsewhere, Tw grades down into unnamed Tertiary sedimentary rocks (Ta).

Tw contains calcified plant debris. It is correlated with the Waite Formation, which is probably Late Miocene at its type section in the Alcoota region (Woodburne 1967).

Discussion

Stratigraphic framework

Although there is gross lithological similarity between the successions in the basins of the Alice Springs area, detailed correlation has been hampered by the weathering of many rock types and the lack of fossils. The lithological distribution in subcrop suggests that the Ti-Tree, Waite, and Aremra Basins were formerly interconnected. The Hale Basin evolved as a separate, isolated feature; it is used as a key reference section because of the better stratigraphic control established there. Dating within the basins is hampered by the poor recovery of palynomorphs from the largely weathered sediments, with only a few

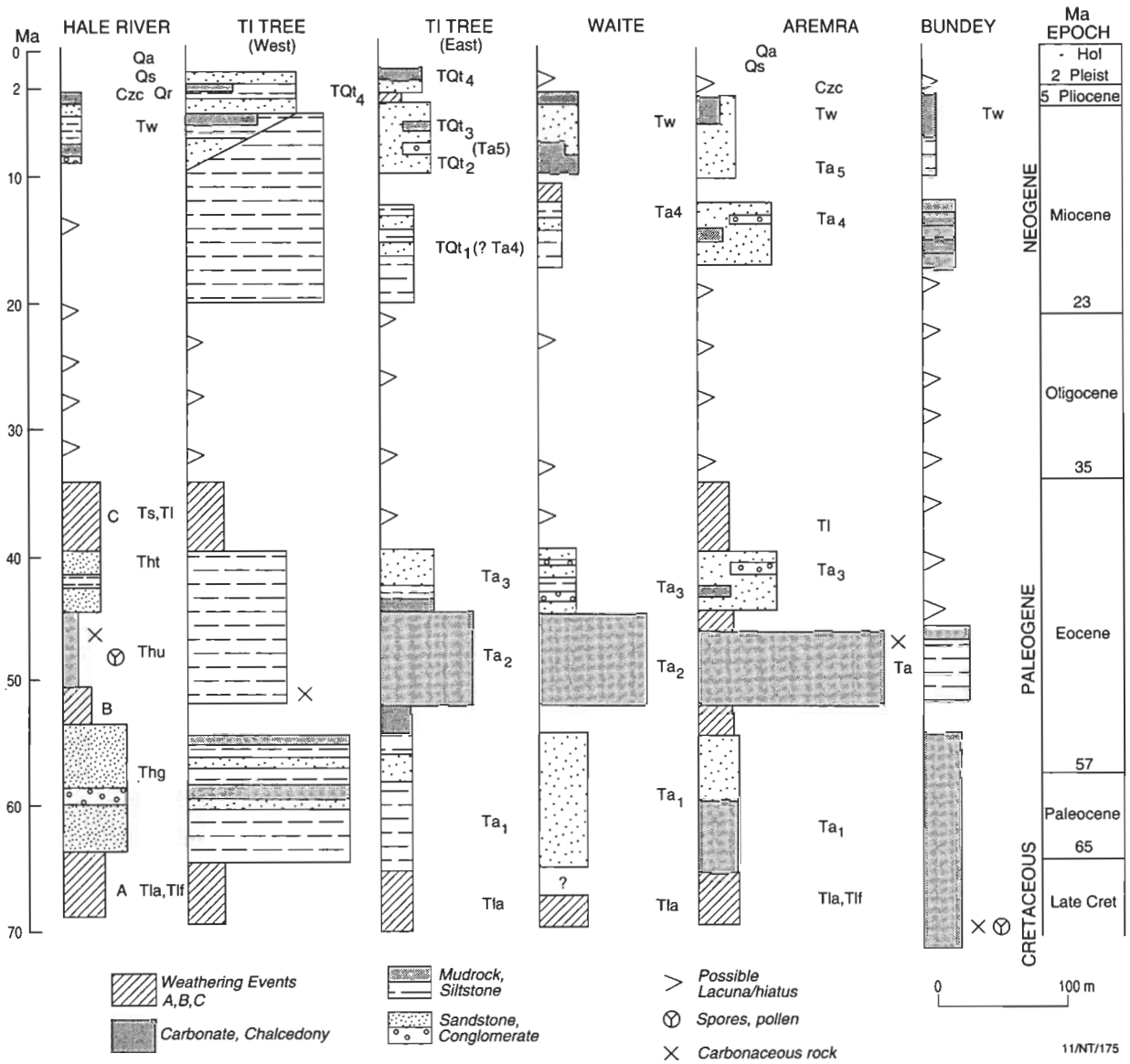

Figure 10. Interpretative time/depth plots for Cainozoic sedimentary units within the main basins overlying the eastern part of the Arunta Block. The timescale (Ma) is that of Harland et al. (1990).

sites yielding spores and pollen.

Although the Hale Basin evolved separately, it has a succession broadly comparable to the basins lying north and east of the Strangways and Harts Ranges (Fig. 1). Of particular interest is an olive-green mudstone unit present in most of the basins. In the Hale Basin, this mudstone grades upwards into a lignite-bearing carbonaceous succession; both the lignite and mudstone contain a rich flora of probable Mid to Late Eocene age. Widely distributed olive-green mudstone units in many of the basins (Fig. 9) possibly correlate with the mudstone in the Hale Basin and suggest the presence of a series of interconnected lakes and swamps during the Mid to Late Eocene.

Younger rocks in these basins consist of oxidised, coarse-grained, poorly sorted sandstone (e.g. Ta_3, Tht), which may have been rapidly deposited in coalescing piedmonts. The weathered profile in these sediments in the Hale Basin records the same Late Eocene magnetic age as weathered profiles preserved on topographically high residuals of Arunta basement. Tectonism and a hiatus in sedimentation may have preceded the deposition of younger sediments because the sites of deposition shifted in some regions. Late Miocene to Early Pliocene fossils reflect a diverse fauna of primitive marsupials, crocodiles, ringtail possums and other vertebrates and invertebrates, suggesting a change to lacustrine environments, probably with vegetated margins, during which interbedded red and green clayey siltstone, sandstone and lacustrine carbonate accumulated (e.g. Tw, TQt). These rocks are now protected from rapid erosion by resistant cappings of chalcedony, and thereby form low plateaus bounded by steep scarps. Sub-surface sedimentary rocks (units Ta_4, Ta_5) comprise some probable pedogenic ferruginous and calcareous layers and may be either equivalent to these lake deposits (i.e. Tw) or represent a longer period characterised by restricted intermittent deposition punctuated by episodes of exposure and erosion.

Figure 10 represents an evolutionary model for the depositional episodes, plotted in terms of current understanding of correlations, inferred age, and rates of deposition. It shows time versus thickness diagrams for the Tertiary segment of basin deposition. The plot is

based on the lithological correlations shown in Figure 9, on presumed breaks in the sedimentary record, corresponding to periods of deep weathering in the Hale Basin (Figs 4 & 5), and, to a lesser extent, on possible correlation with weathering profiles dated palaeomagnetically in the Eromanga Basin (Idnurm & Senior 1978). The time slices adopted are consistent with the international time-scale of Harland et al. (1990), but boundaries are poorly constrained.

The most rapid sedimentation appears to have been in the Palaeogene during deposition of the mudrock unit (Ta_2). Although the order-of-magnitude accumulation rate of 1–15 m/Ma is slow, it is nevertheless within the range of rates recorded in intracratonic basins (cf. Schwab 1986). In order to maintain consistent rates of sediment accumulation, a major break is needed between Paleogene and Neogene sedimentation phases. The apparent lack of a weathered profile equivalent to the Late Oligocene to Early Miocene Canaway profile in the Eromanga Basin in southwest Queensland, may mean that the Oligocene to Early Miocene was a period of active erosion and possibly uplift in central Australia. The plot provides a model for the stratigraphic framework to be tested and refined by future work.

Chronology of chemical weathering

At least two main periods of intense chemical weathering can be identified in the central Australian basins. The first is represented by a relict profile in the Hale Basin, developed near the top of the Hale Formation (weathering event C in Figs 4 & 5). This profile has a Late Eocene preliminary palaeomagnetic age, consistent with a Middle to Late Eocene palynological age for the underlying Ulgnamba Lignite Member (Truswell & Marchant 1986). Its possible age equivalents are found in other Cainozoic basins in central Australia. Examples include thickly weathered intervals in Cainozoic successions intersected by drilling in the Yaloogarie (Stewart 1976) and Ti-Tree Basins (O'Sullivan 1973). An exposed possible equivalent is in breakaways along the northern flanks of the MacDonnell Ranges (unit Tlf of Warren & Shaw 1993). Palaeomagnetic dates suggest ferruginisation of the Arunta basement rocks in the region north of the Hale Basin during the same period, implying that the basement there was exposed.

The second, older weathering period is represented by relict weathered profiles developed in the Arunta basement rocks. In the Bundey and Ayers Rock Basins, their maximum age, obtained by palynological evidence in overlying sediments (Truswell 1987), is either Palaeocene or Late Cretaceous (Harris & Twidale 1991). Similar weathered profiles are widespread in the Arunta basement where it is covered by Cainozoic sediments, including the Hale Basin (weathering event A in Figs 4 & 5). It is possible that basement weathering through central Australia may record the same earliest Tertiary or older event.

In addition to the two main weathering periods, variously oxidised, mottled, silicified, and partly calcified rocks in several of the basin successions indicate other lesser periods of interrupted sedimentation and intense weathering. Examples of such intervals are weathering event B in the Hale Basin (Figs 4 & 5), paleosols at several levels in unit Ta5 in the Aremra Basin, the chalcedonic top of Tw, and the markedly oxidised soils of Qr.

Some weathering events in central Australia may have extended to adjacent regions. In particular, the older period of weathering may be represented in the Eromanga Basin by the Morney profile, dated palaeomagnetically as Late Cretaceous/Early Tertiary (Idnurm & Senior 1978). The same chemical weathering may have ferruginised the Mesozoic Hooray Sandstone along the northwestern margin of the Eromanga Basin and its equivalent in the Hay River 1:250 000 Sheet area. Similarly, weathering event B in the Hale Basin may correlate with an early Middle Eocene hiatus in the Eromanga Basin. On the other hand, the prominent Late Eocene weathering profile in the Hale Basin region (weathering event C) seems to have no age equivalent in the Eromanga Basin: the Canaway profile, which resembles the trizonal Hale Basin profile, has a poorly defined but distinctly younger (approximately Oligocene) palaeomagnetic age. More dates are needed to test the central Australian, as well as inter-regional, tentative correlations.

Palaeoenvironmental and palaeoclimatic implications

Palynological investigations in the Hale Basin have provided both age control and climatic information. Pollen assemblages from the lignites and the underlying green mudstones contain, as very rare elements, pollen types confined to the Mid to Late Eocene interval in southern Australian coastal basins. Pollen assemblages at Hale River are dominated by *Nothofagus* (*Brassospora* spp.), the southern beech, and by pollen of a number of podocarpaceous (southern conifer) genera, suggesting that rainforest trees grew in the vicinity, under conditions of high humidity. Pollen of Casuarinaceae occurs in all assemblages and, assuming that these were non-rainforest species, there may have been some open forest vegetation, possibly on lake margin sites. The pollen cannot, however, be distinguished from rainforest members of the family. Pollen of aquatic plants, reeds and sedges, is locally common.

The pollen suite from the Ulgnamba Lignite bears some resemblance to suites of probable Middle Eocene age described from the Lake Eyre Basin (Sluiter 1991), for which quantitative estimates of palaeoclimates have been made. Some of the Lake Eyre assemblages are similar in that there is a high frequency of *Nothofagus* pollen and Casuarinaceae, but they differ in having a considerable abundance of pollen of Myrtaceae and Cunoniaceae. The two localities are similar in having significant quantities of pollen of aquatic taxa.

Sluiter (1991) used the climatic parameters controlling modern forest taxa as the basis for palaeoclimate estimates. The underlying assumption is that the ecophysiologic characteristics that determine the broad climatic responses of the vegetation are unlikely to have changed through time. On this basis, it was estimated that the mean annual temperature in the Eocene of central Australia was 17–18°C, and the mean annual precipitation around 1500 mm. While the Lake Eyre and Hale Basin microfloras differ in some respects, they were comparable enough to allow conjecture that similar conditions may have pertained in the Hale Basin in the Eocene. A tentative reconstruction of climatic conditions is outlined in Table 2.

Tectonic implications

On a continental scale, changes in the patterns of

subsidence, including those in central Australia, appear to follow major phases of plate realignment and switches in the sites of sea-floor spreading (Table 2). The earliest recognised period of widespread deep weathering in central Australia may have begun in the Late Cretaceous and its termination may have been related to a broad uplift, affecting much of the continent. This uplift was greatest along the Eastern Highlands (see Veevers et al. 1991). Lister et al. (1986) suggested that this uplift of the Eastern Highlands was related to extension immediately prior to sea-floor spreading in the Tasman Sea. The central Australian intermontane basins may have been initiated at this stage or slightly later (i.e. units Ta_1, Thg; Table 2).

The succeeding phase of rapid Eocene infilling in the Cainozoic basins of central Australia (i.e. units Ta_2, Thu, Thc) appears to correspond to the rapid drift of Australia away from Antarctica (cf. Veevers et al. 1991). A major reorganisation of plate motions (Australian–Pacific plates) took place at about 43 Ma (i.e. in the late Mid-Eocene; see Wells 1989), and this event may correspond to minor tilting of piedmont fans (units Ta_3, Tht; see Table 2) as a result of limited doming of the ranges in central Australia. A period of more restricted deposition and widespread deep weathering followed in central Australia (units Tl, Ts and widespread overprinting of Tlf; Table 2). The end of widespread deep weathering is probably recorded by the Late Eocene magnetic date from the Hale Plain and surrounding region. More work is needed to clarify the timing, nature and correlation of these early Tertiary events.

In about the Oligocene, a widespread hiatus and a slight shift in the drainage systems in central Australia was accompanied by a switch in the sites of sedimentation (units Ta_4, TQt, then Tw; see Table 2). It is speculated that this period of apparent uplift of the central Australian ranges may be related to a rearrangement in the Pacific plate and the beginning of the northern Australian collision with Papua New Guinea at about 25–27 Ma (late Oligocene: see Kamp 1991; Etheridge et al. 1991). In this case, the hiatus may be the result of renewed, but slight, regional uplift and erosion of parts of the continent and may be related to compressional tectonism.

A similar, but later, compressional stress may explain the limited uplift of the central Australian ranges, which led to the major drainage reversal of the Sandover River. Tilting of the western MacDonnell Ranges, with some inferred uplift of the MacDonnell Ranges in the region of the Redbank Thrust Zone, probably took place in the latest Pliocene or earliest Pleistocene, as suggested by both the doming of earlier weathering profiles in the MacDonnell Ranges and, to a lesser extent, by the development of extensive fanglomerate deposits (e.g. unit Tuc, previously Czc as in Table 2). At this time, the duricrust capping the Late Devonian conglomerates, the Undandita Member (of the Brewer Conglomerate) appears to have been tilted along the western MacDonnell Ranges (Warren & Shaw 1993). The steep gradient to the Todd River and the beginning of dissection of the Sixteen Mile Basin (Fig. 1) may also date from this period. The inferred doming in the region of the MacDonnell Ranges seems to have been accompanied by subsidence in the region of the Lake Eyre Basin. The possibly Late Pliocene uplift of the MacDonnell Ranges was followed by a period of partial peneplanation and ferruginisation (unit Qr), which pre-dates the last phase of major erosion in the Holocene (units Qa, Qs, Ql, see Shaw & Wells 1983).

Implications for groundwater assessment

Some of the most productive aquifers within the Cainozoic sequences are commonly complex deeper channel sandstones, separated by claystone(and siltstone)-dominated aquicludes (e.g. unit TQt). They represent older drainage systems lying below the present drainage channels. Such aquifers have been investigated for their irrigation potential at Willowra (Morton 1965), and Kulgera (Woolley 1965a, b), the Farm-area Basin near Alice Springs (Woolley 1966; Quinlan & Woolley 1969), and Ti-Tree (McDonald 1988a, b). Groundwaters from these aquifers have variable low to high salt contents. Given the potential of this style of aquifer for recharge, these more permeable and porous upper parts of the Tertiary basins remain an important source for small to moderate renewable water supplies. Consequently, the identification and mapping of palaeodrainage systems within the Neogene fill remains an important target for future investigation.

The older Paleogene sedimentary rocks, lying at even greater depths (e.g. units Ta_2, Thu), tend to be dominated by claystone or mudstone, resulting in poor permeability. Similarly, deeply weathered bedrock generally yields only poor quality water, for which the quality and supply depend on the permeability of the weathered zone.

Future research

Stratigraphic studies need to be extended into the wider region, including the western Arunta Block, the Amadeus Basin and the Eromanga Basin. For example, similar basins overlying the western Arunta basement and the Palaeozoic and Late Proterozoic rocks of the Amadeus Basin should be more accurately delineated, using remote-sensing and techniques that estimate depths to magnetic basement. Further drilling is required in these western basins to see if basin development is similar to that in the eastern part of the Arunta Block. Analogous basins may also include the Horse Creek, Springvale, Marion, Austral Downs, and Noranside Basins, previously described by Paten (1964) in western Queensland. Comparison of sedimentary sequences throughout central Australia may enable a closer analysis of depositional environments and provide a basis for understanding continent-wide Cainozoic stratigraphic evolution.

Preliminary data reported here, together with geological mapping in the Hermannsburg 1:250 000 Sheet area (Warren & Shaw 1993), point to several future research topics concerning the Cainozoic geology of central Australia. These include:

- Detailed stratigraphic, lithologic, petrologic, and petrographic studies of the key successions to select sections suitable for developing models of past climatic regimes.
- A study of Cainozoic warping, as observed from tilted strata, and sediment distribution in relation to peneplain development. For example, the origin of intermontane basins with up to 300 m of sedimentary rocks implies some degree of extension. On the other hand, some compressional tectonism might be explained by the relationships between the exhumation history of peneplain surfaces along the MacDonnell Ranges and the growth and dissection of piedmont fans straddling the MacDonnell Ranges.

- A search for Permian and Mesozoic basins underlying the Cainozoic successions and assessment of their groundwater potential. Although only a thin Permian succession has been identified locally in the subsurface northeast of Haast Bluff (Truswell 1985), it is possible that a much thicker succession is preserved elsewhere. For example, it is likely that a considerable thickness, up to 300 m or more, of sedimentary rocks occurs along the BMR deep seismic line (J. Taylor, AGSO, personal communication, 1991).

- Reconstruction of the palaeogeography as the basis for an assessment of the presence of as yet unknown basin sequences. The extent and boundaries of the known basins are as yet incompletely understood.

- Recharge studies of the Tertiary basins to more accurately determine aquifer characteristics and potential yields of groundwater. For example, the Burt, Sixteen Mile, and Mount Wedge Basins (Fig. 1) deserve particular attention because of their proximity to Alice Springs. In the eastern Mount Wedge Basin, potential recharge is provided by the outwash and alluvial plains of the Derwent and Dashwood rivers. In the Burt Basin, potential for recharge is largely unknown and warrants a more detailed investigation.

- Regolith studies, including relationship of basins to landscape development.

- Further palaeomagnetic studies or implementation of $^{40}Ar/^{39}Ar$ weathered-rock dating techniques for improved age control. In addition, the use of oxygen and hydrogen isotopes should be explored for elucidating past climates, palaeolatitudes, and ages of weathering profiles.

Summary and conclusions

Analyses of Cainozoic sedimentary basin successions, supported by palynological and palaeomagnetic data, indicate two main episodes of deposition in several distinct basins.

- The first episode is represented by thick deposits that date from a Paleocene phase of basin infilling. Locally, as in the Ayers Rock Basin, an even earlier but less-widespread phase may have begun in the Late Cretaceous. Initial fluviatile sand deposition in several of the basins gave way, perhaps in the Middle Eocene, to widespread silt and mud accumulations in a series of interconnected lakes. Swamps and forests were prevalent at this time in regions such as that surrounding the Hale Basin. Then followed deposition of coarse lithic sands with derived weathered rock components, together with scattered woody debris and charcoal. Siliceous and calcareous rock types were chemically precipitated during this interval.

- The second episode of subsidence took place in the Late Miocene to Early Pliocene and was preceded by an extended period of hiatus, possibly spanning the Oligocene. This interval was characterised by deposition of sand, silt and clay, intercalated with calcareous and chalcedonic sediments, some of which appear to represent the products of weathering and groundwater processes.

Between these two episodes, the centres of deposition shifted, implying a change in the tectonic forces affecting the region. The Late Eocene magnetic date obtained for weathering event C is considered to record the time when weathering processes ceased over much of the region as a result of the implied tectonic rearrangement.

For a fuller understanding of the Cainozoic sedimentary sequences of central Australia, there is a particular need for better time control, through palynological and palaeomagnetic studies, as well as other techniques. Dating of clay minerals (e.g. illite, cryptomelane–hollandite) by K-Ar methods shows considerable promise, although possible age modification of the clays by diagenesis and weathering will need to be considered. Stratigraphic studies of clay minerals, using semi-quantitative techniques, may also allow greater precision in correlating sedimentary units and weathering events.

Extension of these techniques to basins surrounding those in central Australia would greatly assist in piecing together the continent-wide Cainozoic successions, leading to an improved knowledge of tectonics and palaeoclimates. Because of the generally poor outcrop, improved drilling techniques leading to better sample recovery would be of considerable benefit. Wireline logging of drill holes is considered essential for improved correlation of both rock units and weathered profiles.

A full assessment of resources in the Cainozoic units warrants further investigations. There is potential for sedimentary uranium, although investigations to date have been largely disappointing. These Cainozoic deposits may well conceal economic mineral deposits in the basement rocks, but geochemical mineral exploration is hampered by the poorly understood effects of deep weathering on chemical dispersal. The presence of potentially commercial lignite and oil shale in basins of comparable age and sedimentary facies, such as the massive Stuart and Rundle deposits in Queensland, means central Australia remains prospective for similar resources.

These basins represent also potential sources of sustainable water supplies for use by small communities or for irrigated agriculture. However, their recharge characteristics remain largely unknown.

Acknowledgements

This report has benefited from comments by Gerry Jacobson, Peter McDonald, Anne Walley, Geoff Hunt and Colin Pain. Four referees provided constructive criticism, namely, Libbie Lau, Graham Taylor, Gerry Wilford, and Mike Macphail. Karl Wolf, as editor, improved the manuscript further.

References

Agip Nucleare Australia Pty Ltd, 1977. Annual Report, Exploration Licence 1056, Illogwa Creek, July 1977. *Northern Territory Geological Survey, Open File Report* CR 77/82 (unpublished).

Agip Nucleare Australia Pty Ltd, 1979. Final Report, Exploration Licence 1056, Illogwa Creek, July 1979. *Northern Territory Geological Survey, Open File Report*, CR 79/63 (unpublished).

BMR Palaeogeographic Group, 1990. *Australia, evolution of a continent*. Bureau of Mineral Resources, Geology and Geophysics, Canberra.

Calf, G.E., McDonald, P.S. & Jacobson, G., 1991. Recharge mechanisms and groundwater age in the Ti–Tree Basin,

Northern Territory. *Australian Journal of Earth Sciences*, 38, 299–306.

Clarke, D., 1975. The Hale River Basin. Alice Springs 1:250 000 Sheet area, SF/53–14, NT, Report 1. Preliminary Review. *Northern Territory Geological Survey Report* G.S. 75/13 (unpublished).

Edworthy, K.J., 1966. Preliminary appraisal of the Ti-Tree groundwater basin, Northern Territory. Report of the Resident Geologist's Office for the Mines Branch, Northern Territory Administration, Alice Springs (unpublished).

Etheridge, M., McQueen, H. & Lambeck, K., 1991. The role of intraplate stress in Tertiary (and Mesozoic) deformation of the Australian continent and its margins: key factor in petroleum trap formation. *Exploration Geophysics*, 22, 123–128.

Freeman, M.J., 1986. Huckitta, Northern Territory 1:250 000 geological series (2nd edition). *Northern Territory Geological Survey, Australia, Explanatory Notes*, SF/53–11.

Galloway, R.W. & Kemp, E.M., 1977. Late Cainozoic Environments in Australia. *Bureau of Mineral Resources, Australia, Record* 1977/40.

Harland, W.B, Armstrong, R.L., Cox, A.V., Craig, L.E., Smith, A.G. & Smith, D.G., 1990. *A geologic time-scale 1989.* Cambridge University Press, Cambridge.

Harris, W.K. & Twidale, C.R., 1991. Revised age for Ayers Rock and the Olgas. *Transactions of the Royal Society of South Australia*, 115(2), 109.

Hays, J., 1967. Landsurfaces and laterites in the north of the Northern Territory. *In* Jennings, J.N. & Mabbutt, J.A. (editors), *Landform studies from Australia and New Guinea.* Australian National University Press, 144–181.

Hughes, F.E. & O'Sullivan, K.N., 1973. Final Report, EL 52, Woola Downs, N.T., CRA Exploration Pty Ltd Report 73/009. *Open File Report, N.T. Geological Survey*, NT 53–10 (unpublished).

Idnurm, M., 1985. Late Mesozoic and Cenozoic palaeomagnetism of Australia—I. A redetermined apparent polar wander path. *Geophysical Journal of the Royal Astronomical Society*, 83, 399–418.

Idnurm, M., 1994. New Late Eocene pole for Australia, time-averaging of remanence directions, and palaeogeographic reference systems. *GeophysicalJournal International*, 117, 827–833.

Idnurm, M. & Senior, B.R., 1978. Palaeomagnetic ages of weathered profiles in the Eromanga Basin, Queensland. *Palaeogeography, Palaeoclimatology, Palaeoecology*, 24, 263–277.

Jacobson, G., Lau, G.C., McDonald, P.S. & Jankowski, J., 1989. Hydrology and groundwater resources of the Lake Amadeus and Ayers Rock region, Northern Territory. *Bureau of Mineral Resources, Australia, Bulletin* 230, 70 pp.

Kamp, P.J.J., 1991. Late Oligocene Pacific-wide tectonic event. *Terra Nova*, 3, 65–69.

Kemp, E. M., 1976. Early Tertiary pollen from Napperby, central Australia. *BMR Journal of Australian Geology & Geophysics* 1, 109–114.

Litchfield, W.H., 1969. Soil surfaces and sedimentary history near the MacDonnell Ranges, Northern Territory. *CSIRO Publication* 25.

Lister, G.S., Etheridge M.A. & Symonds, P.A., 1986. Detachment faulting and the evolution of passive continental margins. *Geology*, 14, 246–250.

Lloyd, A.R., 1968. Outline of the Tertiary geology of Northern Australia. *In* Palaeontological papers, 1965. *Bureau of Mineral Resources, Australia, Bulletin* 80, 105–132.

Mabbutt, J.A., 1967. Denudation chronology in central Australia. Structure, climate, and landform inheritance in the Alice Springs area. *In* Jennings, J.N. & Mabbutt, J.A. (editors), *Landform studies from Australia and New Guinea.* Australian National University Press, Canberra, 144–181.

McDonald, P.S., 1988a. Groundwater studies, Ti-Tree Basin, 1984–1988. *Northern Territory Government, Power and Water Authority, Report* 1/90.

McDonald, P.S., 1988b. Groundwater resources of the central Ti-Tree Basin. M.Appl.Sc. thesis, University of New South Wales, Sydney (unpublished).

Morton, W.H., 1965. The occurrence of groundwater suitable for irrigation, Willowra Station, Northern Territory. *Bureau of Mineral Resources, Australia, Record* 1965/146.

Ollier, C.D., Chan, R.A., Craig, M.A. & Gibson, D.I., 1988. Aspects of landscape history and regolith in the Kalgoorlie region. *BMR Journal of Australian Geology & Geophysics*, 10, 309–321.

Ollier, C.D. & Galloway, R.W., 1990. The laterite profile, ferricrete and unconformity. *Catena*, 17, 97–109.

O'Sullivan, K.N., 1973. Stratigraphic drilling, Ti-Tree area, Northern Territory. *CRA Exploration Pty Ltd, Northern Territory Geological Survey, Open File Report* NT 168 (unpublished).

Paten, R.J. 1964. The Tertiary geology of the Boulia region western Queensland. *Bureau of Mineral Resources, Australia, Report* 77.

Perry, R.A., Mabbutt, J.A., Litchfield, W.H., Quinlan, T., Lazarides, M., Jones, N.O., Slatyer, R.D., Stewart, G.A., Bateman, W. & Ryan, C.R., 1962. General report on lands of the Alice Springs area, Northern Territory, 1956–57. *Scientific and Industrial Research Organisation, Melbourne, Land Research Series*, 6.

Quinlan, T., & Woolley, D.R., 1969. Geology and hydrology, Alice Springs town and inner farm basins, Northern Territory. *Bureau of Mineral Resources, Australia, Bulletin* 89, 64 pp.

Schwab, F.L., 1986. Sedimentary 'signatures' of foreland basin assemblages: real or counterfeit? *International Association of Sedimentologists, Special Publication* 8, 395–410.

Senior, B.R., 1972. Cainozoic laterite and sediment in the Alcoota Sheet area, Northern Territory. *Bureau of Mineral Resources, Australia, Record* 1972/47.

Senior, B.R., & Mabbutt, J.A., 1979. A proposed method of defining deeply weathered rock units based on regional geological mapping. *Journal of the Geological Society of Australia*, 26, 237–254.

Senior, B.R., Mond, A. & Harrison, P.L., 1978. Geology of the Eromanga Basin. *Bureau of Mineral Resources, Australia, Bulletin* 167.

Senior, B.R., Truswell, E.M., Idnurm, M., Shaw, R.D. & Warren, R.G., (in press). Cainozoic sedimentary basins in the Alice Springs region: records of drilling and reconnaissance geology. *Australian Geological Survey Organisation, Record.*

Shaw, R.D. & Langworthy, A.P., 1984. Strangways Range Region, Northern Territory. *Bureau of Mineral Resources, Australia, 1:100 000 Geological Map Commentary.*

Shaw, R.D. & Warren, R.G., 1975. Alcoota, Northern Territory, 1:250 000 geological series. *Bureau of Mineral Resources, Australia, Explanatory Notes* SF/53–10.

Shaw, R.D. & Wells, A.T., 1983. Alice Springs, Northern Territory, 1:250 000 geological series (2nd edition).

Bureau of Mineral Resources, Australia, Explanatory Notes. SF/53–14.

Shaw, R.D., Langworthy, A.P., Offe, L.A., Stewart, A.J., Allen, A.R. & Senior, B.R., 1979a. Geological report on 1:100 000 scale mapping of the southeastern Arunta Block, Northern Territory. *Bureau of Mineral Resources, Australia, Record* 1979/47; *BMR Microform* MF133.

Shaw, R.D., Warren, R,G., Senior, B.R. & Yeates, A.N., 1979b. Geology of the Alcoota 1:250 000 Sheet area, Northern Territory. *Bureau Mineral Resources, Australia, Record* 1975/100; *BMR Microform* MF107.

Shaw, R.D., Freeman, M.J., Offe, L.A. & Senior, B.R., 1982. Geology of the Illogwa Creek 1:250 000 Sheet area, central Australia: preliminary data, 1979–80 surveys. *Bureau of Mineral Resources, Australia, Record* 1982/23; *BMR Microform* MF193.

Shaw, R.D., Rickard, M.J. & Stewart, A.J., 1984. Arltunga–Harts Range region, Northern Territory. *Bureau of Mineral Resources, Australia, 1:100 000 Geological Map Commentary.*

Shaw, R.D., Etheridge, M.A. & Lambeck, K., 1991. Development of the Late Proterozoic to Mid-Proterozoic, intracratonic Amadeus Basin in central Australia: a key to understanding tectonic forces in plate interiors. *Tectonics*, 10(4), 688–721.

Sluiter, I.R.K., 1991. Early Tertiary vegetation and climates, Lake Eyre region, northeastern South Australia. *In* Williams, M.A.J., De Deckker, P. & Kershaw, A.P. (editors), The Cainozoic in Australia: a reappraisal of the evidence. *Geological Society of Australia, Special Publication* 18, 99–118.

Stewart, A.J., 1976. Mount Theo, N.T. 1:250 000 geological series. *Bureau of Mineral Resources, Australia, Explanatory Notes* SF/52–8.

Stewart, A.J., Shaw, R.D., Offe, L.A., Langworthy, A.P., Warren, R.G., Allen, A.R. & Clarke, D.B., 1980a. Stratigraphic descriptions of named units in the Arunta Block, Northern Territory. *Bureau Mineral Resources, Australia, Record* 80/216; *BMR Microform* MF104.

Stewart, A.J., Offe, L.A., Glikson, A.Y., Warren, R.G. & Black, L.P., 1980b. Geology of the northern Arunta Block, Northern Territory. *Bureau of Mineral Resources, Australia, Record* 1980/83; *BMR Microform* MF152.

Truswell, E.M., 1985. Late Permian sediments in the Amadeus Basin, Northern Territory: a palynological examination. *Bureau of Mineral Resources, Australia, Professional Opinion* 85/003 (unpublished).

Truswell, E.M., 1987. Palynology of DDH HUC II, Huckitta Sheet area, Northern Territory. *Bureau of Mineral Resources, Australia, Professional Opinion* 87/002.

Truswell, E.M. & Harris, W.K., 1982. The Cainozoic palaeobotanical record in arid Australia: fossil evidence for the origins of an arid-adapted flora. *In* Barker, W.R. & Greenslade, P.J.M. (editors), *Evolution of the flora and fauna of arid Australia*, Peacock Publications, Frewville, South Australia, 67–83.

Truswell E.M. & Marchant, N.G., 1986. Early Tertiary pollen of probable Droseracean affinity from central Australia. *Special Papers in Palaeontology*, 35, 163–178.

Twidale, C.R. & Harris, W.K., 1977. The age of Ayers Rock and the Olgas, central Australia. *Transactions of the Royal Society of South Australia,* 101, 45–50.

Veevers, J.J., Powell, C.McA. & Roots, S.R., 1991. Review of sea-floor spreading around Australia. I. Synthesis of the patterns of spreading. *Australian Journal of Earth Sciences*, 38, 373–389.

Warren, R.G. & Shaw, R.D., 1993. Hermannsburg, N.T., 1:250 000 geological series. *Bureau of Mineral Resources, Australia, Explanatory Notes* SF/53–13.

Wells, R.E., 1989. The oceanic basalt basement of the Solomon Islands arc and its relationship to the Ontong Java Plateau—insights from Cenozoic plate motion models. *In* Vedder, J.G. & Bruns, T.R. (editors), Geology and offshore resources of Pacific island arcs—Solomon Islands and Bougainville, Papua New Guinea regions. *Circum-Pacific Council of Energy and Mineral Resources, Earth Science Series*, 12, 7–22.

Woodburne, M.O. 1967. The Alcoota fauna, Northern Territory. *Bureau of Mineral Resources, Australia, Bulletin* 87, 187 pp.

Woodburne, M.O., Tedford, R.H., Archer, M., Turnbull, W.D., Plane, M.D. & Lundelius, E.M., 1985. Biochronology of the continental mammal record of Australia and New Guinea. *Department of Mines and Energy, South Australia, Special Publication* 5, 347–363.

Woolley, D.R., 1965a. The availability of groundwater in Utopia irrigation area, Northern Territory—a preliminary proposal. *Bureau of Mineral Resources, Australia, Record* 1965/9.

Woolley, D.R., 1965b. Preliminary appraisal of the prospect of locating supplies of ground water suitable for Kulgera, N.T., town water supply. *Bureau of Mineral Resources, Australia, Record* 1965/79.

Woolley, D.R., 1966. Geohydrology of the Emily and Brewer Plains area, Alice Springs, N.T. Report of the Resident Geologist's Office, NT Administration, Alice Springs, *Northern Territory Geological Survey, Report* GS 66/2, 35 pp.

Woolnough, W.G., 1927. Presidential address. Part 1—The chemical criteria of peneplanation: Part 2—The duricrust of Australia. *Journal of the Royal Society of New South Wales*, 61, 17–53.

Yeates, A.N., 1971. Shallow stratigraphic drilling, western Eromanga Basin and Alcoota area, Northern Territory. *Bureau of Mineral Resources, Australia, Record* 1971/120.

AGSO Journal of Australian Geology & Geophysics, 15(4), 445–468

Oldest Cretaceous sequence, Giralia Anticline, Carnarvon Basin, Western Australia: late Hauterivian–Barremian

S. McLoughlin[1,6], D. W. Haig[1], J. Backhouse[2], M. A. Holmes[3], G. Ellis[4], J. A. Long[5] & K. J. McNamara[5]

Outcrop of the oldest Cretaceous sequence in the Giralia Anticline and the Giralia No. 1 well, penetrating the same sequence, are described and biostratigraphically assessed in detail. The Cretaceous rocks lie on an erosion surface cut into Permian strata. A 10 m thick basal sand unit, the Birdrong Sandstone, is overlain by 56 m of carbonaceous siltstone–mudstone (Muderong Shale). The Birdrong Sandstone in the anticline belongs to the *Muderongia australis* Zone of late Hauterivian–Barremian age, as does the lower part of the Muderong Shale. The age of the upper Muderong Shale is uncertain, as is the age of a 10 m thick sandstone unit (probable Windalia Sand Member) which separates the Muderong Shale from the late Aptian Windalia Radiolarite. Abundant fossil conifer wood, much of it with *Teredolites* borings, is present in outcrop referred to the upper part of the Birdrong Sandstone. Scattered ichthyosauran bones, probable plesiosauran remains, and rare ammonites also are present at this level. A growth-ring analysis of the wood suggests that a seasonal humid mesothermal climate prevailed in the region. Changes in sediment composition, palynomorph assemblages, and foraminiferal biofacies reflect retrogradation of marine facies during deposition of the Birdrong Sandstone and lowermost Muderong Shale, followed by aggradation through most of the Muderong Shale with maximum water depths less than 50 m. Within the sequence, the Birdrong Sandstone and the lowermost Muderong Shale represent a transgressive systems tract, whereas most of the Muderong Shale belongs to a highstand systems tract. The sequence reflects a transgressive pulse that was part of the progressive submergence of vast areas of the Australian continent during the Early Cretaceous. This late Hauterivian–Barremian transgressive pulse is recognised in widely separated basins and may represent a synchronous continent-wide sea-level rise.

Introduction

The Giralia Anticline forms a prominent feature on the Western Australian landscape south of Exmouth Gulf, extending along a north–south axis for over 100 km (Fig. 1; Condon et al. 1956; van de Graaff et al. 1980; Hocking et al. 1985). The structure, folded during the Neogene, exposes a stratigraphic record through about 50 Ma of Cretaceous time, from the late Hauterivian to the Maastrichtian (Fig. 2). The sediments accumulated on a broad continental shelf adjacent to the newly formed passive western continental margin and reflect marine events that are recognised over wide areas of the Australian continent. This paper describes the oldest Cretaceous sequence found in the anticline and a major marine flooding episode coincident with the marine inundation of vast areas elsewhere on the continent.

The oldest sequence in the Cretaceous of the Giralia Anticline lies unconformably above Permian strata of the Byro Group (Johnstone 1955) and includes a basal sandstone unit (transgressive systems tract) and an overlying shale formation (mainly highstand systems tract). Johnstone (1955) identified this stratigraphic succession as the Birdrong Sandstone overlain by the Muderong Shale. The Windalia Radiolarite, overlying the Muderong Shale, represents a distinct depositional sequence of late Aptian to early Albian age (Ellis 1993).

The transition within the Winning Group from shoreface sand to marine shale has been shown to be diachronous across the northern Carnarvon Basin (Wiseman 1979), proceeding from the late Valanginian on the North West Shelf (northern Barrow Sub-basin and central Dampier Sub-basin) to approximately Barremian (in terms of Helby

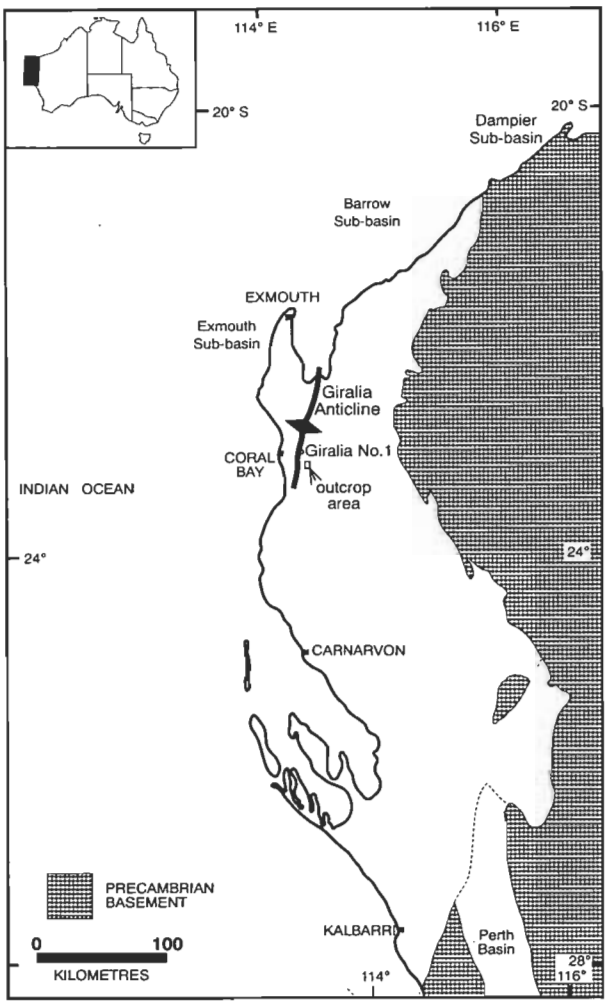

Figure 1. Carnarvon Basin, showing the extent of the Giralia Anticline, the location of Giralia No. 1, and the outcrop area (shown in detail on Fig. 6).

1 Department of Geology and Geophysics, University of Western Australia, Nedlands, WA 6009.
2 Geological Survey of Western Australia, 100 Plain Street, East Perth, WA 6004.
3 Department of Geology, University of Nebraska, Lincoln, Nebraska, 68588-0340, USA.
4 Institut de Géologie et Paléontologie, Université de Lausanne, CH-1014 Lausanne, Switzerland.
5 Department of Earth and Planetary Sciences, Western Australian Museum, Francis Street, Perth, WA 6000.
6 Present address: School of Botany, University of Melbourne, Parkville, Victoria, 3052.

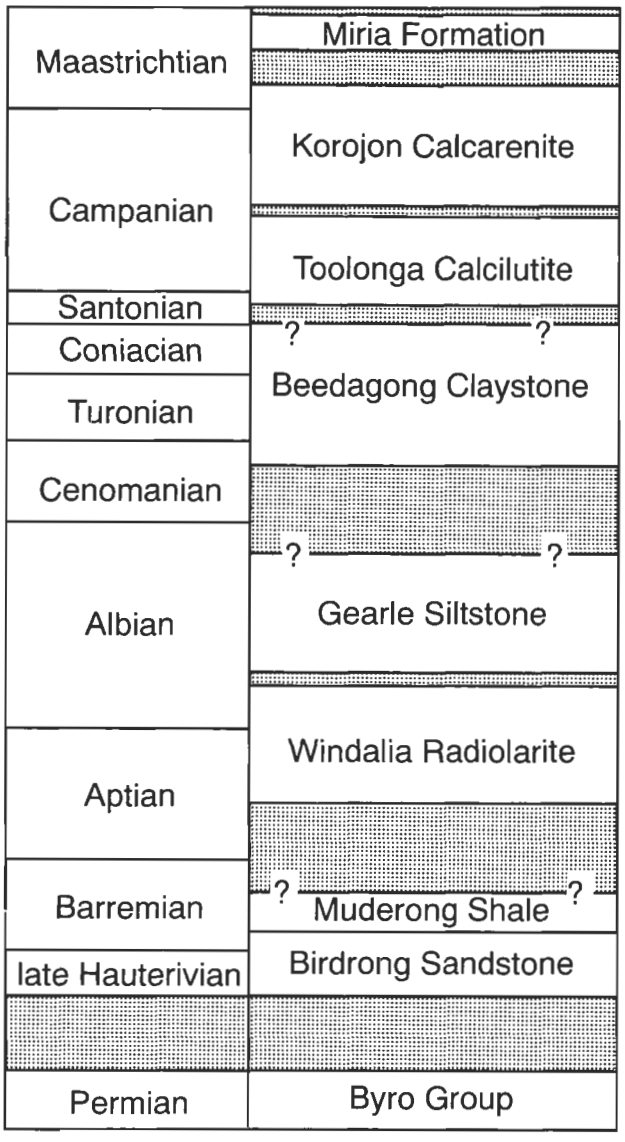

Figure 2. Cretaceous lithostratigraphy of the Giralia Anticline (modified from Condon et al. 1956; van de Graaff et al. 1980; Hocking et al. 1985; Shafik 1990; and our continuing studies).

et al. 1987) in parts of the present-day onshore Carnarvon Basin. The post-Valanginian physiography of the region was established by two main episodes of rifting (Malcolm et al. 1991). A Callovian–Oxfordian episode particularly affected the Barrow and Dampier Sub-basins, establishing a deep depocentre there, and resulted in continental breakup north of Exmouth Plateau. Berriasian to Valanginian rifting particularly affected the Exmouth Sub-basin, through uplift followed by sag, and resulted in continental breakup immediately west of the sub-basin. A widespread hiatus within the Valanginian, marking the end of the second phase of rifting, is present across the northern Carnarvon Basin. The marine Winning Group was deposited on this unconformity (Hocking 1988).

The Giralia Anticline region was part of a relatively stable continental platform during the Early Cretaceous, but was probably affected by transfer and associated tear faults during the Berriasian to Valanginian, as recognised in the adjacent Exmouth Sub-basin (Malcolm et al. 1991). Erosion down through Permian strata may have contributed sediment north to the delta complex of the Barrow Group during this time.

The post-Valanginian onlap of marine shales onto the continental platform presumably took place in a series of cycles reflecting changes in sediment-accommodation space, and resulted from a balance between eustatic sea-level changes, local tectonism, and the rate of sediment accumulation. The marine inundation of the continental platform in the Giralia Anticline region is reflected by the sequence described in this paper. The oldest marine units were previously known only from the few wells drilled in the anticline. During this study, we found outcrop in the central part of the anticline which we believe represents part of the oldest sequence, and we re-examined core material from the nearby WAPET Giralia No. 1 petroleum exploration well (Lat. 22°59′35″S, Long. 114°14′20″E). To determine if the cycle we recognise is reflected elsewhere on the Australian continent: (1) the unit in the central Giralia Anticline has been lithostratigraphically and biostratigraphically assessed in detail; (2) the bathymetry and regional climate have been interpreted from a variety of sedimentological and palaeontological criteria; and (3) comparisons have been made with coeval stratigraphic units elsewhere on the Australian continent.

Stratigraphic setting

The Cretaceous stratigraphy of the Giralia Anticline was outlined by Condon et al. (1956) and revised during later field mapping (van de Graaff et al. 1980; Hocking et al. 1985) and in the micropalaeontological study of Shafik (1990). The Cretaceous lithostratigraphic units are shown on Figure 2. Hocking (1988, 1990) grouped the Cretaceous formations into the following 'depositional sequences': the mainly siliciclastic Mz4b 'Sequence' comprises the Birdrong Sandstone, Muderong Shale, Windalia Radiolarite, and Gearle Siltstone (incorporating the Beedagong Claystone represented on Fig. 2); and the mainly carbonate Mz5 'Sequence' comprises the Toolonga Calcilutite, Korojon Calcarenite, and Miria Formation. Each of these 'sequences' represents a tectonic stage in basin development of an order roughly corresponding to 'supersequences' on the Haq et al. (1988) cycle chart. Mz4b reflects a post-breakup trailing-edge stage in the development of the continental margin, with restricted circulation in the shelf sea; Mz5 reflects a trailing-edge marginal sag situation with open circulation in the shelf sea.

Within the anticline's Mz4b group of formations, we recognise four 'sequences' (of an order somewhat higher than the sequences represented by Haq et al. 1988), each of a different depositional style, bounded by confirmed unconformities or major flooding surfaces (Fig. 2). The oldest of the sequences incorporates units identified as the Birdrong Sandstone and the Muderong Shale. Both these formations have type sections in the onshore Carnarvon Basin to the southeast of the Giralia Anticline.

Giralia No. 1 well section

Lithostratigraphy

The hole penetrated 114 m of Cretaceous strata before passing into Permian units (Fig. 3). Within the Cretaceous interval, ten cores (each 3 m long with generally poor recovery, and now disordered) were taken from depths between 85.3 and 115.8 m. Cuttings were collected from the remainder of the section. Below the base of weathering at 15 m, the borehole penetrated 15 m of a medium to dark grey siltstone. Chips of the rock at 15 m contain

abundant poorly preserved radiolarians forming 25–50% of the rock by volume. The radiolarian skeletons seem to be replaced by a friable recrystallised silica or clay. Minute carbonaceous flecks are common together with rare mica flakes. Between 30 and 40 m a very fine-grained quartz-glauconitic sandstone was encountered. A dark-grey siltstone was penetrated from 40 to 104 m. The washed 150 μm–2 mm sand fractions of cuttings examined from 46 m and 64 m contain abundant small aggregates of siderite crystals as well as common pyrite, including casts of radiolarians and rod-like structures (? pyritised wood debris). A similar grain-type composition was found in equivalent grain-size fractions from material selected from core 1 (85.3–88.4 m), core 3 (91.4–94.5 m) and core 6 (100.6–103.6 m). Siderite is rare in the equivalent sand fractions of studied samples from core 2 (88.4–91.4 m), core 4 (94.5–97.5 m), and core 5 (97.5–100.6 m). In the interval 104–114 m, a medium to coarse, well-sorted sandstone was penetrated. Core recovery in this unit was very poor and the core is in a disaggregated condition. A sample examined from core 7 (103.6–106.7 m) is a slightly indurated glauconitic quartz sandstone. Glauconite grains form about 40% of the 150 μm–2 mm sediment fraction. A sample examined from core 9 (109.7–112.8 m) is a friable quartz sandstone.

Johnstone (1955) referred the interval down to 30 m to the Windalia Radiolarite (in the sense of Condon 1954); the section from 30 to 104 m to the Muderong Formation (= Muderong Shale of Condon 1954); and the sandstone unit between 104 and 114 m to the Birdrong Sandstone (originally defined by Condon 1954). Hocking (1990, p. 149) suggested that the sandstone unit at 30–40 m may be the Windalia Sand Member of the upper Muderong Shale (originally named by Parry, 1967, for the Barrow Island succession). We have adopted this lithostratigraphic subdivision (Fig. 3), although the stratigraphic relation-

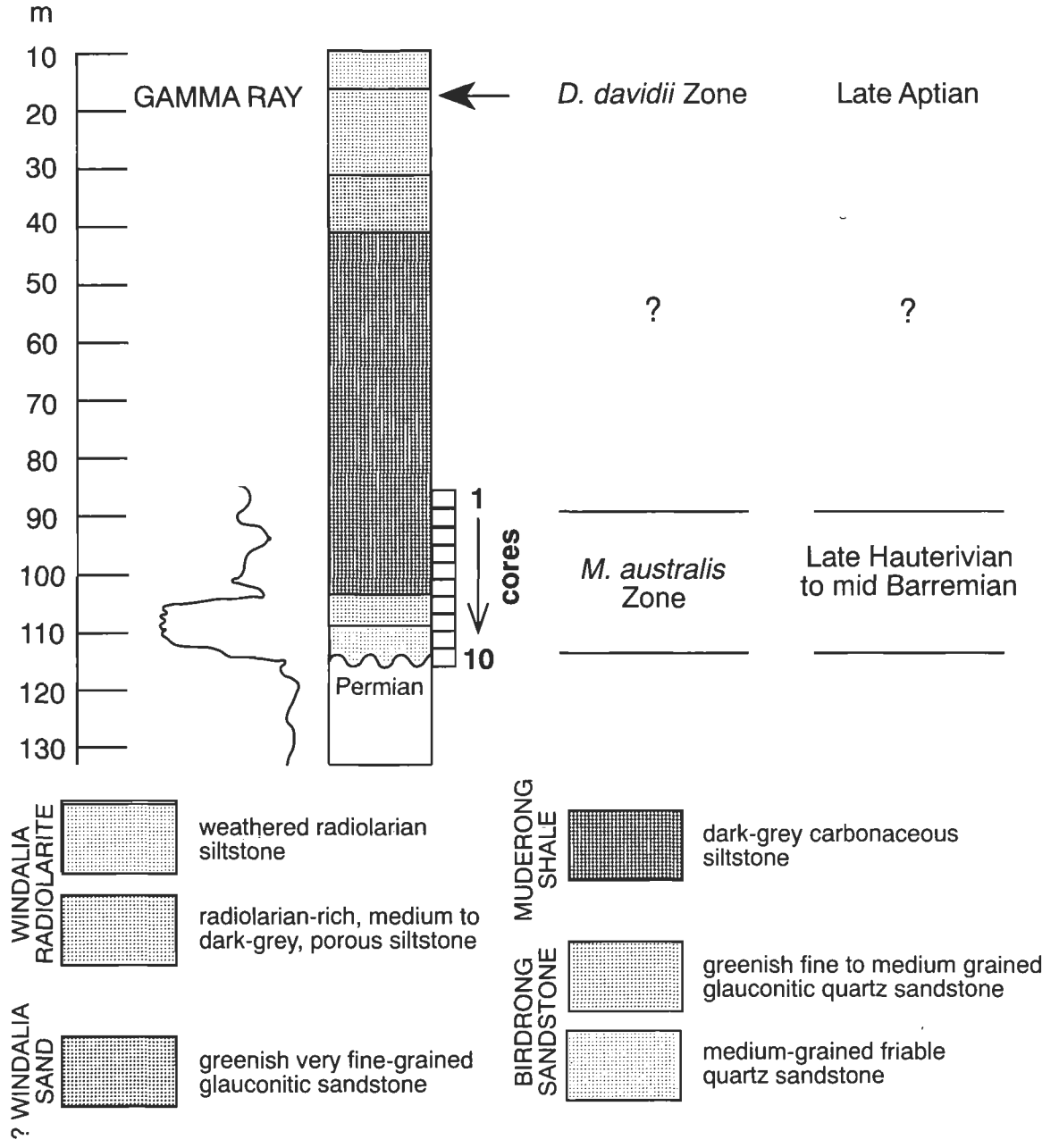

Figure 3. Giralia 1 bore section, showing lithostratigraphy, biostratigraphy, and chronostratigraphy.

ship of the 'Windalia Sand Member' to the Muderong Shale is uncertain.

Biostratigraphy

Palynomorphs. Diverse assemblages of spores–pollen and marine dinoflagellate cysts and acritarchs occur in all Cretaceous units below the weathered zone in Giralia No. 1. Selected species are illustrated in Figure 4 and their distributions recorded in Table 1. Below the Cretaceous, shale samples from cores 11 (115.8–118.9 m) and 12 (134.1–137.2 m) are dated as Early Permian on palynological evidence.

The oldest Cretaceous palynomorphs were recovered from core 10 (112.8–115.8 m) and a similar assemblage from core 7 (103.6–106.7 m), both in the Birdrong Sandstone. Both samples are contaminated by material from higher levels in the well, but in core 7 this seems to be a very minor component of the total assemblage. *Canningia transitoria* is present in both samples and *Scriniodinium attadalense* is a significant component of the core 7 assemblage. Together with the presence of *Muderongia australis* and *Batioladinium jaegeri* and the absence of *Phoberocysta* spp. and other cysts associated with lower zones, this is strong evidence for assignment of the Birdrong Sandstone interval (cores 10–7) to the lower part of the *Muderongia australis* Zone of Helby et al. (1987).

Assemblages from the lowest Muderong Shale in cores 6 (100.6–103.6 m) and 5 (97.5–100.6 m) contain a greater range of dinoflagellates and acritarchs associated with the *M. australis* Zone (Table 1). They are tentatively interpreted as coming from a slightly higher level in the zone than core 7. *Fromea monilifera* and *Ovoidinium cinctum* first appear in core 4 and suggest that the samples from cores 4 (94.5–97.5 m) to 2 (88.4–91.5 m) are from a higher part of the *M. australis* Zone, comparable with the *Fromea monilifera* Zone of the Perth Basin (Backhouse 1987). Assemblages from cores 4–2 also show rather more marine influence, judged by the proportion of marine forms, compared with assemblages below core 4. The interval from core 4 to core 2 is placed in the mid to upper *M. australis* Zone.

The *M. australis* Zone has been variously dated as Barremian (Helby et al. 1987), late Hauterivian to earliest Aptian (Partridge & Helby 1988) and late Hauterivian to Barremian (Helby & McMinn 1992). No ages have been confidently assigned to informal subdivisions of the *M. australis* Zone, but Helby & McMinn (1992) indicated a mid Barremian age for the upper part of the zone.

All the samples assigned to the *M. australis* Zone also belong in the *Balmeiopsis limbata* Miospore Zone of Backhouse (1988), which is equivalent to the upper part of the *Biretisporites eneabbaensis* Spore–pollen Zone as presented in Helby et al. (1987).

The sample from core 1 (85.3–88.4 m) and the cuttings samples examined from 64 to 30 m contain substantial caved material and are inherently unreliable. It is possible that the *Ovoidinium cinctum* (=*Ascodinium cinctum*) and *Odontochitina operculata* zones of Helby et al. (1987) are present within the 85–15 m interval in Giralia No. 1, but this cannot be confirmed from the present samples.

A cuttings sample from 15.2 m, just below the weathered interval, yielded an assemblage with *Diconodinium davidii*, *Endoceratium turneri* and *Odontochitina operculata*. It also contained abundant specimens (>40% of the total dinoflagellates and acritarchs) of a dinoflagellate identified as *Ovoidinium* sp., which is conspecific with *Ascodinium* sp. A of Helby & McMinn (1992). These authors recorded it only from the *Diconodinium davidii* Zone at ODP Site 765. This sample is placed in the *D. davidii* Zone of late Aptian age.

Foraminifera. The distribution of foraminifera in samples from the Giralia No. 1 well section is shown in Table 2, and species are illustrated in Figure 5. Very rare, robust, siliceous agglutinated foraminifera are present in a core sample of glauconitic sandstone within the upper part of the Birdrong Sandstone. In contrast, the agglutinated species in the Muderong Shale are generally smaller in size with deflated siliceous tests. Sparse hyaline benthonic foraminifera are present in cuttings from 30 m. These are associated with rock chips of Windalia Radiolarite.

The foraminifera from the upper Birdrong Sandstone and the Muderong Shale belong to the *Ammobaculites* Association (Haig 1979a; Haig & Lynch 1993) characterised by the presence of siliceous agglutinated species belonging to *Ammobaculites*, *Bimonilina*, *Cribrostomoides*, *Haplophragmoides*, *Lagenammina*, *Psammosphaera*, and possible *Textulariopsis*. *Cribrostomoides* is the revised name for Australian Cretaceous forms included in *Labrospira* by Haig & Barnbaum (1978) and Haig (1980), and in *Recurvoides* by Haig & Lynch (1993), following the generic revision of Jones et al. (1993). The recovered assemblages include species known from the *Ammobaculites australis* and *Lingulogavelinella albiensis* biofacies (Haig 1979b; Haig & Lynch 1993) of the Aptian–Albian in the eastern Australian epeiric basins. None of the species is indicative of age. Based on a comparison with the eastern Australian fauna described by Haig (1979a, 1980, 1981, 1982), Haig & Barnbaum (1978) and Haig & Lynch (1993), the species suggest that the palaeobathymetry was shallow (probably within the range of several metres to 20–30 m), and that conditions on the seafloor were abnormal, possibly dysaerobic and with slightly reduced salinity. The common occurrence of *Ammobaculites humei* in the Muderong core samples suggests that the original fauna may have contained calcareous hyaline species that were dissolved during early diagenesis. In eastern Australia *A. humei* is usually associated with a calcareous microfauna in the *L. albiensis* biofacies (Haig 1979, 1980).

There is a difference in preservation between the recovered Muderong and Windalia assemblages. The agglutinated foraminifera from the Windalia Radiolarite cuttings are non-calcareous like those from the Muderong Shale, but are smaller in size and so deflated and deformed that species cannot be recognised. Although rare and very small in size, the calcareous hyaline types from the Windalia Radiolarite are well preserved. The presence of *Lingulogavelinella* sp. cf. *L. albiensis* suggests the age of the unit is late Aptian or earliest Albian (based on the range of the species in the eastern Australian basins; Haig 1982). The faunal association and biofacies represented in the Windalia Radiolarite cannot be determined because of the low recovery of foraminifera.

Radiolaria. Few pyritised radiolaria are present in the Muderong Shale cores and ditch cuttings within the interval 94.5–46 m; most are indeterminant. Three species

have been tenatively recognised among the pyritic casts found in core 1 (85.3–88.4 m): *Spongodiscus renillaeformis* Campbell & Clark, *Orbiculiforma* sp., and *Arachnosphaera exilis* (Hinde). The ranges of these species have not been firmly established; *S. renillaeformis* has a widespread distribution and is known from the Aptian to lower Cenomanian, and *A. exilis* is abundant in Aptian–Albian deposits elsewhere in Australia (Ellis 1993). In

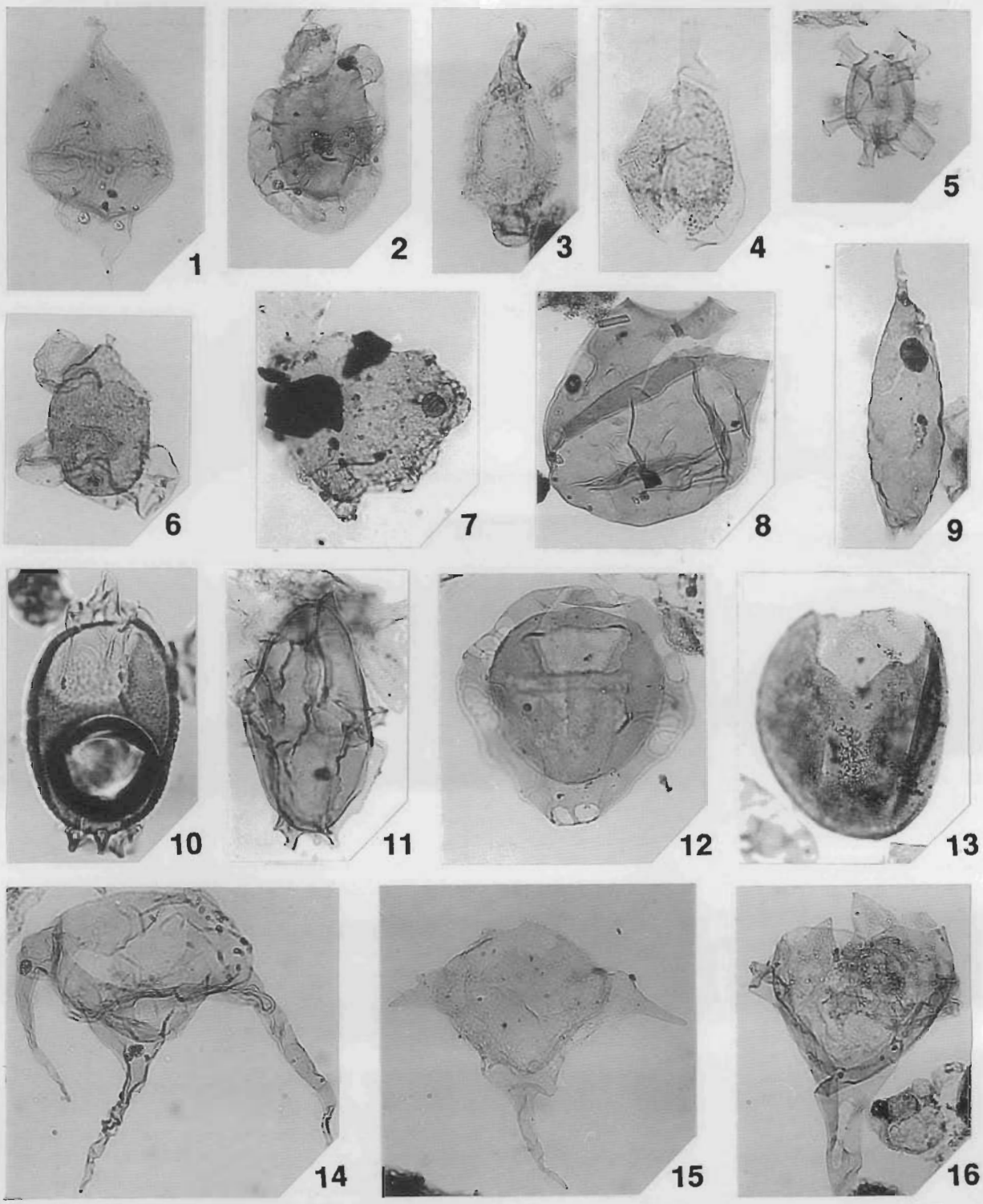

Figure 4. Dinoflagellate cysts and acritarchs from Giralia No. 1 well, all x 500. Sample numbers refer to Geological Survey of Western Australia Fossil Collection, with specimens located by England Finder. 1—*Ovoidinium* sp., cutt. 15.2 m (F49330/1, M10/4); 2—*Platycystidia eisenackii*, core 2, (F49335/1, T29/4); 3—*Belodinium dysculum*, core 5, (F49338/1, T35/2); 4—*Dingodinium cerviculum*, core 2, (F49335/1, M25/3); 5—*Discorsia nanna*, core 5, (F49338/1, T38/1); 6—*Aprobolocysta* sp. cf. *A. alata*, core 5, (F49338/1, U16/0); 7—*Canningia transitoria*, core 10, (F49344/1, K19/1); 8—*Fromea monilifera*, core 2, (F49335/1, R33/1); 9—*Batioladinium jaegeri*, core 2, (F49335/1, S35/3); 10—*Herendeenia postprojecta*, core 3, (F49336/1, T22/1); 11—*Carpodinium granulatum*, core 3, (F49336/1, V28/1); 12—*Scriniodinium attadalense*, core 7, (F49341/1, E17/4); 13—*Batiacasphaera subtilis*, core 7, (F49341/1, U42/1); 14—*Muderongia sp. cf. M. crucis*, core 5, (F49338/1, X17/0); 15—*Muderongia australis*, core 5, (F49338/1, P24/3); 16—*Muderongia* sp. cf. *M. tomaszowensis*, core 2, (F49335/1, S18/1).

Table 1. Distribution of some biostratigraphically significant dinoflagellates and acritarchs in Giralia No. 1 between core 7 and the cuttings sample at 15.2 m.

Core No. / *Cuttings (depth in metres)*	*7*	*6*	*5*	*4*	*3*	*2*	*15.2*
Batiacasphaera subtilis Stover & Helby	x						
Canningia transitoria Stover & Helby	x						
Scriniodinium attadalense (Cookson & Eisenack) Eisenack	x						
Aprobolocysta sp. cf. *A. alata* Backhouse	x	x	x	x	x	x	
Muderongia australis Helby	x	x	x	x	x	x	
Muderongia sp. cf. *M. crucis* Neale & Sarjeant	x		x	x		x	
Muderongia sp. cf. *M. tomaszowensis* Alberti	x					x	
Batioladinium jaegeri (Alberti) Brideaux	x	x	x	x	x	x	x
Dingodinium cerviculum Cookson & Eisenack	x	x	x	x	x	x	x
Epitricysta vinckensis Stover & Helby		x	x	x	x		
Leiosphaeridia perthensis Backhouse		x	x	x	x		
Batiacasphaera aptiensis (Burger) Kumar		x	x	x	x	x	
Platycystidia eisenackii (Mehrotra & Sarjeant) Backhouse		x	x	x	x	x	
Belodinium dysculum Cookson & Eisenack			x				
Discorsia nanna (Davey) Duxbury			x		x	x	
Carpodinium granulatum Cookson & Eisenack				x	x		
Ovoidinium cinctum (Cookson & Eisenack) Davey				x	x		
Fromea monilifera Backhouse				x	x	x	x
Herendeenia postprojecta Stover & Helby					x		
Canningia sp. A (Morgan, 1980a)							x
Canninginopsis intermedia Morgan							x
Diconodinium davidii Morgan							x
Endoceratium turneri (Cookson & Eisenack) Stover & Evitt							x
Odontochitina operculata (O. Wetzel) Deflandre & Cookson							x
Ovoidinium sp.							x
% dinocysts & acritarchs	**39**	**31**	**46**	**68**	**53**	**50**	**70**

Table 2. Distribution of foraminifera in Giralia No. 1 between core 7 and the cuttings sample at 15.2 m.

Core No. / *Cuttings (depth in metres)*	*7*	*6*	*5*	*4*	*3*	*2*	*1*	*64*	*46*	*30*	*15.2*
Agglutinated species											
Ammobaculites humei Nauss	?	x	x	x	x	x	x				
Ammobaculites sp.							x				
Bathysiphon brosgei Tappan		x	x	x	x	x					
Bimonilina sp. cf. *B. engeninensis* (Ludbrook)		x	x		x	x	x				
Cribrostomoides nonioninoides (Reuss)	x		x		x	x	x		x		
Haplophragmoides sp. 1		x	x		x	x	x				
Haplophragmoides sp. 2		x	x			x	x				
Lagenammina lagenoides (Crespin)					x						
Psammosphaera laevigata White		x	x			x			x		
?*Textulariopsis* sp.			x			x	x				
indeterminant agglutinated tests								x		x	x
Hyaline species											
Lenticulina spp. gr. *L. warregoensis* Crespin							x			x	
Lingulogavelinella sp. cf. *L. albiensis* Malapris										x	
"Marginulinopsis" pristipellis Ludbrook										x	
Other mineralised fossil material											
radiolaria (pyritised)				?	x	x	x	x	x		
radiolaria (friable recrystallised silica)										x	x
fish debris	x	x				x	x		?		
? wood debris (pyritised)			?		x	x	x	x	x		

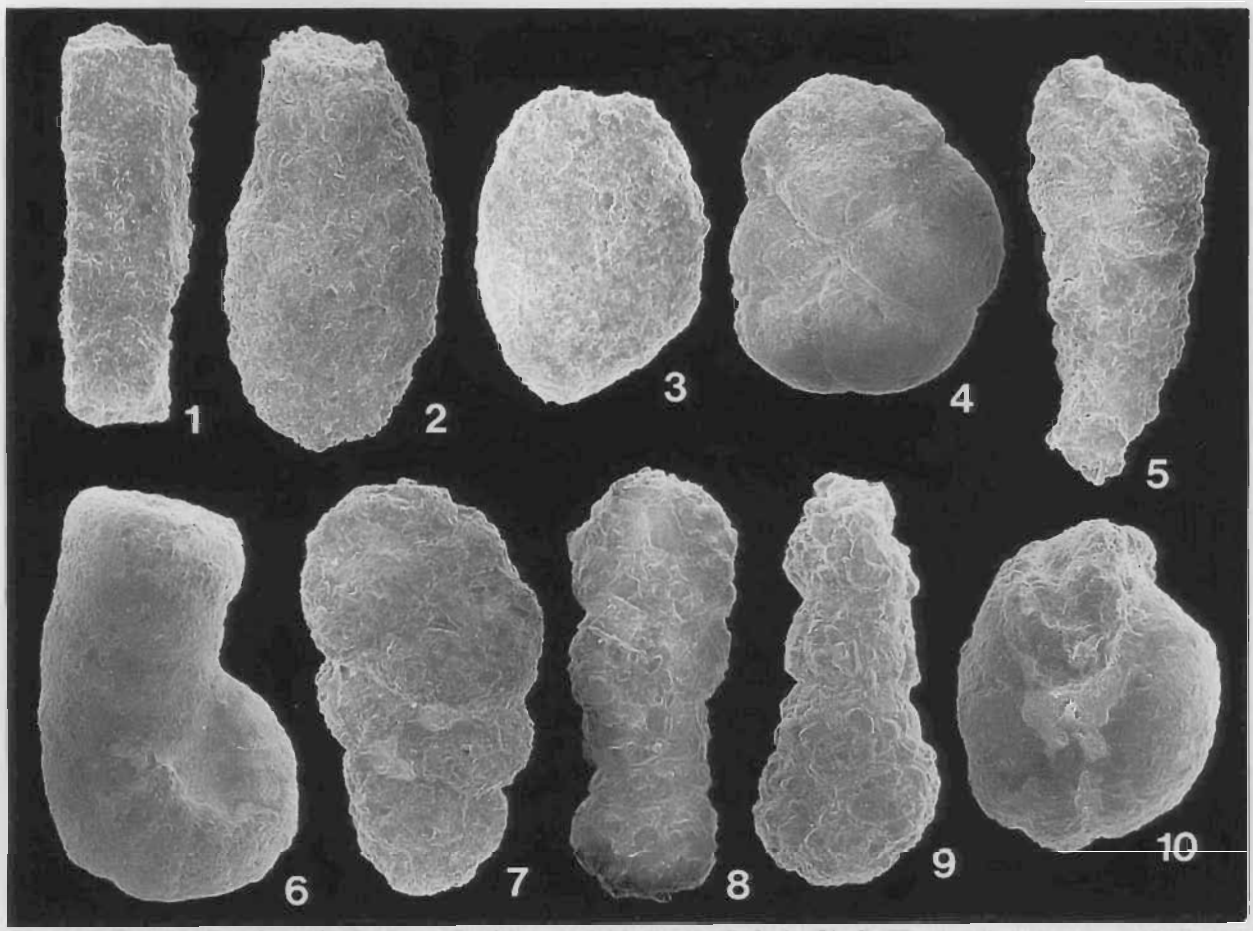

Figure 5. Foraminifera from the Birdrong Sandstone and Muderong Shale in Giralia No. 1. All specimens are housed in the Foraminiferal Species Reference Collection at the University of Western Australia. 1—*Bathysiphon brosgei*, core 5, Muderong Shale, x 95; 2—*Lagenammina lagenoides*, core 3, Muderong Shale, x 135; 3—*Psammosphaera laevigata*, core 5, Muderong Shale, x 160; 4—*Haplophragmoides* sp. 1, core 6, Muderong Shale, x 165; 5—?*Textulariopsis* sp., core 5, Muderong Shale, x 145; 6—*Ammobaculites* sp., core 1, Muderong Shale, x 45; 7—*Bimonilina* sp. cf. *B. engeninensis*, core 6, Muderong Shale, x 90; 8—*Ammobaculites humei*, core 2, Muderong Shale, x 80; 9—*Ammobaculites humei*, core 1, Muderong Shale, x 130; 10—*Cribrostomoides nonioninoides*, core 7, Birdrong Sandstone, x 90.

the Windalia Radiolarite, replacement of the tests by recrystallised silica and clay has made any chance of recovery impossible. Only the distinctive radiolarian outlines remain recognisable and indicate their abundant presence during deposition.

Outcrop in Giralia Anticline

During recent field work in the central part of the anticline, we located flat-lying, glauconitic sandstone beds in a belt to the west of a major lineament seen on aerial photographs (probably a major fault; Fig. 6). Only a few metres of section are exposed here in scattered outcrop, and stratigraphic relationships with adjoining units are obscure. The structural lineament separates the sandstone outcrop from exposures of Windalia Radiolarite immediately to the east. Farther east, material from the basal part of the Gearle Siltstone (with common belemnites) has been exposed in Black Dam, and higher beds of the Gearle Siltstone crop out along Cardabia Creek. To the west of the sandstone belt, in slightly higher country, is an area of no outcrop (possibly weathered Muderong Shale) and, farther west, scattered rubble of Windalia Radiolarite is found. The glauconitic beds may represent the top of an indurated sandstone unit from which overlying friable beds have been eroded.

Lithostratigraphy

Three lithofacies are differentiated in the scattered sandstone outcrop; represented by beds 40–80 cm thick, these appear to be repeated upsection in no particular order.

The first lithofacies is a pale green, very fine greensand with wavy laminae that appear to be ripples. The wavelength of the ripples is 5 cm and amplitude 1 cm. Muscovite flakes and bored wood remnants are also common.

The second facies is a reddish brown, poorly sorted, massive muddy sandstone, with bright red (alteration) and green mottles. The sand is partly cemented by calcite, and late-stage, lesser iron oxide/hydroxide. Dark-red laminae and filled burrows are common. Much of the bored wood on the surface of the ground is similarly stained. The lithofacies contains large (0.50.75 m diameter) calcium carbonate septarian nodules. Limonite nodules are also present and are probably weathered products of former pyrite or siderite nodules.

The sandstone of the second facies is composed of glauconite pellets, quartz grains and some opaque, white grains. The latter are a very minor component, less than

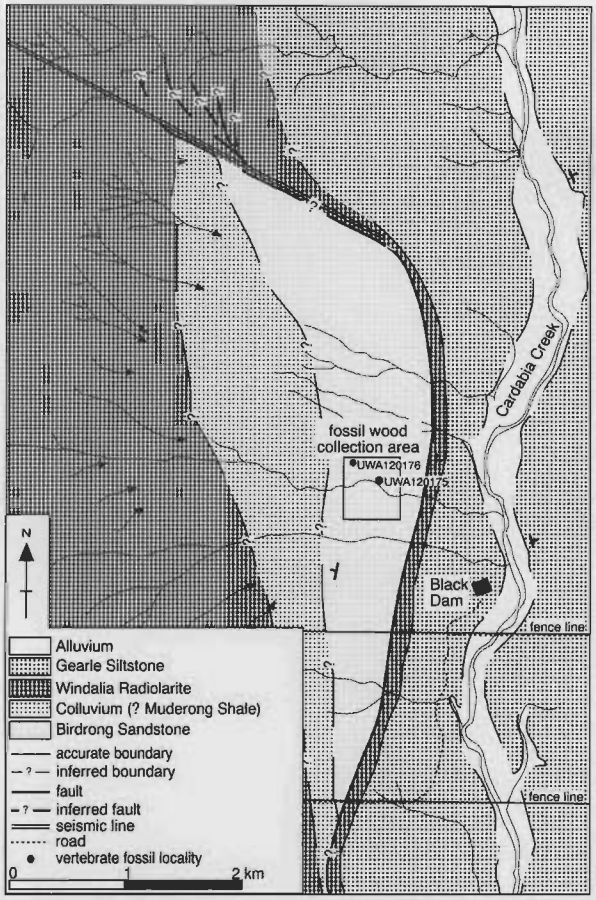

Figure 6. Outcrop area of probable Birdrong Sandstone, central Giralia Anticline, Cardabia Station.

1%, and appear to be kaolinised potassium feldspars. The quartz grains are very rounded to angular, clay-sized to 0.5 mm. Most are clear with some white inclusions. About 5% are frosted and another 5% are pink from iron oxide staining. Glauconite pellets constitute some 60% of the total components. They range in size from 100 μm to aggregates up to 1 mm across. They are faint green in the smaller pellets to dark green in the larger aggregates. The glauconite pellets could not be satisfactorily extracted from the lithified material, as they became crushed and mixed with silt and clay. Consequently, no mineralogical information was obtained on these. The coarse silt fraction (<40 μm) is composed of quartz, a 10/17 Å clay, calcite, goethite, possibly some potassium feldspar and a trace of kaolinite. The clay fraction (2 μm) is composed of an ordered 10/17 Å mixed-layered clay (illite/smectite) with approximately 65% illite layers (35% expandable). Also present are quartz, potassium feldspar, and goethite. There is a barely perceptible trace of kaolinite.

The third lithofacies, is a light-coloured massive glauconitic sand with a white silty infill and spotty gypsum rosette cement. Quartz grains form about 33% of the sand fraction, of which about 15% is fine sand (0.125–0.250 mm) and the rest is very fine sand (0.063–0.125 mm). The quartz is subangular to rounded—most is clear, about 10% is iron-stained pink. The glauconite constitutes about 66% of the sand fraction. It ranges in diameter from 0.63 to 0.25 mm—about 95% is very fine sand. The colour ranges from yellowish white through light to dark green. Many of the grains are globular; others are identifiable as former faecal pellets and foraminiferal moulds, which indicate that much of the glauconite is probably autochthonous. About 1% of the sand-size grains are opaque white to pinkish brown; these are highly kaolinised potassium feldspar grains. Another 1% are opaque black or bright red. Some of the latter appear to be oxidised glauconite pellets. Also present in the sand fraction are wood fragments, <1 mm across. These are opaque black, apparently pyritised or formerly pyritised, now haematitic.

The glauconite pellets in the third lithofacies are composed of expandable 10/17 Å clay with a trace of kaolinite. The exact proportions of smectite and illite in the pellets are difficult to discern from XRD traces. There is probably a range of proportions among the pellets. The coarse silt fraction (<40 μm) comprises gypsum, smectite, quartz, mica, a trace of potassium feldspar and kaolinite. The clay (<2 μm) fraction contains the same components. The smectite is only partly expandable, but interference from the mica and gypsum peaks renders an exact proportion of expandable layers uncertain without more extensive sample preparation (i.e. gypsum removal).

Biostratigraphy

Fossils found in outcrop include ammonoids, marine reptilian bones and fossil wood. The glauconitic sandstone has not yielded any foraminifera and the outcrops are too weathered to preserve palynomorphs.

Ammonoids. Portions of two ammonoid specimens preserved as external moulds in calcareous nodules were collected from the glauconitic sandstone outcrops by Mr R. French of Cardabia Station. The specimens represent two different genera. Because of the fragmentary nature of the material and its preservatiion, only very tentative identifications can be made. The larger of the two specimens (Figure 7b) is an incomplete fragment of body chamber. It has an estimated whorl height of 125 mm. It must be derived from a large genus that had a total diameter of 300–400 mm. The broad, gently sinuous ribs lacking tuberculation are suggestive of the ancyloceratid

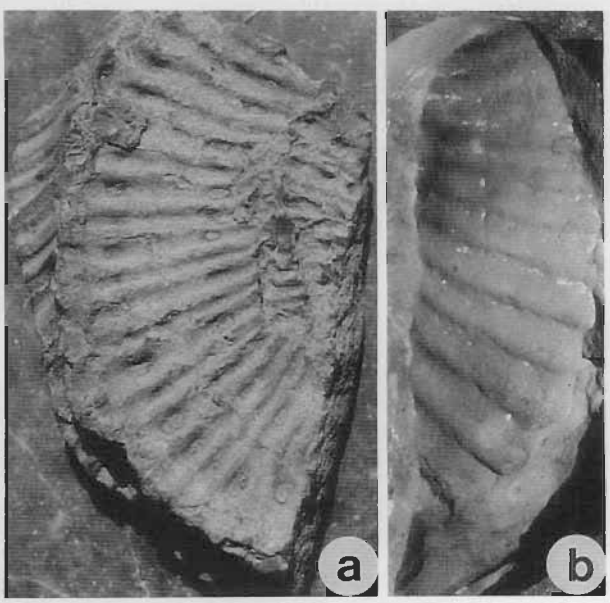

Figure 7. External moulds of Aptian ammonoids from outcrops of the glauconitic sandstone. a—partial remains of three successive whorls of ?*Australiceras* sp. with prominently ribbed tuberculate shell; x 0.5. b—partial remains of a single whorl of ?*Tropaeum* sp. with coarse ribbing; x 0.39.

ammonite *Tropaeum,* which is common in Cretaceous deposits in Queensland (Etheridge 1909; Whitehouse 1926; Day 1974). Congeneric forms, held in the collections of the Western Australian Museum, also occur in glauconitic beds at the top of the Butte Sandstone (considered synonymous with the Birdrong Sandstone by Johnstone et al. 1958) on Murchison House Station (southern Carnarvon Basin). Brunnschweiler (1959) and Ellis (1993) also recorded *Tropaeum* from the Windalia Radiolarite in Western Australia.

While, as Klinger & Kennedy (1977) pointed out, it is difficult to assign fragments of body chamber to any particular species, the specimen from the glauconitic sandstone in the Giralia Anticline is most reminiscent of *T. australe* (Moore) from Queensland (see Etheridge 1892, pl. 31, fig. 1, pl. 32, figs 3–4; Day 1974, pl. 1, fig. 1. pl. 2, fig. 2). *Tropaeum* is a widely distributed genus, having been found in, amongst other places, Russia, Spitzbergen, Greenland, arctic Canada, California, Patagonia, Japan, southern Africa, as well as Australia. It has only been recorded previously from the Aptian.

The second specimen (Fig. 7a) is more complete, consisting of parts of three whorls. The inner whorl has a preserved whorl height of about 25 mm, and shows relatively sinuous, closely spaced, narrow ribs. These bear three pairs of slightly elongate tubercles on each rib—an umbilical, a lateral and a ventrolateral tubercle. The next whorl has a whorl height of about 60 mm. The ribs are closely spaced and quite narrow, but less sinuous than those on the inner whorl. They bear only two sets of tubercles on each whorl—an umbilical and a ventrolateral. Little is preserved of the outermost whorl, but, while also having relatively closely spaced ribs, it appears to lack any tubercles.

The large size of this ammonite (with an estimated diameter of 250–300 mm), combined with the characteristic nature of the ornamentation, suggests that it may be a species of *Australiceras*. The genus has been recorded from the late Aptian (Doncaster Member of the Wallumbillla Formation) of Queensland (Etheridge 1892, 1909; Whitehouse 1926; Day 1974), and from the Windalia Radiolarite of Western Australia (Ellis 1993). Like *Tropaeum* it is a widespread, virtually cosmopolitan genus, occurring in similar regions to *Tropaeum*. It has only been recorded previously from the Aptian.

Marine reptiles. Reptilian bones have weathered out of the surface exposures of the glauconitic sandstone. These are mostly fragmentary specimens, but include some well-preserved individual limb bones. The material includes some large vertebrae of an ichthyosaur (UWA 120176) as well as sauropterygian limb elements (UWA 120175).

The ichthyosaur vertebrae include remains of at least six elements, of which only one (UWA 120176A) is relatively complete. This specimen measures 100.5 mm wide by 98.4 mm high, and is 44 mm thick at the outer margin. In cross-section the middle of the centrum is only 9.5 mm thick. There are no neural arches or transverse processes preserved, nor any sign of ventral paired foramina, which typify plesiosaurians. The largest partial vertebra (UWA 120176B) measures 112 mm in diameter (maximum thickness of 46 mm, minimum thickness only 9.6 mm) being comparable in size with dorsals from the large Queensland species *Platypterygius longmani* (Wade 1984, 1990). This specimen also shows preservation of closely spaced rib apophyses, very similar to that figured by Wade for *Platyptergius* (Wade 1990, fig. 3B) and to indeterminate ichthyosaur vertebrae described by Murray (1985) from the upper Albian Mullaman Beds, near Darwin. At this stage the Giralia Anticline specimens are referred to Ichthyosauria indeterminate.

The reptilian limb elements (UWA 120175) comprise one distal head of a propodial element and four small phalangial bones. The head of the propodial is 94.5 mm wide by 74.6 mm across, the articulatory surface being quite rectangular. Unlike typical ichthyosaur humeri, the specimen tapers rapidly to a narrow shaft, measuring about 49.7 by 51 mm, suggesting that the bone was relatively elongated, and thus more likely to represent a plesiosaurian. The associated phalangial bones are polygonal in outline with broad, rectangular articulatory faces, and could belong to either an ichthyosaur or plesiosaur. As the specimens were found in association from one site it is most likely that they belong with the propodial element and are plesiosaurian.

Fossil Wood. Scattered fossil wood is preserved within the glauconite-rich beds. The wood has been permineralised by silicates and phosphates, but virtually all organic matter has been lost. Xylem cell walls, cell lumens, and fungal hyphae are coated or infilled with cryptocrystalline silica and fluorapatite (Figs 8k, 9g), similar to the preservational style of Cretaceous woods from Alexander Island, Antarctica (Jefferson 1987). The woods are typically fragmentary, seldom bigger than 50 cm long and 17 cm diameter, randomly oriented, and showing extensive biogenic borings. Samples of permineralised wood collected from surface exposures are strongly weathered and have been infiltrated by iron-oxide and clay minerals. Prominent growth banding is evident, but details of the pitting arrangement on individual cell walls is often poorly defined or absent. In most cases, the middle lamella (initially consisting of pectinoid compounds between the primary walls of adjacent cells) has been degraded, producing a wood texture that appears to consist of detached or partially detached tracheids. The cambium, phloem, and bark tissues are invariably not preserved. The primary xylem and pith are poorly preserved or masked by iron oxides (Fig. 8c). Fractures in the wood, generated by compaction, and cavities produced by molluscan borers have been filled with glauconite and quartz sand, chalcedony, or sparry calcite.

The fossil woods consist of secondary xylem tracheids, showing seasonal variations in cell diameter and wall thickness (Figs 8b,l). The small pith content of the plants (pycnoxylic axes) suggests that the woods derive from the dominant arborescent elements of the Australian Early Cretaceous vegetation (viz. the podocarp or araucarian conifers) rather than fern, pteridosperm, or cycadophyte groups that typically contain a large proportion of pith within the stem (manoxylic axes). Permineralised wood belonging to podocarp and araucarian conifers is common in Gondwanan Cretaceous sediments (Sahni 1931; Jefferson 1983; Francis 1986; Frakes & Francis 1990; Francis & Coffin 1992) and the foliage of these plants is abundant in other Western Australian strata of this age (McLoughlin, in press). The wood contains relatively sparse uniseriate xylem rays 1–12 (av. 4) cells high. One group of woods shows rays typically with four or fewer cells (Figs 8d, f, j, m). A second group shows rays with between three and twelve cells (Fig. 8g), but whether these populations

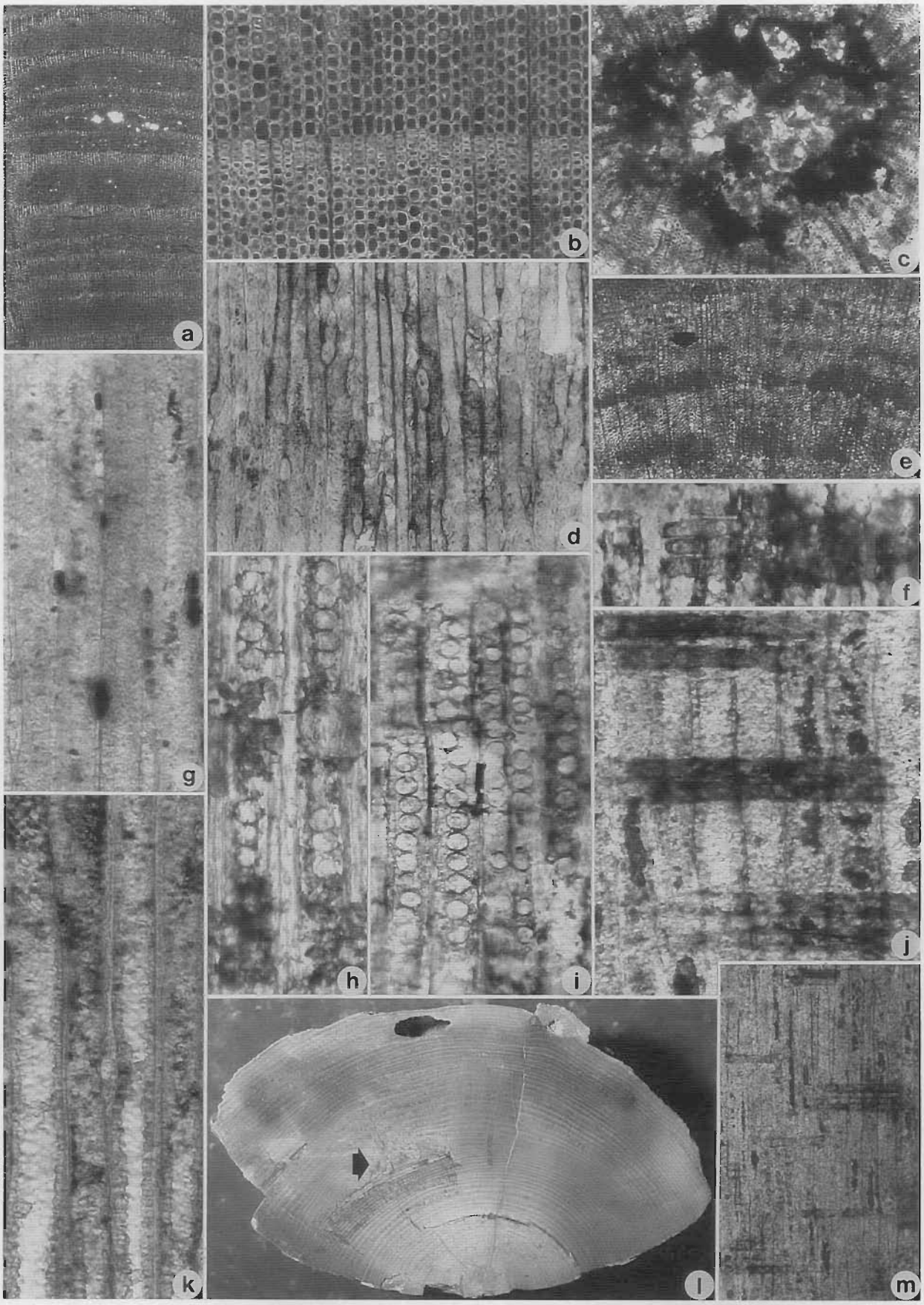
a
b
c
d
e
f
g
h
i
j
k
l
m

represent separate species is uncertain. Uniseriate or rarely biseriate bordered pits are sparsely evident on radial walls of xylem tracheids (Figs 8h, i). Tangential walls are not pitted. Owing to poor preservation, the details of pit apertures and cross-field pit arrangements are not, or are only rarely, discernible (Figs 8f, j, m) but the absence of typically araucariacean closely spaced multiseriate hexagonal bordered pits on radial tracheid walls (Greguss 1955) suggests that these Cretaceous woods have podocarpacean or cupressacean affinities.

Fungi within wood. Several fossil wood specimens show evidence of local degradation of the xylem tissues. These areas are typically represented by partly degraded cell remains or cavities, which are circular, elliptical or irregular in transverse section and spindle-shaped in longitudinal profile. The cavities are up to 10 mm long axially and 0.2–2.5 mm in diameter. The degraded areas most commonly occur within the late wood immediately before the outer margin of the growth band (Fig. 9a), but may also be present in the early wood. In some cases, the degradation of the wood has progressed to an extreme stage, giving the wood a box-work or skeletal texture (Fig. 9d, i). The cells surrounding the cavities mostly show irregular broken walls, but excess lignification of cells around the margins of the cavities also appears to have occurred (Figs 9e, k). The cavities are either vacant (being filled only with secondary iron oxides or silica) or contain ramifying weakly septate filaments (Figs 9b, c, f, g, h, j, l). No clamp connections were observed. The filaments are up to 450 μm long and 4–15 μm wide. The filaments branch irregularly (Fig. 9j), are often coated with prismatic apatite crystals (Fig. 9g) or amorphous silicates or phosphates (Figures 9c, f, j, l), and appear to contain irregularly spaced and poorly defined internal septa (Fig. 9j). Filaments are often in intimate contact with the degraded xylem cells of the cavity margin (Figs 9b, l).

Such filaments are morphologically similar to fungal hyphae described from other fossil woods (Stubblefield et al. 1985; Stubblefield & Taylor 1986, 1988). Moreover, the spindle-shaped cavities produced by fungal saprophytism in the studied woods correspond closely to the style of decay evident in Australian and Antarctic Permian glossopterid gymnosperms (Stubblefield & Taylor 1986; McLoughlin 1992) and to white-pocket rot generated by various basidiomycete fungi in modern angiosperm and conifer woods (Blanchette 1980, 1984). White-pocket rot is also characterised by the destruction of the middle lamella and separation of cells, a feature previously noted as being extensive within these Cretaceous woods. The causes of the concentric distribution of pockets within the Permian, Cretaceous, and modern woods remain unresolved, although they may relate to seasonal fluctuations in the saprophytic activity of the fungi, seasonal physiological susceptibility of the host plants, or the saprophyte's preference for lignin-rich late wood cells. No evidence of wall appositions or callosities (Aist 1976) was seen within individual cells, but strong lignification of the margins of the fungal-degraded cavities may represent a host response limiting pathogen spread. Saprophytic fungal remains have not previously been reported from Australian Cretaceous woods, although epiphyllous fungi and dispersed fungal spores have been recorded (e.g. Douglas 1969, 1973; Dettmann 1985). No fruiting bodies have been clearly identified with the fungal filaments, although some cavities show hyphae associated with darkened spherical bodies, ca. 30 μm diameter, which may represent sporangiate organs (Fig. 9b). However, no individual spores are evident within these bodies. Although morphological and anatomical details are few, such records contribute to the relatively meagre fossil record of fungi and add to knowledge of the evolution and ecological roles of decomposer organisms through time.

Ichnofossils in wood. Much of the fossil wood found in the glauconitic sandstone beds in the Giralia Anticline shows evidence of clavate borings within the woods. Clavate borings in woody substrates are referred to the ichnogenus *Teredolites* Leymerie and are distinguished from morphologically similar borings in lithic substrates assigned to *Gastrochaenolites* Leymerie. Cohesive linings of *Teredolites* borings are sometimes distinguished under *Teredolithus* Bartsch.

Borings in the studied wood are club-shaped, circular in cross-section, expanding from 0.5 to 1 mm in diameter at the outer margins of the wood to maxima of 13 mm in diameter near the base of the excavation. Cavities reach in excess of 8 cm in length. Borings may be straight or more commonly sinuous or variably contorted (Fig. 10a). The sizes, shapes, and degree of contortion of the borings appears to be strongly controlled by the thickness and shape of the woody substrate. The lower (widest) end of each cavity is broadly rounded. Borings very rarely touch or intersect. The cavities are lined by a thin (<0.1 mm) veneer of calcareous material, which, in many cases, has been removed or replaced by silica or iron oxides. The borings are typically filled by glauconitic and quartzose sand (Fig. 10b) or by sparry calcite and siliceous precipitates. Bioglyphic ornaments are not apparent on the exposed walls of lined borings, although faint xenoglyphs of the wood grain are sometimes preserved.

Two common species of *Teredolites* were recognised by

Figure 8. Photomicrographs of anatomical features and growth characteristics of fossil woods from the outcrops of glauconitic sandstone. a—transverse thin-section of wood, showing variable ring dimensions; UWA120187; x 20. b—transverse thin-section, showing transition from small thick-walled cells of late wood (lower) to large thin-walled cells of the succeeeding early season wood (upper); UWA120186; x 100. c—transverse thin-section of pith, showing poor preservation of primary tissues and masking by opaque iron oxides; UWA120233; x 55. d—tangential longitudinal thin-section of wood, showing uniserial rays of 1–4 cells; UWA120199; x 137. e—transverse thin-section of wood, showing development of false growth ring (arrowed); UWA120186; x 40. f—radial longitudinal thin-section of wood, showing ray cells with poorly defined circular cross-field pits; UWA120232; x 275. g—tangential longitudinal thin-section of wood, showing uniseriate rays with up to nine cells per ray; UWA120217; x 275. h—radial longitudinal thin-section of wood, showing uniseriate circular pits on tracheid radial walls; UWA120232; x 275. i—radial longitudinal thin-section of wood, showing uniseriate or rarely biseriate circular to elliptical pits on tracheid radial walls. Pit apertures rarely preserved; UWA120231; x 275. j—radial longitudinal thin-section of wood, showing rays rarely preserving cross-field pits; UWA120187; x 275. k—tangential longitudinal thin-section of wood, showing tracheid walls coated by silicate or phosphate minerals; UWA120217; x 275. l: Transverse section of a permineralised log, showing relatively uniform growth rings, except where disrupted by a branch trace (arrowed); UWA120192; x 0.8. m—radial longitudinal thin-section of wood, showing 1–4 celled vascular rays; UWA120187; x 100.

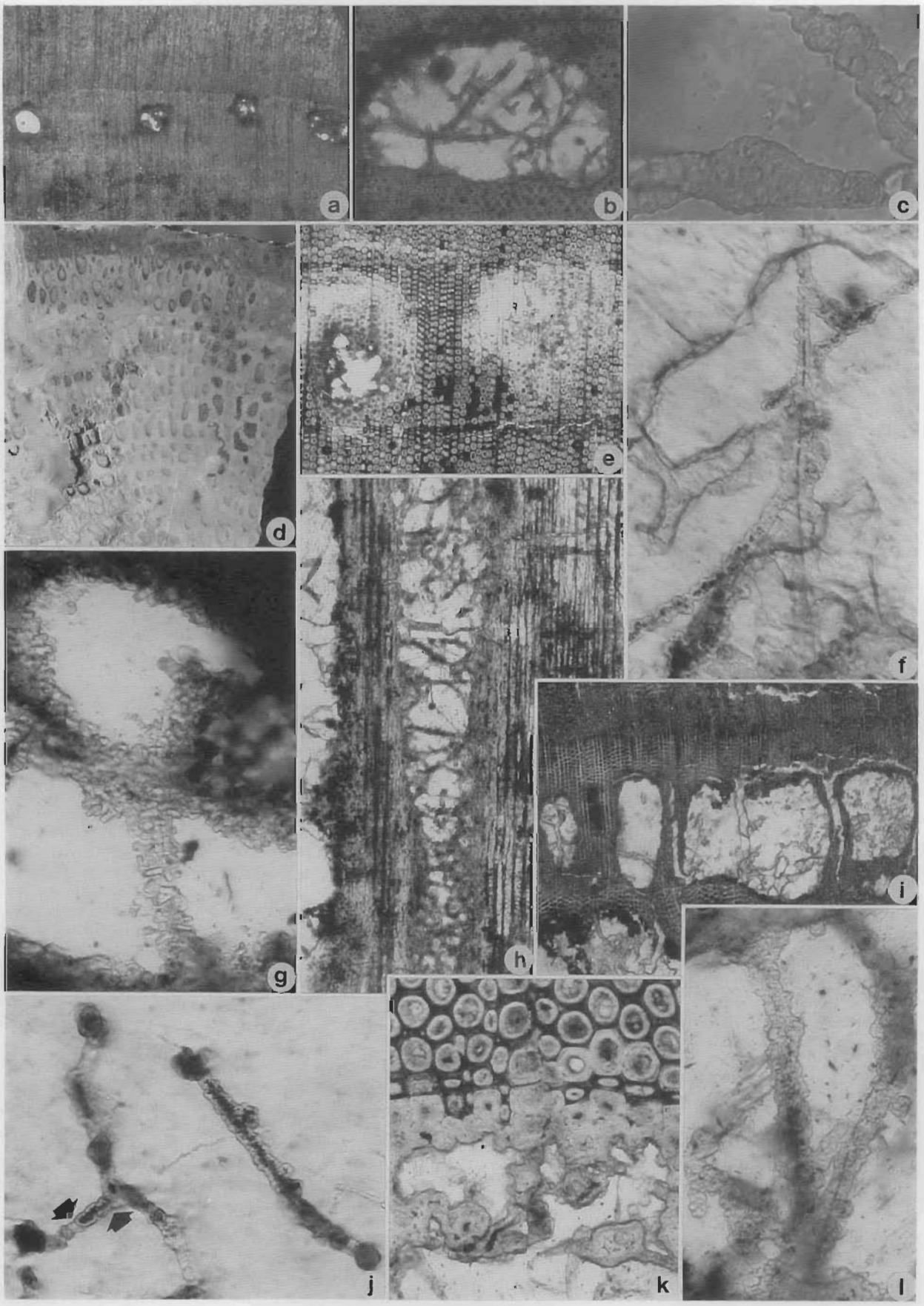
a
b
c
d
e
f
g
h
i
j
k
l

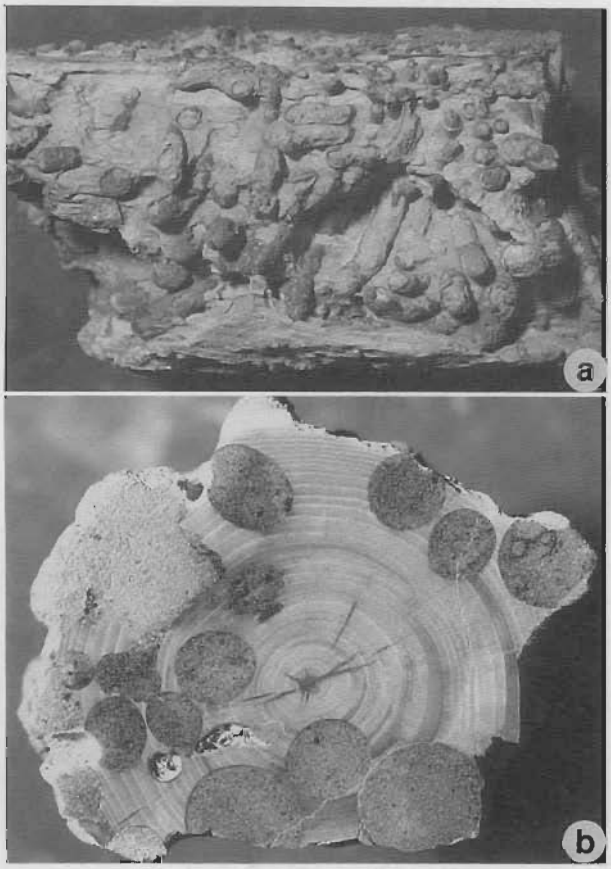

Figure 10. Infillings of molluscan borings (*Teredolites longissimus*) within Early Cretaceous conifer woods from the outcrops of glauconitic sandstone. a—external view of a weathered permineralised log, showing club-shaped borings, which commonly twist at right angles where borings reach opposite margin of log; UWA120235; x 0.9. b—transverse section of wood, showing borings with a thin calcite lining infilled by glauconite and quartz sand; UWA120208; x 2.

Kelly & Bromley (1984), based on the length:width ratio of the cavities and the orientation of the borings with respect to the wood grain. *Teredolites clavatus* Leymerie has a length:width ratio of <5, is usually straight, typically oriented perpendicular to the wood grain, and is recognised in Jurassic to recent woods. Borings of this type are produced by the modern pholadid bivalve *Martesia*. *Teredolites longissimus* Kelly & Bromley has a length:width ratio >5, is commonly sinuous or contorted, predominantly orientated parallel to the wood grain, and is recognised from Cretaceous to recent substrates. Modern borings of this type are produced by the bivalve *Teredo*. The present wood specimens contain borings falling into both categories with a complete intergradation. Borings typically initiate perpendicular to the wood, but, owing to constraints of the substrate, commonly twist and extend parallel to the grain during later stages of development. Kelly (1988) also found intergradation between these categories when describing borings in Cretaceous Antarctic woods. The differentiation of the above species of *Teredolites* may be invalidated by the occurrence of the described intergradational forms. However, important palaeoecological information may be gained where discrete populations of short and long borings are recognised, as short borings are often produced by filter feeders, whereas long excavations are typically generated by bivalves with a wood-digesting caecum (Kelly 1988).

None of the present wood borings appears to contain the shell of the original excavator organism. Early and Late Cretaceous woods from marine sediments of Alexander and James Ross Islands near the Antarctic Peninsula do contain remains of bivalve borers belonging to various representatives of the family Pholadidae (Kelly 1988). Similar borings are also produced by teredinid bivalves and isopods (Plint & Pickerill 1985), but attribution of simple borings in fossil woods to genera or families of borer organisms is impossible without the preservation of the borer's skeletal remains.

Correlation between outcrop and Giralia No 1 section

Based on regional lithostratigraphy and biostratigraphy, the outcropping glauconitic sandstone beds are clearly lower than the Windalia Radiolarite. In Giralia No. 1, about 15 km north of the outcrop area, two Cretaceous sandstone units are present below the Windalia Radiolarite—the basal Birdrong Sandstone, unconformably overlying Permian strata, and the sandstone unit (probable Windalia Sand Member) between the Muderong Shale and the Windalia Radiolarite.

In terms of rock type, the outcropping sandstone corresponds more closely to the upper Birdrong Sandstone than to the 'Windalia Sand Member' in the Giralia No. 1 section. The 'Windalia Sand Member' in the well, as originally described by Johnstone (1955) and observed by us in cuttings, is a very fine quartz-glauconitic sand which lacks the coarser grained components present in some of the outcrop beds. The 'Windalia Sand Member' is overlain by the Windalia Radiolarite, which weathers to a resistant porcellaneous siliceous rock in outcrop. The mapped sandstone beds are apparently overlain by a friable unit (probably the Muderong Shale) which has been intensely weathered and eroded (Fig. 6).

The lithostratigraphic correlation is tentative, however, because of the divergent chronostratigraphic determinations obtained from the ammonites in outcrop (tentatively identified, but suggesting an Aptian age) and from the

Figure 9. Photomicrographs of fossil wood from the outcrops of glauconitic sandstone, showing aspects of fungal decay and phosphatic permineralisation. a—transverse thin-section of wood, showing development of fungal-degraded pockets in late-wood tissues; UWA120186; x 20. b—transverse thin-section of pocket in wood, showing ramifying fungal hyphae coated by phosphates or silicates; UWA120186; x 100. c—enlargement of fungal hyphae in Fig. 9b; x 1000. d—transverse section of wood, showing advanced pocket rot; UWA120231; x 2. e—transverse thin-section of wood, showing early stages of cell degradation in the development of pocket rot; UWA120221; x 27.5. f—transverse thin-section of pocket within wood, showing thin, dark, fungal hyphae coated by amorphous phosphates or silicates; UWA120232; x 275. g—transverse thin-section of pocket within wood, showing fungal hyphae and walls of pocket coated by apatite crystals; UWA120187; x 275. h—radial longitudinal thin-section of wood, showing part of a spindle-shaped pocket traversed by numerous fungal filaments; UWA120232; x 55. i—transverse thin-section of wood, showing advanced fungal decay with coalescing pockets; UWA120232; x 27.5. j—transverse thin section of pocket in wood, showing branched, septate?, fungal hyphae (arrowed); UWA120232; x 275. k—transverse thin-section of pocket margin in wood, showing thickening of cell walls and infilling of lumens in cells surrounding the pocket; UWA120221; x 137. l—transverse thin-section of pocket within wood, showing fungal hyphae coated by amorphous phosphates or silicates; UWA120232; x 275.

dinoflagellates in the well section (suggesting a late Hauterivian–early Barremian age). The ammonite determinations must be viewed with considerable caution because: (1) the identifications are based on two fragmentary specimens which represent only small portions of external moulds; (2) the Australian ammonoid fauna of the Hauterivian–Barremian is very poorly known; and (3) the knowledge of the stratigraphic ranges of *Tropaeum* and *Australiceras* in the Australian region is based mainly on rare and scattered records in the Surat, Eromanga, and Carpentaria Basins, where marine conditions suitable for ammonite habitation existed only during the late Aptian and Albian.

Seismic coverage across the region is also difficult to interpret, because of the large number of faults shown in the seismic profiles (R. Bunt, pers. comm. July 1994). The stratigraphic position of the sandstone outcrops may be solved only by drilling through these beds to determine the stratigraphic succession and the presence of Permian strata beneath the unit.

For the present, we think that the outcropping sandstone belongs to the upper part of the Birdrong Sandstone, as it is recognised in this region, rather than to a higher unit. We believe the outcrop represents the uppermost indurated section of the Birdrong Sandstone seen in Giralia No. 1, which has been exposed by the erosion of friable Muderong Shale. The glauconitic beds may be better placed with the Mardie Greensand (Hocking et al. 1988) rather than with the upper Birdrong Sandstone, but further work needs to be done on time–facies relationships in the region before this correlation can be confirmed.

Climate and bathymetry

Growth analysis of fossil wood related to climate

Introduction. Modern trees growing in high-latitude seasonal climates show distinctive banding in their wood, whereas trees in humid tropical climates typically show only minor or no banding (Richards 1952), although there are some exceptions (Creber & Chaloner 1984). The similar range of growth patterns evident in fossil woods has been used to interpret past climatic conditions (Chaloner & Creber 1973; Fritts 1976). A number of environmental factors may influence the periodic and total production of carbohydrates which are ultimately reflected in the growth increments of a plant's woody tissues. Such factors include: length of season and day, radiation intensity and solar periodicity, temperature, water supply, mineral nutrient supply, atmospheric humidity, storm damage, herbivore and parasite attack, inter-plant competition, the orientation (lean) of the plant, volcanic ash fall, substrate instability, and palaeoseismic damage (Fritts 1976; Creber & Chaloner 1984; Sheppard & Jacoby 1989; Kurths et al. 1993; Filion & Quinty 1993). Ideally, palaeoclimatic interpretations based on plant growth indices should be derived from autochthonous stumps of the same species positioned relatively close together so that many of the competing environmental factors will apply to all specimens. In this study, forty-eight allochthonous permineralised conifer logs were analysed from outcrops of the glauconitic sandstone. The logs, deposited under marine conditions, had clearly been transported from relatively distant terrestrial environments and had been subjected to intense boring by pholadid or teredinid bivalves. Hence, it is possible that the wood samples were derived from a range of hinterland habitats. Nevertheless, a study of the growth parameters of these Early Cretaceous woods was deemed worthwhile for comparison with similar studies of fossil wood from roughly coeval strata in South Australia and Antarctica (Jefferson 1983; Francis 1986; Frakes & Francis 1990).

Growth features. Several qualitative and quantitative measures have been established for analysing growth bands in assessing palaeoclimate (Chaloner & Creber 1973; Fritts 1976; Creber 1977; Creber & Chaloner 1984, 1985). Simple qualitative considerations include the recognition of growth rings and their degree of prominence within the plant axis. Quantitative analysis includes measurement of growth-ring widths, relative proportions of early and late wood production, variation in size between the cells of early and late wood, the number of cells produced per season, and several measures of variation of ring widths between seasons. The variability of growth rings in successive seasons probably offers the most valuable information about past climatic conditions. Annual sensitivity is a measure of the difference in width between a pair of consecutive growth bands divided by their average width (Creber 1977). Mean sensitivity (Fritts 1976) is a measure of the average of these values for each tree, and provides an indication of the plant's growth response to variable climatic factors [see Jefferson (1983) or Francis (1986) for calculation method]. Trees having a mean sensitivity measure of <0.3 are considered 'complacent' and probably grew under climates of low interseasonal variability. Those having mean sensitivities >0.3 are regarded as 'sensitive' and probably grew under more variable climatic conditions. Growth rings of the studied woods were measured on cut and polished slabs under a dissecting microscope and in petrographic thin sections. Where possible, measurements of growth rings were taken along a single radius, although patches of poor wood preservation necessitated continuation of some measurements along adjacent radii.

Forty-eight wood specimens, 2.2–17 cm in diameter and showing 5–117 growth bands, were collected and examined from the exposures of glauconitic sandstone (identified as uppermost Birdrong Sandstone) in the Giralia Anticline. These Early Cretaceous woods show distinctive seasonal growth banding (Fig. 8I), a feature common to other Australian and Antarctic woods of this age. Widths of growth rings within the studied woods vary from 0.033 mm to 12.340 mm and averages for individual axes are in the range 0.177–9.390 mm. Some woods show relatively little interseasonal variability, whereas others show marked fluctuations in wood production between seasons (Figs 8a, 11). The variation between the narrowest and broadest growth increments for individual axes ranges from 154% to 7367%. Woods display mean sensitivity measurements ranging from complacent to mildly sensitive (0.148–0.673) with the average mean sensitivity (0.348) falling within the 'sensitive' field (Figs 11, 12). Annual sensitivity measurements range from 0 to 1.765. Most ring couplets plot within the 0–0.3 'complacent' growth field (Fig. 13), although some woods show a broad spread of annual sensitivity measurements, indicative of irregular but marked growth fluctuations. Some annual sensitivity histograms appear to show a small subsidiary peak in ring couplet variability around 0.3–0.7 (Fig. 13). Whether this is due to a regular periodicity in climatic variability or to some other factor, such as sporadic pathogen attack, is indeterminate.

Certain axes show differential production of wood around the circumference by as much as 500%, which may reflect responses to localised environmental factors, including shading, tree leaning or production of the wood in a lateral branch rather than a vertical stem. Indeed several specimens display obvious branching. All ring measure-

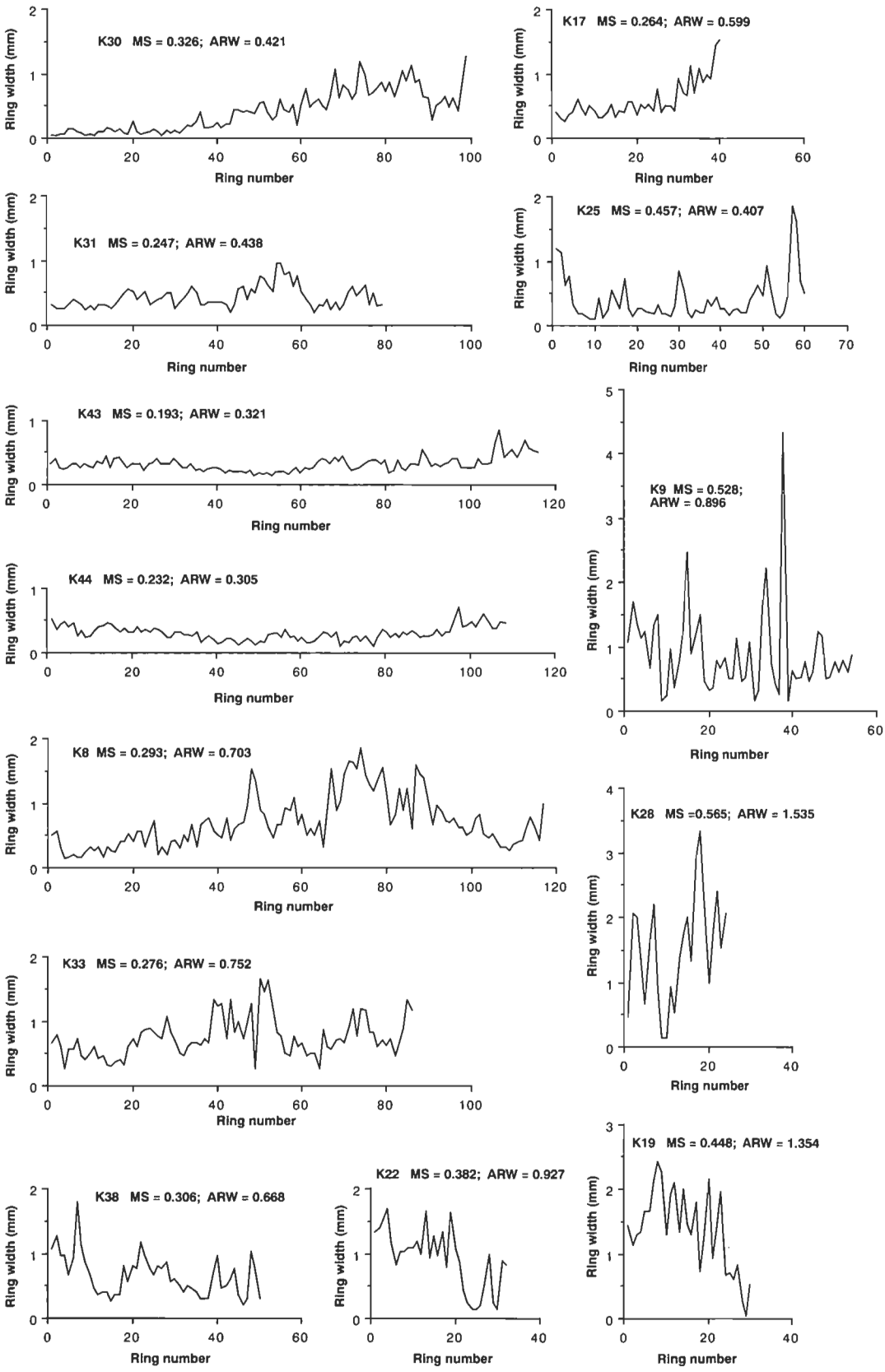

Figure 11. Plots of the variation in growth-ring widths for selected fossil woods from the outcrop area, showing examples with mean sensitivity ranging from strongly complacent to strongly sensitive. MS = mean sensitivity; ARW = average ring width.

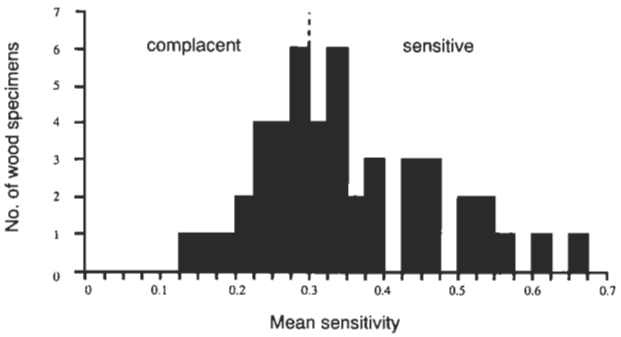

Figure 12. Histogram of the frequency of mean sensitivity values recorded for woods from the outcrop area.

ments were taken from the main axis of each specimen in areas away from branch traces. False growth rings are produced in modern trees by adverse environmental conditions during the normal growth season. They show gradual reduction in cell diameters followed by gradual increases and are differentiated from true growth rings, which show abrupt transitions between the narrow thick-walled cells of the late wood and the broad thin-walled cells of the early wood of the succeeding season. Although they are uncommon in the studied woods, sporadic false growth rings are present in some axes (Fig. 8e).

The variation in width of growth bands within and between the wood samples also corresponds to considerable variation in the number of cells produced per band. Broad growth rings on some specimens may have more than 300 cells per band, while some specimens show narrow growth increments with as few as 10 cells per season. Early and late wood cells are readily distinguished by the latter's smaller size and thickened walls. Early wood typically represents 80–90% of growth bands. Within individual growth bands, radial cell diameters are typically 25–45 μm in the early wood to just 5–10 μm in the late wood. Cells produced at the end of each growth season show almost complete occlusion of the cell lumens (Figure 8b). Cell walls are 2–4 μm thick in the early wood to 2–6 μm in the late wood.

Palaeoclimatic implications. The collection of forty-eight specimens provides a fair representation of the variation in fossil wood growth patterns found among specimens preserved in the glauconitic sandstone beds within the Giralia Anticline. Other assemblages of Early Cretaceous fossil wood from the Australia–Antarctica region (then a connected landmass) include those from the Otway and Gippsland Basins (Douglas & Williams 1982), the Eromanga Basin (Frakes & Francis 1990), the Carpentaria Basin (White 1961), Alexander Island (Jefferson 1983, 1987), and the Antarctic Peninsula (Francis 1986). Early Cretaceous woods from all of these localities display marked seasonal banding as might be expected in high-latitude floras, although the few illustrated Carpentaria Basin woods (White 1961) also appear to show abundant false growth rings typical of more erratic climatic conditions. Palaeomagnetic data indicate latitudes of 75–85° for the Gippsland and Otway Basins, 65–75° for the Eromanga Basin, and around 45–50° for the Carnarvon basin during the Early Cretaceous (Veevers et al. 1991). Suggested palaeolatitudes for Alexander Island and the tip of the Antarctic Peninsula are 70–80° and 60–70° respectively (Jefferson 1983; Francis 1986), although these were tectonically active regions during the Cretaceous and their precise position within Gondwanan plate configurations is still disputed (Dalziel & Elliot 1982; Lawver et al. 1985; Wilson et al. 1989).

Early Cretaceous woods from the Antarctic Peninsula have relatively wide and uniform growth rings (average annual ring widths of 0.99–5.57 mm and low mean sensitivities of 0.125–0.239) and seem to reflect conditions similar to those experienced by the temperate araucarian conifer and deciduous *Nothofagus* forests to the north of the modern Magellanic rainforests of southern Chile (Francis 1986). Similar-aged woods from Alexander Island show broad, but more variable, growth rings (mean ring widths up to 2.5 mm, with sporadic large rings up to 9.55 mm wide, and mean sensitivities of 0.4–0.45) suggesting more significant fluctuations in climatic conditions between growth seasons (Jefferson, 1983). Jefferson (1983) likened such growth parameters to those of *Phyllocladus* species presently growing in New Zealand and Tasmania, where light availability has an important limiting affect on growth. Francis (1986), emphasising the difference in mean sensitivities between the Antarctic Peninsula and Alexander Island woods, suggested that the highly variable growth patterns of the latter group may represent the marginal limits of the Cretaceous Antarctic Peninsula forests.

Although Early Cretaceous permineralised gymnosperm axes from the Gippsland and Otway Basins show prominent seasonal banding (Douglas & Williams 1982), no detailed analyses of the growth rings are yet available. Eromanga Basin allochthonous fossil coniferous woods show average annual ring widths of 0.34–4.53 mm and mean sensitivities of 0.104–0.366, the vast majority having complacent mean sensitivities of <0.3 (Frakes & Francis 1990). However, Frakes & Francis (1990) noted two distinct populations in their samples: one (population A) with consistently narrow rings, <1 mm wide and an average mean sensitivity of 0.157, and another (population B) with uniform rings about 2 mm wide and an average mean sensitivity of 0.202. No false growth rings were noted in the Eromanga Basin woods. Frakes & Francis (1990) interpreted the population distinctions in their fossil assemblages as a result of the woods being derived from vegetation sources growing under different hinterland climatic settings. They compared their narrow-ringed woods to growth patterns witnessed in the modern cool-temperate evergreen *Nothofagus* forests of Magellanic Chile, where relatively uniform rainfall and consistently low temperatures support trees showing narrow but very regular growth rings. They compared the second population with broader, though still relatively uniform, growth rings to cool temperate (microthermal) forests of modern New Zealand and Tasmania. By contrast, Late Jurassic conifer woods associated with evaporitic sediments in southern England (basal Purbeck Formation) show prominent false growth rings, average true ring widths of 0.52–2.28 mm, and high mean sensitivities in the range of 0.290–0.788 (average: 0.527) comparable to wood growth in climatically variable 'Mediterranean' vegetation types (Francis 1984).

The Carnarvon Basin woods, having growth rings of 0.0333–12.339 mm (average 0.305–9.390 mm) and average mean sensitivities of 0.348, fall between the complacent growth values shown by the 'population B' Eromanga Basin woods and the sensitive growth parameters displayed by the Alexander Island woods. The Giralia Anticline woods show considerable variation in mean sensitivities from complacent to strongly sensitive values,

probably reflecting their origin from a range of hinterland habitats. Taking into account the palaeolatitude of the Carnarvon Basin, the sporadic presence of false growth rings, the range in seasonal growth ring widths, and the relatively high average mean sensitivity measure, a seasonal mesothermal conifer-dominated vegetation is envisaged for the basin hinterland during the Early Cretaceous. Fluctuations in climatic conditions may have been slightly more irregular than in areas peripheral to the higher latitude epicratonic Eromanga Basin. Early Cretaceous macrofloras from the Perth, Carnarvon, and Canning Basins of Western Australia are dominated by araucarian and podocarp conifers, cycadophytes, pteridosperms, ferns, and isoëtalean lycophytes (McLoughlin, in press). Many of the taxa have affinities to families and genera living in modern humid warm temperate (mesothermal) southern hemisphere forests (McLoughlin, in press). Other assemblages of Early Cretaceous fossil wood occur further

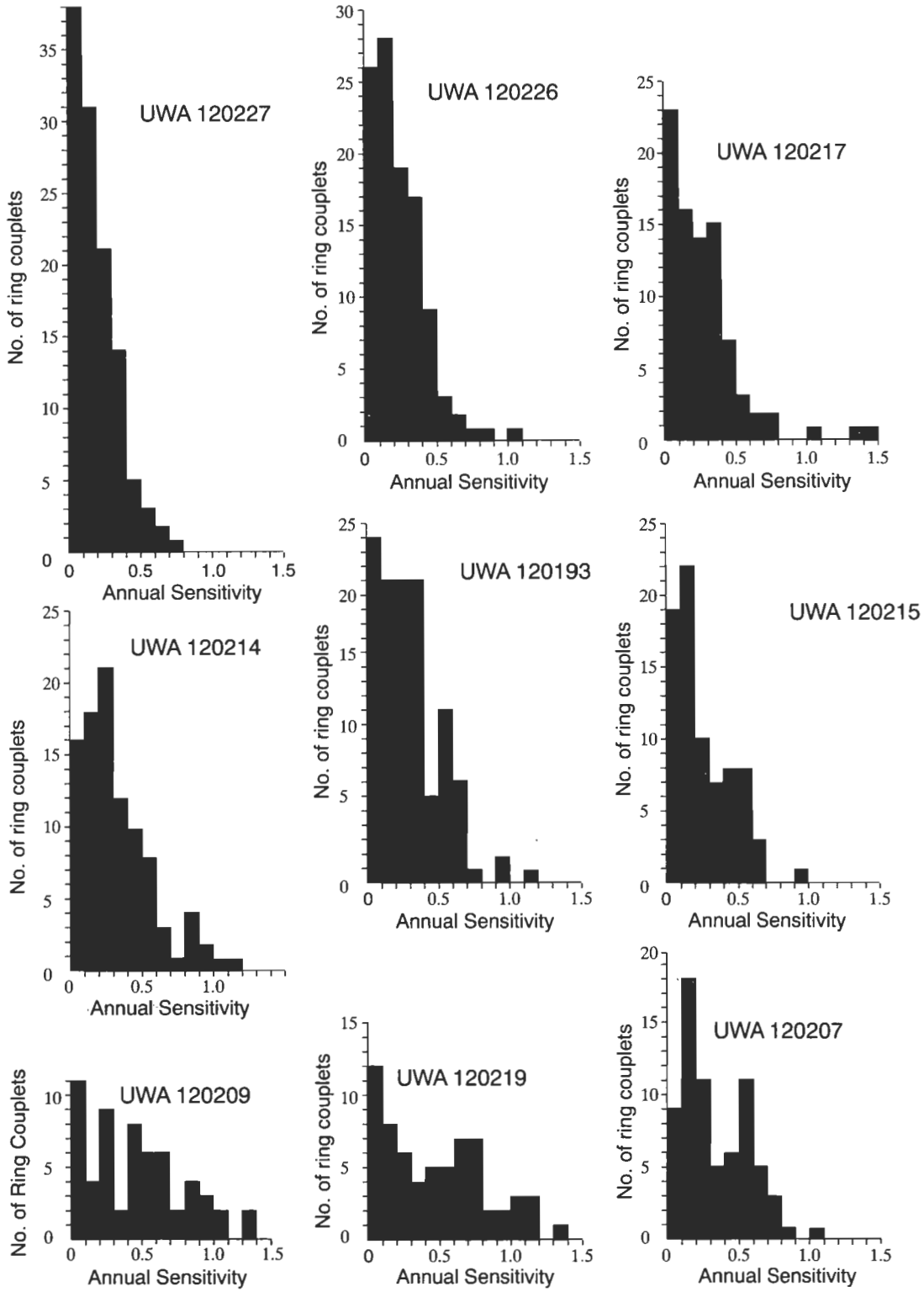

Figure 13. Histograms of the frequency of annual sensitivity values recorded for ring couplets in selected fossil woods from the outcrop area.

to the south, in exposures of the 'Birdrong Sandstone' at Kalbarri and in the coeval Dandaragan Sandstone of the Perth Basin (Simpson 1912). Further studies of the Western Australian, Gippsland, and Carpentaria Basin fossil woods would better resolve their botanical affinities and growth patterns and would enhance understanding of Australian Early Cretaceous climates.

Bathymetric interpretation

The main criteria used to interpret the palaeobathymetry are (1) sedimentary features, (2) foraminiferal facies, and (3) microplankton abundances. The transition from quartz-rich sandstone (lower Birdrong Sandstone) through glauconite-rich sandstone (upper Birdrong Sandstone) to carbonaceous siltstone and mudstone (Muderong Shale) suggests that bathymetry changed during deposition of the Birdrong–Muderong sequence. The change is reflected also by variations in foraminiferal assemblages and in the relative abundance of marine dinoflagellates and acritarchs among the palynomorphs.

Lower Birdrong Sandstone. Dinoflagellates and acritarchs constitute about 23% of the palynomorph assemblage in Core 10 of Giralia No. 1, but, because of caving evident in the sample, this figure is inherently unreliable. Nevertheless, it seems that marine palynomorphs form a relatively small part of the assemblage compared with higher samples, and this may reflect shallower water conditions. Permian spores and pollen constitute 1–2% of the palynomorph assemblage in Core 10 (lower Birdrong Sandstone) and may reflect reworking of the unit exposed on the transgressive surface.

Upper Birdrong Sandstone. Core 7 in Giralia No. 1 gave a sample with 39% dinoflagellates and acritarchs, which suggests continuing shallow marine conditions. The abundance of glauconite, the presence of occasional ripples, and the 30–80 cm thickness of the beds support a shallow marine origin for the upper Birdrong Sandstone. Following the facies models outlined in Reading (1978) and Reineck & Singh (1980), all three facies described from outcrop on Cardabia Station represent transgressive, foreshore deposits, from the upper shoreface (ripples in parts of our 'Facies 1') to lower shoreface (strong bioturbation, high glauconite contents in our 'Facies 2').

Greensands often have phosphorite associated with them, although the phosphate does not often replace wood (Pettijohn 1975, p. 427–434; Odin & LeTolle 1980). In such cases, the seawater in the depositional environment is considered to have been oxic, while the sediment was somewhat anoxic with a slightly lowered pH (McRae 1972; Pettijohn 1975, p. 427–434). Such a setting, coupled with the low depositional rates associated with these facies, suggests some restriction of the bottom-water circulation to fully open marine waters. The presence of robust siliceous agglutinated foraminifera of the benthonic *Ammobaculites* Association also supports the interpretation of restricted bottom-water conditions (based on the facies model of Haig & Lynch 1993).

The ammonites present in the outcropping glauconitic sandstone beds (upper Birdrong Sandstone) are probably posthumous drifters washed in from the open sea to their shoreface burial site. The wood, much with *Teredolites* borings, represents driftwood washed from hinterland localities into the sea, and stranded in the shoreface deposits.

Pholadid bivalves and *Teredolites* borings have been recorded from modern and ancient deep marine to fluvial sediments in tropical to cool temperate latitudes (Wrigley 1929; Turner & Johnson 1971; Turner 1972, 1973; Howard & Frey 1984; Plint & Pickerill 1985). Their association with other marine fossils and glauconitic sediments implies a marine depositional setting in this instance. Bromley et al. (1984) established the term '*Teredolites* ichnofacies' for consolidated xylic (persistent peat or coal) substrates showing abundant *Teredolites* borings in ?high energy marine environments. As the present fossil axes occur as dissociated driftwood fragments, they do not conform precisely to the definition of a 'woodground' as proposed by the above authors, and their bathymetry and hydrodynamic energy levels at deposition are uncertain. As in some other cases (e.g. Savrda 1991) the studied woods, together with vertebrate remains and ammonoids, appear to be concentrated in a relatively thin interval (<6 m) in this case at the top of the formation. Such accumulations of dispersed woody material have been described as 'log-grounds' by Savrda (1991) and are common features of transgressive systems tracts. The exceptional wood accumulations result from three chief processes during trangressive pulses: (1) inundation of subaerially exposed coastal settings and consequent influx of wood to marine environments, (2) hydraulic concentration of previously bored and buried xylic substrates by coastal erosion, exhumation, and redeposition of the woods, and (3) preferential landward trapping of sediments and sediment starvation seawards, resulting in accumulations of driftwood in offshore areas where they are not diluted by clastic sediments (Savrda, 1991).

Our findings support previous interpretations of the Birdrong Sandstone at other localities as a basal transgressive sand (e.g. Parry 1967; Hocking et al. 1987; Malcolm et al. 1991).

Muderong Shale. In contrast to the underlying Birdrong Sandstone, the lower Muderong Shale in Giralia No. 1 lacks glauconite and quartz sand, and apparently does not contain shelly macrofossils or large wood fragments (although millimetre-size pyritised wood debris and carbonaceous flecks are abundant). It is considered to be an offshore deeper water deposit than the Birdrong Sandstone.

Foraminifera are common in the Muderong Shale, but belong to a low diversity assemblage of siliceous agglutinated types characteristic of the benthonic *Ammobaculites* Association (Haig 1979a). As noted above, the assemblage is typical of that found in the *Ammobaculites australis* and *Lingulogavelinella albiensis* Biofacies (Haig 1979; Haig & Lynch 1993) in the eastern Australian epeiric basins, and may be part of the *L. albiensis* Biofacies from which the calcareous hyaline components have dissolved. The foraminiferal assemblage suggests that water depths remained shallower than 50 m during Muderong Shale deposition. In the Giralia 1 section, the first appearance of radiolarians at a position about 10 m above the base of the formation and a slight increase in proportions of dinoflagellates and acritarchs among the palynomorphs (from 31% in a near basal sample to about 50% or more in samples about 8–15 m above the base) may indicate that water depths increased slightly during deposition of the lower Muderong Shale. The lack of a shelly macrofauna, the presence of the *Ammobaculites* Association of foraminifera and the preservation of organic debris suggest that dysaerobic or anaerobic

conditions existed on the seafloor and within the sediment. The organic debris may have been washed out to sea in sediment plumes coming from hinterland rivers. Slightly brackish water conditions are suggested by the foraminiferal association.

The fine sandstone unit between 30 and 40 m in Giralia No. 1 (tentatively correlated with the Windalia Sand Member by Hocking 1990) probably represents reappearance of the shoreface facies, because of the presence of sand-size quartz and glauconite. As explained below, we are unsure of the relationship of the sandstone unit to the Muderong Shale.

Correlations of Birdrong–Muderong sequence

Sequence recognition

In the Giralia Anticline study area, the Birdrong Sandstone is recognised as a transgressive systems tract, based on its stratigraphic position and the changes in bathymetry outlined above. The base of the unit, overlying an erosion surface cut into Permian strata, probably belongs within the upper Hauterivian–lower Barremian. The transition through the upper Birdrong Sandstone to the lower Muderong Shale reflects retrogradation of the shoreface facies. According to the dinoflagellate zonation (viz. *Muderongia australis* Zone), the transition in Giralia No. 1 well lies within the late Hauterivian–Barremian. The lower 20 m of the Muderong Shale belongs also within the *Muderongia australis* Zone of late Hauterivian–Barremian age. The age of the upper siltstone–mudstone part of the Muderong Shale in the study region has not been determined, because of a lack of uncontaminated samples. A slight increase in sediment accommodation space occurred during initial deposition of the Muderong Shale, but most of the unit seems to have accumulated in an aggradational setting as part of a highstand systems tract (with water depths remaining less than 50 m).

The fine sandstone unit between typical Muderong Shale and the Windalia Radiolarite in the Giralia No. 1 well section may represent either progradation of the shoreface facies (as the terminal part of the highstand systems tract) or the basal part of a transgressive systems tract overlying the Birdrong–Muderong sequence. We have insufficient data to resolve this problem.

The Windalia Radiolarite is late Aptian in age, at least in the lower 15 m, and represents a younger sequence (mainly highstand systems tract) overlying the Birdrong–Muderong sequence.

Correlations to other western Australian basins

The dinoflagellate and acritarch succession from the Birdrong Sandstone and Muderong Shale in Giralia No. 1 is comparable to that previously described in the western margin basins of Australia. At ODP Site 765 on the Argo Abyssal Plain, 850 km north-northeast of Giralia No. 1, Helby & McMinn (1992) described a section ranging from the Berriasian to Aptian. The *M. australis* to *D. davidii* Zone interval at this site, dated as late Hauterivian to late Aptian, appears to be continuous and is approximately 200 m thick. It is closely comparable with the succession in Giralia No. 1, although with a much higher microplankton to spores–pollen ratio. Dating of the ODP Site 765 section is supported, in part, by nannofossils, radiolarians and foraminifers.

Shorter intervals with *M. australis* Zone were described from Vinck No. 1 (350 km northwest of Giralia No. 1) between 1949.8 and 1989.1 m by Stover & Helby (1987a), and from Houtman No. 1 (650 km south of Giralia No. 1) between 753.5 and 761.3 m by Stover & Helby (1987b). In Houtman No. 1 only the lowest sample contains *C. transitoria* and *S. attadalense*.

Further south, in the Vlaming Sub-basin and Dandaragan Trough of the Perth Basin, Backhouse's (1987, 1988) *B. jaegeri* and *F. monilifera* Zones are age equivalents of the *M. australis* Zone and represent the maximum onlap of pre-Albian sediments in the onshore Perth Basin. *C. transitoria* and *S. attadalense* do not range above the lower part of the *B. jaegeri* Zone (= lower *M. australis* Zone; Backhouse, 1988), thus mirroring the situation in Houtman No. 1 and Giralia No. 1.

Undoubtedly, the *M. australis* Zone represents a significant transgressive marine unit along the west coast of Australia. It also extended over some of the inland basins—as far as Browne No. 1 in the Officer Basin (Kemp 1976; Morgan 1980a; Backhouse 1988) and, less certainly, into the central Eucla Basin in Madura No. 1 (Ingram 1968; Backhouse 1988).

Correlations to eastern Australian basins

According to the palaeogeographic compilations of Frakes et al. (1987) and Dettmann et al. (1992), a major marine transgression during the late Valanginian through Barremian covered large tracts of the Carpentaria, Eromanga, and Surat Basins in eastern Australia, and portions of the Canning–Officer–Eucla Basins in the western sector of the continent. The marine transgression commenced during the Valanginian, more-or-less coincident with the transition from shoreface sands to marine shale in deeper parts of the Carnarvon Basin on the western margin of the continent and with the base of the marine Ieru Formation in the Papuan Basin on the northern continental margin. A major transgressive pulse occurred during the late Hauterivian–Barremian (time of the *M. australis* Zone and the oldest Giralia sequence) with a significant increase in the submerged continental area. A more extensive marine transgression took place during the late Aptian when radiolarian-rich marine muds covered about 60% of continental Australia (Ellis 1993; Haig & Barnbaum 1978; Haig 1979b); and a further significant transgressive pulse occurred during the late early Albian (Haig & Lynch 1993), when the deepest water developed in the epeiric basins.

The Birdrong–Muderong sequence of the Giralia Anticline correlates with parts of the Bungil Formation (Kingull Member) in the Surat Basin (Helby et al. 1987, based on presence of *F. wonthaggiensis* Zone of Valanginian to earliest Aptian age), middle to upper parts of the Cadna-Owie and Gilbert River Formations in the Eromanga and Carpentaria Basins (Burger 1986; first transgression–regression cycle of Morgan 1977, 1980b); and the upper Alene Member in the Ieru Formation of the western Papuan Basin (Phelps & Denison 1993; Granath & Hermeston 1993). It coincides with the upper part of the K1 Sequence of Valanginian to ?early Aptian age recognised by Welsh (1990) in the western Papuan Basin. Welsh's (1990) *Cassiculosphaeridia magna* Zone (roughly equivalent to the *Ascodinium cinctum* Zone of Helby et

al. 1987), which overlies the *Muderongia australis* Zone, is missing in many wells in the western Papuan Basin. According to Welsh (1990), the K1 Sequence is overlain by the late Aptian to early Albian K2 Sequence (Juha Member of Ieru Formation).

There seems to be broad correspondence in the stratigraphic patterns in most of the basins. The Birdrong–Muderong sequence coincides with an increasing marine influence in sandy units of the same age in the epeiric basins of eastern Australia. The transition from the Birdrong–Muderong sequence (late Hauterivian–Barremian) to the late Aptian–early Albian Windalia Radiolarite in the Giralia Anticline is mirrored in the change from the basal sandy units to the mud-dominated Wallumbilla Formation in the Surat, Eromanga and Carpentaria Basins in eastern Australia and the succession from K1 Sequence to K2 Sequence in the western Papuan Basin.

Precise correlations, within an accuracy of less than 1 m.y., between the Australian basins are hampered by a lack of fine biostratigraphic control for the Hauterivian to Barremian in the region. The dinoflagellate *Muderongia australis* Zone ranges from late Hauterivian through the Barremian (Helby et al. 1987; Partridge & Helby 1988), spanning about 3.5 m.y. according to the time scale of Haq et al. (1988), although tentative informal subdivisions of the zone are now being developed. The associated spore pollen zones (viz. the *Balmeiopsis limbata* Zone in western Australia and the *Foraminisporis wonthaggiensis* Zone in northern Queensland and the Papuan Basin) are stratigraphically much broader (Helby et al. 1987). The foraminiferal assemblages from this interval are of low diversity and fall below the Aptian–Albian zonation established within the northeastern epeiric basins by Haig (1979b). Nannofossils have not been recorded in the Hauterivian–Barremian of the present-day onshore Australian basins. The macrofossil record is sparse and, in northeastern Australia, is dominated by endemic bivalves.

Eustasy

As Powis (1993) noted, many Australian biostratigraphic and seismic data were used by the Exxon group to establish the cycle chart of Haq et al. (1987). Because of the possibility of circular deduction, caution is required when using this chart as an aid to Australian sequence correlation. The Birdrong–Muderong sequence of the Giralia Anticline forms part of the Lower Zuni B-3 Supercycle of Haq et al. (1987), but we cannot correlate it more finely to any of the five third-order cycles that apparently constitute the supercycle. As explained above, the biostratigraphic schemes available for correlation of the Australian deposits are chronostratigraphically broad and do not permit correlations with the same time resolution as third-order cycles. As Miall (1992) pointed out, correlation with the cycle chart requires a precision of ± 0.5 m.y., a level of accuracy far higher than even the best biostratigraphic schemes can achieve for the Cretaceous. At present, there is no method available to independently check the chronostratigraphic correlations suggested by the cycle chart.

The Birdrong–Muderong sequence in the Giralia Anticline reflects a transgressive pulse that was part of progressive Early Cretaceous submergence of vast areas on the Australian continent. This late Hauterivian–Barremian transgressive pulse is particularly apparent in the coastal basins of Western Australia and is also recognised in widely separated basins across the Australian continent. It may represent a synchronous continent-wide and, therefore, probably eustatic sea-level rise. The Early Cretaceous marine flooding episodes in Australia seem to be associated with rapid expansion of the Indian Ocean to the west of the continent (with continental breakup along the south-western margin during the Berriasian–Valanginian; Veevers et al. 1991), but may also be associated with terminal developments in a volcanic arc with Chilean-type subduction along the eastern margin (Veevers 1991).

Conclusions

The oldest Cretaceous sequence in the central part of the Giralia Anticline lies on an erosion surface cut into Permian strata and includes a basal sandstone unit, 10 m thick, correlated to the Birdrong Sandstone, overlain by 56 m of dark grey siltstone (Muderong Shale). The sandstone unit consists of friable quartz sand at the base passing upwards into more indurated quartz-glauconitic sandstone. In outcrop, glauconitic sandstone containing abundant fossil wood, scattered bones of marine reptiles (ichthyosaurs and probable plesiosaurs), and rare ammonites seems to belong to the upper Birdrong Sandstone. Dinoflagellate palynomorphs from subsurface samples indicate that the Birdrong Sandstone is of late Hauterivian–Barremian age (*Muderongia australis* Zone), as is the lower 16 m of the Muderong Shale. The age of the upper part of the Muderong Shale is unknown, as is the age of the 10 m thick sandstone unit (possibly Windalia Sand) which separates the Muderong Shale from the late Aptian Windalia Radiolarite.

Siliceous and apatitic permineralised conifer wood from the outcrop of probable Birdrong Sandstone displays prominent growth rings, indicative of a strongly seasonal climate. However, the presence of sporadic false growth rings and the relatively high average mean sensitivity measure (0.348) for the 48 studied samples suggest that the parent plants experienced substantial intra-seasonal and inter-seasonal climatic variability. The broad range of mean sensitivity values also suggests that the fossil logs were derived from a number of hinterland habitats. The presence of a range of hydrophilous pteridophytes, lycophytes and pteridosperms and abundant probable warm-climate cycadophytes in coeval Western Australian non-marine strata, the 45–50° palaeolatitude of the Carnarvon Basin during the Neocomian–Aptian, and the measured wood growth indices suggest that the Carnarvon Basin hinterland experienced seasonal humid mesothermal conditions.

Fossil hyphae preserved in spindle-shaped cavities within the permineralised conifer wood represent the first Cretaceous saprophytic fungi recorded from Australia. An absence of fruiting bodies or clamp connections prevents their precise identification, but the mode of wood decay is similar to pocket rot evident in modern trees and in Permian glossopterid gymnosperms induced by a range of basidiomycete fungi. Probable pholadid bivalve borings within the permineralised wood are referable to the ichnospecies *Teredolites clavatus* and *T. longissimus*. The abundant mollusc-bored fossil wood is characteristic of a 'log-ground' ichnofacies, which is typically developed in condensed sedimentary successions within transgressive systems tracts.

The transition from quartz-rich sandstone (lower Birdrong Sandstone) through glauconitic-rich sandstone (upper Birdrong Sandstone) with a higher dinoflagellate content, and robust agglutinated foraminifera of the *Ammobaculites* Association, to carbonaceous siltstone and mudstone with an abundant and diverse dinoflagellate microflora and the low diversity *Ammobaculites* Association suggests that sediment accommodation space increased, but remained less than 50 m. Initial retrogradation through the Birdrong Sandstone to lower Muderong Shale was followed by aggradation during most of Muderong deposition. Within the sequence, the Birdrong Sandstone and lowermost Muderong Shale represents a transgressive system tract, whereas most of the Muderong Shale is a highstand systems tract. The relationship to the Birdrong–Muderong sequence of the probable Windalia Sand unit is uncertain.

The Birdrong–Muderong sequence, as recognised in the Giralia Anticline, correlates with an increasing marine influence in sandy units of similar age in the epeiric basins of eastern Australia, and this reflects a continent-wide marine transgressive pulse during the late Hauterivian–Barremian (time of *Muderongia australis* Zone). However, precise correlations are hampered by a lack of fine biostratigraphic control. The continent-wide sea-level rise coincides with rapid expansion of the Indian Ocean to the west and possibly with terminal developments in a volcanic arc on the eastern margin.

Acknowledgements

This study, initiated by David Haig at the University of Western Australia, forms part of a broader project relating the Cretaceous–Cenozoic stratigraphy of the onshore Carnarvon Basin to continent-wide marine events. Haig wishes to acknowledge the following students, whose work on younger sequences in the Giralia Anticline provided part of the stratigraphic background for the present study: Scot Bishop, Don Clarke, Ian Copp, Kim Grey, Greg Milner, and Margaret Smith. During our work in the Giralia Anticline, we have always received a friendly welcome and invaluable assistance and guidance from Rick French of Cardabia Station, who drew our attention to the outcrops of Birdrong Sandstone. During our field study of the Birdrong Sandstone, we received geological assistance from Stefan Revets and Richard Howe of the University of Western Australia and David Watkins of the University of Nebraska. Marisa Worth assisted with the drafting of several text-figures. Access to Giralia No. 1 cores and cuttings samples was kindly provided by West Australian Petroleum Pty Ltd. We are grateful to Richard Bunt of Carnarvon Petroleum N.L. for discussing with us the seismic coverage of the study area. We thank Majorie Apthorpe, George Chaproniere, Peter Barber, and John Gorter for helpful reviews of the manuscript, . Stephen McLoughlin was funded by an Australian Research Council Postdoctoral Fellowship at the Department of Geology and Geophysics, University of Western Australia. Glynn Ellis was supported by the Swiss National Science Foundation (project No. 20-27633.89 and 20-36040.92) while at the Université de Lausanne, Switzerland. John Backhouse publishes with the permission of the Director of the Geological Survey of Western Australia.

References

Aist, J.R., 1976. Papillae and related wound plugs of plant cells. *Annual Review of Phytopathology*, 14, 290–301.

Backhouse, J., 1987. Microplankton zonation of the Lower Cretaceous Warnbro Group, Perth Basin, Western Australia. *Association of Australasian Palaeontologists, Memoir* 4, 205–225.

Backhouse, J., 1988. Late Jurassic and Early Cretaceous palynology of the Perth Basin, Western Australia. *Geological Survey of Western Australia, Bulletin* 135, 233 pp.

Blanchette, R.A., 1980. Wood decomposition by *Phellinus (Fomes) pini*: a scanning electron microscopy study. *Canadian Journal of Botany*, 58, 1496–1503.

Blanchette, R.A., 1984. Screening wood decay by white rot fungi for preferential lignin degradation. *Applied Environmental Microbiology*, 48, 647–653.

Bromley, R.G., Pemberton, S.G. & Rahmani, R.A. 1984. A Cretaceous woodground: the *Teredolites* ichnofacies. *Journal of Paleontology*, 58, 488–498.

Brunnschweiler, R.O., 1959. New Aconeceratinae (Ammonoidea) from the Albian and Aptian of Australia. *Bureau of Mineral Resources, Australia, Bulletin* 54, 1–19.

Burger, D., 1986. Palynology, cyclic sedimentation, and palaeoenvironments in the Late Mesozoic of the Eromanga Basin. *Geological Society of Australia, Special Publication* 12, 53–70.

Chaloner, W.G. & Creber, G.T., 1973. Growth rings in fossil woods as evidence of past climates. *In* Tarling, D.H. & Runcorn, S.K. (editors), *Implications of continental drift to the earth sciences.* Academic Press, *London*, 425–437.

Condon, M.A., 1954. Progress report on the stratigraphy and structure of the Carnarvon Basin, Western Australia. *Bureau of Mineral Resources, Australia, Report* 15.

Condon, M.A., Johnstone, D., Prichard, C.E. & Johnstone, M.H., 1956. The Giralia and Marrilla Anticlines, North-west Division, W.A. *Bureau of Mineral Resources, Australia, Bulletin* 25, 1–86.

Creber, G.T., 1977. Tree rings: a natural data storage system. *Biological Reviews*, 52, 349–383.

Creber, G.T. & Chaloner, W.G., 1984. Climatic indications from growth rings in fossil woods. *In* Brenchley, P.J. (editor), *Fossils and climate.* John Wiley, Chichester, 49–77.

Creber, G.T. & Chaloner, W.G., 1985. Tree growth in the Mesozoic and Early Tertiary and the reconstruction of palaeoclimates. *Palaeogeography, Palaeoclimatology, Palaeoecology*, 52, 35–60.

Dalziel, I.W.D. & Elliot, D.H, 1982. West Antarctica: Problem child of Gondwanaland. *Tectonics*, 1, 3–19.

Day, R.W., 1974. Aptian ammonites from the Eromanga and Surat basins, Queensland. *Geological Survey of Queensland, Palaeontological Paper* 34, 1–19.

Dettmann, M.E., 1985. Early Cretaceous palynoflora of subsurface strata correlative with the Koonwarra Fossil Bed, Victoria. *Association of Australasian Palaeontologists, Memoir* 3, 79–110.

Dettmann, M.E., Molnar, R.E., Douglas, J.G., Burger, D., Fielding, C., Clifford, H.T., Francis, J., Jell, P., Rich, T., Wade, M., Rich, P.V., Pledge, N., Kemp, A. & Rozefelds, A., 1992. Australian Cretaceous terrestrial faunas and floras: biostratigraphic and biogeographic implications. *Cretaceous Research*, 13, 207–262.

Douglas, J.G., 1969. The Mesozoic floras of Victoria, Parts 1 and 2. *Geological Survey of Victoria, Memoir* 28, 1–310.

Douglas, J.G., 1973. The Mesozoic floras of Victoria, Part 3. *Geological Survey of Victoria, Memoir* 29, 1–185.

Douglas, J.G. & Williams, G.E., 1982. Southern polar

forests: the Early Cretaceous floras of Victoria and their palaeoclimatic significance. *Palaeogeography, Palaeoclimatology, Palaeoecology*, 40, 199–212.

Ellis, G., 1993. Late Aptian–early Albian Radiolaria of the Windalia Radiolarite (type section), Carnarvon Basin, Western Australia. *Eclogae Geologicae Helvetiae*, 86, 943–995.

Etheridge, R., 1892. *In* Jack, R.L. & Etheridge, R., The geology and palaeontology of Queensland. *Geological Survey of Queensland, Publication* 92. 2 vols.

Etheridge, R., 1909. Lower Cretaceous fossils from the sources of the Barcoo, Ward and Nive Rivers, south central Queensland. Part 2, Cephalopoda. *Australian Museum, Record* 7, 135–165, 235–240.

Filion, L. & Quinty, F., 1993. Macrofossil and tree-ring evidence for a long-term forest succession and mid-Holocene hemlock decline. *Quaternary Research*, 40, 89–97.

Frakes, L.A. & Francis, J.E., 1990. Cretaceous palaeoclimates. *In* Ginsburg, R.N. & Beaudoin, B. (editors), *Cretaceous resources, events and rhythms.* Kluwer Academic Publishers, Dordrecht, 273–287.

Frakes, L.A., Burger, D., Apthorpe, M., Wiseman, J., Dettmann, M., Alley, N., Flint, R., Gravestock, D., Ludbrook, N., Backhouse, J., Skwarko, S., Scheibnerova, V., McMinn, A., Moore, P.S., Bolton, B.R., Douglas, J.G., Christ, R., Wade, M., Molnar, R.E., McGowran, B., Balme, B.E. & Day, R.A., 1987. Australian Cretaceous shorelines, stage by stage. *Palaeogeography, Palaeoclimatology, Palaeoecology*, 59, 31–48.

Francis, J.E., 1984. The seasonal environment of the Purbeck (Upper Jurassic) fossil forests. *Palaeogeography, Palaeoclimatology, Palaeoecology*, 48, 285–307.

Francis, J.E., 1986. Growth rings in Cretaceous and Tertiary wood from Antarctica and their palaeoclimatic implications. *Palaeontology*, 29, 665–684.

Francis, J.E. & Coffin, M.F., 1992. Cretaceous fossil wood from the Raggatt Basin, southern Kerguelen Plateau (Site 750). *In* Wise, S.W., Schlich, R., et al., *Proceedings of the Ocean Drilling Program, Scientific Results*, 120, 273-280. College Station, Texas (Ocean Drilling Program), .

Fritts, H.C., 1976. *Tree rings and climate.* Academic Press, London, 576 pp.

Granath, J.W. & Hermeston, S.A., 1993. Relationship of the Toro Sandstone Formation and the Alene Sands of Papua to the Woniwogi Formation of Irian Jaya. *In* Carman, G.J. & Carman, Z. (editors), Petroleum exploration and development in Papua New Guinea, *Proceedings of the Second PNG Petroleum Convention, Port Moresby, 31st May–2nd June 1993*, 201–206.

Greguss, P., 1955. *Identification of living gymnosperms on the basis of xylotomy.* Akadémiai Kaidó, Budapest, 263 pp.

Haig, D.W., 1979a. Global distribution patterns for mid-Cretaceous foraminiferids. *Journal of Foraminiferal Research*, 9, 29–40.

Haig, D.W., 1979b. Cretaceous foraminiferal biostratigraphy of Queensland. *Alcheringa*, 3, 171–187.

Haig, D.W., 1980. Early Cretaceous textulariine foraminiferids from Queensland. *Palaeontographica A.*, 170, 87–138.

Haig, D.W., 1981. Mid-Cretaceous foraminiferids from the Wahgi Valley, Central Highlands of Papua New Guinea. *Micropaleontology*, 27, 337–351.

Haig, D.W., 1982. Early Cretaceous milioline and rotaliine benthic foraminiferids from Queensland. *Palaeontographica A.*, 177, 1–88.

Haig, D.W. & Barnbaum, D., 1978. Early Cretaceous microfossils from the type Wallumbilla Formation, Surat Basin, Queensland. *Alcheringa*, 2, 159–178.

Haig, D.W. & Lynch, D.A., 1993. A late early Albian marine transgressive pulse over northeastern Australia, precursor to epeiric basin anoxia: foraminiferal evidence. *Marine Micropaleontology*, 22, 311–362.

Haq, B.U., Hardenbol, J. & Vail, P.R., 1988. Mesozoic and Cenozoic chronostratigraphy and cycles of sea level change. *In* Wilgus, C.K., Hastings, B.S., Kendall, C.G.St.C., Posamentier, H.W., Ross, C.A., & Van Wagoner, J.C. (editors), Sea level changes: an integrated approach. *Society of Economic Paleontologists and Mineralogists, Special Publication* 42, 71–108.

Helby, R. & McMinn, A., 1992. A preliminary report of Early Cretaceous dinocyst floras from Site 765, Argo Abyssal Plain, northwest Australia. *In* Gradstein, F.M., Ludden, J.N. et al., *Proceedings of the Ocean Drilling Program, Scientific Results*, 123, 407–420.

Helby, R., Morgan, R. & Partridge, A.D., 1987. A palynological zonation of the Australian Meosozoic. *Association of Australasian Palaeontologists, Memoir* 4, 1–94.

Hocking, R.M., 1988. Regional geology of the northern Carnarvon Basin. *In* Purcell, P.G. & Purcell, R.R. (editors), The North West Shelf, Australia. *Proceedings of Petroleum Exploration Society, Australia Symposium, Perth, 1988*, 97–114.

Hocking, R.M., 1990. Carnarvon Basin. *In* Geology and Mineral Resources of Western Australia. *Geological Survey of Western Australia, Memoir* 3, 457–495.

Hocking, R.M., Moors, H.T. & van de Graaff, W.J.E., 1987. Geology of the Carnarvon Basin. *Geological Survey of Western Australia, Bulletin* 133, 1–289.

Hocking, R.M., Voon, J.W.K., & Collins, L.B., 1988. Stratigraphy and sedimentology of the basal Winning Group, northern Carnarvon Basin. *In* Purcell, P.G. & Purcell, R.R. (editors), The North West Shelf, Australia. *Proceedings of Petroleum Exploration Society, Australia Symposium, Perth, 1988*, 203–224.

Hocking, R.M., Williams, S.J., Lavaring, I.H., & Moore, P.S., 1985. Winning Pool–Minilya, Western Australia. *Geological Survey of Western Australia, 1:250 000 Geological Series, Explanatory Notes.*

Howard, J.D. & Frey, R.W., 1984. Characteristic trace fossils in nearshore to offshore sequences, Upper Cretaceous of east-central Utah. *Canadian Journal of Earth Science*, 21, 200–219.

Ingram, B.S., 1968. Stratigraphical palynology of Cretaceous rocks from bores in the Eucla Basin, Western Australia. *Geological Survey of Western Australia, Annual Report for 1967*, 64–67.

Jefferson, T.H., 1983. Palaeoclimatic significance of some Mesozoic Antarctic fossil forests. *In* Oliver, R.L., James, P.R., & Jago, J.B. (editors), *Antarctic earth science.* Australian Academy of Science, Canberra, 593–598.

Jefferson, T.H., 1987. The preservation of conifer wood: examples from the Lower Cretaceous of Antarctica. *Palaeontology*, 30, 233–249.

Johnstone, D., Condon, M.A., & Playford, P.E., 1958. Stratigraphy of the Lower Murchision River area and Yaringa North Station, Western Australia. *Journal of the Royal Society of Western Australia*, 41, 13–16.

Johnstone, M.H., 1955. Giralia No. 1 Test, Geological Completion Report. Western Australian Petroleum Pty. Ltd. (unpublished)

Jones, R.W., Bender, H., Charnock, M.A., Kaminski, M.A. & Whittaker, J.E., 1993. Emendation of the foraminif-

eral genus *Cribrostomoides* Cushman, 1910, and its taxonomic implications. *Journal of Micropalaeontology*, 12, 181–193.

Kelly, S.R.A., 1988. Cretaceous wood-boring bivalves from Western Antarctica with a review of the Mesozoic Pholadidae. *Palaeontology,* 31, 341–372.

Kelly, S.R.A. & Bromley, R.G., 1984. Ichnological nomenclature of clavate borings. *Palaeontology*, 27, 793–807.

Kemp, E.M., 1976. Palynological observations in the Officer Basin, Western Australia. *Bureau of Mineral Resources, Australia, Bulletin* 160, 23–39.

Klinger, H.C. & Kennedy. W.J., 1977. Cretaceous faunas from Zululand, South Africa and southern Mozambique—the Aptian Ancyloceratidae (Ammonoidea). *Annals of the South African Museum*, 73, 215–359.

Kurths, J., Spiering, Ch., Müller-Stoll, W. & Striegler, U., 1993. Search for periodicities in Miocene tree ring widths. *Terra Nova*, 5, 359–363.

Lawver, L.A., Schlater, J.G. & Meinke, L., 1985. Mesozoic and Cenozoic reconstructions of the South Atlantic. *Tectonophysics*, 114, 233–254.

Malcolm, R.J., Pott, M.C. & Delfos, E., 1991. A new tectono-stratigraphic synthesis of the North West Cape area. *The Australian Petroleum Exploration Association Journal,* 31(1), 154–176.

McLoughlin, S., 1992. Late Permian plant megafossils from the Bowen Basin, Queensland, Australia: part 1. *Palaeontographica*, 228B, 105–149.

McLoughlin, S., in press. *A guide to the Cretaceous plant fossils of Western Australia*. Publication of the Department of Earth and Planetary Sciences, Western Australian Museum.

McRae, S.G., 1972. Glauconite. *Earth Science Reviews*, 8, 397–440.

Miall, A.D., 1992. Exxon global cycle chart: an event for every occasion? *Geology*, 20, 787–790.

Morgan, R., 1977. New dinoflagellate zones and a depositional model for the Great Australian Basin. *Geological Survey of New South Wales, Quarterly Notes*, 28, 10–18.

Morgan, R., 1980a. Palynostratigraphy of the Australian Early and Middle Cretaceous. *Geological Survey of New South Wales, Palaeontology Memoir* 18, 1–153.

Morgan, R., 1980b. Eustasy in the Australian Early and Middle Cretaceous. *New South Wales Geological Survey, Bulletin* 27, 105 pp.

Murray, P.F. 1985. Ichthyosaurs from Cretaceous Mullaman Beds near Darwin, Northern Territory. *The Beagle, Occasional Papers of the Northern Territory Museum, Arts and Sciences* 2(1), 39–55.

Odin, G.S. & LeTolle, R., 1980. Glauconitization and phosphatization environments: a tentative comparison. *Society of Economic Paleontologists and Mineralogists, Special Publication* 29, 227–237.

Odin, G.S. & Matter, A., 1981. De glauconarium origine. *Sedimentology*, 28, 611–641.

Parry, J.C., 1967. The Barrow Island Oilfield. *The Australian Petroleum Exploration Association Journal,* 7(1), 130–133.

Partridge, A. & Helby, R., 1988. Cretaceous global cycle chart for the Cretaceous with Australian biostratigraphy, based on Haq et al. 1987 (unpublished).

Pettijohn, F.J., 1975. *Sedimentary rocks*. 3rd edition. Harper & Row, New York.

Phelps, J.C. & Denison, C.N., 1993. Stratigraphic thickness variations and depositional systems of the Ieru Formation, Southern Highlands and Western Provinces, Papua New Guinea. *In* Carman, G.J. & Carman, Z. (editors), Petroleum exploration and development in Papua New Guinea, *Proceedings of the Second PNG Petroleum Convention, Port Moresby, 31st May–2nd June 1993*, 169–190.

Plint, A.G. & Pickerill, R.K., 1985. Non-marine *Teredolites* from the Middle Eocene of southern England. *Lethaia*, 18, 341–347.

Powis, G.D., 1993. The sequence stratigraphy of the Mesozoic reservoirs of the Gobe Anticline, Papuan Thrust Belt. *In* Carman, G.J. & Carman, Z. (editors), Petroleum exploration and development in Papua New Guinea, *Proceedings of the Second PNG Petroleum Convention, Port Moresby, 31st May–2nd June 1993*, 155–167.

Reading, H.G., 1978. *Sedimentary environments and facies*. Blackwell Scientific, Oxford, 557 pp.

Reineck, H.E. & Singh, I.B., 1980. *Depositional sedimentary environments*. Springer-Verlag, New York, 549 pp.

Richards, P.W., 1952. *The tropical rain forest: an ecological study*. Cambridge University Press, Cambridge, 450 pp.

Sahni, B., 1931. Revision of Indian fossil plants. Pt. II. Coniferales (b. petrifactions). *Geological Survey of India, Palaeontographica Indica, Memoir* 11, 51–124.

Savrda, C.E., 1991. *Teredolites*, wood substrates, and sea-level dynamics. *Geology*, 19, 905–908.

Shafik, S., 1990. Late Cretaceous nannofossil biostratigraphy and biogeography of the Australian western margin. *Bureau of Mineral Resources, Geology and Geophysics, Australia, Report* 295, 164 pp.

Sheppard, P.R. & Jacoby, G.C., 1989. Application of tree-ring analysis to palaeoseismicity: two case studies. *Geology*, 17, 226–229.

Simpson, E.S., 1912. Unusual types of petrifaction from Dandarragan. *Journal of the Natural History Scientific Society of Western Australia*, 4, 33–37.

Stover, L.E. & Helby, R., 1987a. Early Cretaceous dinoflagellates from the Vink-1 well, offshore Western Australia. *Association of Australasian Palaeontologists, Memoir* 4, 227–259.

Stover, L.E. & Helby, R., 1987b. Early Cretaceous dinoflagellates from the Houtman-1 well, Western Australia. *Association of Australasian Palaeontologists, Memoir* 4, 261–295.

Stubblefield, S.P. & Taylor, T.N., 1986. Wood decay in silicified gymnosperms from Antarctica. *Botanical Gazette*, 147, 116–125.

Stubblefield, S.P. & Taylor, T.N., 1988. Recent Advances in palaeomycology. *New Phytology*, 108, 3–25.

Stubblefield, S.P., Taylor, T.N. & Beck, C.B., 1985. Studies of Paleozoic fungi. V. Wood decay in the Upper Devonian progymnosperm , *Callixylon newberryi*. *American Journal of Botany*, 72, 1765–1773.

Turner, R., 1972. A new genus and species of deep water wood-boring bivalve (Mollusca, Pholadidae, Xylophagainae). *Basteria*, 36, 97–104.

Turner, R.D., 1973. Wood-boring bivalves: opportunistic species in the deep sea. *Science*, 180, 1377–1379.

Turner, R. & Johnson, A.C., 1971. Biology of marine wood-boring molluscs. *In* Jones, E.B.G. & Eltringham, S.K. (editors), *Marine borers, fungi and fouling organisms*. Organization for Economic Co-operation and Development, Paris, 259–301.

van de Graaff, W.J.E., Denman, P.D., Hocking, R.M. & Baxter, J.L., 1980. Yanrey–Ningaloo, Western Australia. *Geological Survey of Western Australia, 1:250 000 Geological Series, Explanatory Notes*.

Veevers, J.J., 1991. Mid-Cretaceous tectonic climax, Late

Cretaceous recovery and Cainozoic relaxation in the Australian region. *Geological Society of Australia, Special Publication* 18, 1–14.

Veevers, J.J., Powell, C.McA., & Roots, S.R., 1991. Review of seafloor spreading around Australia. 1. Synthesis of the patterns of spreading. *Australian Journal of Earth Science*, 38, 373–389.

Wade, M. 1984. *Platypterygius australis*, an Australian Cretaceous ichthyosaur. *Lethaia* 17, 99–113.

Wade, M. 1990. A review of the Australian Cretaceous longipinnate ichthyosaur *Pletypterygius* (Ichthyosauria, Ichthyopterygia). *Queensland Museum, Memoir* 28 (1), 115–137.

Welsh, A., 1990. Applied Mesozoic biostratigraphy in the western Papuan Basin. *In* Carman, G.J. & Carman, Z. (editors), Petroleum exploration in Papua New Guinea, *Proceedings of First PNG Petroleum Convention, Port Moresby, 12–14th February 1990*, 369–379.

White, M.E., 1961. Report on 1960 collections of Mesozoic plant fossils from the Northern Territory. *Bureau of Mineral Resources, Australia, Record* 1961/146, 1–26.

Whitehouse, F. W., 1926. The Cretaceous Ammonoidea of eastern Australia. *Queensland Museum, Memoir* 8, 195–242.

Wilson, K.M., Rosol, M.J., Hay, W.W. & Harrison, C:G.A., 1989. A new model for the tectonic history of west Antarctica: a reappraisal of the fit of Antarctica in Gondwana. *Eclogae geologicae Helvetiae*, 82, 1–35.

Wiseman, J.F., 1979. Neocomian eustatic changes—biostratigraphic evidence from the Carnarvon Basin. *The Australia Petroleum Exploration Association Journal*, 19 (1), 66–73.

Wrigley, A., 1929. Notes on English Eocene boring mollusca, with descriptions of new species. *Proceedings of the Geologist Association*, 40, 376–383.

AGSO Journal of Australian Geology & Geophysics, 15(4), 469–474

Earthquake duration magnitudes in southeast Australia, accounting for site, seismograph and source

J. Wilkie,[1] G. Gibson [2] & V. Wesson[2]

A new expression with superior consistency in the calculation of magnitude from earthquake coda duration has been developed. The need to take into consideration the site, the seismograph characteristics and the source has been investigated. The expression is valid for distances up to 1000 km in southeast Australia except where the source is located on some other major geological foundation, for example the Australian shield or the Tasman Sea.

The expression takes the form:

$M_D = p_1 + p_2(\log(S_D D))^{p_3} + p_4 R e^{-p_5 R}$

M_D is duration magnitude, and the parameters in the above expression are determined by regression based on local magnitude M_L. Duration, D, is in seconds, R is the hypocentral distance in kilometres, and p_n are parameters. Parameter p_1 zeroes the function to give values similar to M_L and accounts for the definition of duration; p_2 and p_3 give the shape of the variation with duration; and p_4 and p_5 give the variation with distance. S_D is the 'duration site correction factor', which varies from site to site and can be easily determined by comparing particular site durations with average durations. If the network data are electronically recorded, the value of S_D for all sites can be continually monitored and updated.

Because of the different methods of estimating D for the analogue and digital seismographs, a value of the parameter p_1 for each seismograph type is necessary.

analogue $M_D = -0.46 + 0.45(\log(S_D D))^{2.4} + 0.0045Re^{-0.002R}$
digital $M_D = -0.20 + 0.45(\log(S_D D))^{2.4} + 0.0045Re^{-0.002R}$

The above expressions present the relationship between M_D, D (measured to double the background level) and R in southeast Australia for magnitudes between M_D 0 and 5 and for distances from a few km to 1000 km.

Introduction

The size of an earthquake can be measured in a variety of ways. Most magnitude scales are based on peak amplitudes, while earthquake moment is based on low-frequency spectral content. The effect of an earthquake depends on the amplitude of the motion, the frequency content and the duration of motion. The number of cycles of motion may determine damage levels or whether liquefaction occurs, and depends on both frequency content and duration.

Duration magnitude could be defined in many ways, but it is convenient to use a definition which gives average numerical values similar to amplitude-based magnitudes. However, some short-duration earthquakes will inherently give lower duration magnitudes, while others have long durations and give higher values. A duration magnitude scale is a separate and distinct measure of the size of an earthquake. A duration magnitude is not just a simple way of determining the size of an earthquake, but is a measure of a different aspect of earthquake size. As with amplitude-based magnitude, duration magnitudes are affected by transmission path and seismograph site effects as well as the source effects, and these must be taken into account.

The duration of an earthquake at a seismograph site is usually defined as the time in seconds from the onset of the recording of the event to the time the average signal amplitude falls below a particular noise level. The decaying amplitude of the coda is a characteristic feature of the recordings of local earthquakes, and is caused by the scattering of seismic waves in the Earth's crust. Duration of an earthquake can be used as a measure of magnitude and has the advantage that off-scale recording during large or close events does not affect the measurement. In practice, duration is influenced by seismograph characteristics, location of the source, seismograph foundation, and hypocentral distance (Bakun 1984). Empirical formulae have been devised by many authors and duration magnitudes are estimated by many networks (Lee & Stewart 1981; Denham 1982; Tsumura 1967; Real & Teng 1973).

Most formulae are of the following forms :

$$M_D = p_1 + p_2 \log D + p_3 \Delta,$$

$$M_D = p_1 + p_2 \log D + p_3 (\log D)^2 + p_4 \Delta,$$

$$M_D = p_1 + p_2 \log D + p_3 \Delta + p_4 h.$$

D is duration (seconds), Δ is epicentral distance (kilometres), h is earthquake depth (kilometres) and p_n are parameters.

In the following analysis, duration magnitudes for SRC seismograph sites (Fig. 1) are studied using parametric expressions with respect to:

(i) the applicability of duration magnitudes for hypocentral distances to 1000 km,

(ii) the possibility of the adoption of one M_D formula for the whole southeast of Australia with a single site correction parameter.

The following definition of duration was adopted at the workshop on Australian earthquake magnitude scales (Denham 1982): 'duration is the time from the first motion to the finish time when the coda amplitude drops to double the background amplitude level existing before the event'. Duration could also be defined using the S-phase arrival time to a finish time related to the level of noise or a fixed trace amplitude (Bakun & Lindh 1977). Alternatively, a definition using the coda decay rate might be possible. Herrmann (1975) suggested duration might be better defined with respect to the origin time. Clearly, any definition involving the background noise is unsatisfactory, because noise differs from site to site and in the short and long term and has a strong influence on the estimation of event duration.

In this analysis, both analogue and digital recorders were used, and differences between durations for the two instrument types had to be taken into account. The instruments have different frequency responses and the

[1] Department of Applied Physics, Victoria University of Technology, PO Box 14428 MMC, Melbourne, Vic. 3000, Australia

[2] Seismology Research Centre, Royal Melbourne Institute of Technology, Plenty Rd, Bundoora, Vic. 3083, Australia

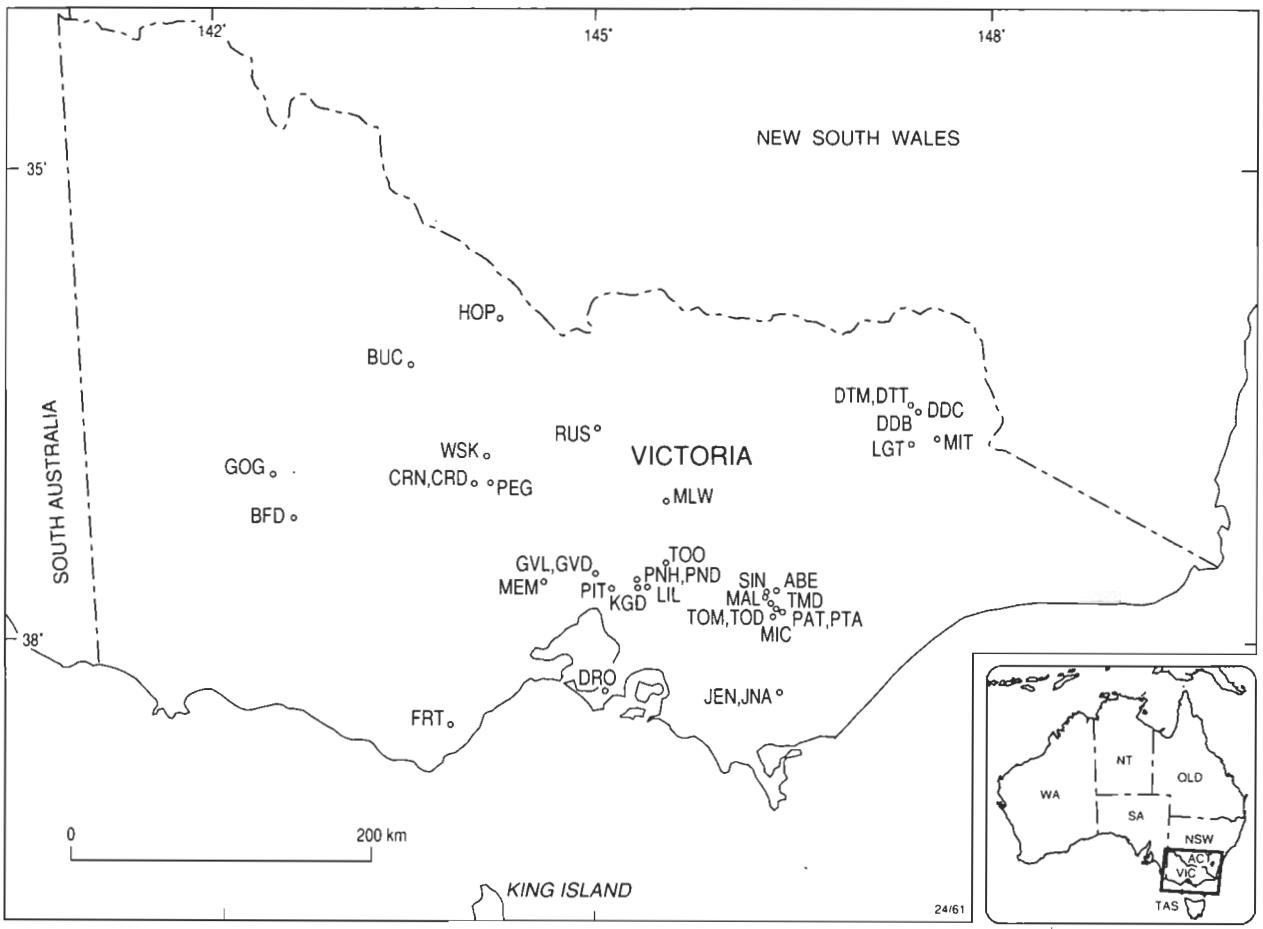

Figure 1. Map of the Victoria region showing the location of seismograph sites.

finish time as defined above (Denham 1982), in the case of analogue records, was estimated by eye, and for digital recorders was determined by computer. Digital seismographs can easily maintain a running average signal level corresponding to the background seismic noise, and this inherently has an arbitrary time constant. The finish time of an event is automatically recorded by the SRC network digital recorders and when the P-phase arrival time is measured, a duration is assigned to the earthquake.

Analysis

The SRC network of seismographs is optimised to record local microearthquakes, both in its spatial distribution and in the frequency response of the seismographs used. The recorders are either Sprengnether MEQ–800 single-component analogue instruments or triggered digital three-component recorders developed by the Seismological Research Centre. Either Sprengnether S6000, S7000 or Mark Products L4C seismometers are used. Further details of the network are given in Wilkie et al. (1993).

A data set of local magnitude values, distances, and durations at nine analogue and nine digital seismographs was studied. The number of magnitude, duration, distance combinations for each seismograph is given in Table 1.

The parametric expression initially used for the non-linear least squares regression analysis of the data, including hypocentral distances over 1000 km, was that used by Cuthbertson (1977)

$$M_D = p_1 + p_2(\log D)^{p_3} + p_4 R. \quad (1)$$

Table 1. Parameter values obtained from regression analysis of all data using expression (3), with p_2 to p_5 fixed at chosen values for southeast Australia. N is the number of earthquakes used in the analysis and SD is the standard deviation of the calculated M_D magnitudes with respect to the assigned M_L magnitudes for each earthquake.

Error = 2 · standard error.

Sites	p_1	p_1 *error*	*SD*	*N*
Analogue				
GVL	−0.357	0.047	0.250	113
PNH	−0.587	0.038	0.257	185
LIL	−0.429	0.055	0.286	109
KGD	−0.546	0.041	0.233	128
TOM	−0.528	0.032	0.283	319
PEG	−0.646	0.043	0.268	155
JEN	−0.352	0.040	0.264	196
FRT	−0.184	0.073	0.290	64
MLW	−0.480	0.062	0.240	60
		mean analogue SD	0.263	
Digital				
PAT	−0.245	0.058	0.311	113
TOD	−0.192	0.050	0.272	114
HOP	−0.552	0.060	0.322	115
ABE	0.011	0.070	0.373	114
MAL	0.332	0.093	0.299	41
MIC	0.049	0.076	0.325	73
BUC	−0.359	0.072	0.266	55
TMD	−0.305	0.073	0.308	71
RUS	−0.351	0.122	0.372	37
		mean digital SD	0.316	
		mean overall SD	**0.291**	

For the analogue seismographs (where R extended beyond 1000 km) p_4 was found to be about 0.0005, but for the digital seismographs (for which R ranged to approximately 300 km) the p_4 value was much higher at about 0.0020. This lead to the conclusion that the term p_4R needed to be replaced by a function of R which allowed this term to initially increase approximately linearly with R and then reduce in value with increasing R.

Further numerical analysis was carried out on the duration data using the expression

$$MD = p_1 + p_2(\log D)^{p_3} + p_4 R e^{-p_5 R} \quad (2)$$

The choice of the form of the term $p_4Re^{-p_5R}$ was made to give the minimum and simplest change to the term p_4R, yet accommodate the trend of the decreasing proportional contribution of the term with R. It is empirical and has no theoretical basis. A comparison of the performance of the two expressions can be made using the mean standard deviation. For expression (1) the mean standard deviation for all sites was 0.295, and for expression (2) the mean standard deviation was 0.272. For the analogue seismograph sites the mean standard deviation improved from 0.282 for expression (1) to 0.257 for expression (2). For each site the standard deviation using expression (2) was less than or equal to the standard deviation using expression (1).

We assume the p_1 term of equation (2) relates to the definition of 'duration', especially the determination of finish time, which was estimated by eye for the analogue seismograms and by automatic comparison of average noise before the event with a running mean of the absolute signal value for the digital instruments. The parameters p_2 to p_5 in the other two terms relate the duration of scattered waves and distance to magnitude. Values were determined for p_2 to p_5 for south east Australia. This was achieved by the adoption of representative values for individual parameters one at a time, taking cross-correlation coefficients into account, with repeated regression analysis determining new values of the remaining parameters, finally giving the expression

$$MD = p_1 + 0.45(\log D)^{2.4} + 0.0045Re^{-0.002R} \quad (3)$$

The data for all seismographs cannot be combined for the above analysis because this would introduce bias, owing to the different numbers of events analysed for each site.

Table 1 presents the results of the application of expression (3). The first nine sites in the table have analogue seismographs, the rest are digital. The mean standard deviation for the analogue sites increased slightly to 0.263, and the digital to 0.316. The overall mean standard deviation increased to 0.291. A higher value for the standard deviation of residuals for the digital recorders could be attributed to anomalous values of duration determined as a result of natural or artificial changes in background noise.

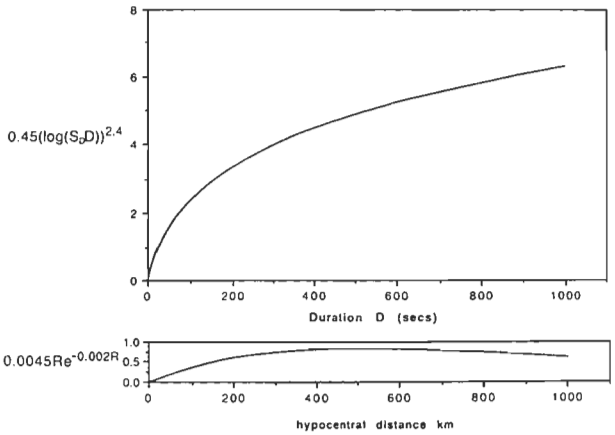

Figure 2. Plot of the contribution of the term $0.45(\log D)^{2.4}$ to the duration magnitude value (S_d = 1). Plot of the contribution of the term $0.0045Re^{-0.002R}$ to the duration magnitude value.

Figure 2 shows the magnitude contribution of the term $0.45(\log D)^{2.4}$ versus D and the contribution of the term $0.0045Re^{-0.002R}$ versus R. Note the relatively small but not insignificant contribution to magnitude of the distance term. The former reflects the conversion from a log of duration scale to the equivalent of the ML (log of maximum amplitude) magnitude scale. The latter accounts for the dependence of the duration on R, which possibly includes a data-induced dependence of magnitude on R, because the earthquakes whose duration is measured at large values of R will have the higher values of magnitude, with the smaller earthquakes not being detected.

The duration and duration magnitude are related by a non-linear function, so at least two parameters are required. The effect of distance is also non-linear, also requiring at least two parameters. Parameter p_1 combines the constant terms for both, and provides similar numeric values to ML. The expression used is the simplest possible that will incorporate both these non-linear functions.

Source effects and transmission path

Some distant earthquakes had particularly large residuals with respect to the assigned magnitude for each recording site. These earthquakes are listed in Table 2. The mean residual, MD – ML, for all analogue seismographs for the Leigh Creek and Milparinka earthquakes was +0.8 and +0.7, respectively, and for the Tasman Sea earthquake, –0.6. These large residual values can be attributed to the earthquake source region. Both Leigh Creek and Milparinka are on the Australian shield, which has lower attenuation than in southeast Australia (Wilkie et al. 1993, fig. 6,) and, therefore, earthquakes recorded at SRC sites which have part of their travel path in the shield region will record longer durations than southeast Australian events. Bakun (1984), in his parametric expression for duration magnitude for central California, included a recording site correction parameter and an earthquake

Table 2. Earthquakes giving large residual values of duration magnitude.

Place	*Date*	*Time (UT)*	*ML*	*MD*	*Longitude° E*	*Latitude° S*	*Depth*
Leigh Creek	29/12/83	1741	4.2	5.0	138.609	30.589	20
Milparinka	20/6/83	1732	4.0	4.5	141.885	30.453	17
Milparinka	8/4/83	1933	3.6	4.5	142.242	30.159	17
Tasman Sea	25/11/83	1956	5.9	5.3	155.039	40.167	36

source correction parameter.

Because of the existence of regions of differing scattering attenuation characteristics, it would appear that in the application of this type of analysis, geological regions would have to be defined for the applicability of the formula and parameters. If the earthquake and seismograph were each in different geological regions the equations must be used with caution.

The application of expression (3) above to the restricted data (with the events from other geological regions removed) gave considerable improvement in the standard deviation for the analogue sites (0.263 to 0.238). The large residual magnitudes from different geological regions were for distant earthquakes, which were only detected by the analogue seismographs.

Using expression (3) for earthquakes with transmission path longer than 250 km, with the earthquakes from other tectonic regions (Table 2) removed, the standard deviation for the distant earthquakes was in all cases, except for PNH, slightly larger than the overall standard deviation. When it is considered that the signal received from the distant earthquakes is usually small and the rate of decay of the coda is much slower than that of close earthquakes, making the estimation of finish time difficult, the higher standard deviation for the distant events is acceptable.

Site correction

Duration is affected by site effects as well as source and transmission path effects. The site to site variation in duration was investigated for particular magnitude ranges. A duration site correction factor S_D was defined to be the ratio of the average duration for the magnitude range over the duration for the site (Tables 3 and 4). Note that for each site there is little change in S_D with magnitude range. Sites which record a long duration coda have S_D less than 1.0, while those recording short durations give S_D greater than 1.0.

The mean values from Tables 3 and 4 are given in Table 5 with p_1 and corresponding standard deviation. The duration site correction factor can then be applied in expression (3), where S_D is a factor normalising D to the mean. This has practical applications, in that rather than having a correction in the calculated site magnitude, the correction here is applied to the measured quantity duration, which is directly affected by the site and seismograph characteristics. Duration is then converted by empirical parametric formulae to a magnitude value.

This site correction can be attributed to three main sources: site amplification, site noise, and instrument gain. Bakun (1984) found clear evidence of duration being related to instrument gain. At sedimentary foundation sites, horizontal components are usually significantly amplified and, although there can be some amplification of the vertical component (Wilkie et al. 1994), the effects of site amplification are minimised in our measurements of duration, because the analogue seismographs only record the vertical component, and only the vertical component is used to measure duration on the digital instruments. Because there have been many changes in the frequency response and gain (by orders of magnitude) over the period for which the data have been extracted, only a superficial assessment of the effects of gain and noise can be made. However, clearly both have considerable effect. For example, taking the extremes, HOP has a high gain at a very quiet site and has a duration correction factor of 0.78, whereas FRT, which has a low gain at a very noisy site, has a duration correction factor of 1.25. This corresponds to a change in magnitude of approximately 0.2 for a magnitude ML 2.0 earthquake.

Considerable differences in frequency response characteristics exist between the analogue and digital seismographs. In general the analogue seismographs respond to frequencies in the 5–10 Hz range and the digital seismographs respond to a broader range of frequencies of 1–25 Hz or higher. Thus, it is reasonable to adopt separate p_1 parameters for the analogue and digital seismographs, leaving the factor S_D as the only parameter which changes from site to site in the calculation of the duration magnitude.

The separate values of p_1 (Table 5) adopted are:

p_1 (analogue) = –0.46

p_1 (digital) = –0.20

Table 3. S_D for *analogue* seismograph sites expressed as the ratio of the mean duration for the magnitude range over the duration for the site.

ML	*GVL*	*PNH*	*KGD*	*LIL*	*TOM*	*FRT*	*PEG*	*JEN*	*MLW*
2	1.143	0.935	0.960	1.014	0.960	1.241	0.837	1.000	0.878
2.5	1.126	0.863	0.995	1.078	0.941	1.262	0.900	0.950	0.987
3	1.086	0.866	1.055	1.003	0.933	1.145	0.909	1.070	0.909
3.5	1.133	0.943	0.831	1.171	0.923	1.362	0.860	0.980	1.091
4	1.047	0.935	0.978	0.974	0.921	1.133	1.037	1.013	
4.5	1.110	0.848	0.788	0.909	1.020	1.372	1.067	1.016	

Table 4. S_D for *digital* seismograph sites expressed as the ratio of the mean duration for the magnitude range over the duration for the site.

Ml	*PAT*	*TOD*	*HOP*	*ABE*	*MAL*	*MIC*	*BUC*	*TMD*	*RUS*
1	1.104	0.997	0.883	1.404	1.545	1.065	0.773	1.004	0.718
2	0.911	1.004	0.609	1.157	1.587	1.366	0.843	0.976	1.077
2.5	1.041	1.082	0.739	1.261	1.600	1.231	0.894	0.844	0.812
3	1.133	1.124	0.741	1.172	1.524	1.247	0.841	0.797	0.890
3.5	0.853	1.163	0.815	1.735		1.027	0.844		0.763
4	1.045	0.947	0.898	1.076	1.326	1.129	0.980	0.845	0.870

Table 5. Values of average duration site correction factor S_D, the parameter p_1 and the corresponding standard deviation for each seismograph site resulting from regression analysis using expression (3) with D replaced by $S_D D$.

Site	S_D	p_1	*SD*	*Site*	S_D	p_1	*SD*
GVL	1.111	–0.458	0.207	PAT	1.014	–0.245	0.311
PNH	0.893	–0.455	0.232	TOD	1.053	–0.244	0.272
LIL	1.020	–0.427	0.220	HOP	0.781	–0.292	0.321
KGD	0.926	–0.458	0.225	ABE	1.300	–0.254	0.393
TOM	0.952	–0.474	0.274	MAL	1.515	–0.112	0.327
PEG	0.926	–0.548	0.243	MIC	1.162	–0.104	0.325
JEN	1.020	–0.366	0.258	BUC	0.862	–0.180	0.267
FRT	1.250	–0.454	0.249	TMD	0.893	–0.193	0.291
MLW	0.962	–0.490	0.242	RUS	0.855	–0.154	0.361
mean analogue p_1		–0.458		mean digital p_1		–0.197	
mean analogue SD			0.239	mean digital SD			0.319

Thus the final expressions for the calculation of MD for the analogue and digital seismographs from expression (3) are:

analogue

$$M_D = -0.46 + 0.45(\log(S_D D))^{2.4} + 0.0045Re^{-0.002R} \quad (4)$$

digital

$$M_D = -0.20 + 0.45(\log(S_D D))^{2.4} + 0.0045Re^{-0.002R} \quad (5)$$

Using the expressions (4) and (5), the final mean values of the standard deviations achieved for the analogue and digital seismographs were 0.242 and 0.326, respectively.

No uncertainty estimates in the parameters have been expressed, because the values are adopted from different data sets for each seismograph site with a wide variety of sample numbers in each set, making it impossible to determine meaningful uncertainty values. The criterion for adoption of the parameter values was the minimisation of the overall standard deviation for the large total data set used. The difference of –0.26 between the values of p_1 in the above expressions is a combination of the different instrument frequency characteristics and the different methods of measuring finish time.

If a particular site has an analogue and a digital seismograph and the same set of earthquakes is considered, then it would be expected that the same S_D is used for both. The measured durations for each recorder will differ, and each will be adjusted by the same factor S_D. The parameter p_1 then gives the correction to MD, depending on how the duration was defined and measured.

Discussion

Although the above parametric expressions (4) and (5) achieve a reasonable standard deviation for values of R out to approximately 1000 km, they are empirical only, and parameters have not been related to physical phenomena.

The expressions (4) and (5) above are valid for distances up to 1000 km in southeast Australia, except where the source is located on some significantly different major geological foundation, for example the Australian shield or the Tasman Sea.

Expressions are of the form:

$$M_D = p_1 + p_2(\log(S_D D))^{p_3} + p_4 Re^{-p_5 R} \quad (6)$$

The parameters and form of (6) present the relationship between MD, D, and R for the data set used, from ML 0 to 5 and distance from a few km to 1000 km. The parameters p_2, p_3 and especially p_4 and p_5 take into account the wave transmission path, so values of these will change for other areas. Figure 2 shows that the effect of distance given by p_4 and p_5 is small but not insignificant.

Characteristics of the site have been incorporated in the expressions (4) and (5) in the duration site correction factor S_D. Because of the significantly different frequency

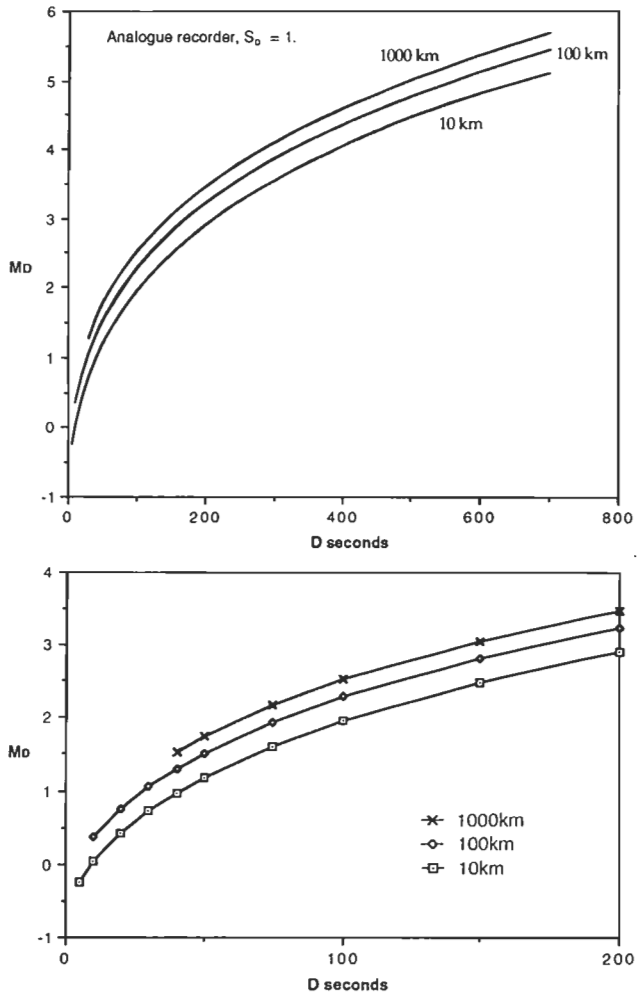

Figure 3. Plot of MD versus D for analogue seismographs with S_D = 1, for quick evaluation of earthquake magnitude for distances of 10, 100, and 1000 km. An expanded plot for durations up to 200 seconds is included.

characteristics of the analogue and digital seismographs and the different ways durations are measured for the analogue and digital seismographs, two values of p_1 are necessary. However, once the p_n parameters have been determined, the only parameter which varies from site to site is the duration site correction factor S_D. Once recording begins at a particular site, this can be easily determined by comparing the site durations with average durations for a set of earthquakes. If the network data are electronically recorded, the values of S_D for all sites can be continually monitored and updated. The value of S_D may change if there is a significant change in noise level or instrumentation sensitivity. The value of p_1 may change if there is a change in the duration criteria for either analogue or digital measurements.

Duration is usually in the range from a few seconds to a few hundred seconds, and since log10 = 1, log1000 = 3, the range of values of logD is usually in the range from 1 to 3 and these quantities have to be converted to the larger range of numbers of the ML scale, perhaps from 1 to 5 or more. A magnitude ML 2.0, for example, has a duration of about 80 seconds. A change of 10% in the estimation of the duration will give a change of approximately 0.1 in magnitude.

Figure 3 can be used to quickly evaluate magnitudes. Alternatively, expression (5) can be included in software for automatic and routine digital seismological processing.

Acknowledgments

The authors thank the referees for their helpful reviews of the paper. J. Wilkie thanks the Victoria University of Technology for supporting the research with a grant of leave, and the director, Gary Gibson, and staff of the Seismology Research Centre, RMIT, for their generous cooperation.

References

Bakun, W.H., 1984. Magnitudes and moments of duration. *Bulletin of the Seismological Society of America*, 74(6), 2335–2356.

Bakun, W.H. & Lindh, A.G., 1977. Local magnitudes, seismic moments, and coda durations for earthquakes near Oroville, California. *Bulletin of the Seismological Society of America*, 67(3), 615–629.

Cuthbertson, R.J., 1977. PIT Seismology Centre network calibration and magnitude determination. B.Sc. honours thesis, University of Melbourne (unpublished).

Denham, D., 1982. Proceedings of the workshop on Australian earthquake magnitude scales. *Bureau of Mineral Resources, Australia, Record* 1982/29.

Herrmann, R.B., 1975. The use of duration as a measure of seismic moment and magnitude. *Bulletin of the Seismological Society of America*, 65(4), 899–913.

Lee, W.H.K. & Stewart, S.W.(editors), 1981. Principles and applications of microearthquake networks. *Advances in Geophysics, Supplement 2, Academic Press.*

Real, C.R. & Teng,T.-L., 1973. Local Richter magnitude and total signal duration in southern California. *Bulletin of the Seismological Society of America*, 63(5), 1809–1827.

Tsumura, K., 1967. Determination of earthquake magnitude from total duration of oscillation. *Bulletin of Earthquake Research Institute (Japan)*, 45, 7–18.

Wilkie J., Gibson G. & Wesson V., 1993. Application and extension of the MI magnitude scale in the Victoria region. *AGSO Journal of Australian Geology & Geophysics*, 14(1), 35–46.

Wilkie J., Gibson G. & Wesson V., 1994. Richter magnitudes and site corrections using vertical component seismograms. *Australian Journal of Earth Sciences*, 41(3), 221–228.

AGSO Journal of Australian Geology & Geophysics, 15 (4), 475–499

Upper Ordovician conodonts from the Malongulli Formation, Cliefden Caves area, central New South Wales

J. A. Trotter[1] & B. D. Webby[2]

Thirty-seven spicule-dominated clasts from limestone breccia in the lower part of the Upper Ordovician Malongulli Formation of the Cliefden Caves area, central New South Wales, have yielded a collection of 2657 conodonts. These have been assigned to 48 species, dominated by *Belodina confluens* Sweet, *Besselodus* sp., *Dapsilodus mutatus* (Branson & Mehl)?, *Drepanoistodus suberectus* (Branson & Mehl), '*Oistodus*' cf. *venustus* Stauffer, *Panderodus gracilis* (Branson & Mehl), *Paroistodus*? sp. A Nowlan & McCracken, *Scabbardella altipes* subsp. B Orchard and *Walliserodus amplissimus* (Serpagli). Two new species are described, *Pseudobelodina*? *anceps* and *Taoqupognathus tumidus*. This allochthonous assemblage is a mixture of North American Midcontinent and North Atlantic-type pelagic elements, reflecting derivation from warm shallow and cooler deeper zones of the low-latitude, offshore Malongulli site. These spicule-dominated clasts probably formed initially as periplatform-ooze deposits at the outer margins of an island platform, then were incorporated in debris flows and transported basinward to become associated with the basal, *in situ*, graptolitic siltstone–shale Malongulli succession. The graptolite horizons are late Eastonian in age (Zone of *Dicranograptus hians kirki*). There is little evidence of reworking of the conodonts from older horizons. Twelve species have close North American Midcontinent affinities and may be correlated, using graphic methods, with the lower half of the Zone of *Oulodus velicuspis*, i.e. within the North American mid-upper Edenian Stage. This establishes upper limits for the age of the underlying pre-Malongulli carbonate succession, and confirms the Malongulli Formation as distinctive and much younger than the Darriwilian–early Gisbornian Malongulli-type succession to the east of Cliefden Caves.

Introduction

The acid-etched residues of allochthonous limestone from breccias in the lower part of the Ordovician Malongulli Formation, in the Cliefden Caves area of central New South Wales, contain a rich and varied conodont fauna. These are the same clasts that produced diverse assemblages of siliceous sponges (mainly demosponges and hexactinellids), discrete sponge spicules and radiolarians, described, respectively, by Rigby & Webby (1988), Webby & Trotter (1993) and Webby & Blom (1986). Altogether, 2657 conodont specimens have been recovered from the spicule-rich clasts, and these are assigned to 48 species (24 genera) (Table 1). Each clast from the three main breccia localities has been individually processed: specifically, 23 clasts (CM1–23) from Coppermine Creek (Fig. 1, locality 1), 11 (GC1–11) from Gleesons Creek (Fig. 1, locality 2), and 3 (AB1–3) from the small breccia on the Angullong side of the Belubula River (Fig. 1, locality 3). All are from similar stratigraphic levels in the lower part of the Malongulli Formation (Fig. 2). Separate upper and lower Gleesons Creek limestone breccias were previously mapped (Rigby & Webby 1988), but are now regarded as representing one very thick graded unit, repeated by thrust faulting. The most common elements of the Malongulli spicule-rich fauna are *Belodina confluens* Sweet (126 specimens), *Besselodus* sp. (140 specimens), *Dapsilodus mutatus* (Branson & Mehl)? (108 specimens), *Drepanoistodus suberectus* (Branson & Mehl) (225 specimens), 'Oistodus' cf. *venustus* Stauffer (356 specimens), *Panderodus gracilis* (Branson & Mehl) (409 specimens), *Paroistodus*? sp. A Nowlan & McCracken (229 specimens), *Scabbardella altipes* subsp. B Orchard (131 specimens), and *Walliserodus amplissimus* (Serpagli) (152 specimens).

Little descriptive work on the Middle–Upper Ordovician conodont faunas of central New South Wales (and the Australian Capital Territory) has previously been published. Savage (1990) documented the assemblage (many of them new taxa) from the lower part of the Cliefden Caves Limestone Group (Fossil Hill Limestone), in the same area as this study, but from a stratigraphically much lower level (Fig. 2). Other papers have only provided brief reports of conodont occurrences and their age significance; for example, those from Ordovician limestone–volcanic associations west of Parkes and near Sofala (Packham 1967; Pickett 1978; Pickett & Ingpen 1990), and from the more widely distributed Ordovician quartz-rich greywacke–slate–chert associations of the Lachlan Fold Belt, specifically from the slates and cherts (Nicoll 1980; Stewart & Glen 1986; Pickett 1991).

The Malongulli Formation of the Cliefden Caves area has two stratigraphically distinct graptolite assemblages, which establish the age range for the succession and, by inference, that of the limestone breccia in the lower part of the unit (Fig. 2). The graptolite association from near the base of the Malongulli Formation (Moors 1970), which directly underlies the main breccia, contains *Dicranograptus* cf. *hians kirki*, *Leptograptus eastonensis*, *Dicellograptus elegans*, and *Normalograptus tubuliferus*. This assemblage has been assigned to the Eastonian Zone of *Dicranograptus hians kirki* (Ea3), which probably corrrelates with the British *Pleurograptus linearis* Zone (VandenBerg *in* Webby & Nicoll 1989; VandenBerg & Cooper 1992), i.e. at or close to the Caradoc–Ashgill boundary. Alternatively, the assemblage may, following Williams (1982), equate with a slightly lower level, spanning an interval from the upper part of the *Dicranograptus clingani* Zone to the lower part of the *Pleurograptus linearis* Zone, that is, late Caradoc age (Fig. 3). The upper part of the Malongulli Formation has been referred to the early Bolindian Zone of *Climacograptus uncinatus* (Bo1) (Percival 1976; Jenkins 1978), which represents a level in the early-mid Ashgill. In terms of North American stages, the Malongulli Formation probably spans an interval from Edenian through Maysvillian to early Richmondian age (Fig. 3).

Two types of limestone clasts are found in the lower Malongulli Formation breccia—a coral-dominated biofacies, which probably derived from the nearby contemporaneous island-shelf carbonate succession (middle-upper Cargo Creek Limestone and equivalents to the west—see Webby & Packham 1982, fig. 6), and a distinctive

[1] CSIRO Division of Petroleum Resources, North Ryde Laboratories, PO Box 136, North Ryde, NSW 2113

[2] Department of Geology & Geophysics, University of Sydney, NSW, 2006, and Centre for Ecostratigraphy & Palaeobiology, School of Earth Sciences, Macquarie University, NSW 2109

Table 1. Distribution of conodont specimens in clasts of limestone breccia at Coppermine Creek, Gleesons Creek and on the Angullong side of the Belubula River, lower part of the Malongulli Formation, Cliefden Caves area.

SPECIES \ LOCALITY & CLAST	COPPERMINE CREEK																						ANGULLONG SIDE OF BELUBULA			GLEESONS CREEK										TOTAL
	CM1	CM2	CM3	CM4	CM5	CM6	CM8	CM9	CM10	CM11	CM12	CM13	CM14	CM15	CM16	CM17	CM18	CM19	CM20	CM21	CM22	CM23	AB1	AB2	AB3	GC1	GC2	GC3	GC4	GC5	GC6	GC7	GC8	GC9	GC10	GC11	
Ansella sp.	5	1								3	5	1	3		1	1	2																1				23
Belodina confluens Sweet	2	2	1	8	7	2	6	4		12	11	2	4	6	7	2	18		4		15		1		1		2	6		3							126
Belodina sp.A	1	1	1	1	1			1			2				1		4		2		1																16
Belodina sp.B		1			1				1								1				4																8
Belodina sp.C					1														2		7																10
Belodina sp.D										2							1												1								3
Belodina sp.E		2																																			2
Belodina sp.F											1										1																2
Belodina sp.G				1															1																		2
Besselodus sp.	13	8			27	2	1	12	1	1	1	2	9	16	6		10				16						1	3			1	2			7	1	140
Chirognathus duodactylus Branson & Mehl?															1		1																				2
Culumbodina? sp.				2		1	1	1					1				1										1										8
Dapsilodus mutatus (Branson & Mehl)?	16	5		11	5	3	3	6	1	4	1	8	8	1	3		7			1	17						4			1				1	2		108
Drepanoistodus suberectus (Branson & Mehl)	23	3		5	9	16	1	9	2	38	6	4	6	5	12	5	14	1		2	39			1	4		5	1		3		1	3		7		225
Istorinus? sp.	5							3		10	2	1		3		1					1												1		3		30
"Oistodus" cf. venustus Stauffer	50	4		2	28	9	9	4		37	35	10	17	20	27	9	21	3	1	1	45			2	1	1				1		1	5	5		6	3	356
Oulodus cf. oregonia (Branson, Mehl & Branson)																	1																				1
Ozarkodina sesquipedalis Nowlan & McCracken	2				1		4			4		1	2		1		11				7					4								2			39
Panderodus gracilis (Branson & Mehl)	58	15		33	15	26	14	14	8	17	12	23	18	36	17	11	21	4	4	4					5	7	8	9		14	1	1	1	3	7	3	409
Panderodus sp.A	27				1				2	4	3	7	8	13	4	2	3			1													1				76
Panderodus sp.B										2						1	1																				4
Panderodus sp.C				3								1		1	1																						6
Panderodus sp.D	4	1			3	1				10			5		7	1	7		2		8				1	3		1		1			1				56
Panderodus? liratus Nowlan & McCracken														1											1												2
Paroistodus sp.	5					7		2		10	4	1	4	2	2		4				7						1			3						1	53
Paroistodus? sp. A. Nowlan & McCracken	52				10	1	7	11		13	23	19	15	32	11	6	7	4			10			2							3	2			1	229
Periodon grandis Ethington	2										2				1										1												6
Periodon? sp.																	1																				1
Phragmodus undatus Branson & Mehl	4					1		2		24	7	3	5	1	1	1		1								2		1				1	1		5		60
Protopanderodus insculptus (Branson & Mehl)					1	10		2		4	6								1	3	18										1					1	47
Protopanderodus liripipus Kennedy, Barnes & Uyeno	1					11											5																				17
Pseudobelodina dispansa (Glenister)	11	1		5	7		7			1	2	4	3	6	2	2	27			1	16	1				2				1	2					101
Pseudobelodina inclinata (Branson & Mehl)	4	1		5			1		1							1													1								14
Pseudobelodina sp.A								1																													1
Pseudobelodina sp.B										1																											1
Pseudobelodina? anceps sp. nov.	26				2		2		1	2		17	14	19	2	3					3	1														1	93
Pseudooneotodus beckmanni (Bischoff & Sannemann)					1						1																1										3
Pseudooneotodus mitratus (Moskalenko)					1	2				1	1						2																				7
Scabbardella altipes subsp.B Orchard	11	2		2	3	20	3	5	1	11	6	5	4	8	1	1	20			1	15	1		1	1		1			3	3	1			1		131
Strachanognathus parvus Rhodes	1				1	3											1				1																7
Taoqupognathus tumidus sp. nov.	3	1		3	4	1	2	2		3	3	1	2				6				6	1															38
Walliserodus amplissimus (Serpagli)	19	1		3	8	2	1	6		25	7	4	4	9	7	1	5	1	1		28		1		2	1		4		3		5	1	1	2		152
Yaoxianognathus? tunguskaensis (Moskalenko)																	2																	2			4
Zanclodus levigatus Nowlan & McCracken					2						2			1			2										1										8
Gen. et sp. indet.A																	1																				1
Gen. et sp. indet.B																										1											1
Gen. et sp. indet.C	8			1	2	2		1		1		4		7																							26
Gen. et sp. indet.D	1																																				1
																																					2657

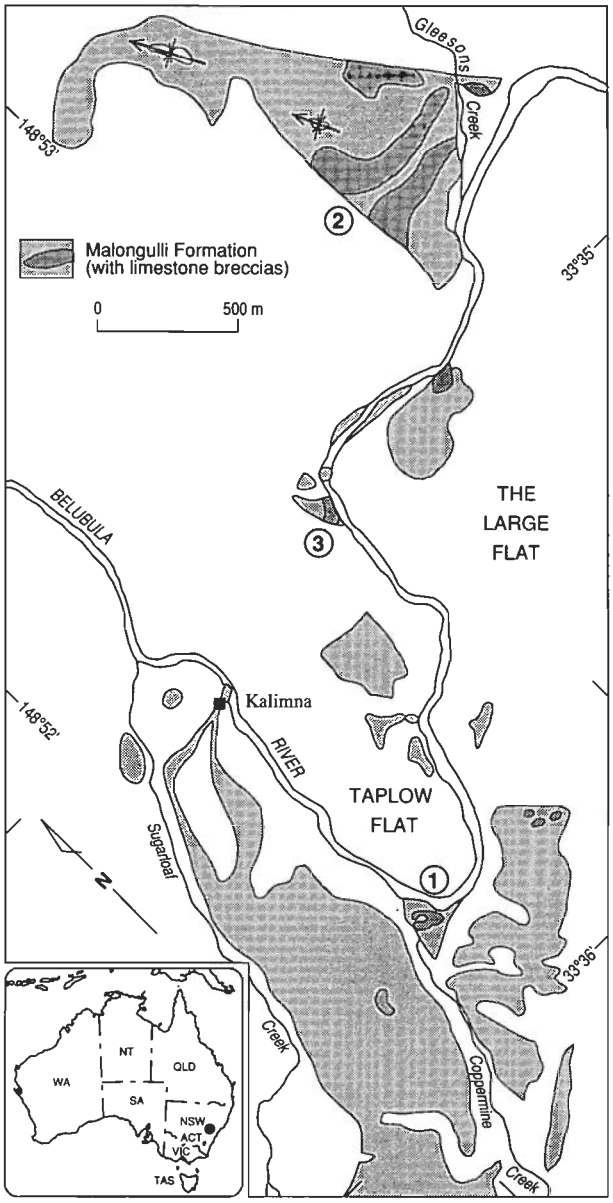

Figure 1. Location of the Cliefden Caves area and outcrop of the Malongulli Formation with associated limestone breccia, central New South Wales. Note the location of the conodont-bearing breccia at Coppermine Creek (1), Gleesons Creek (2), and on the Angullong side of the Belubula River (3).

sponge-dominated 'periplatform ooze' biofacies (tabular blocks, distinctively laminated and containing abundant siliceous spicules). The 'periplatform ooze' biofacies is not known from the associated *in situ* island-shelf carbonate sequence (see Webby 1992, fig. 6). The tabular, spicule-rich clasts were probably eroded from the outer island-shelf or upper slope by debris flows moving basinward from the island shelf (Rigby & Webby 1988; Webby 1992). The conodont faunas described herein come exclusively from the spicule-rich, 'periplatform ooze'-derived breccia clasts.

It has previously been noted (Rigby & Webby 1988; Webby 1992) that the shallow-water carbonates of the underlying Cliefden Caves Limestone Group (Fossil Hill to Vandon Limestones inclusive; see Fig. 2) with their warm-water coral and stromatoporoid associations formed on volcanic highs at low-latitudes off the Gondwana continental margin. The high concentrations of siliceous organisms (sponges and radiolarians) in the tabular clasts of the Malongulli breccias suggest that a favourable slope environment may have existed, possibly because of a ready supply of nutrients associated with upwelling at the equatorial convergence (Rigby & Webby 1988; Webby 1992).

There is little evidence to suggest that the clasts of the Malongulli breccia were reworked from significantly older horizons. The compound cerioid rugose coral *Favistina*, specifically *F. floweri*, occurs in the island-shelf deposits to the west, notably in the upper parts of the Cargo Creek and Canomodine Limestones (Webby 1988) and is not known from older stratigraphic levels of the island-shelf

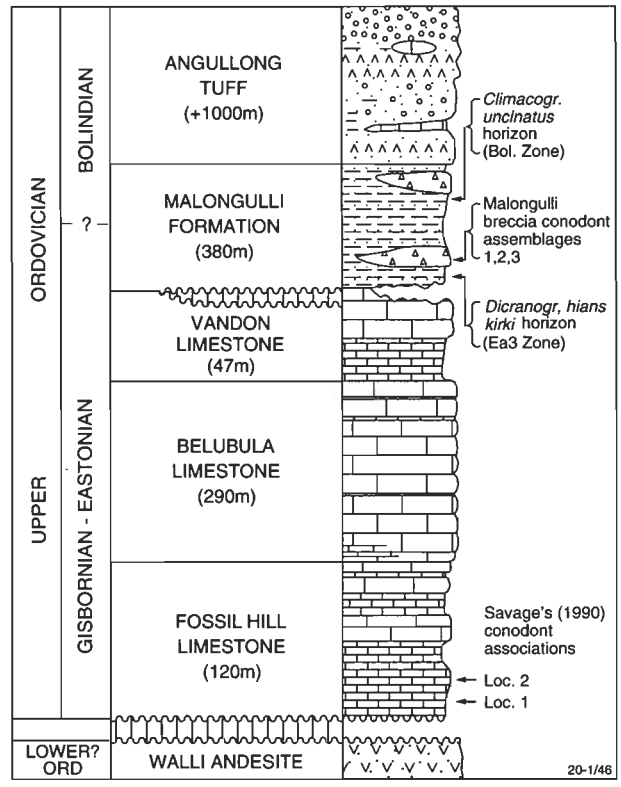

Figure 2. Generalised stratigraphic column of the upper Ordovician sequence in the Cliefden Caves area, showing horizons with Savage's (1990) conodont associations in the lower part of the Fossil Hill Limestone, and the lower Malongulli breccia with the Coppermine Creek (1), Gleesons Creek (2) and Angullong side of the Belubula River (3) conodont assemblages. The graptolite zonal indicators in the basal and upper parts of the Malongulli Formation are also shown. The Fossil Hill, Belubula Limestone and Vandon Limestone are the component formations of the Cliefden Caves Limestone Group.

successions; indeed, it is a diagnostic representative of the biostratigraphically distinct coral–stromatoporoid fauna IIIb (Webby *in* Webby et al. 1981; *in* Webby & Nicoll 1989). This same species of *Favistina* is present in clasts of the lower Malongulli breccias, establishing that it was reworked from contemporaneous, not older, deposits.

The spicule-rich clasts, derived from environmental settings further offshore, also show little indication of being reworked from older deposits of ages. Of the 2657 conodonts processed, only the occurrences of *Ansella* sp. (23 specimens) and *Chirognathus duodactylus* (two speci-

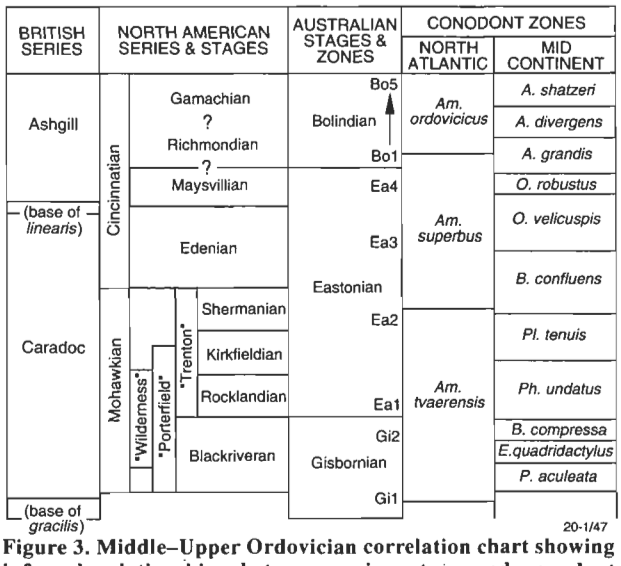

Figure 3. Middle–Upper Ordovician correlation chart showing inferred relationships between series, stage and conodont zonal schemes (based on Bergström 1990; Fortey et al. 1991; VandenBerg & Cooper 1992; MacKenzie & Bergström 1993). Note that the Australian column is based on graptolite zones (Gi1–2, Ea1–4 & Bo1–5), and that in the British column the levels at the base of *Nemagraptus gracilis* Zone and the base of *Pleurograptus linearis* Zone are shown (the base of the *linearis* Zone is equivalent to the top of the *Dicranograptus clingani* Zone).

mens) suggest reworking from older (?Middle Ordovician) horizons; but they represent less than one per cent of the total fauna.

Palaeoenvironments

The conodonts from the spicule-rich clasts comprise a diverse fauna dominated by cosmopolitan species (taxa occurring in both North Atlantic and North American Midcontinent 'provinces' of Sweet & Bergström 1984) as well as species of characteristic North American Midcontinent-type. The cosmopolitan species appear mainly to have been derived from North Atlantic forms, and are represented by *Dapsilodus mutatus* (Branson & Mehl)?, *Protopanderodus insculptus* (Branson & Mehl), *Protopanderodus liripipus* Kennedy, Barnes & Uyeno, *Strachanognathus parvus* Rhodes, and *Periodon grandis* Ethington. Other taxa of more restricted North Atlantic affinity are primarily represented by *Scabbardella altipes* Subsp. B Orchard and *Walliserodus amplissimus* (Serpagli). *W. amplissimus* is known from the Carnic Alps (Serpagli 1967) and England and Wales (Orchard 1980), but has also been reported from Canada by Nowlan et al. (1988). Elements characteristic of Chinese and Siberian faunal 'provinces' are rare, being represented by *Taoqupognathus tumidus* sp.nov., *Yaoxianognathus? tunguskaensis* (Moskalenko), and *Culumbodina*? sp.

Species characteristic of the North American Midcontinent fauna include *Panderodus gracilis* (Branson & Mehl), *Belodina confluens* Sweet, *Pseudobelodina dispansa* (Glenister), *Paroistodus*? sp. A Nowlan & McCracken, and *Phragmodus undatus* Branson & Mehl. Rare specimens of *Oulodus* cf. *oregonia* (Branson, Mehl & Branson), *Chirognathus duodactylus* Branson & Mehl?, and *Zanclodus levigatus* Nowlan & McCracken were also recovered. *Phragmodus undatus* (Branson & Mehl) is characteristic of the North American Midcontinent 'province', though it also occurs rarely in North Atlantic faunas, while *Drepanoistodus suberectus* (Branson & Mehl) is truly cosmopolitan, being equally represented in both faunal provinces (Sweet & Bergström 1984).

In terms of overall percentages, the cosmopolitan species in the fauna constitute 34.5% of the total, elements characteristic of the North American Midcontinent make up 37%, and elements of the North Atlantic, almost 11% of the total. Minor additions are the Siberian–Chinese (1.9%) and a proportion of undiagnostic elements (15.6%).

Individually, the most common taxa are *Panderodus gracilis* (15.5% of the total), '*Oistodus*' cf. *venustus* (13.5%), *Paroistodus*? sp. A Nowlan & McCracken (9.0%), and *Drepanoistodus suberectus* (8.5%). The belodinans comprise 14% of the fauna, of which *Belodina confluens* and *Pseudobelodina dispansa* alone make up 8.5%. *B. confluens* and *P. dispansa* probably represent a part of the same apparatus (S.M. Bergström pers. comm. 1994). Bergström (1990) has recorded *B. confluens* as an important constitutent of the North American Midcontinent fauna and present in Scottish, Polish, and Swedish successions. In contrast, the most dominant North Atlantic species are *Walliserodus amplissimus* (6%) and *Scabbardella altipes* subsp. B (5% of the total).

There is a strong association between some elements of the Malongulli spicule-clast fauna and the D1–4 species clusters of Sweet & Bergström's (1984) Late Ordovician *Oulodus velicuspis* 'Chronozone' (late Edenian–early Maysvillian). Species present in both faunas are *Belodina confluens*, *Drepanoistodus suberectus*, *Phragmodus undatus*, *Periodon grandis*, *Pseudobelodina inclinata*, *Panderodus gracilis*, *Protopanderodus liripipus*, and *Dapsilodus mutatus* (the latter being only tentatively identified in the Malongulli fauna). Sweet & Bergström (1984), using cluster analysis of conodont data across the equatorially disposed North American Platform during the *O. velicuspis* zonal interval, were able to differentiate species into site clusters A–D. Many with wide distributions were grouped in clusters D1–4. As Sweet & Bergström (1984) further noted, the species in the D1–4 clusters, also had extra-North American, essentially cosmopolitan, distributions in Late Ordovician seas. The Malongulli (D1–4) species constitute 36% (40% if *Pseudobelodina dispansa* is regarded as belonging to the *Belodina confluens* apparatus) of the total New South Wales fauna.

Additionally, Sweet & Bergström (1984) recognised a number of specific environmental differences between the D-clustered North American occurrences. *Drepanoistodus suberectus* was regarded as a eurythermal, cosmopolitan species with equal representation in cold and warm-water faunas; *Panderodus gracilis*, *Dapsilodus mutatus* and *Protopanderodus liripipus* as stenothermal, inhabiting the deeper, cold-water (or North Atlantic) realm of low latitudes; and *Belodina confluens* and *Phragmodus undatus* as characteristic of the warm-water realm.

The presence of stenothermal *Panderodus gracilis*, *Dapsilodus mutatus*? and *Protopanderodus liripipus*, as well as *Drepanoistodus suberectus* and *Periodon grandis*, in the Malongulli fauna confirms the existence of a relatively deeper and cooler water mass. Together, these components of the Malongulli fauna constitute 31% of the total. Significantly, Sweet & Bergström (1984) have also noted that on the North American Platform the deepest *O. velicuspis* 'Chronozone' conodont biofacies is typified by

an abundant association of *Periodon grandis* and *Dapsilodus mutatus*. *Scabbardella altipes* subsp. B and *Walliserodus amplissimus* are additional restricted North Atlantic (cooler water) elements in the Malongulli fauna.

Phragmodus undatus is recognised as a warm-water indicator and, in the North American Upper Ordovician, as characterising a comparatively shallow, offshore biofacies, above the deep-water association with *Dapsilodus mutatus*? and *Periodon grandis* (Sweet & Bergström 1984). In the Cincinnati region, Sweet (1988) showed *P. undatus* as the chief representative of an oxygenated and well-lit water mass above the deep bottom waters and offshore from the shallow shelf environments. Nowlan & Barnes (1981) have noted in the Vauréal Formation (Richmondian) of Anticosti Island that increased abundance of *P. undatus* in the succession reflects a phase of the deeper subtidal conditions. In the spicule-bearing clasts of the Malongulli breccia, this species represents some 2.3% of the total fauna.

The shallowest component of the Malongulli fauna is suggested by typical warm-water, North American Midcontinent-type species, such as *Belodina confluens*, *Pseudobelodina dispansa*, *Oulodus* cf. *oregonia*, *Chirognathus duodactylus*?, *Zanclodus levigatus*, and *Besselodus* sp. However, only *B. confluens* and *P. dispansa* (possibly part of the same apparatus) are present in sufficient numbers (8.5% of the fauna) to suggest that a component of the very shallow, nearshore *Pseudobelodina* biofacies (Sweet & Bergström 1984) may also be represented.

It seems, in conclusion, that the conodont fauna of this particular offshore, deeper water, siliceous sponge-dominated, low-latitude Malongulli site comprised a mixture of pelagic elements—North American Midcontinent types, derived from warm, shallow surface waters, and North Atlantic and cosmopolitan types, which accumulated from cooler, deeper, possibly near-bottom, waters.

Biostratigraphy

The graptolite assemblage in the lower part of the Malongulli Formation has a late Eastonian age (Ea3 Zone) (Moors 1970; VandenBerg *in* Webby et al. 1981), and the contemporaneous, conodont-bearing, spicule-rich clasts of the associated breccia are likely to be of similar age. In the absence of close ties between the graptolite and conodont zonal schemes, it is difficult to precisely relate this late Eastonian (Ea3) zonal level to the well-established North American or European conodont biozonations. It equates with a level in the Early Cincinnatian (Edenian–early Maysvillian) or Late Caradoc to Caradoc–Ashgill boundary (Fig. 3), but the precise correlation to zonal level is difficult.

As already noted, elements of the Malongulli fauna have close ties with components of the North American fauna at the level of the Late Ordovician *O. velicuspis* Zone (late Edenian–early Maysvillian), but a more precise means of correlation is needed. This may be provided by comparing the Malongulli species with the conodont ranges established numerically, using the graphic correlation methods of Sweet (1984) for the upper Middle and Upper Ordovician rocks of the North American Midcontinent 'province'. Based on a composite standard section (CSS), a numerical time-range was allocated to each North American conodont species, and to each zone and stage subdivision.

Twelve Malongulli species have similar occurrences to the North American forms. Five in particular have comparatively short numerical CSS ranges—*Belodina confluens* (1025–1169), *Periodon grandis* (968–1149), *Pseudobelodina inclinata* (1092–1268), *Chirognathus duodactylus* (967–987), and *Oulodus oregonia* (1014–1111). The last two are only tentatively assigned in the Malongulli fauna (*Ch. duodactylus*? and *O.* cf. *oregonia*). The six longer ranging forms and four of the five short-ranging species have common occurrences through the 1092–1111 interval, which equates with the lower part of the *O. velicuspis* Zone, i.e. middle to late Edenian. The fifth, short-ranging species is *Ch. duodactylus*? and is excluded because it is not identical with the North American *Ch. duodactylus* (having lower CSS values 967–987). If *Oulodus* cf. *oregonia* is also excluded, because of its tentative assignment, the remaining three short-ranging species have common occurrences through the 1092–1149 interval, which correlates with almost the entire *O. velicupis* Zone, i.e. from mid-Edenian to early Maysvillian.

A further point of qualification is that, although Sweet (1984, 1988) recognised *B. confluens* as having its last appearance in the mid-Maysvillian, Nowlan et al. (1988) recorded it from a Richmondian fauna in the Northwest Territories of Canada. Bergström (1990) has similarly noted that *B. confluens* may range upwards into the lower part of the North Atlantic *Amorphognathus ordovicicus* Zone (Fig. 3), but has mainly been recorded from the *A. superbus* Zone (i.e. equivalent to ranging through the Shermanian, Edenian to early Maysvillian).

Most North Atlantic elements of the fauna are long-ranging species, of little value for precise correlation. *Walliserodus amplissimus* is a representative of the *Amorphognathus ordovicicus* Zone fauna in the British Isles (Orchard 1980), and occurs in the Ashgill of the Carnic Alps (Serpagli 1967) and Richmondian of the Northwest Territories, Canada (Nowlan et al. 1988). *Protopanderodus insculptus* is also a characteristic species of the *A. ordovicicus* Zone (Bergström 1971; Kennedy et al. 1977), and has been recorded from Ashgill deposits (Viira 1974; Serpagli 1967) as well as from the upper part of the underlying *Amorphognathus superbus* Zone of the late Caradoc (Dzik 1978). *Protopanderodus liripipus* has been reported from the *A. ordovicicus* Zone of Wales (Savage & Bassett, 1985) and the upper part of the *A. tvaerensis* Zone (middle Caradoc) of Tasmania (Burrett et al 1983). *Dapsilodus mutatus* has been recorded as having a similarly long range in Scotland (*A. tvaerensis* to *A. ordovicicus*), while *Scabbardella altipes* occurs in both the *A. superbus* and *A. ordovicicus* Zones of Scotland (Bergström 1990). *Strachanognathus parvus* is considered a characteristic conodont species of the *A. ordovicicus* Zone (Bergström 1971), but is known from much older (Arenig) strata (Löfgren 1978, p.112).

Remarks on other local Ordovician conodont faunas

Conodonts from the Fossil Hill Limestone, Cliefden Caves area

Savage (1990) described the Upper Ordovician conodont faunas (many of them new taxa) from the lower part of the Cliefden Caves Limestone Group, specifically from two horizons (his localities 1 and 2) in the lower part of the Fossil Hill Limestone, some 400 m stratigraphically

below the Malongulli breccia fauna described here (Fig. 2). He recorded new species of *Aphelognathus*, *Belodina*, *Yaoxianognathus*, and *Taoqupognathus*, in addition to reporting *Panderodus gracilis*, *Belodina confluens*, and *Phragmodus? tunguskaensis* in the fauna. Savage claimed, mainly on the basis of the range of *B. confluens* in the North American Midcontinent Province, a middle to late Caradoc (mid-Shermanian to mid-Edenian) age for the lower part of the Fossil Hill succession, in contrast to the earlier view of Webby et al. (1981) and Webby & Packham (1982) of an early to middle Caradoc (late Gisbornian) age for this basal part of the succession.

Unfortunately, the fauna described by Savage (1990) is undiagnostic, and his use of *B. confluens* for defining the lower age limit of his assemblages does not help. According to Sweet (1984) and Bergström (1990), *B. confluens* ranges down into the upper *A. tvaerensis* Zone, which correlates with the middle Caradoc (or a level in the Kirkfieldian or Shermanian). Packham (*in* Webby 1969) and Barnes (*in* Webby & Kruse 1983) suggested, from preliminary determinations of the conodont faunas, that the horizons in the lower part of the Cliefden Caves succession were of late Porterfield? or early Wilderness (i.e. Blackriveran) aspect (Fig. 3). This was an important basis for Webby et al. (1981) suggesting a late Gisbornian (early to middle Caradoc) age.

The basal part of the overlying Malongulli Formation, with its conodont-bearing, spicule-rich clasts, is late Eastonian (Ea3 Zone) and probably correlates with the North American middle to late Edenian. It is at least 400 m higher than the Fossil Hill units containing Savage's conodont fauna (Fig. 2) and, based on studies of other fossil groups, this 400 m represents the stratigraphic equivalent of at least one biozone. The intervening Vandon Limestone, for example, has coral/stromatoporoid, trilobite and brachiopod assemblages which are biostratigraphically distinct from underlying, and laterally equivalent, overlying carbonate sequences (Webby 1974; Webby *in* Webby & Nicoll 1989; Percival 1992) and cannot be younger than middle Eastonian (Ea2). The underlying Fossil Hill Limestone and Belubula Limestone (Fig. 2) must be early to middle Eastonian or older (but probably no older than late Gisbornian). In terms of North American stages, this is about equivalent to the Rocklandian or Kirkfieldian (Fig. 3). Current work by Dr Zhen Yongyi (University of Sydney, personal communication, October 1994) on the conodont assemblages of the Fossil Hill Limestone confirms the presence of important diagnostic elements additional to those studied by Savage. A species of *Tasmanognathus* occurs in the lower part, then *Phragmodus undatus* appears towards the middle of the Fossil Hill sequence. The lower member of the Benjamin Limestone in Tasmania shows a similar record of appearances through assemblages OT12 to 14 of Banks & Burrett (1980), and this part of the Tasmanian sequence is usually equated with the late Gisbornian (Blackriveran) to early Eastonian (Rocklandian–Kirkfieldian) interval (Banks & Burrett 1989; Webby 1991).

Conodonts from the Coombing Formation (formerly 'Smith's Malongulli Formation'), east of Cliefden Caves

The Malongulli Formation was originally defined by Stevens (1952) based on a 'calcareous facies' developed only in the Cliefden Caves area. However, the conception of the formation was widened by Stevens (1957) to include a 'siltstone–arenite' facies in the region to the east, in the mistaken belief that both facies have a similar age. Since the 1970s, the type Malongulli Formation in the Cliefden Caves area (Moors 1970; Percival 1976) has been established as having a late Eastonian to early Bolindian age. The 'siltstone–arenite facies' is now recognised as a distinctly older, Darriwillian (Da3)–early Gisbornian (Gi1) unit. It contains graptolites *Cryptograptus tricornis*, *Pseudotrigonograptus ensiformis*, *Loganograptus logani*, *Amplexograptus* sp., *Isograptus* sp., and *Tetragraptus* sp. of probable Da3 age (Smith 1966; Packham 1969) and assemblages with *Glyptograptus* sp. (previously referred to *G. teretiusculus*, but possibly *G.* sp.A of VandenBerg & Cooper 1992, p.44), *Dicellograptus* sp., and *Nemagraptus gracilis* (C.J. Jenkins *in* Taylor 1988). A few localised limestone pods have produced conodonts *Periodon aculeatus*, *Belodella jemtlandica*, *Protopanderodus* cf. *robustus*, and platform-element *Eoplacognathus* sp. of broadly similar age range (Taylor 1988; Pickett 1992).

Webby (1973, p. 446; 1974; 1976; *in* Webby et al. 1981, p.30) has consistently referred to this distinctive Darriwillian–early Gisbornian unit as Smith's 'Malongulli Formation'. Taylor (1988) informally renamed it the 'Weemalla Beds', and Wyborn (1992, fig. 1) mapped the area with the fossil occurrences as a part of his 'Coombing Formation', but many other workers have, since the 1970s, failed to distinguish the unit from the type Malongulli Formation.

Systematic descriptions

All the illustrations in Plates 1–7 are SEM photomicrographs. Figured specimens bearing the prefix CPC are deposited in the Commonwealth Palaeontological Collection of the Australian Geological Survey Organisation, Canberra. For details of the localities within the Malongulli Formation of the Cliefden Caves area, see the Canowindra 1:50 000 topographic maps 8630-I and IV (First edition, 1978). Details of these localities and horizons are given in Rigby & Webby (1988) and Webby & Trotter (1993). The main localities (see Fig. 1) have the following grid references: lower limestone breccia at Coppermine Creek, FC736810 (locality 1); lower (and tectonically repeated) limestone breccia at Gleesons Creek, FC757829 to FC757830 (locality 2); and lower limestone breccia at the Belubula River (Angullong side), FC745823 (locality 3). Numbers of conodont species are listed for each clast in Table 1. Details of clast numbers of all figured specimens are included in brackets in the plate captions.

The Malongulli conodonts are mainly well preserved, especially those from the limestone breccias at Coppermine Creek. The specimens characteristically have Colour Alternation Index (CAI) values of 4 to 6, suggesting heating of the host rocks to temperatures higher than 200°C (Epstein et al. 1977).

Phylum **Conodonta** Pander, 1856

Class **Conodontata** Pander, 1856

Order **Conodontophorida** Eichenberg, 1930

Genus ***Ansella*** Fåhraeus & Hunter, 1985

Type species. *Belodella jemtlandica* Löfgren, 1978

Ansella sp.

Pl. 1, figs 1–5; Pl. 2, figs 5 & 6; ?Pl. 5, fig. 32

Remarks. The association assigned to this species comprises mainly denticulate elements (Pl. 1, figs 1–5), a few adenticulate elements (Pl. 2, figs 5 & 6) and a probable geniculate element (Pl. 5, fig. 32). The denticulate elements are characterised by a high sinuous blade-like structure that becomes denticulate orally. The denticles of *A. jemtlandica* (Löfgren) and *A. sinuosa* (Stouge) differ in being fewer, usually coarser, lower and more clearly differentiated basally. Stouge (1984) included a fine, 'hairlike' denticulate form as *A. jemtlandica* (Löfgren) which may be conspecific with *A.* sp., although the geniculate element of the former differs greatly from that tentatively assigned to *A.* sp. (Pl. 5, fig. 32). This latter geniculate element features a truncated anterobasal corner, and has a straight upper basal margin, which is expanded posteriorly. *Ansella nevadensis* (Ethington & Schumacher) is distinctly triangular in basal cross-section and accommodates a strong anterolateral furrow and carina, whereas *A.* sp. features 1 or 2 fine keels along the anterior margin.

Genus ***Belodina*** Ethington, 1959

Type species. *Belodus compressa* Branson & Mehl, 1933

Belodina confluens Sweet, 1979

Pl. 2, figs 7?, 18–20, 24, 25, 27–30

1979 *Belodina confluens* Sweet 1979, p. 59–60, fig. 5 (10, 17), fig. 6 (9).

1981 *Belodina confluens* Sweet; Sweet *in* Ziegler, p. 73–77, pl. 2, figs 8–14.

1988 *Belodina confluens* Sweet; Nowlan & McCracken, *in* Nowlan et al., p. 12, pl. 1, figs 16–21 (*cum. syn.*)

1989 *Belodina confluens* Sweet; McCracken & Nowlan, p. 1888, pl. 1, figs 19–21; pl. 2, figs 1 & 2.

1990 *Belodina confluens* Sweet; Uyeno, p. 71, pl. 1, figs 8 & 9.

1990 *Belodina confluens* Pickett & Ingpen, p. 6, cover photo, K.

Remarks. The compressiform elements are distinguishable from those of other species by their uniformly curved anterior margin closely paralleled by a thin carina on the concave furrowed side. The element represented by Pl. 2, fig. 7 differs slightly in being more compressed.

Belodina sp. A

Pl. 2, figs 12 & 13

Remarks. These grandiform elements have a roundly terminated cusp apex, which allies them to *Belodina*. However, they differ from *B. confluens* in having an anterior margin that is not uniformly arcuate, and slightly flattened basally. They also exhibit similarities in outline to elements of *Pseudobelodina inclinata*, but lack the flatter, broader denticles.

Belodina sp. B

Pl. 2, fig. 14

Remarks. The large size of this grandiform element and its characteristic broadly rounded cusp readily distinguish this form from other species of the genus.

Belodina sp. C

Pl. 2, fig. 15

?1978 *Belodina* sp. D. Palmieri, p. 15, Pl. 3, figs 16 & 17.

Remarks. This strongly compressiform element closely resembles the elements of *Belodina* sp. D illustrated by Palmieri (1978, pl. 3, figs 16 & 17), although the latter features distinctly discrete denticles.

Belodina sp. D

Pl. 2, figs 16, 17, 22 & 23

Remarks. This species is characterised by the irregular curvature of the anterior margin. A change of near 90 degrees occurs between the anterobasal margin and cusp margin, becoming widely keeled at this point.

Belodina sp. E

Pl. 2, fig. 21

Remarks. The nature of the heel may suggest affinities to *B.* sp. F described below (see Pl. 2, fig. 26).

Belodina sp. F

Pl. 2, fig. 26

Remarks. This large, short and wide eobelodiniform element resembles the stratigraphically older *B. monitorensis* Ethington & Schumacher; this latter is similarly robust, has an exceptionally short wide heel, and is slightly bowed to the unfurrowed side. *B.* sp. F also appears to have affinities with the compressiform elements *Belodina* sp. C and sp. E as they also feature an unusually short, wide heel. However, the latter species differs greatly in size.

Belodina sp. G

Pl. 2, figs 3 & 4

Remarks. Elements are long with a narrow base, and are characterised by 8 to 9 evenly sized spatula-like denticles with well-rounded tips. Blade shape and the nature of denticulation, therefore, distinguish this species.

Genus ***Besselodus*** Aldridge, 1982

Type species. *Besselodus arcticus* Aldridge, 1982

Besselodus sp.

Pl. 3, fig 7, 12–18

Remarks. Nowlan & McCracken (*in* Nowlan et al. 1988) recognised four types of distacodiform (S) elements and a geniculate oistodiform (M) element as constituting the *Besselodus* apparatus. In the Malongulli collection, Sa (= c), Sb (= b), Sc (= a), and M (= e) elements are recognised, the latter being closer to *B. borealis* Nowlan & McCracken than *B. arcticus* Aldridge with its anterobasal margin extending past the line of geniculation of the cusp and base. The Malongulli form also shares the medial positioning of the costa, though is not as strongly developed. The S elements tend to develop a more distinctive posterobasal 'heel' than that of the Canadian species, causing the triangular base to be a right-angle triangle.

These elements are assigned to *Besselodus* Aldridge in preference to *Dapsilodus* Cooper, as all elements are unbowed and differ in general shape to those assigned to *Dapsilodus*, and because geniculate M elements are also present.

Genus ***Chirognathus*** Branson & Mehl, 1933

Type species. *Chirognathus duodactylus* Branson & Mehl, 1933

Chirognathus duodactylus Branson & Mehl, 1933?

Pl. 4, fig. 23

?1933 *Chirognathus duodactylus* Branson & Mehl, p. 28, pl. 2, figs 1 & 2

?1982 *Chirognathus duodactylus* Branson & Mehl; Sweet, p. 1038, pl. 1, figs 12–17.

?1991 *Chirodactylus duodactylus* Branson & Mehl; Sweet, *in* Ziegler, p. 47–50, pl. 1, figs 11–16 (*cum syn.*)

Remarks. The two specimens are probably Pb elements of *C. duodactylus* Branson & Mehl, following the reassessment given by Sweet (1982). The Malongulli material shares the distinct antero-posteriorly flaring basal cavity and reclined cusp, the latter twisted distally and being twice as long as the next largest denticle which is accommodated by the longer process. However, well-developed denticles on the shorter lateral process are lacking, yet are shown to be developed in other illustrated forms (Sweet 1982, pl. 1, fig. 12; Webers 1966, pl. 5, fig. 5). As only one specimen is complete and the other fragmentary, and the species is typically recorded elsewhere from Middle Ordovician strata, only a tentative assignment is proposed here.

Genus ***Culumbodina*** Moskalenko, 1973

Type species. *Culumbodina mangazeica* Moskalenko, 1973

Culumbodina? sp.

Pl. 5, figs 16–18; ?Pl. 2, figs 1 & 2

1978 *Panderodus* sp. B Palmieri, p. 23, Pl. 2, fig. 10, Fig. 3 (7a–d).

?1978 *Panderodus* sp. A Palmieri, p. 23, Pl. 2, figs 1–6; Pl. 9, figs. 1–3; Fig. 4 (1a–1d).

Remarks. The Malongulli forms (Pl. 5, figs 16–18) appear similar to those described by Palmieri (1978, pl. 2, fig. 10) as *Panderodus* sp. B from the Fork Lagoons Beds, central Queensland, principally in regard to the posterior serrations and general outline of the latter. These features are reminiscent of *Culumbodina* Moskalenko, but the serrations of the Malongulli specimens do not develop the denticle overgrowths of typical representatives of the genus *Culumbodina* Moskalenko. Furthermore, the *Culumbodina*? sp. elements are slightly bowed toward the furrowed side, the opposite direction to elements of *Culumbodina* Moskalenko. The much stouter elements represented in Pl. 2, figs 1 and 2 have a similar denticulation and may, therefore, also be included, though tentatively, as a part of the apparatus.

Genus ***Dapsilodus*** Cooper, 1976

Type species. *Distacodus obliquicostatus* Branson & Mehl, 1933

Dapsilodus mutatus (Branson & Mehl, 1933)?

Pl. 3, figs 19, 20 & 22

?1933 *Belodus*(?) *mutatus* Branson & Mehl, p. 126, pl. 10, fig. 17.

?1980 *Dapsilodus mutatus* (Branson & Mehl); Orchard, p. 20, pl. 5, figs 6, 15, 16, 21 (*cum syn.*).

Remarks. Acodiform elements only were recovered, each with a long posterolateral costa almost extending to the aboral margin. The smaller elements (Pl. 3, figs 19 & 22), however, seemingly lack the oblique anterobasal striae characteristic of *Dapsilodus* Cooper.

Genus ***Drepanoistodus*** Lindström, 1971

Type species. *Oistodus forceps* Lindström, 1955

Drepanoistodus suberectus (Branson & Mehl, 1933)

Pl. 5, figs 27–31

1933 *Oistodus suberectus* Branson & Mehl, p. 111, pl. 35, figs 22–27.

1988 *Drepanoistodus suberectus* (Branson & Mehl); Nowlan & McCracken, *in* Nowlan et al., pl. 16, pl. 3, figs 19–22 (*cum syn.*)

1990 *Drepanoistodus suberectus* (Branson & Mehl); Uyeno, p. 76, pl. 1, figs 13, 16–18.

Remarks. Suberectiform Sa elements, drepanodiform Sb elements and very few oistodiform M elements were recovered from the Malongulli collection.

Genus ***Istorinus*** Knupfer, 1967

Type species. *Istorinus erectus* Knüpfer, 1967

Istorinus? sp.

Pl. 3, figs 29–32

Remarks. Similar elements were previously assigned to '*Carniodus*' Walliser by Serpagli (1967) and Palmieri (1978), who illustrated fragmented forms comprising a flexed, laterally compressed blade with a long, erect cusp flanked by one or two denticles. Sweet & Bergström (1984) revised the taxonomy of the European faunas, reassigning Serpagli's '*Carniodus*' Walliser to *Istorinus erectus* Knüpfer; however, the latter is believed to be composed of more complete elements.

Genus ***Oistodus*** Pander, 1856

Type species. *Oistodus lanceolatus* Pander, 1856

'***Oistodus***' cf. ***venustus*** Stauffer 1935

Pl. 3, figs 27 & 28

cf. 1935 *Oistodus venustus* Stauffer, p. 147, pl. 12, fig. 12.

1988 *Paroistodus*? sp. A Nowlan & McCracken; *in* Nowlan et al., p. 24, pl. 9, figs 4, 20–22 (*cum syn.*, 'e' element only).

1989 *Paroidstodus*? sp. A Nowlan & McCracken; McCracken & Nowlan, p. 1889, pl. 3, fig. 6

1990 '*Oistodus*' cf. '*O.*' *venustus* Stauffer; Bergström, p. 22, pl. 3, fig. 13.

Remarks. This geniculate element is variable in its development of costae, being weaker in some specimens, and they may be medially or more posteriorly positioned. The length of the base is usually subequal to the cusp, but may be somewhat shorter. Such variations are typical of the morphological range of this form species.

The affinity of this element is not clear, many similar forms having previously been assigned to or compared with *O. venustus* (e.g. Hamar 1966; Winder 1966; Weyant 1968). Nowlan & McCracken (*in* Nowlan et al. 1988) regarded such forms as 'e' elements of their *Paroistodus*? sp. A apparatus (see also description of *Paroistodus*? sp. A Nowlan & McCracken, herein). The Malongulli representatives of '*Oistodus*' cf. *venustus* differ from *O. venustus* as originally described and illustrated by Stauffer (1935), in that the former features a sharper, almost pointed, anterobasal corner than the latter.

Genus ***Oulodus*** Branson & Mehl, 1933

Type species. *Cordylodus serratus* Stauffer, 1930

Oulodus cf. ***oregonia*** (Branson, Mehl & Branson, 1951)

Pl. 4, figs 16 & 17

cf. 1951 *Prioniodina oregonia* Branson, Mehl & Branson, p. 15–16, pl. 3, fig. 18, pl. 4, figs 28–32.

cf. 1975 *Oulodus subundulatus* Sweet, Turco, Warner & Wilkie; Sweet & Schönlaub, p. 47, pl. 2, figs 13–18 (Pb element, fig. 14).

non 1975 *Oulodus oregonia* (Branson, Mehl & Branson); Sweet & Schönlaub, p. 48, pl. 2, figs 1–6 [=*O. velicuspis* (Pulse & Sweet, 1960)].

cf. 1981 *Oulodus oregonia* (Branson, Mehl & Branson); Sweet, *in* Ziegler, p. 199–200, pl. 1, fig. 1–6.

Remarks. This specimen is virtually identical to the Pb element of *O. subundulatus* (Sweet, Turco, Warner & Wilkie) as described by Sweet & Schönlaub (1975, pl. 2, fig. 14). Sweet (*in* Ziegler 1981) synonymised this form with *O. oregonia* (Branson, Mehl & Branson) and reassigned the elements of the same name described by Sweet & Schönlaub (1975) to *O. velicuspis* (Pulse & Sweet). Sweet's revised classification is followed here for the Malongulli specimen, the specimen seemingly closest to *O. oregonia*; but without the presence of the diagnostic M element, this assignment must remain tentative. *Oulodus* sp. Barnes figured by An (1985) is also similar to the Malongulli specimen; however, a description is lacking, so preventing further comparison.

Genus ***Ozarkodina*** Branson & Mehl, 1933

Type species. *Ozarkodina typica* Branson & Mehl, 1933

Ozarkodina sesquipedalis Nowlan & McCracken, *in* Nowlan et al., 1988

Pl. 6, figs 13–25

1988 *Ozarkodina sesquipedalis* Nowlan & McCracken, *in* Nowlan et al., p. 18, Pl. 5, figs 1–15.

Remarks. Pa, Pb, M, and Sc elements (equivalent to 'f', 'g', 'e', 'a' elements) of *O. sesquipedalis* Nowlan & McCracken (*in* Nowlan et al., 1988, p. 18) were recovered. Minor variations between these specimens and the Canadian forms include the additional denticles in the P elements of the Malongulli collection. The Pa element may accommodate up to 17 denticles (Pl. 6, fig. 25) while the Pb element may develop up to 8 rather than 6 along its anterior process (Pl. 6, fig. 17). It is also noted that the posterior process of the Pb element accommodates alternating large and small denticles, which are shorter and more discrete than those forming the anterior process.

As noted in the original descriptions of Nowlan & McCracken (*in* Nowlan et al. 1988, p. 19), the Sc element closely resembles *Plectodina florida* Sweet, but can be distinguished by its smaller, irregular, posterior denticles that are fused rather than discrete, and by its proportionately higher base.

The P elements of the Malongulli material are remarkably similar to elements of *Yaoxianognathus yaoxianaensis* An (1985, pl. II, figs 6 & 7) and may well be synonymous. The assignment to *O. sesquipedalis* Nowlan & McCracken is followed, however, as there is a greater range of elements included in this form, and the more distinctive 'zygognathiform' and 'hibbardelliform' elements of the Chinese species are absent from the Malongulli collection.

Genus ***Panderodus*** Ethington, 1959

Type species. *Paltodus unicostatus* Branson & Mehl, 1933

Panderodus gracilis (Branson & Mehl, 1933)

Pl. 5, figs 1–4, 9, 10, 12–15

1933 *Paltodus gracilis* Branson & Mehl, p. 108, pl. 8, figs 20 & 21.

1988 *Panderodus gracilis* (Branson & Mehl); Nowlan & McCracken, *in* Nowlan et al., p. 21, pl. 7, figs 1–10, 12–13, 19 (*cum syn.*).

1990 *Panderodus gracilis* (Branson & Mehl); Uyeno, p. 69–70, pl. 1, figs 14, 19–20.

Remarks. Following Orchard's (1980) assessment of element positions M, Sa and Sb, representatives of this species have been recovered: (1) broad, symmetrical, laterally compressed M elements, which were originally described as *Paltodus compressus* Branson & Mehl, 1933; (2) slender, costate, graciliform Sa elements, featuring two anterolateral costae, one each side; and (3) an intermediate Sb element with only one anterolateral costa on the reverse side. A seemingly transitional form between the Sa and Sb elements is also exhibited (see Pl. 5, figs 4 & 9, 1 & 10).

The basal transverse section delineates the typically broad rounded anterior, a strongly pinched centre, and a narrow, laterally compressed, posterior. Hence, they are typical representatives of this species and do not differ from the range illustrated by Orchard (1980), and by Nowlan & McCracken (*in* Nowlan et al. 1988).

Panderodus sp. A

Pl. 1, figs 10–12

Description. Elements small, laterally compressed with two symmetrically disposed anteromedian carinae, one extending the length of each face. Carinae taper apically, become flattened basally, and in one, bounded posteriorly by a fine slit-like groove or furrow. Cusp proclined, margins sharp and keeled, anterobasal corner slightly truncated, and posterobasal corner with rounded lip.

Posterior margin irregularly serrated to almost finely denticulate in some forms. Base may be relatively high and long, with basal wrinkles.

Remarks. These elements show some resemblance to *Pseudobelodina*? *anceps* n. sp., particularly in basal outline and the square-faced lateral carinae, but lack denticles.

Panderodus sp. B

Pl. 5, figs 6 & 11

Remarks. *Panderodus* sp. B differs from the other illustrated forms primarily by the notch-like depression at the posterobasal margin. This basal outline is reminiscent of *P. panderi* Stauffer; however the former is generally acostate. Additionally, the compressiform element is smaller and less blade-like than that of *Panderodus gracilis* (Branson & Mehl), and with a more recurved cusp.

Panderodus sp. C

Pl. 1, figs 15 & 19

Description. Elements small, laterally compressed and scythe-shaped with broadly flattened base and uniformly curved, keeled margins. Basal wrinkles present, cusp twisted in some, and slightly bowed to the furrowed side. Weak posteromedian and anteromedian carina accommodated by the unfurrowed and furrowed faces, respectively; the latter extending to basal margin. Furrow developed as fine slit-like groove that extends the entire exposed length (apex not preserved) of specimens.

Remarks. These small panderodontid elements resemble elements of *Zanclodus* Nowlan & McCracken and could well belong to this apparatus. The former differs in lacking the posteriorly expanded base and the weak 'heel' characteristic of *Zanclodus* Nowlan & McCracken.

Panderodus sp. D

Pl. 5, figs 24–26

?1978 *Panderodus* sp. aff. *P. panderi* (Stauffer); Palmieri, p. 22, pl. 1, figs 9, 13 & 14, text fig. 3(4–5).

Description. Strongly recurved coniform elements compressed laterally; commonly with weakly developed anterior and posterior keels. One or two weak nodes or denticles, typically represented just above mid-height on posterior margin of cusp.

Remarks. Palmieri (1978) described similar forms as *Panderodus* sp. aff. *P. panderi* [pl. 1, figs 9, 13 & 14 and text-figs 3 (4 & 5)]; however, none of these elements show the thickened upturned base characteristic of *P. panderi* (Stauffer). *P.* sp. D is distinguished from *Culumbodina*? sp. by having much smaller and less conspicuous denticles (characteristically positioned above rather than below mid-height) and a greater recurvature of the cusp, and by lacking the posteriorly expanded base. It probably represents a new species of *Panderodus*.

Panderodus*? *liratus Nowlan & Barnes 1981

Pl. 5, figs 5, 7 & 8

1981 *Panderodus liratus* Nowlan & Barnes, p. 17, pl. 6, figs 21, 22, 24, 28 & 29, text-figs 7C & D.

1988 *Panderodus*? *liratus* Nowlan & Barnes; Nowlan & McCracken, *in* Nowlan et al., p. 21, pl. 7, figs 11, 15–18, 22 (*cum syn.*).

Remarks. The Malongulli specimens are referred to *P.*? *liratus* Nowlan & Barnes, a species reported specifically from Late Ordovician successions of Anticosti Island (Nowlan & Barnes 1981) and the Northwest Territories of Canada (Nowlan et al. 1988), because they exhibit a distinctive heel-like extension at the posterobasal corner of the cusp.

Genus ***Paroistodus*** Lindström, 1971

Type species. *Oistodus parallelus* Pander, 1856

Paroistodus sp.

Pl. 5, figs 19–23

Remarks. These geniculate elements are similar to the oistodiform elements of the stratigraphically older species *Paroistodus parallelus* (Pander). As the diagnostic drepanodiform elements are lacking in this collection, a further species assignment is not possible.

Paroistodus? sp. A Nowlan & McCracken, 1988

Pl. 3, fig. 21

1988 *Paroistodus*? sp. A Nowlan & McCracken, *in* Nowlan et al., p. 24–26, pl. 9, figs 1, 3, 5, 6, 9, 10, 14 & 15 (*cum syn.*, 'a' elements only).

1989 *Paroistodus*? sp. A Nowlan & McCracken; McCracken & Nowlan, p. 1889, pl. 3, fig. 1.

Remarks. The elements assigned to *Paroistodus*? sp. A Nowlan & McCracken are acodiform and lack oblique anterobasal striae. Thus, they closely conform to the Sc (= 'a') elements of Nowlan & McCracken's species. Of the other elements of Nowlan & McCracken's *Paroistodus*? sp. A apparatus, only the 'e' elements are well represented in the Malongulli assemblages. They are here referred to form species '*Oistodus*' cf. *venustus* Stauffer 1935 (see above).

Genus ***Periodon*** Hadding, 1913

Type species. *Periodon aculeatus* Hadding, 1913

Periodon grandis (Ethington, 1959)

Pl. 4, figs 13, 14, 27 & 28

1959 *Loxognathus grandis* Ethington, p. 281, pl. 40, fig. 6.

1981 *Periodon grandis* (Ethington); Lindström, *in* Ziegler, p. 243–244, pl. 1, figs. 13–18.

1989 *Periodon grandis* (Ethington); McCracken & Nowlan, p. 1889, pl. 3, figs 7–9.

1990 *Periodon grandis* (Ethington); Bergström, p. 11, pl. 3, fig. 7.

Remarks. Ramiform and prioniodiniform elements are represented in this collection, the latter (particularly Pl. 4, fig. 14) being similar to elements described by Ethington (1959, p. 284, pl. 41, fig. 14) and that illustrated by Sweet (1979, fig. 8: 20), but differing slightly from the latter in having a slightly higher and wider flaring base. The Malongulli ramiform elements are nearly identical to those illustrated by Bergström & Sweet (1966, pl. 30, figs 7 & 8).

Periodon? sp.

Pl. 5, fig. 34

Remarks. This incomplete element is probably related to *Periodon* Hadding; it features relatively large denticles. The lateral process, though broken, shows a large denticle apparently exceeding the size of the cusp.

Genus ***Phragmodus*** Branson & Mehl, 1933

Type species. *Phragmodus primus* Branson & Mehl, 1933

Phragmodus undatus Branson & Mehl, 1933

Pl. 6, figs 2–11 (1 & 12)?

1933 *Phragmodus undatus* Branson & Mehl, p. 115–116, pl. 8, figs 22–26.

1966 *Phragmodus undatus* Branson & Mehl; Philip, p. 112, fig. 1–5.

1988 *Phragmodus undatus* Branson & Mehl; Nowlan & McCracken, *in* Nowlan et al., p. 26–27, pl. 10, figs 1–3, 6 & 7 (*cum syn.*).

1989 *Phragmodus undatus* Branson & Mehl; McCracken & Nowlan, p. 1889, pl. 3, figs 10–12.

Remarks. The Malongulli material includes representatives of the Pa, Pb, M, Sa, Sb and Sc elements. One rather 'robust' Sc element (Pl. 6, fig. 1), similar to that illustrated by Pulse & Sweet (1960), may not belong to this species, as was previously suggested by Nowlan & Barnes (1981). The other less-typical specimen is the large Pa element (Pl. 6, fig. 12), which has broad, irregularly developed denticles and the cusp base accommodating a longitudinal ridge.

Genus ***Protopanderodus*** Lindström, 1971

Type species. *Acontiodus rectus* Lindström, 1955

Protopanderodus insculptus (Branson & Mehl, 1933)

Pl. 4, figs 1, 7–12

1933 *Phragmodus insculptus* Branson & Mehl, p. 124, pl. 10, figs 32–34.

1978 *Protopanderodus insculptus* (Branson & Mehl); Palmieri, p. 25, pl. 2, figs 26–29, text-fig. 4 (10a–10c) (*cum syn.*).

Remarks. According to Kennedy et al. (1979), *Protopanderodus insculptus* is readily distinguished from the very similar *P. liripipus* (see Pl. 4, figs 2–6) by the development of a denticle on its base. Plate 4, figure 1 features a lobate, flange-like basal process with only the basal remnants of its posterior denticle. Palmieri (1978, pl. 2, fig. 26) illustrated a form from central Queensland, which shows the remains of the base of the broken secondary denticle, but none show the prominent anterobasal flange that is apparent in the Malongulli representatives. Most elements are either symmetrical or slightly asymmetrical, the only exception being that in Plate 4, figure 8. The last is markedly asymmetrical, featuring a cusp that is strongly costate on one face with a correspondingly short weak costa on the other.

Protopanderodus liripipus Kennedy, Barnes & Uyeno, 1979

Pl. 4, figs 2–6

1979 *Protopanderodus liripipus* Kennedy, Barnes & Uyeno, p. 546–550, pl. 1, figs 9–19.

1983 *Protopanderodus liripipus* Kennedy, Barnes & Uyeno; Burrett, Stait & Laurie, p. 184, fig. 9A & B.

1985 *Protopanderodus liripipus* Kennedy, Barnes & Uyeno; Savage & Bassett, p. 708, pl. 86, fig. 15.

1988 *Protopanderodus liripipus* Kennedy, Barnes & Uyeno; Nowlan & McCracken, *in* Nowlan et al., p. 29, pl. 11, figs 18, 20 (*cum syn.*).

1989 *Protopanderodus liripipus* Kennedy, Barnes & Uyeno; McCracken & Nowlan, p. 1890, pl. 4, fig. 1.

Remarks. These specimens are recognised as symmetrical, slightly asymmetrical, and markedly asymmetrical protopanderodiform elements of *Protopanderodus liripipus*, in accordance with the description given by Kennedy et al. (1979). They are distinguishable from similar forms by their elongate, pointed base and the absence of a basal denticle. As in *P. insculptus* (Branson & Mehl), the anterobasal flange is variably developed.

Genus ***Pseudobelodina*** Sweet, 1979

Type species. *Belodina kirki* Stone & Furnish, 1959

Pseudobelodina dispansa (Glenister, 1957)

Pl. 1, figs 21–26, 31–33, (27–29, 34 & 35)?

1957 *Belodus dispansus* Glenister, p. 729–730, pl. 88, figs 14 & 15.

1988 *Pseudobelodina*? *dispansa* (Glenister) Nowlan & McCracken, *in* Nowlan et al., p. 30–31, pl. 12, figs 8–26 (*cum. syn.*).

1978 *Belodina* sp. D Palmieri, p. 15, pl. 3, figs 18, 19 & 22.

1989 *Pseudobelodina*? *dispansa* (Glenister); McCracken & Nowlan, p. 1890, pl. 4, figs 2–4.

1990 *Pseudobelodina dispansa* (Glenister); Uyeno, p. 73, pl. 1, fig. 24, 30.

Remarks. S.M. Bergström (Ohio State University, personal communication, May 1994) regards this taxon as a part of the same apparatus as *Belodina confluens*. The forms here assigned to the group vary in curvature of the anterior margin and in number and size of the denticles. Specimens shown in Plate 1, figures 31–33 compare closely with the original material described by Glenister (1957), though one specimen illustrated has only four denticles. Specimens illustrated in Plate 1, figures 23 and 24 have much enlarged denticles, while the bases of Plate 1, figures 21, 22, and 25 are longer and narrower. The latter are equivalent to forms illustrated by Nowlan & McCracken (*in* Nowlan et al. 1988, pl. 12, figs 8–26), McCracken & Nowlan (1989, pl. 4, fig. 2), and Uyeno (1990, pl. 1, fig. 24, 30). The specimen in Plate 1, figure 29 is tentatively assigned to this taxon as an aberrant form with only three proclined denticles. However, its general morphology shows affinities to elements within this group. Plate 1, figures 27 and 28 may be considered as shorter, broader, compressiform varieties of the forms represented in Plate 1, figures 23 and 24, with a blade of higher, longer denticles compared to those at the other end of the spectrum represented by Plate 1, figures 31–33. Elements with a long cusp, low heel and three to four proclined denticles (Pl. 1, figs 34 & 35) are also tentatively grouped within this apparatus.

Pseudobelodina inclinata (Branson & Mehl, 1933)

Pl. 2, figs 8–11

1933 *Belodus inclinatus* Branson & Mehl, p. 125–126, pl. 10, fig. 24.

1979 *Pseudobelodina inclinata* (Branson & Mehl); Sweet, p. 69, figs 6.11, 6.15, 6.16, & 6.22 (*cum syn.*).

1988 *Pseudobelodina inclinata* (Branson & Mehl); Nowlan & McCracken, *in* Nowlan et al., p. 31, pl. 13, figs 5–20, pl. 14, figs 1–6.

Remarks. The aspect of the posterobasal corner varies in the Malongulli material from being truncated (Pl. 2, figs 8, 10 & 11) to extending basally (Pl. 2, fig. 9). The latter feature is illustrated by the original material from the Maquoketa Shale (Branson & Mehl 1933; Sweet *in* Ziegler 1981; Sweet 1979) and in specimens from the Whittaker Formation, illustrated by Nowlan & McCracken (*in* Nowlan et al. 1988). The present material also differs in featuring a flattened anterobasal corner.

Pseudobelodina sp. A

Pl. 1, fig. 20

Remarks. This species differs from others of this genus in that the heel is almost non-existent. The lateral faces are completely covered with striae and the anterior margin is rounded basally, then straight along much of its length—in other species this margin is uniformly curved.

Pseudobelodina sp. B

Pl. 1, fig. 30

Remarks. *Pseudobelodina* sp. B has a uniformly curved anterior margin as does *P. dispansa* (Glenister), see above, but differs from the latter in denticulation and by developing a more distinct heel.

Pseudobelodina? anceps n. sp.

Pl. 1, figs 6–9, 13–14

Material. Ninety-three elements from Coppermine Creek and Gleesons Creek clasts (CM1, 2, 5, 8, 10, 11, 13–17, 22, and GC11). Figured specimens CPC 32987–88 (Form 1), CPC 32983–84 (Form 2) and CPC 32985–86 (Form 3); designated holotype is the form-2 element, CPC32983.

Derivation of name. Latin *anceps*, meaning two-edged, alluding to the doubled ridges on the medially flattened lateral face.

Description. Three forms were recognised, ranging from long and narrowly coniform to shorter, wider-based elements with a variably proclined to recurved cusp. Elements are slightly bowed to the more convex side or straight as in Form 3. Basal cross-section varies from subrounded to ovate. Lateral faces bear a single thin, median costa or ridge along the carina of the more convex side and two—one upper and one lower—bounding the flattened carina of the other face in one element type (Pl. 1, fig. 13–14); the second element type (Pl. 1, figs 6 & 9) repeats the former costate plan, but is slightly laterally compressed with an ovate basal section, a higher heel and, thus, longer basal margin; the third (Pl. 1, figs 7 & 8) has symmetrically disposed costae, two on each side, a more rounded and restricted basal opening as in Form 1, and a heel that develops as a high blade, extending the basal margin further than the intermediate Form 2.

Remarks. The medially flattened lateral face bounded by prominent doubled ridges distinguishes *P.? anceps* n. sp. from other belodinids. Its affinities are likely to be related to *Pseudobelodina* Sweet, as it features strong lateral coastae, a 'wrinkled' base and a 'panderodontid-like' furrow. This furrow is bearly discernible in Plate 1, figure 8, as it is obscured by the upper lateral ridge. *P.? anceps* lacks the sinuous blade-like denticulate structure that characterises *Ansella* sp.

Genus ***Pseudooneotodus*** Drygant, 1974

Type species. *Oneotodus? beckmanni* Bischoff & Sannemann, 1958

Pseudooneotodus beckmanni (Bischoff & Sannemann, 1958)

Pl. 4, figs 29 & 30

1958 *Oneotodus? beckmanni* Bischoff & Sannemann, p. 98, pl. 15, figs 22–25.

1981 *Pseudooneotodus beckmanni* (Bischoff & Sannemann); Nowlan & Barnes, p. 23, pl. 2, figs 20 & 21 (*cum syn.*)

1990 *Pseudooneotodus beckmanni* (Bischoff & Sannemann); Uyeno, p. 99–100, pl. 1, figs 36 & 37.

Remarks. The Malongulli specimens are identical to the Canadian forms from the Vauréal Formation figured by Nowlan & Barnes (1981) and the laterally compressed ovate representatives of the type material from Germany (Bischoff & Sannemann 1958, pl. 15, fig. 25).

Pseudooneotodus mitratus (Moskalenko, 1973)

Pl. 4, figs 21 & 22

1973 *Ambalodus mitratus mitratus* Moskalenko, p. 86, pl. 17, figs 9–11.

1973 *Ambalodus mitratus nostras* Moskalenko, p. 87, pl. 17, figs 12–14, ?15.

1978 *Pygodus*? sp. Palmieri, p. 25, pl. 4, figs 24, 27–29 only.

1988 *Pseudooneotodus mitratus* (Moskalenko); Nowlan & McCracken, *in* Nowlan et al., p. 34, pl. 16, figs 2–6 (*cum syn.*).

1989 *Pseudooneotodus mitratus* (Moskalenko); McCracken & Nowlan, p. 1890, pl. 4, fig. 8.

Remarks. Two different forms are apparent: (1) an asymmetrical, nodose variety with weak concentric ornamentation (Pl. 4, fig. 21); and (2) a form which lacks nodes (Pl. 4, fig. 22). The elements are equivalent to the type material from the Siberian Platform illustrated by Moskalenko (1973); the nodose variety was originally described as the subspecies *P. mitratus nostras* Moskalenko and the smooth form as *P. mitratus mitratus* Moskalenko. Intermediate forms have often featured in other collections (e.g. Nowlan et al. 1988), but these subspecies have not been recognised here.

Genus ***Scabbardella*** Orchard, 1980

Type species. *Drepanodus altipes* Henningsmoen, 1948

Scabbardella altipes (Henningsmoen, 1948) subsp. B Orchard, 1980

Pl. 3, fig. 1–6, 8–11

1948 *Drepanodus altipes* Henningsmoen, p. 420, pl. 25, fig. 14 (*partim*?).

1980 *Scabbardella altipes* (Henningsmoen) subsp. B Orchard, p. 26, pl. 5, figs 2, 3, 14, 18, 20, 23, 24, 30 & 33.

1989 *Scabbardella altipes* (Henningsmoen) subsp. B Orchard; Nowlan & McCracken, *in* Nowlan et al., p. 36, pl. 16, figs 7–20, pl. 17, figs 1–3, 5, 6, 8 & 9 (*cum syn.*).

Remarks. A variety of Sc elements are the predominant representatives of this species. Some (Pl. 3, figs 3 & 4) are equivalent to *Acodus similaris* Rhodes, as illustrated by Serpagli (1967, pl. 7, figs 5 & 6), and to some Canadian representatives of *S. altipes* subsp. B Orchard (Nowlan & McCracken *in* Nowlan et al. 1988, particularly pl. 16, figs 7–10); such elements are strongly laterally compressed and broader than the other elements of this collection. The other Sc elements feature a narrow, recurved cusp and either a long narrow base (Pl. 3, figs 6, 10 & 11) or a short widely triangular base (Pl. 3, figs 2, 5 & 9). The former are closely comparable to those from the Keisley Limestone illustrated by Rhodes (1955, pl. X, figs 10 & 26) as *Acodus similaris* Rhodes. The latter are similar, in general outline, to the M (= 'e-3') elements figured by Nowlan & McCracken (*in* Nowlan et al. 1988), but lack the second costa. Plate 3, figure 2 is also unusually ornamented with relatively strong closely spaced longitudinal striae.

The Sa (= 'c') element has the same form as those from the Whittaker Formation, Canada (Nowlan & McCracken *in* Nowlan et al. 1988, pl. 16, figs 17–20) and features finer striae and ridges associated with the primary posterolateral costae (Pl. 3, fig. 8).

Genus ***Strachanognathus*** Rhodes, 1955

Type species. *Strachanognathus parvus* Rhodes, 1955.

Strachanognathus parvus Rhodes, 1955

Pl. 4, figs 24–26

1955 *Strachanognathus parvus* Rhodes, p. 132, pl. 7, fig. 16, pl. 8, figs 1–4.

1978 *Strachanognathus parvus* Rhodes; Löfgren, p. 112, pl. 1, fig. 29 (*cum syn.*).

1978 *Strachanognathus parvus* Rhodes; Palmieri, p. 27, pl. 6, figs 27 & 28, text-fig. 6 (8a–8c).

1980 *Strachanognathus parvus* Rhodes; Orchard, p. 26, pl. 14, figs 34 & 35.

1990 *Strachanognathus parvus* Rhodes; Bergström, pl. 1, fig. 10.

Remarks. The Malongulli specimens are fairly typical representatives of this species, thus being closely comparable to the type material from the Keisley Limestone (Rhodes 1955).

Genus ***Taoqupognathus*** An, 1985

Type species. *Taoqupognathus blandus* An, 1985.

Taoqupognathus tumidus n. sp.

Pl. 7, figs 10–24

1978 *Drepanodus*? *altipes*? Henningsmoen; Palmieri, p. 19, pl. 2, figs 24 & 25, Fig. 4 (3a–c).

?1978 *Drepanodus*? cf. *altipes* Henningsmoen; Palmieri, p. 19, pl. 2, figs 22 & 23.

Material. Thirty-eight elements from 14 clasts in the breccia at Coppermine Creek (CM1–2, 4–9, 11–14, 18, 22, & 23); 13 figured specimens CPC 33162–74; holotype designated Sc? type 'c' element CPC 33171.

Derivation of name. From Latin *tumidus*, swollen, alluding to the portly, penguin-like outline.

Description. Blade-like coniform panderodontid elements, featuring basal wrinkles and a medial furrow on outer face, from base to cusp tip. Characteristic flange-like posterior process is exhibited in all but one element, and a variably developed ledge marks the base and cusp junction. Posterobasal corner of all elements is extended posteriorly and an anterobasal protruberance marks the height of basal ledge. Four groups of elements are recognised, with the Sb? and Sc? elements further subdivided into two and three types, respectively:

(1) **M? elements** (Pl. 7, figs 21 & 22) are symmetrical or slightly asymmetrical, slender and coniform; they lack costae and posterior process, have a convex anterior margin, concave posterior margin, recurved cusp and reduced lateral basal ledge; the unfurrowed side is smooth.

(2) **Sb? elements** are asymmetrical unicostate and with posterior process; and they are subdivided into:

- **type 'a'** (Pl. 7, figs 17 & 18) is composed of short, stout asymmetrical elements exhibiting an almost straight anterior margin, with cusp tip slightly higher than flange-like posterior process; posterior process almost extends full length of margin; furrowed side convex; unfurrowed side concave and accommodating prominent anteromedial costa developed as lateral process;

- **type 'b'** (Pl. 7, figs 14 & 15) comprises flattened and more elongate coniform elements (in comparison to Sb? type 'a' forms), with proclined cusp, prominent basal ledge and small nodular or lobe-like process developed along posterior margin near mid-length; furrowed side convex; unfurrowed side concave and accommodating posterior costa, developed as short lateral process, bounding posterior flange and extending to cusp tip.

(3) **Sc? elements** asymmetrical, and may feature short medial ridge with expanded posterior flange-like process, with cusp in transverse section sinusoidally bowed; subdivided into:

- **type 'a'** (Pl. 7, figs 10 & 11), which consists of forms with cusp sub-erect and anterior margin gently arcuate, posterior margin featuring distinct but narrow, lobe-like process (larger than the Sb? type 'b' element) near mid-height; basal ledge prominent; furrowed side convex; unfurrowed side concave, featuring median ridge on upper half between process and cusp tip;

- **type 'b'** (Pl. 7, figs 12–13), which has a convex anterior margin, posterior margin showing high flange-like process and prominent basal ledge; posterior

process extends from base for three-fifths of length of element; furrowed side convex; unfurrowed side concave with short, weak median ridge towards cusp tip;

- **type 'c'** (Pl. 7, figs 19 & 20), which exhibits an almost straight anterior margin, and posterior margin with high flange-like process (greater than Sc? type 'b' element); posterior process extends from base for three-quarters of element length; basal ledge prominent; furrowed side convex; unfurrowed side concave and smooth.

(4) **P? elements** (Pl. 7, figs 16, 23 & 24) asymmetrical and showing lateral twisting of cusp tip; anterior margin convex; posterior margin concave; basal ledge reduced; furrowed side convex; unfurrowed side convex, smooth and strongly bowed with cusp twisted laterally, becoming displaced toward the unfurrowed side at junction of posterior process; flange-like posterior process high (greater than that of the Sc? type 'b' element), extending along much of posterior margin

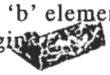

Remarks. The genus was first illustrated by An (1985 pl. II, figs 18 & 19) based on *Taoqupognathus blandus* An, and featuring elements equivalent to those described above as occupying the Sb? type 'b' position. Savage (1990) described and illustrated a new species, *Taoqupognathus philipi* Savage from the lower part of Cliefden Caves Limestone Group (Fossil Hill Limestone), naming six different element types, using Greek numerals, from a smallest 'alpha' element to a largest 'zeta' element. This size gradation is not apparent in the Malongulli material, though three elements are very similar to forms identified in the Cliefden Caves succession. The M? (=Savage's 'delta') and the Sb? type 'b' (='beta') elements are quite similar, though the latter is a more elongate element in the Malongulli fauna, tending towards the shape of Savage's 'gamma' element. Neither costae nor posterolateral processes are mentioned in Savage's descriptions, although a prominent costa or ridge is shown in his illustration of the 'beta' element (see Savage 1990, fig. 8-4). Savage's 'gamma' element apparently lacks this feature. The Sc? type 'c' elements of *T. tumidus* (equivalent to the 'zeta' elements of Savage's *T. philipi*) are much broader, with the posterior process being wider and terminating orally almost at right-angles to the cusp. P?, Sb? type 'a', Sc? type 'a' and Sc? type 'b' elements are difficult to identify in Savage's species, and close comparisons are limited without essential descriptive details such as presence or absence of lateral costae or processes.

The specimens Palmieri (1978) described previously from the Late Ordovician Fork Lagoons Beds of central Queensland, which he referred tentatively to *Drepanodus* Pander, should now be interpreted as P? and M? elements of *T. tumidus*.

Genus ***Walliserodus*** Serpagli, 1967

Type species. *Acodus curvatus* Branson & Branson, 1947

Walliserodus amplissimus (Serpagli, 1967)

Pl. 7, figs 1–9

1967 *Drepanodus amplissimus* Serpagli, p. 66, pl. 15, figs. 1–5.

1978 *Drepanodus* sp. aff. *D. amplissimus* (Serpagli); Palmieri, p. 20, pl. 2, figs 15 & 16, text-fig. 4 (8a–c).

1988 *Walliserodus amplissimus* (Serpagli); Nowlan & McCracken *in* Nowlan et al., p. 40, pl. 19, figs 1–15 (*cum syn.*).

1989 *Walliserodus amplissimus*? (Serpagli); McCracken & Nowlan, p. 1892, pl. 4, fig. 11.

Remarks. Sa, Sb?, and M elements ('c', 'b', and 'e', types, respectively, following the nomenclature of Nowlan & McCracken *in* Nowlan et al. 1988) are recognised from the Malongulli collection. They are fairly typical representatives, comparing closely with those from the Carnic Alps (Serpagli 1967), and from the Whittaker Formation, Canada (Nowlan et al. 1988).

The Sa elements (Pl. 7, figs 1, 3–4) are distinctly triangular in basal transverse section, developing an anterior face with each edge defined by a single sharp anterolateral costa. The posterior margin is thinly keeled and a posterolateral costa is developed on one side only. These elements are equivalent to those in Serpagli (1967, pl. 31, figs 8 & 11) and Nowlan & McCracken (*in* Nowlan et al. 1988, pl. 19, figs 4, 14 & 15). The M elements (Pl. 7, figs 6–9) are equivalent to the carinate forms illustrated in Nowlan et al. (1988, pl. 19, figs 12 & 13), Serpagli (1967, pl. 15, fig. 2), and Palmieri (1978, pl. 2, figs 15 & 16). They are characterised by a strong posterior taper, creating a sharp widely keeled margin, a broader cusp, and the smooth curvature of the anterior and posterior margins, in contrast to the abrupt recurvature of the cusp in other elements.

The Sb? elements (Pl. 7, figs 2 & 5) have a sharp anterolateral costa on the flatter side and a posterolateral costa on the convex side. Plate 7, figure 5 features an additional keel or costa along the posterior margin. The cusps of both specimens are bowed to the convex side. The obvious difference between these two forms is the shorter base in one (see Pl. 7, fig. 5) in contrast to the much higher base in the other (see Pl. 7, fig. 2). The positioning of the costae equates these elements to those of Serpagli (1967, pl. 31, fig. 5).

Genus ***Yaoxianognathus*** An, 1985

Type species. *Yaoxianognathus yaoxianensis* An, 1985.

Yaoxianognathus? tunguskaensis (Moskalenko, 1973)

Pl. 4, figs 18–20

1973 *Phragmodus*? *tunguskaensis* Moskalenko, 1973, p. 74, Pl. XII, figs 1–3.

1983 *Phragmodus*? (*Spinodus*?) *tunguskaensis* Moskalenko; Moskalenko, Fig. 4.Z.

1985 *Oulodus*? *tunguskaensis* (Moskalenko); An, p. 108, pl. II, fig. 9.

1988 *Spinodus*? n. sp. A Nowlan & McCracken, *in* Nowlan et al., p. 38, pl. 17, figs 17–22.

1990 *Phragmodus*? *tunguskaensis* Moskalenko; Savage, p. 830, figs 10.7 & 10.8.

Remarks. The species has previously been assigned tentatively to various genera, including *Phragmodus*, *Oulodus* and *Spinodus* (Moskalenko 1973, 1983; An 1985; Nowlan & McCracken *in* Nowlan et al. 1988; Savage 1990). Savage (1990) described the species from the underlying Fossil Hill Limestone of the Cliefden Caves area (Fig. 2) and, following Moskalenko's (1973) original assignment, placed it tentatively in the genus *Phragmodus*.

However, the material seems better tentatively grouped in *Yaoxianognathus* An, especially given the similarities to the 'cordylodiform form' (Sc) elements of that genus. The Siberian elements that feature a prominent anterior denticle (e.g. Moskalenko 1973, pl. XII, fig. 1) resemble *Yaoxianognathus* sp. A of An (1985), and the latter also features a prominent denticle near mid-length of the posterior process.

The specimens from the present collection are closely similar to the type material from the Siberian Platform, and, in particular, to the holotype (Moskalenko 1973, pl. XII, fig. 3) with a much reduced anterior process, rather than to the paratypes of Moskalenko, which have developed a true denticle. The material illustrated by Nowlan & McCracken (*in* Nowlan et al. 1988) as *Spinodus*? n. sp. A is conspecific and also features the reduced anterior process.

Genus ***Zanclodus*** Nowlan & McCracken, *in* Nowlan et al., 1988

Type species. *Zanclodus levigatus* Nowlan & McCracken, *in* Nowlan et al., 1988

Zanclodus levigatus Nowlan & McCracken, *in* Nowlan et al., 1988

Pl.3, figs 23–26

1988 *Zanclodus levigatus* Nowlan & McCracken, *in* Nowlan et al., p. 43–44, pl. 19, figs 1–15.

Remarks. Nowlan & McCracken (*in* Nowlan et al. 1988) erected the genus *Zanclodus* to accommodate panderodontacean conodonts with a distinct, but weakly developed, posterior heel, and often truncated anterobasal margin. Elements of the type species show greater variation in flexure, being bowed to the unfurrowed side (group 1), bowed to the furrowed side (group 2), or unbowed (group 3).

The Malongulli collection features elements from groups 1 and 3, and is typical of the type material from the Whittaker Formation. The elements assigned to group 3 show the typical square-shaped base in profile, owing to the short, broad base, distinct posterior heel and truncated anterior margin (Pl. 3, figs 24–26). The group 1 representative (Pl. 3, fig. 23) is bowed to the unfurrowed side by definition, slightly more laterally compressed, features a very weakly developed posterior heel, and the truncation of the anterobasal margin is less abrupt compared to the group 3 elements. However, the 'characteristic' *Zanclodus* Nowlan & McCracken base is still distinguishable.

Gen. et sp. indet. A.

Pl. 5, fig. 33

Remarks. This small and incomplete element features an anterior, posterior and lateral process. The anterior process accommodates one small denticle, the lateral process is irregularly denticulate with four small and one large denticle, and the posterior process develops from the posterior costa of the cusp into a small flaring aboral lip.

Gen. et sp. indet. B

Pl. 5, fig. 35

Remarks. This large robust blade accommodates ten stout denticles. The denticles are uniformly short, rounded and erect, but become proclined anteriorly. Narrow lips flank a very shallow basal cavity, which is truncated posteriorly. Another distinguishing feature is the lateral deflection of the anterior end of the blade, which terminates with a larger (broken) denticle.

Gen. et sp. indet. C

Pl. 1, figs 16–18

?1978 *Acodus mutatus* (Branson & Mehl); Palmieri, p. 6–7, pl. 2, fig. 17 & 18, text-fig. 4(a–c).

Remarks. This small, blade-like element with a broadly sub-triangular profile has similarities to forms assigned to the genus *Acodus* Pander by Palmieri (1978, Pl. 2, figs 17 & 18) and Stouge (1984, pl. 14, figs 20 & 22). Those assigned by Palmieri are essentially the same as the Malongulli elements, although it seems to develop a slightly convex, rather than flat to concave, furrowed side. Those assigned by Stouge from Newfoundland have the same general outline. However, in the Malongulli material, the costa does not appear to be as prominent, as it is almost developed as a lateral process. The opposite face is not described by Stouge and is assumed to be featureless.

Gen. et sp.indet. D

Pl. 4, fig. 15

Remarks. Specific assignment is prevented by the lack of diagnostic elements, although this zygognathiform element shows similarities with the Sb element of *Plectodina florida* Sweet (1979, fig. 8:17).

Acknowledgements

This study has been carried out with the support of a Sydney University research grant during 1988 and 1989 and Australian Research Council support during 1993 and 1994 (A39230628). We thank Drs S.M. Bergström (Columbus, Ohio), G.S. Nowlan (Calgary, Canada), R. Mawson (Macquarie University, Sydney), and J.H. Shergold (AGSO, Canberra) for constructively helpful comments on the manuscript. We also appreciate support of Drs Ian Percival and Zhen Yongyi in final stages of preparation of the manuscript.

References

Aldridge, R.J., 1982. A fused cluster of coniform conodont elements from the Late Ordovician of Washington Land, western North Greenland. *Palaeontology*, 25, 425–430.

An, T., 1985. Ordovician conodonts from Yaoxian and Fuping, Shaanxi Province, and their stratigraphic significance. *Acta Geologica Sinica,* 59, 97–108 (in Chinese).

Banks, M.R. & Burrett, C.F., 1980. A preliminary Ordovician biostratigraphy of Tasmania. *Journal of the Geological Society of Australia*, 26, 363–376.

Banks M.R. & Burrett, C.F., 1989. The Gordon Group (Early Ordovician to Early Silurian)— mainly platform carbonates. *In* Burrett, C.F. & Martin, E.L. (editors), Geology and mineral resources of Tasmania. *Geological Society of Australia, Special Publication*, 15, 201–224.

Bergström, S.M., 1971. Conodont biostratigraphy of the Middle and Upper Ordovician of Europe and eastern North America. *Geological Society of America, Memoir*,

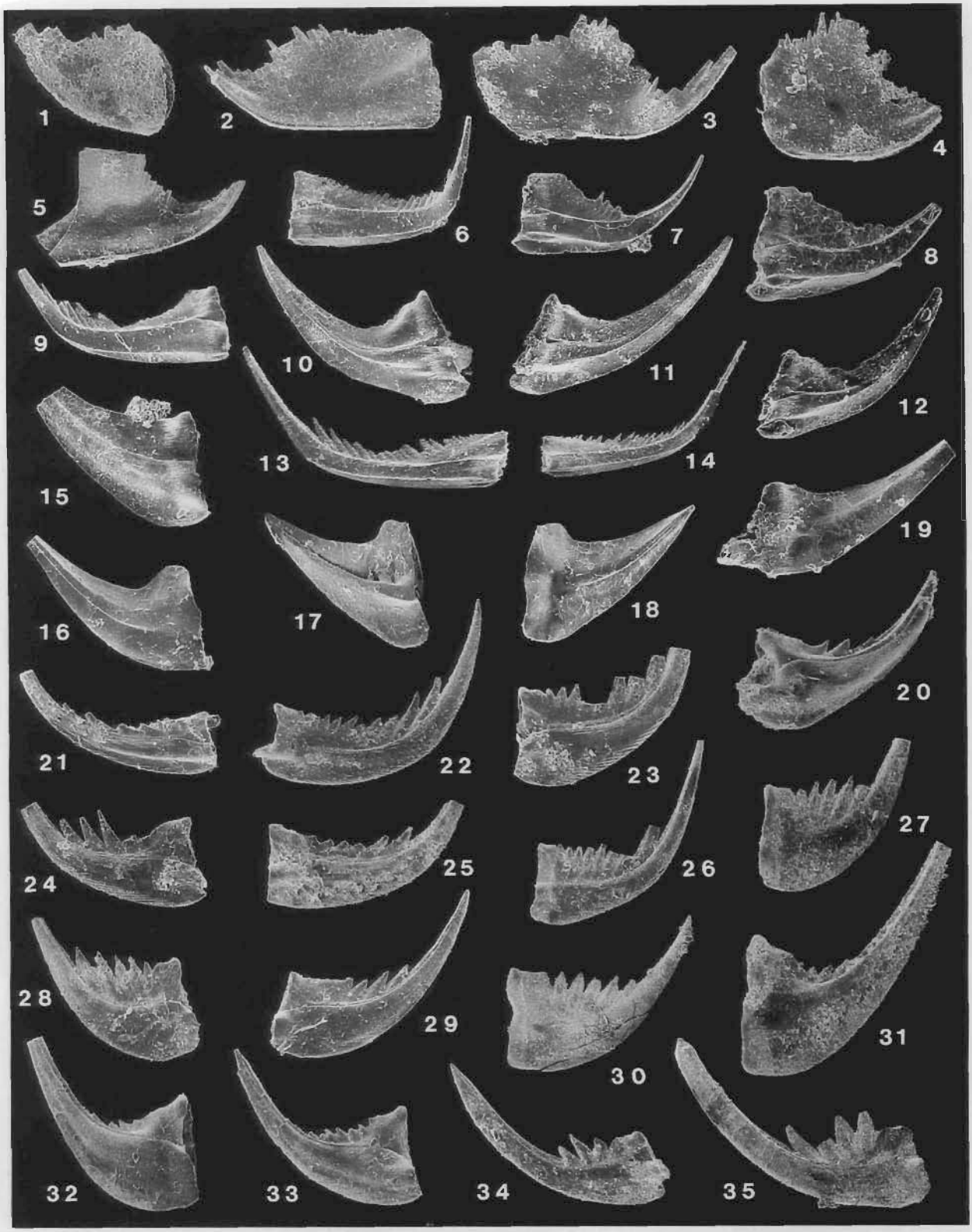

Plate 1. Figs 1–5, *Ansella* sp.; respectively CPC 32978 (CM12), x72; CPC 32979 (CM18) x72; CPC 32980 (CM1), x72; SUP CPC 32981 (CM13), x90; CPC 32982 (GC8), x90. Figs 6–9, 13 & 14, *Pseudobelodina*? *anceps* sp.nov.; 6, 9, Form 2, respectively holotype CPC 32983 (CM15), x90; CPC 32984 (CM15), x90; 7–8, Form 3, respectively CPC 32985 (CM23), x108; CPC 32986 (CM10), x99; 13–14, Form 1, respectively CPC 32987 (CM13), x90; CPC 32988 (CM13), x90. Figs 10–12, *Panderodus* sp. A; respectively CPC 32989 (CM15), x90; CPC 32990 (CM17), x90; CPC 32991 (CM11), x90. Figs 15, 19, *Panderodus* sp. C; respectively CPC 32992 (CM4), x90; CPC 32993 (CM4), x90. Figs 16–18, Gen. et sp. indet. C; 16, CPC 32994 (CM1), x117; 17–18, CPC 32995 (CM6), x90. Fig. 20, *Pseudobelodina* sp. A, CPC 32996 (CM9), x72. Figs 21–26, 31–33, *Pseudobelodina dispansa* (Glenister, 1957); 21–26, respectively CPC 32997 (CM8), x99; CPC 32998 (CM18), x72; CPC 32999 (CM18), x90; CPC 33000 (CM1), x108; CPC 33001 (CM8), x72; CPC 33002 (CM18), x72; 31–33, respectively CPC 33003 (CM22), x72; CPC 33004 (CM4), x72; CPC 33005 (CM4), x72. Figs 27–29, 34 & 35, *Pseudobelodina dispansa* (Glenister, 1957)?; 27–29, respectively CPC 33006 (CM18), x81; CPC 33007 (CM18), x72; CPC 33008 (CM13), x72; 34–35, respectively CPC 33010 (CM18), x72; CPC 33011 (GC6), x45. Fig. 30, *Pseudobelodina* sp. B; CPC 33009 (CM11), x45.

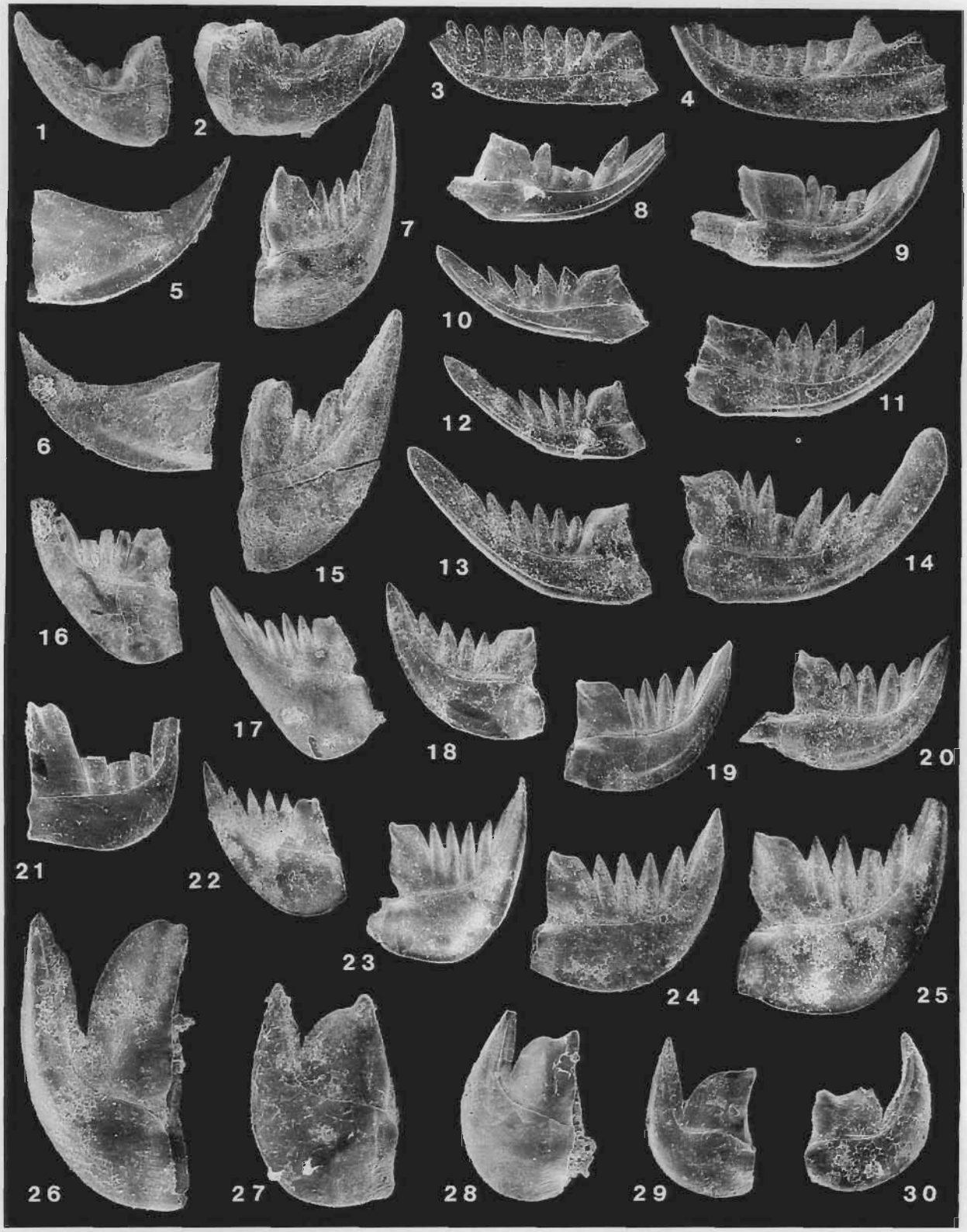

Plate 2. Figs 1 & 2, *Culumbodina*? sp.?; respectively CPC 33012 (CM4), x90; CPC 33013 (CM14), x72. Figs 3 & 4, *Belodina* sp. G; respectively CPC 33014 (CM20), x72; CPC 33015 (CM4), x72. Figs 5 & 6, *Ansella* sp.; CPC 33016 (CM11), x63. Fig. 7, *Belodina confluens* Sweet 1979?; CPC 33017 (CM4), x54. Figs 8–11, *Pseudobelodina inclinata* (Branson & Mehl, 1933); respectively CPC 33018 (CM8), x99; CPC 33019 (GC5), x36; CPC 33020 (CM1), x108; CPC 33021 (CM4), x81. Figs 12 & 13, *Belodina* sp. A; respectively CPC 33022 (CM22), x54; CPC 33023 (CM9), x54. Fig. 14, *Belodina* sp. B; CPC 33024 (CM18), x54. Fig. 15, *Belodina* sp. C; CPC 33025 (CM22), x54. Figs 16, 17, 22 & 23, *Belodina* sp. D; respectively CPC 33026 (GC4), x45; CPC 33027 (CM11), x36; CPC33028 (CM11), x54; CPC 33039 (CM18), x36. Figs 18–20, 24, 25, 27–30, *Belodina confluens* Sweet, 1979; 18–20, 24–25, compressiform elements, respectively CPC33029 (CM11), x54; CPC33030 (CM6), x54; CPC 33031 (CM3), x54; CPC33032 (CM18), x54; CPC 33033 (CM22), x54; 27–30, eobelodiniform elements, respectively CPC 33034 (CM11), x90; CPC 33035 (GC3), x90; CPC 33036 (CM1), x90; CPC 33037 (CM20), x90. Fig. 21, *Belodina* sp. E; CPC 33038 (CM2), x108. Fig. 26, *Belodina* sp. F, CPC33040 (CM22), x72.

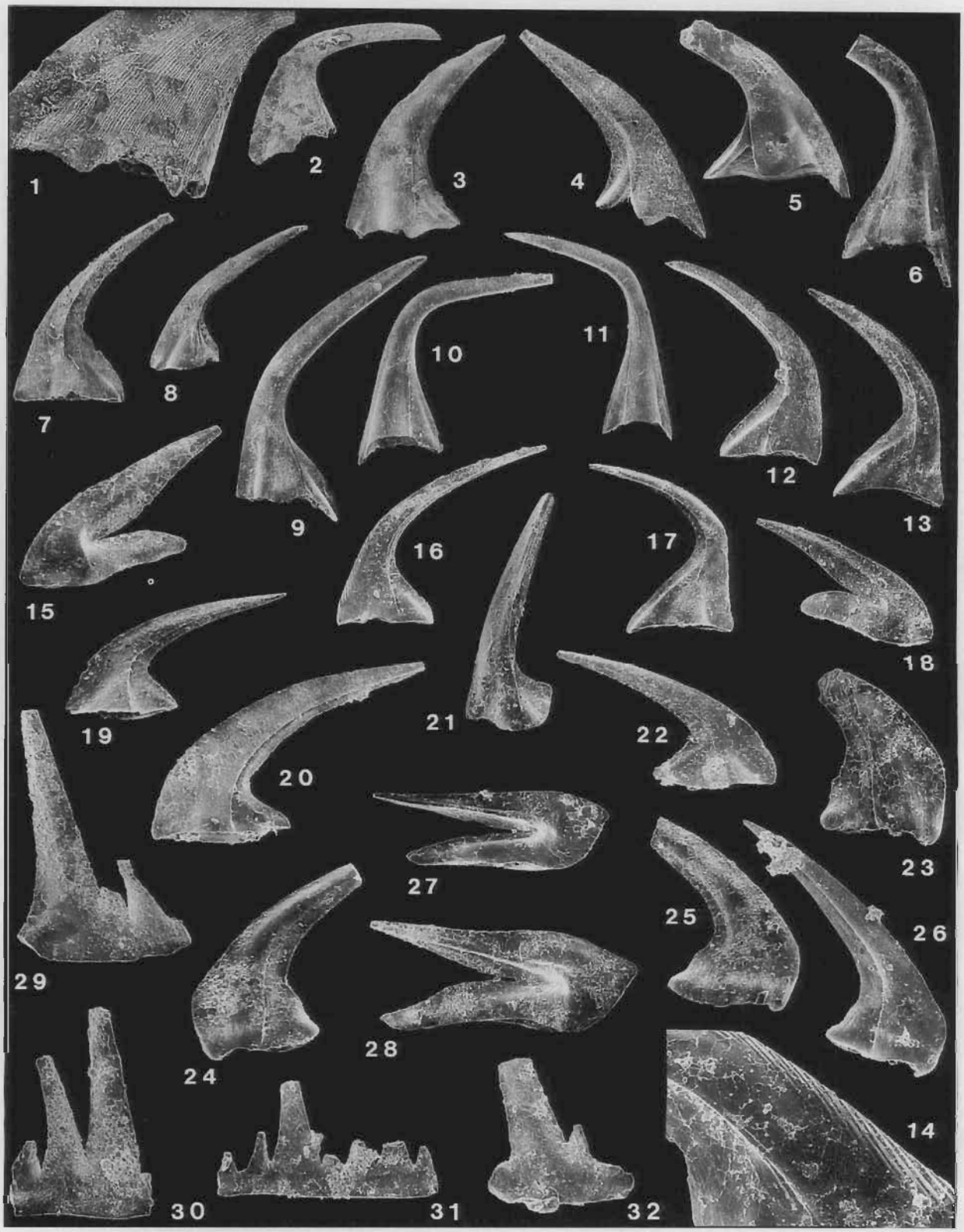

Plate 3. Figs 1–6, 8–11, *Scabbardella altipes* subsp. B Orchard, 1980; 1–6, 9–11, Sc elements, respectively CPC 33041 (GC6), x90 & x36; CPC 33042 (CM18), x22.5; CPC 33043 (CM18), x22.5; CPC 33044 (CM18), x27; CPC33045 (CM11), x27; CPC 33046 (CM6), x18; CPC 33047 (CM18), x36; CPC33048 (CM23), x36; 8, Sa element, CPC 33049 (CM18), x27. Figs 7, 12–18, *Besselodus* sp.; 7, 13–14, Sc elements, respectively CPC 33050 (GC10), x63; CPC 33051 (CM5), x54 & x324; 12, 16–17, Sb elements, respectively CPC 33052 (GC10), x54; CPC 33053 (CM5), x54; CPC 33054 (CM13), x54; 15, 18, M elements, respectively CPC 33055 (CM6), x72; CPC 33056 (CM13), x72. Figs 19–20, 22, *Dapsilodus mutatus* (Branson & Mehl, 1933)?; Sc elements, respectively CPC 33057 (CM13), x72; CPC 33058 (GC2), x63; CPC 33059 (CM1), x72. Fig. 21, *Paroistodus*? sp. A Nowlan & McCracken, 1988; Sc element, CPC33060 (CM19), x72. Figs 23–26, *Zanclodus levigatus* Nowlan & McCracken, 1988; 23, Group 1 element, CPC 33061 (CM18), x108; 24–26, Group 3 elements, respectively CPC 33062 (CM18), x90; CPC 33063 (CM15), x90; CPC 33064 (GC3), x90. Figs 27–28, *'Oistodus'* cf. *venustus* Stauffer 1935; respectively CPC 33065 (CM6), x72; CPC 33066 (CM11), x72. Figs 29–32, *Istorinus*? sp.; respectively CPC 33067 (CM11), x90; CPC 33068 (CM11), x90; CPC 33069 (CM1), x90; CPC 33070 (CM9), x90.

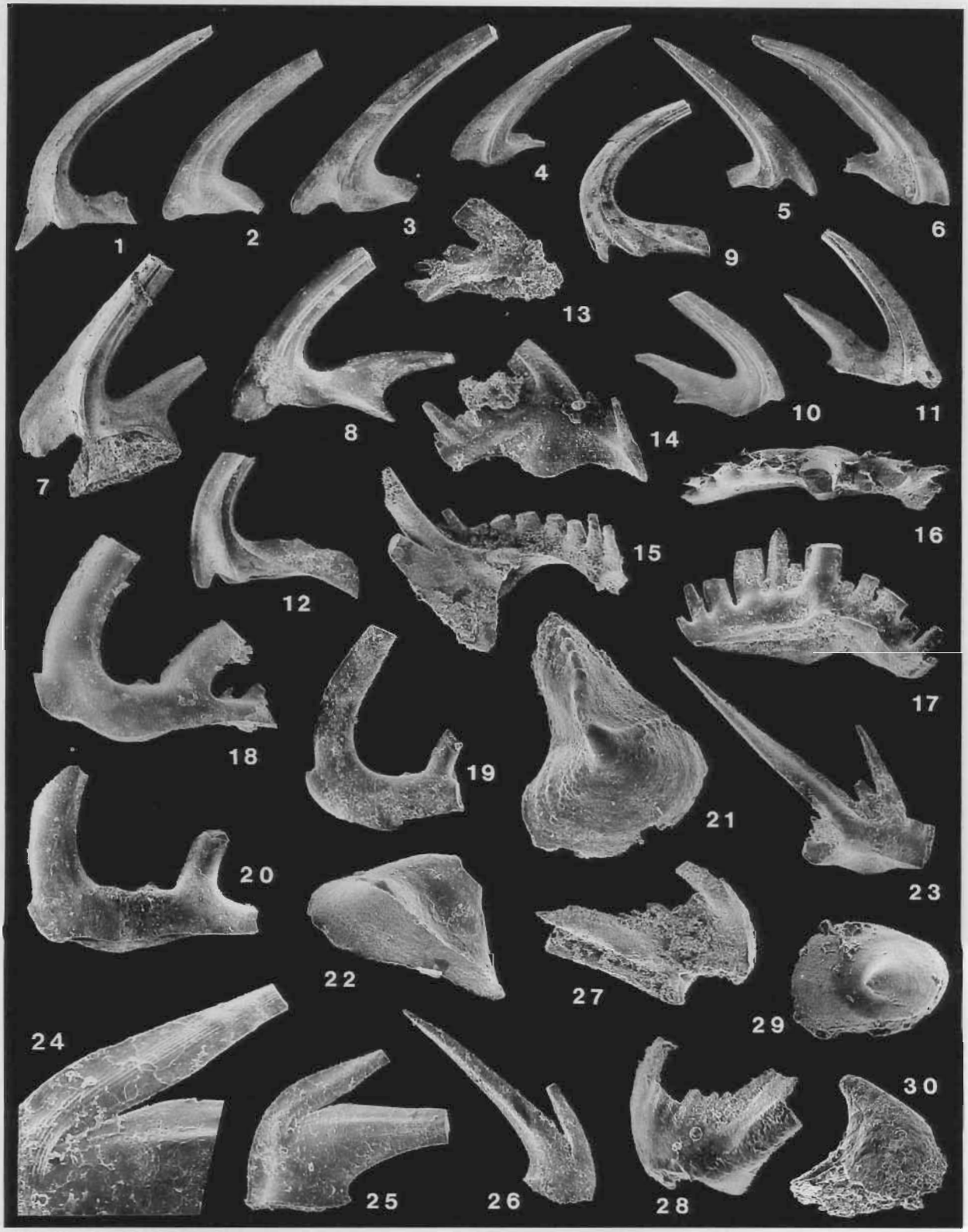

Plate 4. Figs 1, 7–12, *Protopanderodus insculptus* (Branson & Mehl, 1933); respectively CPC 33071 (GC6), x27; CPC 33072 (CM6), x27; CPC 33073 (CM22), x27; CPC 33074 (CM6), x36; CPC 33075 (CM22), x27; CPC 33076 (GC11), x27; CPC 33077 (CM6), x36. Figs 2–6, *Protopanderodus liripipus* Kennedy, Barnes & Uyeno, 1979; respectively CPC 33078 (CM6), x27; CPC 33079 (CM18), x27; CPC 33080 (CM6), x27; CPC 33081 (CM6), x27; CPC 33082 (CM6), x27. Figs 13, 14, 27–28 *Periodon grandis* (Ethington 1959). 13–14 P (prioniodiniform) elements, respectively CPC 33083 (CM1), x90; CPC 33084 (CM1), x90; 27–28, S (periodontiform) element, CPC 33085 (CM16), (inner & outer views), x90. Fig. 15, Gen. et sp. indet. D; CPC 33086 (CM1), x63. Figs 16 & 17, *Oulodus* cf. *oregonia* (Branson, Mehl & Branson, 1951); Pb element, CPC 33087 (CM18), (oral & lateral views), x63. Figs 18–20, *Yaoxianognathus*? *tunguskaensis* (Moskalenko, 1973), respectively CPC 33088 (CM18), x54; CPC 33089 (GC9), x54; CPC 33090 (GC9), x54. Figs 21 & 22, *Pseudooneotodus mitratus* (Moskalenko, 1973); 21, nodose element, CPC 33091 (CM6), x63; 22, element lacking nodes, CPC 33092 (CM5), x117. Fig. 23, *Chirognathus duodactylus* Branson & Mehl, 1933?; Pb element, CPC 33093 (CM18), x72. Fig. 24–26, *Strachanognathus parvus* Rhodes, 1955; 24 & 25, CPC 33095 (CM6), x205 & x90; 26, CPC 33096 (CM6), x72. Figs 29 & 30, *Pseudooneotodus beckmanni* (Bischoff & Sannemann, 1958); respectively CPC 33097 (GC3), x135; CPC 33098 (CM12), x135.

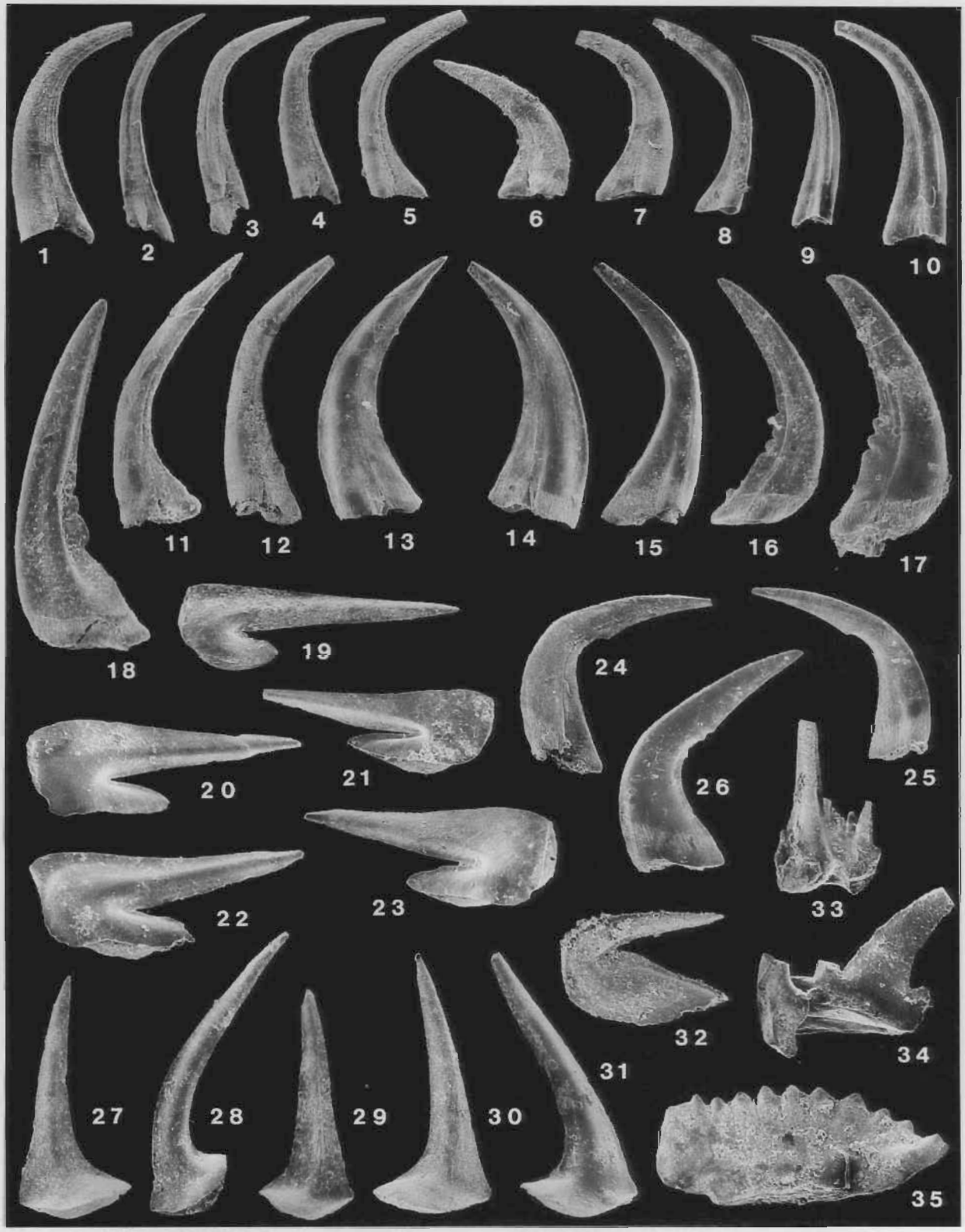

Plate 5. Figs 1–4, 9 & 10, 12–15, *Panderodus gracilis* (Branson & Mehl, 1933); 1, 4, 9, 10, Sa–Sb elements, 1, 10, CPC 33099 (GC10), x72; 4, 9, CPC 33100 (GC10), x72; 2–3, Sa elements, respectively CPC 33101 (GC3), x45; CPC 33102 (CM13), x54; 12, 15, Sb element, CPC 33103 (CM9), x45; 13 & 14, M elements, respectively CPC 33104 (CM6), x45; CPC 33105 (CM6), x45. Figs 5, 7 & 8, *Panderodus*? *liratus* Nowlan & Barnes 1981; 5, 8, CPC 33106 (AB3), x54; 7, CPC 33107 (CM15), x72. Figs 6, 11, *Panderodus* sp. B, respectively CPC 33108 (CM17), x72; CPC 33109 (CM18), x90. Figs 16–18, *Culumbodina*? sp.; respectively CPC 33110 (CM4), x81; CPC 33111 (CM9), x72; CPC 33112 (CM6), x72. Figs 19–23, *Paroistodus* sp.; respectively CPC 33113 (CM11), x72; CPC 33114 (CM9), x72; CPC 33115 (GC5), x72; CPC 33116 (CM6), x72; CPC 33117 (GC2), x72. Figs 24–26, *Panderodus* sp. D, 24–25, CPC 33118 (GC3), x72 & x72; 26, CPC 33119 (CM22), x72. Figs 27–31, *Drepanoistodus suberectus* (Branson & Mehl, 1933); 27, 29–31, oistodiform elements, respectively CPC 33120 (CM11), x63; CPC 33121 (AB3), x63; CPC 33122 (CM11), x63; CPC 33123 (CM22), x63; 28, drepanodiform element, CPC 33124 (CM9), x45. Fig. 32, *Ansella* sp.?; CPC 33125 (CM1), x90. Fig. 33, Gen. et sp. indet. A, CPC 33126 (CM18), x72. Fig. 34, *Periodon*? sp.; CPC 33127 (CM18), x72. Fig. 35, Gen. et sp. indet. B; CPC 33128 (GC1), x45.

Plate 6. Figs 2–11, *Phragmodus undatus* Branson & Mehl, 1933; 5, 8, 11, Sc elements, respectively CPC 33129 (CM1), x63; CPC 33130 (CM11), x63; CPC 33131 (CM1), x63; 2–4, M elements, respectively CPC 33132 (CM13), x63; CPC 33133 (CM11), x63; CPC 33134 (CM14), x63; 6, Pb element, CPC 33135 (CM11), x63; 7, Pa element, respectively CPC 33138 (GC1), x63; 9, Sa element, CPC 33136 (CM11), x63; 10, Sb element, CPC 33137 (CM11), x63. Figs 1 & 12. *Phragmodus undatus* Branson & Mehl, 1933?; 1, Sc element, CPC 33140 (CM11), x63; 12 Pa element CPC 33139 (CM11), x63. Figs 13–25, *Ozarkodina sesquipedalis* Nowlan & McCracken, 1988; 13, 15, Sc elements, respectively CPC 33152 (GC1), x72; CPC 33153 (CM8), x90; 14, Sb element, CPC 33141(CM18), x54; 16, 20-21, 23-25, Pa elements, respectively CPC 33146 (CM5), x72; CPC33147 (CM18), x72; CPC 33148 (CM22), x72; CPC 33149 (CM18), x72; CPC 33150 (GC1), x72; CPC 33151 (GC9), x72; 17-19, Pb elements, respectively CPC 33142 (CM18), x72; CPC 33143 (CM18), x72; CPC33144 (CM1), x72; 22, M element, CPC 33145 (CM18), x72.

127, 83–157.

Bergström, S.M., 1990. Biostratigraphic and biogeographic significance of Middle and Upper Ordovician conodonts in the Girvan succession, south-west Scotland. *Courier Forschungsinstitut Senckenberg*, 118, 1–43.

Bergström, S.M. & Sweet, W.C., 1966. Conodonts from the Lexington Limestone (Middle Ordovician) of Kentucky and its lateral equivalents in Ohio and Indiana. *Bulletin of American Paleontology*, 50(229), 271–441.

Bischoff, G. & Sannemann, D., 1958. Unterdevonische Conodonten aus dem Frankenwald. *Notizblatt hessisches Landesamt für Bodenforschung*, 86, 87–110.

Branson, E.B. & Branson, C.C., 1947. Lower Silurian conodonts from Kentucky. *Journal of Paleontology*, 21, 549–556.

Branson, E.B. & Mehl, M.G., 1933. Conodont studies. *University of Missouri Studies*, 8 (1–4), 1–343.

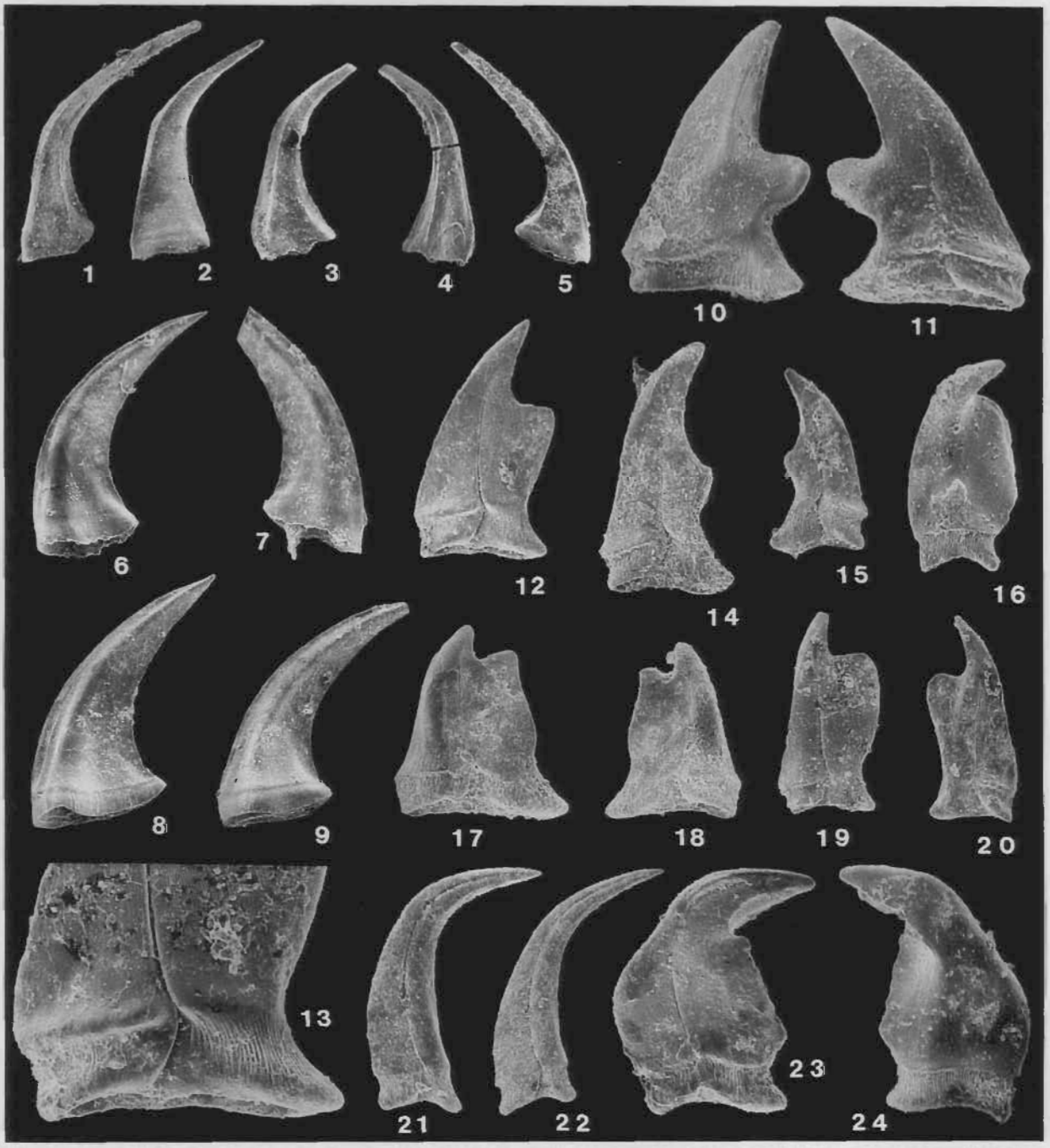

Plate 7. Figs 1–9, *Walliserodus amplissimus* (Serpagli, 1967); 1, 3 & 4, Sa elements, 1, CPC 33156 (CM11), x72; 3 & 4, CPC 33157 (GC10), x72; 2, 5, Sb? elements, respectively CPC 33154 (CM13), x72; CPC 33155 (CM11), x63; 6–9, M elements, respectively CPC 33158 (GC3), x63; CPC 33160 (AB3), x72; CPC 33161 (CM6), x54; CPC 33159 (GC7), x63. Figs 10–24, *Taoqupognathus tumidus* sp.nov.; 10 & 11, Sc? type 'a' elements, respectively CPC 33162(CM18), x108; CPC 33163 (CM18), x108; 12 & 13, Sc? type 'b' element, CPC 33164 (CM5), x108 & x225; 14 & 15, Sb? type 'b' elements, respectively CPC 33165 (CM11), x90; CPC 33166 (CM18), x90; 16, 23 & 24, P? elements, 16, CPC 33167 (CM4), x108; 23 & 24, CPC 33168 (CM6), x108; 17 & 18, Sb? type 'a' elements, respectively CPC 33169 (CM5), x108; CPC 33170 (CM12), x108; 19 & 20, Sc? type 'c' elements, respectively CPC 33172 (CM2), x108; holotype CPC 33171 (CM23), x108; 21 & 22, M? elements, respectively CPC 33173 (CM8), x108; CPC 33174 (CM4), x90.

Branson, E.B., Mehl, M.G. & Branson, C.C., 1951. Richmond conodonts of Kentucky and Indiana. *Journal of Paleontology*, 25, 1–17.

Burrett, C., Stait, B. & Laurie J., 1983. Trilobites and microfossils from the Middle Ordovician of Surprise Bay, southern Tasmania, Australia. *Memoir of the Association of Australasian Palaeontologists*, 1, 177–193.

Cooper, B. J., 1976. Multielement conodonts from the St. Clair Limestone (Silurian) of Southern Illinois. *Journal of Paleontology*, 50, 205–217.

Drygant, D.M., 1974. Prostye Konodonty Silura i nizhov Devona Volyno-Podolya [Simple conodonts from the Silurian and lowermost Devonian]. *Paleontologicheskiy Sbornik*, 10, 64–69.

Dzik, J., 1976. Remarks on the evolution of Ordovician conodonts. *Acta Palaeontologica Polonica*, 21, 395–455.

Eichenberg, W., 1930. Conodonten aus dem Culm des Harzes. *Paläontologisches Zeitschrift*, 12, 177–182.

Epstein, A.G., Epstein, J.B. & Harris, L.D., 1977. Conodont color alteration—an index to organic metamorphism. *U.S. Geological Survey Professional Paper*, 995, 1–20.

Ethington, R.L., 1959. Conodonts of the Ordovician Galena Formation. *Journal of Paleontology*, 33, 257–292.

Fåhraeus, L.E. & Hunter, D.R., 1985. Simple-cone conodont taxa from the Cobbs Arm Limestone (Middle Ordovician), New World Island, Newfoundland. *Canadian Journal of Earth Sciences*, 22, 1171–1182.

Fortey, R.A., Bassett, M.G. Harper, D.A.T., Hughes R.A., Ingham, J.K., Molyneux, S.G. Owen, A.W., Owens, R.M., Rushton, A.W.A., & Sheldon, P.R., 1991. Progress and problems in the selection of stratotypes for the bases of series in the Ordovician System of the historical type area in the U.K. *In* Barnes C.R. & Williams, S.H. (Editors). Advances in Ordovician Geology, *Geological Survey of Canada Paper*, 90-9, 5–25.

Glenister, A. T., 1957. The conodonts of the Ordovician Maquoketa Formation in Iowa. *Journal of Paleontology*, 31, 715–736.

Hadding, A., 1913. Undre dicellograptusskiffern i Skåne jämte några därmed ekvivalenta bildningar. *Lunds Universitets Årsskrift, Avd.*, 2, 9, 1–90.

Hamar, G., 1966. The Middle Ordovician of the Oslo region, Norway 22. Preliminary report on conodonts from the Oslo-Asker and Ringerike districts. *Norsk Geologisk Tidsskrift*, 46, 27–83.

Henningsmoen, G., 1948. The *Tretaspis* Series of the Kullatorp Core. *The Bulletin of the Geological Institutions, University of Uppsala* 32, 374–432.

Jenkins, C.J., 1978. Llandovery and Wenlock stratigraphy of the Panuara area, central New South Wales. *Proceedings of the Linnean Society of New South Wales*, 102, 109–130.

Kennedy, D.J., Barnes, C.R. & Uyeno, T.T., 1979. A Middle Ordovician conodont faunule from the Tetagouche Group, Camel Back Mountain, New Brunswick. *Canadian Journal of Earth Sciences*, 16, 540–551.

Knüpfer, J., 1967. Zur Fauna und Biostratigraphie des Ordoviziums (Gräfenthaler Schichten) in Thüringen. *Freiberger Forschungshefte*, C220, 1–81.

Lindström, M., 1955. Conodonts from the lowermost Ordovician strata of south-central Sweden. *Geologiska Föreningens i Stockholm Förhandlingar*, 76, 517–604.

Lindström, M., 1971. Lower Ordovician conodonts of Europe. *In* Sweet, W.C. & Bergström, S.M. (Editors). Symposium on Conodont Biostratigraphy. *Geological Society of America, Memoir*, 127, 21–61.

Löfgren, A., 1978. Arenigian and Llanvirnian conodonts from Jämtland, northern Sweden. *Fossils and Strata*, 13, 1–129.

MacKenzie, P. & Bergström, S.M., 1993. Discovery of the zonal index conodont *Amorphognathus ordovicicus* in the Richmondian of Indiana: Implications for the regional correlation of the North American Upper Ordovician Standard. *Geological Society of America, Abstracts with Programs*, 25, 472.

McCracken, A.D. & Nowlan, G.S., 1989. Conodont paleontology and biostratigraphy of Ordovician carbonates and petroliferous carbonates on Southampton, Baffin, and Akpatok islands in the eastern Canadian Arctic. *Canadian Journal of Earth Sciences*, 26, 1880–1903.

Moors, H.T., 1970. Ordovician graptolites from the Cliefden Caves area, Mandurama, N.S.W., with a re-appraisal of their stratigraphic significance. *Proceedings of the Royal Society of Victoria*, 83, 253–287.

Moskalenko, T.A., 1973. Conodonts of the Middle and Upper Ordovician on the Siberian Platform. *Akademiy Nauk SSSR, Sibirskoe Otdelenie, Trudy Instituta Geologii i Geofiziki* 137, 1–143, Novosibirsk (in Russian).

Moskalenko T.A., 1983. Conodonts and biostratigraphy in the Ordovician of the Siberian Platform. *Fossils and Strata*, 15, 87–94.

Nicoll, R.S., 1980. Middle Ordovician conodonts from the Pitman Formation, Canberra, A.C.T. *BMR Journal of Australian Geology & Geophysics*, 5, 150–153.

Nowlan, G.S. & Barnes, C.R., 1981. Late Ordovician conodonts from the Vauréal Formation, Anticosti Island, Quebec. *Geological Survey of Canada, Bulletin*, 329, Part I, 1–49.

Nowlan, G.S., McCracken, A.D. & Chatterton, B.D.E., 1988. Conodonts from Ordovician-Silurian boundary strata, Whittaker Formation, MacKenzie Mountains, Northwest Territories. *Geological Survey of Canada, Bulletin* 373, 1–99.

Orchard, M.J., 1980. Upper Ordovician conodonts from England and Wales. *Geologica et Palaeontologica*,14, 9–44.

Packham, G.H., 1967. The occurrence of shelly Ordovician strata near Forbes, New South Wales. *The Australian Journal of Science*, 30, 106–107.

Packham, G.H., 1969. The geology of New South Wales. *Geological Society of Australia, Journal*, 16, 1–654.

Palmieri, V., 1978. Late Ordovician conodonts from the Fork Lagoons Beds, Emerald area, central Queensland. *Geological Survey of Queensland, Publication* 369, *Palaeontological Paper*, 43, 1–55.

Pander, C.H., 1856. Monographie der fossilen Fische des Silurischen Systems der russisch-baltischen Gouvernements. *Akademie der Wissenschaften, St. Petersburg*, 1–91.

Percival, I.G., 1976. The geology of the Licking Hole Creek area, near Walli, central-western New South Wales. *Journal and Proceedings of the Royal Society of New South Wales*, 109, 7–23.

Percival, I.G., 1992. Ordovician brachiopod biostratigraphy of central-western New South Wales. *In* Webby, B.D. & Laurie, J.R. (editors), *Global perspectives on Ordovician geology*, 215–229. Balkema, Rotterdam.

Philip, G.M., 1966. The occurrence and palaeogeographic significance of Ordovician strata in northern New South Wales. *The Australian Journal of Science*, 29, 112–113.

Pickett, J.W., 1978. Further evidence for the age of the Sofala Volcanics. *Quarterly Notes of the Geological Survey of New South Wales*, 31, 1–4.

Pickett, J.W., 1991. Conodonts from cherts of the Ordovician 'Foxlow Formation' west of Numerella. Geological Survey of New South Wales, Unpublished Palaeontological Report 1991/2 (GS 1991/130).

Pickett, J.W., 1992. Conodont assemblages from limestones north of 'Millamolong', via Mandurama. Geological Survey of New South Wales, Unpublished Palaeontological Report 1992/11 (GS 1992/356).

Pickett J.W. & Ingpen, I.A., 1990. Ordovician and Silurian strata south of Trundle, New South Wales. *Quarterly Notes of the Geological Survey of New South Wales, 78*, 1–14.

Pulse, R.R. & Sweet, W.C., 1960. The American Upper Ordovician Standard. III. Conodonts from the Fairview and McMillan Formations of Ohio, Kentucky and Indiana. *Journal of Paleontology*, 34, 237–264.

Rigby J.K. & Webby, B.D., 1988. Late Ordovician sponges from the Malongulli Formation of central New South Wales, Australia. *Palaeontographica Americana*, 56, 1–147.

Rhodes, F.H.T., 1955. The conodont fauna of the Keisley Limestone. *Quarterly Journal of the Geological Society of London,* 11, 117–142.

Savage, N.M., 1990. Conodonts of Caradocian (Late Ordovician) age from the Cliefden Caves Limestone, southeastern Australia. *Journal of Paleontology,* 64, 821–831.

Savage, N. & Bassett M.G., 1985. Caradoc-Ashgill conodont faunas from Wales and the Welsh Borderland. *Palaeontology*, 28, 679–713.

Serpagli, T.J.M., 1967. I conodonti dell'Ordoviciano Superiore (Ashgilliano) delle Alpi Carniche. *Bolletino della Società Paleontologica Italiana,* 6, 30–111.

Smith, R.E., 1966. The geology of Mandurama-Panuara. *Journal and Proceedings of the Royal Society of New South Wales*, 98, 239–262.

Stauffer, C.R., 1930. Conodonts from the Decorah Shale. *Journal of Paleontology*, 4, 121–128.

Stauffer, C.R., 1935. Conodonts of the Glenwood Beds. *Geological Society of America, Bulletin*, 46, 125–168.

Stevens, N.C., 1952. Ordovician stratigraphy at Cliefden Caves, near Mandurama, New South Wales. *Proceedings of the Linnean Society of New South Wales*, 77, 114–120.

Stevens, N.C., 1957. Further notes on Ordovician formations of central New South Wales. *Journal and Proceedings of the Royal Society of New South Wales,* 90, 44–50.

Stewart, I.R. & Glen, R.A., 1986. An Ordovician age for part of the Girilambone Group at Yanda Creek, east of Cobar. *Geological Survey of New South Wales, Quarterly Notes* 64, 23–25.

Stone, G.L. & Furnish, W.M., 1959. Bighorn conodonts from Wyoming. *Journal of Paleontology*, 33, 211–228.

Stouge, S., 1984. Conodonts of the Middle Ordovician Table Head Formation, western Newfoundland. *Fossils and Strata*, 16, 1–145.

Sweet, W.C., 1979. Late Ordovician conodonts and biostratigraphy of the western Midcontinent Province. *Brigham Young University Geology Studies*, 26, 45–86.

Sweet, W.C., 1982. Conodonts from the Winnipeg Formation (Middle Ordovician) of the northern Black Hills, South Dakota. *Journal of Paleontology,* 56, 1029–1049.

Sweet, W.C., 1984. Graphic correlation of upper Middle and Upper Ordovician rocks, North American Midcontinent Province, U.S.A., *In* Bruton, D.L. (editor). Aspects of the Ordovician System. *Palaeontological Contributions from the University of Oslo*, 295, 23–35.

Sweet, W.C., 1988. *The Conodonta: morphology, taxonomy, paleoecology, and evolutionary history of a long-extinct animal phylum.* Clarendon Press, Oxford, x + 212 pp.

Sweet, W.C. & Bergström, S.M., 1984. Conodont provinces and biofacies of the Late Ordovician. *Geological Society of America, Special Paper* 196, 69–87.

Sweet, W.C. & Schönlaub, H.P., 1975. Conodonts of the genus *Oulodus* Branson & Mehl, 1933. *Geologica et Palaeontologica*, 9, 41–59.

Taylor, J.M. 1988. The geology of 'Weemalla' and 'Narambon' near Panuara, central western New South Wales. Unpublished B.Sc. thesis, University of Sydney, 1-138 pp.

Uyeno, T.T., 1990. Biostratigraphy and conodont fauna of Upper Ordovician through Middle Devonian rocks, eastern Arctic Archipelago. *Geological Survey of Canada, Bulletin*, 401, 1–211.

VandenBerg, A.H.M. & Cooper, R.A., 1992. The Ordovician graptolite sequence of Australasia. *Alcheringa* 16, 33–85.

Viira, V., 1974. Konodonty ordovika Pribaltiki. *Eesti NSV Teaduste Akadeemia Geoloogia Instituutt,* 1–142, Valgus, Tallinn (In Russian).

Webers, G.F., 1966. The Middle and Upper Ordovician conodont faunas of Minnesota. *Minnesota Geological Survey, Special Publication*, 4, 1–123.

Webby, B.D., 1969. Ordovician stromatoporoids from New South Wales. *Palaeontology*, 12, 637–662.

Webby, B.D., 1973. *Remopleurides* and other Upper Ordovician trilobites from New South Wales. *Palaeontology*, 16, 445–475.

Webby, B.D., 1974. Upper Ordovician trilobites from central New South Wales. *Palaeontology*, 17, 203–252.

Webby, B.D., 1976. The Ordovician System in south eastern Australia. *In* Bassett, M.G. (editor). *The Ordovician System.* University of Wales Press & National Museum of Wales, Cardiff, 417–446.

Webby, B.D., 1991. Ordovician stromatoporoids from Tasmania. *Alcheringa,* 15, 191–227. Webby, B.D., 1992. Ordovician island biotas: New South Wales record and global implications. *Journal and Proceedings of the Royal Society of New South Wales*, 125, 51–77.

Webby, B.D. & Blom, W., 1986. The first well-preserved radiolarians from the Ordovician of Australia. *Journal of Paleontology*, 60, 145–167.

Webby, B.D. & Kruse, P.D., 1983. The earliest heliolitines: a diverse fauna from the Ordovician of New South Wales. *Palaeontographica Americana*, 54, 164–168.

Webby, B.D. & Nicoll, R.S., 1989. Australian Phanerozoic Timescales 2: Ordovician. *Bureau of Mineral Resources, Australia, Record* 1989/32, 1–42, 1 chart.

Webby, B.D. & Packham, G.H., 1982. Stratigraphy and regional setting of the Cliefden Caves Limestone Group (Late Ordovician), central-western New South Wales. *Journal of the Geological Society of Australia*, 29, 297–317.

Webby, B.D. & Trotter, J., 1993. Ordovician sponge spicules from New South Wales, Australia. *Journal of Paleontology,* 67, 28–41.

Webby, B.D., VandenBerg, A.H.M., Cooper, R.A., Banks, M.R., Burrett, C.F., Henderson, R.A., Clarkson, P.D, Hughes, C.P., Laurie, J., Stait B., Thomson, M.R.A. & Webers, G.F., 1981. The Ordovician System in Australia, New Zealand and Antarctica. Correlation

Chart and Explanatory Notes. *International Union of Geological Sciences Publication*, 6, 1–69.

Weyant, M., 1968. Conodontes ordoviciens de I'lle Hoved (Archipel Arctique Canadien). *Bulletin de la Société Linnéenne de Normandie, 10 série*, 9, 20–66.

Williams, S.H., 1982. Upper Ordovician graptolites from the top Lower Hartfell Shale Formation (*D. clingani* and *P. linearis* zones) near Moffat, southern Scotland. *Transactions of the Royal Society of Edinburgh, Earth Sciences*, 72, 229–255.

Winder, C.G., 1966. Conodonts from the upper Cobourg Formation (late Middle Ordovician) at Colbourne, Ontario. *Journal of Paleontology*, 40, 46–63.

Wyborn, D., 1992. Stratigraphy and geochemistry of Ordovician volcanics from the Lachlan Fold Belt in central New South Wales. *In* Webby, B.D. & Laurie, J.R. (editors), *Global perspectives on Ordovician geology*. Balkema, Rotterdam, 495–497.

Ziegler, W. (editor), 1981. *Catalogue of Conodonts*, Vol.4. Schweizerbart'sche Verlagsbuchhandlung, Stuttgart. v + 445 pp.

Ziegler, W. (editor), 1991. *Catalogue of Conodonts*, Vol.5. Schweizerbart'sche Verlagsbuchhandlung, Stuttgart. iv + 212 pp.

AGSO Journal of Australian Geology & Geophysics, 15(4), 501–509

Pb-isotope data from base-metal deposits in central Australia: implications for Proterozoic stratigraphic correlations

R.G. Warren[1], R.I. Thorpe[2], J.A. Dean[3] & J.K. Mortensen[4]

Pb-isotope data for samples of lead-bearing minerals collected in central Australia provide useful age information, based on recently developed Pb-isotope mixing models. The Strangways Metamorphic Complex and the Bonya Metamorphics in the Arunta Block are hosts to stratabound base-metal lodes with model Pb-ages clustered with that of vesicle-filling galena from the lower Hatches Creek Group in the southern Tennant Creek Block. It is suggested, therefore, that these units in the northern and central Arunta Block are time-depositional equivalents of the Hatches Creek Group, the age of which has been independently established by zircon geochronology as 1820–1810 Ma. This time interval was an episode of extension, rift-style deposition and generation of volcanogenic base-metal deposits in the northern and central Arunta Block. The model Pb-age of the Oonagalabi prospect, and hence its host, the Bungitina metamorphics, appears younger than that for the Strangways Metamorphic Complex, but field evidence requires a more complex interpretation, involving metasomatic addition of radiogenic lead. Other deposits in the northern Arunta Block have Pb-isotope characteristics that show they are younger than their host rocks, and are thus related to granite intrusion or later tectonism. Home of Bullion lead has a range of compositions that can be interpreted to indicate formation probably in the Late Proterozoic.

The isotopic composition of lead in the gold lodes of the Tennant Creek district indicates model Pb-ages consistent with introduction shortly after deposition of their host rocks, during folding and granite emplacement.

Introduction

The results of two studies have been combined in this paper. A set of samples with lead minerals, collected from base-metal deposits during regional mapping by the Bureau of Mineral Resources (now the Australian Geological Survey Organisation, AGSO) in central Australia, was analysed by the Geological Survey of Canada (GSC). The other data set was assembled by SIROTOPE (CSIRO Division of Exploration and Mining isotope consultancy) in the assessment of sulphide or gossan occurrences for base-metal exploration programs. The latter data are released with the permission of the companies for which the research was conducted.

Some samples are from deposits in the Arunta Block interpreted as syngenetic, either stratabound or metamorphosed volcanogenic (Warren & Shaw 1985): one aim is to test the agreement of model Pb-ages with interpreted host-rock ages. If precise ages (i.e. ion microprobe SHRIMP ages on zircon) can be established for the host rocks to some of the deposits, the data will also be useful in a program initiated by the Geological Survey of Canada to evaluate and refine models for Pb-isotope evolution in the Proterozoic.

Data are also presented for four Au deposits hosted by the turbiditic Warramunga Formation (formerly Carraman Formation) in the Tennant Creek Block.

Recent Pb-isotope modelling (R.I.T. in prep.) has resulted in the recognition of a number of distinct lead sources (see below). Mixing isochrons based on a number of combinations of these sources yield several sets of possible model ages for the Arunta ore leads. Assessment of the analytical results permits the correlation of stratigraphic units that otherwise lack geochronological data, and indicates the timing of mineralisation in the northern and central Arunta Block. In particular, it gives new insight into the time–tectonic development of the northeastern and central segments of the Arunta Block during the Early to Mid Proterozoic.

[1] Australian Geological Survey Organisation, GPO Box 378, Canberra, ACT 2601

[2] Geological Survey of Canada, Ottawa, Canada

[3] Division of Exploration and Mining, CSIRO, North Ryde, NSW

[4] University of British Columbia, Vancouver, Canada

Regional setting

The Arunta Block comprises a terrane of metamorphic rocks and igneous intrusions at the southern edge of the North Australian Proterozoic Domains (Fig. 1). To the northwest, it is probably continuous with the poorly exposed Granites–Tanami Block, and it is separated from the Tennant Creek Block to the north by a trough of late Proterozoic to Palaeozoic sediments connecting the Wiso and Georgina Basins. The Tennant Creek Block forms an elongate ridge of basement, flanked to the east and west by the Georgina and Wiso Basins.

Regional mapping has shown that the Arunta Block can be subdivided into three provinces, elongated essentially east–west, which are characterised by distinctly different tectonic regimes (Shaw et al. 1984a). Stratigraphic correlations across the major faults that separate the provinces have been no better than speculative. Isotopic age data that record events before a widespread intense metamorphism at 1760–1750 Ma are sparse, and are invariably ages of intrusion; thus providing minimum ages for the depositional sequences. Intrusive rocks in the southeastern and northwestern parts of the Arunta Block have been dated at 1880 Ma (Zhao & Cooper 1992; Young et al. 1992). Zircon ages for other intrusions range down to 1160 Ma (Black & Shaw 1992).

The oldest rocks in the Tennant Creek Block, the Warramunga Formation (host to mineralisation), and the overlying Flynn Subgroup and granites, are in the central part of the ridge. These are overlain to the north by the Thompson Creek beds and to the south by the Hatches Creek Group. A review of geochronological data by Donnellan et al. (1994) led them to consider a depositional age of about 1860 Ma probable for the Warramunga Formation, followed by granite intrusion at about 1850 Ma. The Hatches Creek Group, in the southern part of the Tennant Creek Block (Davenport sub-province), has been placed in the interval 1820–1800 Ma (Blake & Page 1988). Affinity between the Northern Arunta Province and the Tennant Creek Block (e.g. Shaw et al. 1984a), is supported by recent age determinations in the northern Arunta Block (e.g. Williams et al. 1992; Young et al. 1992).

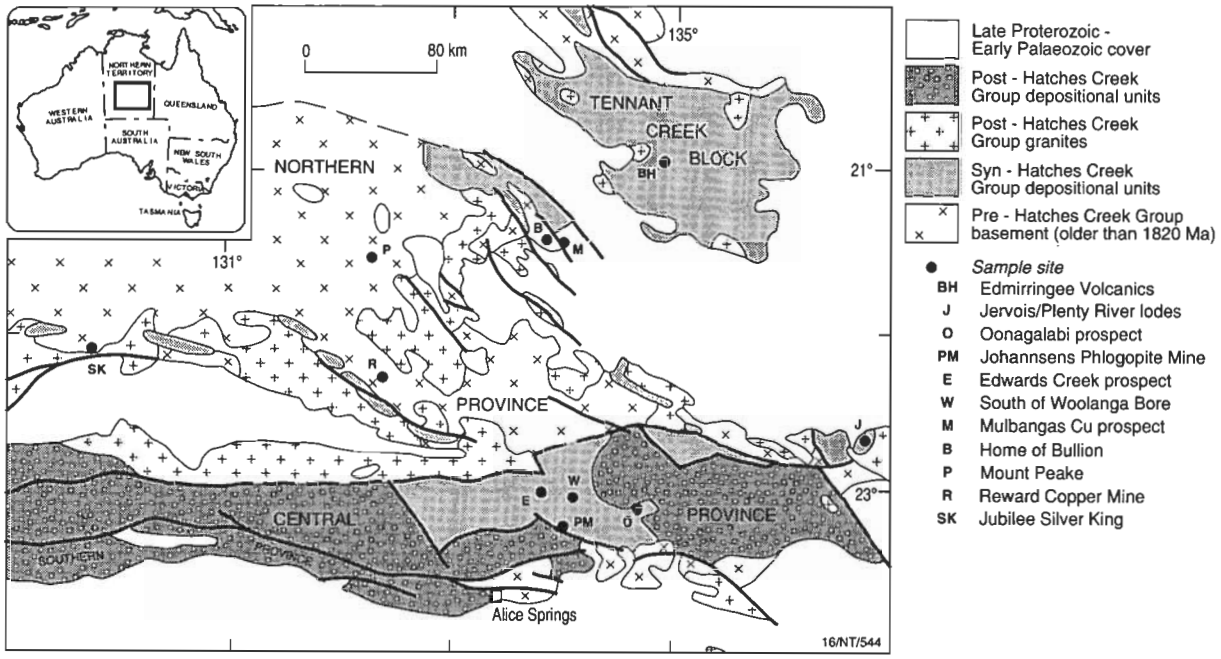

Figure 1. Map of the southern Tennant Creek Block and part of the Arunta Block, showing the locations from which specimens were collected. Locations of the Tennant Creek goldfield deposits are shown in Figure 1 of Gulson et al. (1988).

Exposure in the northern part of the Arunta Block is discontinuous, and the characteristics and distribution of the lithologies are obscured by deep weathering, thin Tertiary sediments and sand sheets. The rocks within the Hatches Creek Block are well exposed, but those within the central part of the Tennant Creek Block are poorly exposed and deeply weathered.

The samples

The northern and central Arunta Provinces contain a number of small base-metal lodes (Fig. 1), some of which have supported small mining ventures. All have been investigated by pits and shafts, and core from exploratory drilling is available for some lodes. The prospects are hosted by a number of stratigraphic units (Table 1). The Jervois deposits (also known as Plenty River) are stratabound, possibly distal, volcanogenic (e.g. Watson 1976; Freeman 1986), whereas the Oonagalabi, Johannsen's Phlogopite Mine, and the Edwards Creek prospect are interpreted as metamorphosed volcanogenic deposits (Warren & Shaw 1985). The sulphides in all these are, therefore, considered syngenetic with their host sequences. The Woolanga Bore prospect consists of an isolated outcrop of impure carbonate rock with disseminated galena. The remaining samples are from lodes that show discordant features (Home of Bullion, Mulbangas Cu prospect, Jubilee Silver King, Reward Copper, Mount Peake) and are expected to be younger than their hosts. Sulphides in the lower Hatches Creek Group fill vesicles in volcanic rocks and are considered essentially co-temporal with their hosts.

The lodes in the Tennant Creek mining district consist of Au, Cu and Bi in massive magnetite and/or hematite lenticular or pipe-like bodies hosted by turbidites of the Warramunga Formation (revised stratigraphy of Donnellan et al. 1994; previously the Carraman Formation, Gulson

Table 1. Sample location, host formation, and type of mineral deposit. (SMC—Strangways Metamorphic Complex).

Deposit/Occurrence	*Formation*	*Type*	*Lat & Long*
Oonagalabi	Bungitina metamorphics (SMC)	Syngenetic: volcanogenic	23°08′S 134°51′S
Edwards Creek Prospect	Yamba granulite (SMC)	Syngenetic: volcanogenic	23°01′S 134°01′S
Johannsen's Phlogopite Mine	Erontonga Granulite (SMC)	Syngenetic: volcanogenic	23°13′S 134°06′S
Mount Peake Lead Prospect	Lander Rock beds	Quartz vein in amphibolite	21°32′S 133°05′S
Jubilee Silver King	Lander Rock beds	Lode in pegmatite body near fold hinge	22°07′S 131°11′S
Woolanga Bore	upper Cadney metamorphics (SMC)	?: disseminated sulfides in fosterite marble	23°07′S 134°13′S
Home of Bullion	Bullion Schists	Discordant: in fault	21°31′S 134°10′S
Mulbangas Cu prospect	Bullion Schists	Discordant: in amphibolite	21°29′S 134°04′S
Lower Hatches Creek Group	Edmirringee Volcanics	Syngenetic?: galena in vesicles	20°59′S 135°54′S
Reward Copper Mine	Lander Rock beds	Discordant: quartz vein parallel to schistosity	22°11′S 132°49′S
Jervois Lodes (Plenty River Mine)	Bonya Metamorphics	Stratabound: syngenetic, distal volcanic?	22°39′S 136°25′S
Juno	Warramunga Formation	Hydrothermal	19°42′S 134°14′S
Argo	Warramunga Formation	Hydrothermal	19°28′S 134°06′S
Gecko	Warramunga Formation	Sedimentary/Hydrothermal?	19°26′S 134°03′S
Peko	Warramunga Formation	Hydrothermal	19°27′S 133°49′S

Table 2. Pb isotope data for central Australian ore leads

Sample	*Deposit/occurrence*	$^{206}Pb/^{204}Pb$	$^{207}Pb/^{204}Pb$	$^{208}Pb/^{204}Pb$	*Lab. and Date*	*Pb content*
TQ87-66	Oonagalabi	15.852	15.363	35.469	Geospec. Cons. 1988	galena
I107	Oonagalabi	15.851	15.351	35.434	CSIRO 1993	n.d.
dupl.	Oonagalabi	15.847	15.351	35.424	CSIRO 1993	2520 ppm
I109	Oonagalabi	15.852	15.360	35.463	CSIRO 1993	2690 ppm
TQ87-67	Edwards Creek	15.823	15.378	35.438	Geospec Cons. 1988	galena
H615	Edwards Creek	15.838	15.375	35.427	CSIRO 1992	4350 ppm
H616	Edwards Creek	15.863	15.392	35.455	CSIRO 1992	6050 ppm
H617	Edwards Creek	15.853	15.375	35.432	CSIRO 1992	7800 ppm
TQ87-68	Johanssen's Phlogopite M.	15.832	15.393	35.485	Geospec Cons. 1988	galena
dupl.	Johanssen's Phlogopite M.	15.830	15.394	35.464	Geospec Cons. 1988	galena
TQ87-69	Mount Peake Pb showing	21.032	16.054	40.615	Geospec Cons. 1988	galena
TQ88-30	Jubilee Silver King	15.822	15.417	35.474	Univ. Alberta 1993	Pb rich
TQ88-31	S. of Woolanga Bore	15.851	15.398	35.481	G.S.C. 1990	galena
TQ88-32	Home of Bullion	16.015	15.402	35.654	G.S.C. 1992	galena
I454	Home of Bullion	15.984	15.390	35.605	CSIRO 1993	>3%
I455	Home of Bullion	15.870	15.365	35.454	CSIRO 1992	cpy; 1190 ppm
I456	Home of Bullion	17.156	15.564	36.912	CSIRO 1994	>2%
TQ88-33	basal Hatches Creek Gp.	15.852	15.408	35.496	G.S.C. 1992	galena
TQ88-34	Reward Copper Mine	15.813	15.396	35.464	G.S.C. 1990	galena
TQ88-35	Jervois Lodes	15.857	15.394	35.492	G.S.C. 1990	galena
F137	Plenty River	15.844	15.377	35.451	CSIRO 1990	galena
dupl.	Plenty River	15.845	15.376	35.436	CSIRO 1990	galena
F138	Plenty River	15.835	15.366	35.423	CSIRO 1990g	alena
K227	Mulbangas	20.943	16.087	40.874	CSIRO 1994	1540 ppm
R27790	Juno	15.776	15.388	35.379	CSIRO 1984	galena
P866	Gecko	15.757	15.395	35.394	CSIRO 1985	n.d.
P867	Gecko	15.748	15.385	35.372	CSIRO 1985	2.2%
A672	Peko	15.769	15.379	35.366	CSIRO 1985	1770 ppm
A673	Peko	15.775	15.390	35.394	CSIRO 1985	2320 ppm
A489	Argo	15.785	15.399	35.377	CSIRO 1985	9700 ppm

n.d. not determined; cpy chalcopyrite

et al. 1988). The genesis of these lodes is controversial, but they are thought to be younger than their host rocks (e.g. Wedekind et al. 1988, 1990). Previously unpublished Pb-isotope data for four deposits in the central Tennant Creek field (Juno, Argo, Peko and Gecko) have been provided by Dr Brian Gulson of CSIRO.

The majority of samples used in these studies contain galena. However, some from the Edwards Creek, Oonagalabi, Home of Bullion, Mulbangas Cu prospect and the Tennant Creek lodes were oxidised Pb-rich material. The sample from Jubilee Silver King consists of secondary minerals from the oxidised zone, and contains beaverite, a hydrated sulphate of copper, lead and ferric iron.

Pb-isotope results

The Pb-isotope results for the central Australian samples are presented in Table 2. Twenty-three analyses have been obtained for ten separate deposits and occurrences in the Arunta Block, and seven analyses for five localities in the Tennant Creek Block. Results from the lodes in the central Tennant Creek Block are the least radiogenic and those from the Mount Peake and Mulbangas Cu prospects are highly radiogenic. The Home of Bullion data show a range of values from close to the Oonagalabi composition to values that are significantly more radiogenic. Data for the remaining seven localities are reasonably well clustered (Figs 2 and 3), although lead from Jubilee Silver King appears to be a little older, and lead from Oonagalabi a little younger, than that in the remaining deposits.

On the basis of recent Pb-isotope modelling, terrestrial lead evolution can be explained in terms of a number of distinct sources that have each continuously evolved throughout the history of the Earth. The evidence for these sources and the nature of their evolution will be presented elsewhere (R.I.T. in prep.). The sources have been defined in relation to primitive lead at $^{206}Pb/^{204}Pb = 9.3$ and $^{207}Pb/^{204}Pb = 10.297$ at an age of 4560 Ma, and the evolution of each is defined by the parameters μ and ε (Table 3).

Table 3. End-member lead sources recognised on the basis of linear Pb-isotope trends for volcanogenic massive sulphide deposits of a wide range of ages. The parameters are relative to a common primary composition of $^{206}Pb/^{204}Pb = 9.3$ and $^{207}Pb/^{204}Pb = 10.297$ at 4560 Ma.

Source	μ	ε*(x10-9/year)*
B	12.64478	0.0918161
C	14.63223	0.1146440
D	14.7958	0.1216569
E	18.23574	0.1238578
F	23.23296	0.1554803
G	9.862745	0.0525467
H	8.983918	0.0531951

The ε parameter is a rate factor as defined by Cumming & Richards (1975). Sources B, C, D, and G have been recognised in whole-rock Pb-isotope data from modern oceanic settings, as well as in massive sulphide deposits ranging in age from Archaean to Cenozoic. In contrast, source H has long-lived highly depleted characters (i.e. H is low μ), and sources E and F, long-lived highly enriched characters. Source E is believed to be a sub-continental lithospheric source.

The Pb-isotope compositions can be explained by empiri-

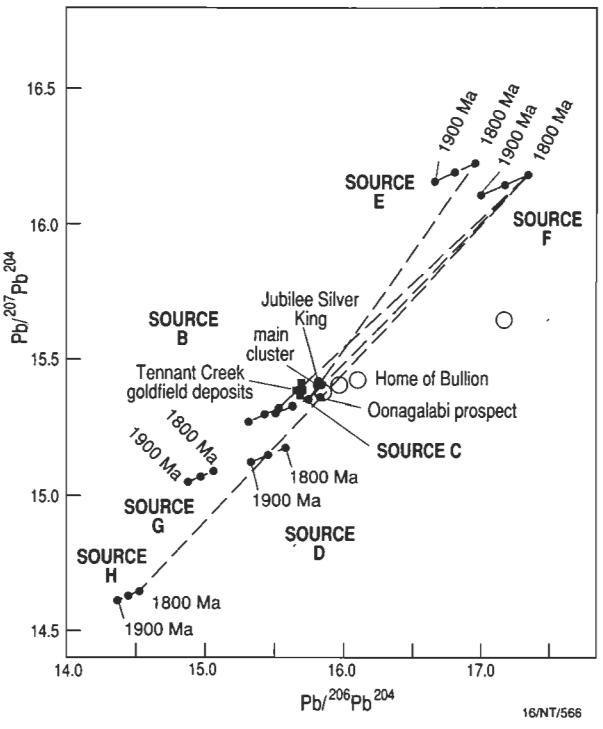

Figure 2. Plot of the Pb-isotope data, with the exception of the Mount Peake and Mulbangas values, in relation to the lead sources that have been recognised from modelling studies based on well-dated volcanogenic massive sulphide deposits. The mixing trends at 1800 Ma, corresponding to 4 of the 5 mixing combinations listed in Table 3, are shown by connecting lines.

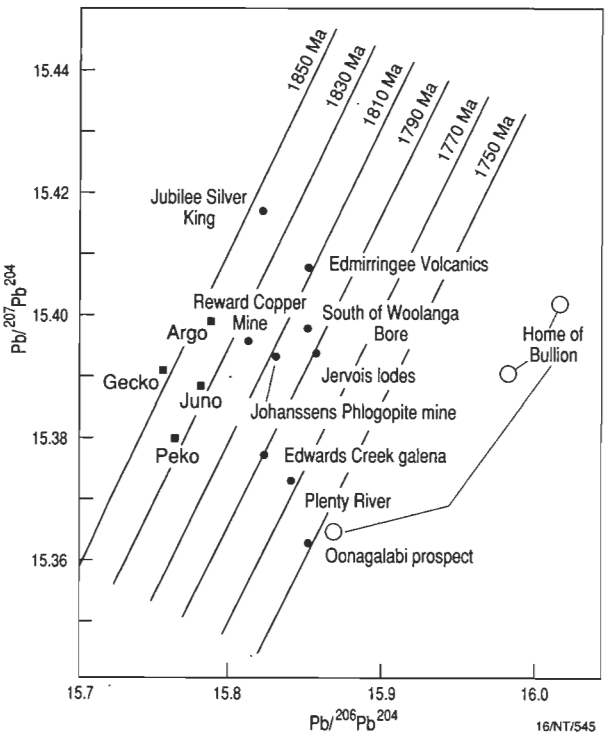

Figure 3. A detailed plot of the Pb-isotope data, with the highly radiogenic Mount Peake and Mulbangas values again omitted, in relation to mixing isochrons based on mixing between sources C and F. The parameters for these sources are given in Table 3.

cal mixing, in several different ways, of the possible model lead sources discussed above. The model ages based on five possible sets of mixing isochrons are listed in Table 4 for the samples from the Jubilee Silver King, Oonagalabi, Hatches Creek, and main cluster (Reward Copper, Johannsens Phlogopite Mine, Edwards Creek, Woolanga Bore and Jervois/Plenty River). Aside from the question of which of the mixing isochrons should be applied, there are other uncertainties to be attached to the model ages. These amount to ± 5 Ma, based on the analytical uncertainties in the Pb-isotope ratios (about 0.064% for $^{206}Pb/^{204}Pb$, and 0.068% for $^{207}Pb/^{204}Pb$ for analyses carried out by Geospec Consultants Limited and by the Geological Survey of Canada), perhaps ± 8 Ma due to the uncertainties in ages of Proterozoic volcanogenic massive sulphide deposits (particularly those in Sweden, Finland and Wisconsin, U.S.A.) on which the modelling is partly based, and some unknown, but probably small, additional modelling uncertainties. Each model age is, consequently, believed to be accurate to about ± 15 Ma, when the pertinent sources have been positively established. However, provided the lead in the different deposits was from the same sources, the data will define the relative ages of deposits more accurately than this.

Mixing between the B and F sources has been recognised in Archaean deposits of the southern Slave Province, Canada, and between the C and E sources in similar deposits in the west-central Slave Province. H–F mixing is known in the Proterozoic Skellefte massive sulphide district in Sweden and in Archaean deposits of the Whim Creek district and at Coppin Gap in the Pilbara Craton, Western Australia. The other possible trends, C–F and D–E, have not previously been documented. Model ages from B–F mixing and H–F mixing seem to be too young and too old, respectively, in relation to the few established age constraints for the host rock sequences in the Arunta Block (see below). Model ages based on the remaining three mixing trends all seem possible and are not greatly different, ranging from 1769 to 1838 Ma for the deposits of the main cluster. Although mixing between the C and F sources has not yet been documented elsewhere, model ages based on such a mixing process fit best with the known age constraints and are thus tentatively preferred. The model ages obtained in this manner are presented in Table 5 (except for those for Home of Bullion, Mount Peake and Mulbangas Cu prospect). Pb-isotope analyses for the volcanogenic massive sulphide deposits in Wisconsin (Afifi et al. 1984; unpublished data of G.L. Cumming and R.I. Thorpe), which have an age of about 1860 Ma (Sims et al. 1989), define a linear trend that appears to require a radiogenic end-member that lies between sources E and F. The central Australian deposits may have had analogous lead sources and their best model ages could thus lie between the two sets of values in Table 5.

Syngenetic deposits: stratigraphic correlations

A key regional stratigraphic marker in the northern Arunta and southern Tennant Creek Blocks is the unconformity at the base of the Hatches Creek Group and its correlatives, the Reynolds Range Group and the Ledan Schist–Utopia Quartzite succession (Fig. 4). The published age of 1813 ± 5 Ma (conventional zircon, maximum age) for the Treasure Volcanics in the lower Hatches Creek Group has been taken as placing this unconformity at about 1820 Ma and the Hatches Creek Group in the interval 1820–1810 Ma (Blake & Page 1988).

Table 4. Possible sets of model ages for the central Australian ore leads based on different mixing combinations between recognised lead sources. Average values are given for deposits where there is more than one analysis. Uncertainties are ± 15 Ma.

	Model ages based on mixing isochrons			
Mixing of sources	*Jubilee Silver King*	*Main cluster*	*Hatches Creek*	*Oonagalabi*
B and F	1754 Ma	1688–1725 Ma	1716 Ma	1639 Ma
H and F	1886 Ma	1838–1868 Ma	1857 Ma	1805 Ma
C and F	1843 Ma	1772–1822 Ma	1811 Ma	1744 Ma
C and E	1815 Ma	1769–1804 Ma	1791 Ma	1750 Ma
D and E	1848 Ma	1812–1838 Ma	1825 Ma	1792 Ma

If it is assumed that the galena infilling the vesicles in the sample from the lower Hatches Creek Group is essentially syngenetic with its host, then the zircon-based age of the Hatches Creek Group acts as a control for the model Pb-age (Table 5, Fig. 3).

The Bonya Metamorphics, in the northeastern part of the Arunta Block, are predominantly metasediments, but contain interlayered mafic and felsic volcanic units (Shaw et al. 1984a). They host a discontinuous line of stratabound lenses, referred to collectively as the Jervois lodes (alternatively, Plenty River Mines; the samples are from the Reward and the Green Parrot lodes). Textures reminiscent of volcanic breccias occur in drill core from the interval in which the lodes occur, suggesting these probably originated through distal volcanic exhalative processes, though the evidence is inconclusive (see also Watson 1976; Freeman 1986). The samples from Jervois give model Pb-ages slightly younger than the lower Hatches Creek sample. The Bonya Metamorphics appear to be penecontemporaneous with the Strangways Metamorphic Complex or slightly younger and to have formed at the same time as the Hatches Creek Group. Previously, the only constraint on the age of the Bonya Metamorphics was provided by the age of the post-tectonic Jervois Granite at about 1760 Ma (Black 1980; Zhao 1992). All the model Pb-ages are older than the age of the granite, but indicate a short time between deposition and granite intrusion.

Oonagalabi, Edwards Creek, and the sulphide-bearing rocks at Johannsen's Phlogopite Mine have been interpreted as metamorphosed exhalative–volcanogenic deposits, and their country rocks (units in the lower Strangways Metamorphic Complex, see Table 1), as bimodal volcanic suites (Warren & Shaw 1985). A small prospect south of Woolanga Bore consists of an isolated outcrop of galena-bearing forsterite marble, apparently part of the upper Cadney metamorphics, in the upper Strangways Metamorphic Complex. For the Edwards Creek prospect, Johannsen's Phlogopite Mine, and the prospect south of Woolanga Bore, the galena model Pb-ages (1792 ± 15 Ma, 1807 ± 15 Ma and 1799 ± 15 Ma, based on C–F mixing) confirm the supposed similar ages of these deposits and, thus, of their country rocks. Moreover, the age of their host formations is very similar to that of the Bonya Metamorphics and apparently only marginally less (in relative age) than that of the Hatches Creek Group. The inference drawn from these results is that the depositional age of the Strangways Metamorphic Complex is essentially the same as that of the Hatches Creek Group. Previously, the best indications of the age of the Strangways Metamorphic Complex were a Rb–Sr whole-rock isochron at 1820 ± 60 Ma (data from Iyer et al. 1976, using revised decay constants), a Rb–Sr isochron age of 1790 ± 35 Ma (interpreted by Black et al., 1983, as dating metamorphism), a conventional zircon age of 1763 Ma for a metadiorite near Johannsen's Phlogopite Mine (Black & Shaw 1992), and a conventional zircon age (Cooper et al. 1988) of 1747^{+3}_{-2} Ma for the Bruna Gneiss, which has intruded the overlying Harts Range Group.

Gossanous material from Edwards Creek prospect is slightly more radiogenic than the lead in galena from the carbonate rocks. This may indicate a minor radiogenic component in the gossan data derived *in situ* due to their lower Pb contents (<8000 ppm).

The Oonagalabi prospect is hosted by the upper Bungitina metamorphics. This unit has been considered, on structural criteria (e.g. Shaw & Wells 1983; Sivell 1988), to be basement to the Harts Range Group and, therefore, part of the Strangways Metamorphic Complex. The model age of about 1752 Ma for Oonagalabi would appear to indicate the host Bungitina metamorphics may not be a time-equivalent of the Strangways Metamorphic Complex, but, even allowing for analytical uncertainties, would confine deposition of the Harts Range Group to an improbably short timespan at about 1750 Ma. Such a strict stratigraphic interpretation of the Oonagalabi model age may not be necessary. Oonagalabi lead has a lower $^{207}Pb/^{204}Pb$ ratio than the other Strangways samples, suggesting a slightly different source of Pb. The deposit has been severely deformed, metamorphosed to granulite grade, and subsequently almost entirely rehydrated to amphibolite grade. Galena in the analysed specimen is a very minor constituent, and it may be that the isotopic composition of the lead has been somewhat altered by the introduction of a component of remobilised, more

Table 5. Model ages (with uncertainity of ± 15 Ma) based on the two preferred mixing relationships. Home of Bullion and deposits with very radiogenic lead (Mount Peake and Mulbangas) omitted.

Deposit	*Model ages derived from isochrons*	
	C–E mixing	*C–F mixing*
Jubilee Silver King	1815 Ma	1843 Ma
Reward Copper Mine	1804 Ma	1822 Ma
Hatches Creek galena	1791 Ma	1811 Ma
Johannsens Phlogopite Mine	1791 Ma	1807 Ma
Woolanga Bore	1783 Ma	1799 Ma
Edwards Creek	1783 Ma	1792 Ma
Jervois Lodes	1777 Ma	1790 Ma
Plenty River Mine	1769 Ma	1772 Ma
Oonagalabi galena	1754 Ma	1752 Ma
Oonagalabi gossans	1748 Ma	1741 Ma
Juno	1819 Ma	1837 Ma
Gecko	1834 Ma	1856 Ma
Peko	1819 Ma	1835 Ma
Argo	1826 Ma	1843 Ma

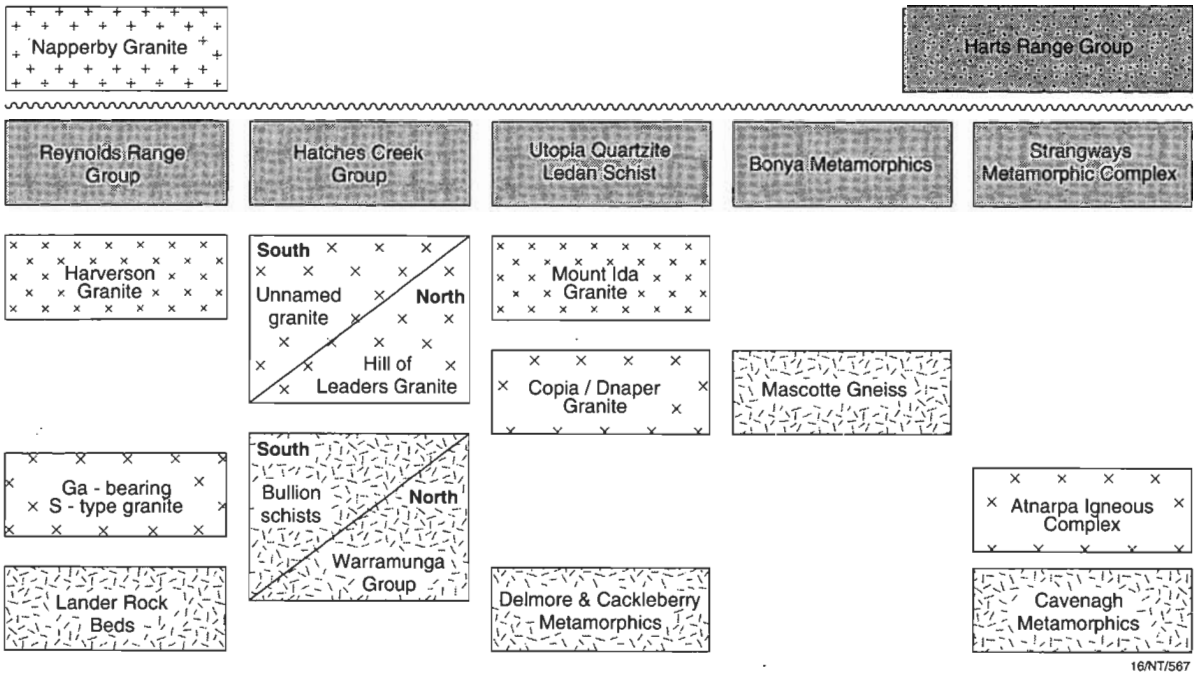

Figure 4. Stratigraphic correlation chart for the southern Tennant Creek Block and part of the Arunta Block, based in large part on the results of the Pb-isotope study. The age of the Atnarpa Igneous Complex is from Zhao & Cooper (1992).

radiogenic lead. Such open-system behaviour might have been possible during retrogression, when abundant fluid was introduced into the wall rocks to form the gedrite-bearing assemblages so characteristic of Oonagalabi.

Mineral deposits younger than their host rocks

The Au deposits of the central Tennant Creek Block have model Pb-ages, based on C–F mixing, of about 1856–1835 Ma. They are hosted by the Warramunga Formation (formerly the Carraman Formation), which is presently considered to have been deposited at about 1860 Ma (Donnellan et al. 1994). The model Pb-ages of the mineralisation are similar to, to younger than, the age of the enclosing rocks. Wedekind & Love (1990) have proposed a genetic model for the Warrego deposit and, by analogy, the other massive magnetite lodes in the Tennant Creek goldfield, involving dewatering of sediments and precipitation of iron hydroxides in structural traps during folding. They concluded that the mineralisation then occurred in response to a distinct major tectonothermal event, which they suggested may have been the intrusion of granites at about 1850 Ma (Cabbage Gum Granite dated at 1846 ± 8 Ma; Black 1984) and which localised the lodes centred on the major structural features. Main et al. (1990) favoured a model for Gecko based on remobilisation of a sediment-hosted massive sulphide deposit. The model age for Gecko (1856 ± 15 Ma, Table 3) is compatible with this model. However, the younger ages for the other deposits are closer to the age of the granite. Previously, the best indication of the age of mineralisation, based on the Rb/Sr ages of muscovite from several of the hydrothermal alteration zones exposed in the mines, has been about 1810 Ma (Black 1977).

The Jubilee Silver King lode is hosted by the Lander Rock beds, the age of which is presently constrained by an intrusive S-type granite, with an ion-probe zircon age of 1880 ± 5 Ma (Young et al. 1992). As a secondary lead mineral was used to obtain the model age, some disturbance of the Pb-isotopic system by secondary processes (deep weathering) in the late Mesozoic to present is possible. Even so, the 1843 ± 15 Ma model age result indicates that the Jubilee Silver King lode formed before deposition of the Reynolds Range Group. The model age falls close to the (approximately) 1850 Ma event which is significant to the north, with the Whitewater Volcanics (Halls Creek Inlier) at 1850 ± 5 Ma (Page & Hancock 1988), the Cabbage Gum Granite in the Tennant Creek Block at 1846 ± 8 Ma (conventional zircon, Black 1984), and activity in the Pine Creek and Mount Isa Inliers (see Page 1988). At present, there is little evidence for significant events of this age in the Arunta Block.

Galena from the Reward Copper Mine, also hosted by the Lander Rock beds is, at most, slightly older than the Hatches Creek Group. Its model age of 1822 ± 15 Ma suggests it is related to emplacement of the nearby Harverson Granite at 1818 ± 8 Ma (Williams et al. 1992).

The Home of Bullion Mine occupies a fault cutting the Bullion Schist, which is considered to underlie the Hatches Creek Group (Haines et al. 1991). The data, comprising analyses of primary ore and gossans, exhibit a range of Pb-isotopic compositions from close to the Oonagalabi value to significantly more radiogenic. The Mulbangas Cu prospect, some 10 km west-northwest of Home of Bullion, occurs in amphibolites of the Bullion Schist. The Home of Bullion and Mulbangas Cu prospect data define a linear trend on a $^{207}Pb/^{204}Pb$ vs $^{206}Pb/^{204}Pb$ diagram which has a low MSWD (mean square of weighted deviates) of 0.3. This may be interpreted as a mixing isochron which, if a source rock age of about 1850 Ma is assumed, gives a mineralisation age of about 700 Ma. The inference is that the Mulbangas Cu prospect and at least the more radiogenic data from the Home of Bullion lode were formed by fluids generated in a Late Proterozoic tectonothermal event, rather than having a genetic rela-

tionship to granite intrusions, as previously proposed (Sullivan 1953; Haines et al. 1991).

Mount Peake occurs in an area which includes granite with high U and Th (similar to the Mount Doreen suite emplaced at about 1550 Ma, Young et al. 1992). Lead from this prospect is highly radiogenic, and thus does not give reliable age information about the surrounding terrane. A two-stage interpretation of the data for this prospect, assuming the initial source composition was the same as that of the lead in the Reward Copper Mine at an age of 1820 Ma, gives an age of about 425 Ma for the mineralisation. This suggests the Mount Peake prospect may be as young as the mid-Palaeozoic Alice Springs Orogeny, the last major tectonic upheaval in central Australia. No other evidence provides a limiting minimum age on this occurrence.

Tectonic environment of the Strangways Metamorphic Complex and the Bonya Metamorphics (Figs 1 & 2).

The Northern Arunta Province is essentially the southern continuation of the Tennant Creek Block and was sialic basement by about 1820 Ma, when the Hatches Creek Group and its equivalents were deposited. The layered arrangement of well-sorted shallow-water arenaceous sediments in the Hatches Creek Group shows it was deposited in an extensive ensialic basin (Blake et al. 1987). The Ledan Schist–Utopia Quartzite succession is essentially a southern outlier of the lower Hatches Creek Group (Haines et al. 1991). The Reynolds Range Group, now preserved in synclinal keels as relics of more extensive cover, was deposited over sialic basement (Fig. 1).

The lithological succession in the Hatches Creek Group is consistent with a rift-and-sag model of basin development (Blake & Page 1988). In the early (rift) stage, rapid sedimentation was accompanied by abundant felsic and mafic volcanism and penecontemporaneous subvolcanic intrusive activity. Some of the clastic sediments were externally derived, some were locally derived volcanic detritus (Blake et al. 1987). The upper (sag-stage) Hatches Creek Group is predominantly sedimentary, but includes with a volcanic component in its lower part.

An ensialic tectonic environment seems valid for the Bonya Metamorphics. The Mascotte Gneiss, to the west of the Bonya Metamorphics, has been regarded as older basement (e.g. Shaw et al. 1984a), so pre-Bonya sialic crust extended at least as far east as the Jervois region and perhaps beyond, into the poorly exposed far-eastern Arunta Block. Certainly, farther to the east, sialic crust of the Mount Isa Inlier predates the Bonya Metamorphics (e.g. Page 1988). The internal stratigraphy of the Bonya Metamorphics has been mapped only by lithology, but fits rift-and-sag deposition. The sequence evolved from early felsic and mafic volcanic rocks to mainly sedimentary rocks, including calc-silicate rocks, at the top in the core of the syncline in the Bonya Hills (Shaw et al. 1984a; Freeman 1986). However, early down-warping must have outpaced deposition sufficiently to create deepwater conditions suited to formation of volcanogenic base-metal deposits.

South of the present outcrop of the Strangways Metamorphic Complex, sialic crust had formed well before 1820 Ma, as the Atnarpa Igneous Complex had been emplaced at 1880 Ma (Zhao & Cooper 1992). The northern margin of the complex is the Delny–Mount Sainthill Fault Zone, which is the southern boundary of the Northern Arunta Province. Most of the eastern Strangways Metamorphic Complex is overlain by the platform-like Harts Range Group; the western edge is faulted against the Narwietooma Metamorphic Complex. The early (rift) stage of the lower Strangways Metamorphic Complex consists mainly of metavolcanic units (e.g. the Yamba Granulite, which hosts the Edwards Creek prospect). The predominantly sedimentary Cadney metamorphics formed in the late (sag) stage. Again, early down-warping must have outstripped deposition.

Clearly, more data in the form of ion-microprobe zircon ages are required to test these correlations. Additional testing can be made through detailed geochemical studies of units in the Bonya Metamorphics and Strangways Metamorphic Complex, and comparison with the Hatches Creek Group. The proposed tectonic environment is in keeping with the regime proposed by Shaw et al. (1984b), who considered the Arunta Block to have evolved by repeated extensional and compressional events.

Conclusions

On the basis of the Pb-isotope data presented above, the Jervois lodes and the small volcanogenic base-metal lodes in the Strangways Metamorphic Complex were formed in the same tectono-stratigraphic episode and, thus, the Bonya Metamorphics and the Strangways Metamorphic Complex are time-stratigraphic equivalents. They appear to have been contemporaneous with the Hatches Creek Group. The probable ages of the Bonya Metamorphics and Strangways Metamorphic Complex are consistent with deposition on a pre-existing ensialic basement in an extensional environment. Recognition that a substantial part of the Central Province is younger than was previously known has implications for palinspastic reconstructions of the earlier stages of the Arunta Block. The model Pb-age for Oonagalabi is best viewed as a disturbed one, but the age of its host, the Bungitina metamorphics, needs clarification.

Deposits with model Pb-ages younger than the age of their host rocks are related to later events, either intrusion of granitic plutons or metamorphism. The model Pb-ages for Au mineralisation in the central Tennant Creek Block cluster around the age of granite emplacement at about 1850 Ma, but the data for Gecko are a little older, and a sedimentary origin cannot be ruled out. The range of isotopic compositions for Home of Bullion and the Mulbangas Cu prospect suggests the mineralisation may be much younger than the host rocks. The Mount Peake prospect may be as young as the mid-Palaeozoic Alice Springs Orogeny.

Acknowledgements

This paper was prepared with enthusiastic encouragement from S.S. Sun (AGSO). We are indebted to A.J. Stewart (AGSO) and to R.B. Thompson (formerly Northern Territory Geological Survey) for supplying the Hatches Creek and Jervois Lodes specimens, respectively. Dr. G.L. Cumming (University of Alberta, Edmonton) kindly contributed an analysis for the Pb-bearing sulphate specimen from the Jubilee Silver King deposit. Mount Isa Mines Limited and Aberfoyle Resources Limited are thanked for allowing J.A.D. to publish data. Dr B. Gulson (CSIRO)

is thanked for allowing publication of the Tennant Creek data. Barbara Gardner and Michael Korsch are thanked for undertaking analyses and maintaining the mass spectrometer at CSIRO. Nguyen Khanh Kim (GSC) did the final drafting of the lead isotope plots in Figures 2 and 3. Figures 1 and 4 were drafted by AGSO's Cartographic Services Unit. Helpful reviews were made by L. Anglin (GSC), J.W. Sheraton, A.J. Stewart, S.S. Sun, and D.H. Blake (AGSO).

References

Afifi, A., Doe, B.R., Sims, P.K. & Delevaux, M.H., 1984. U-Th-Pb isotope chronology of sulfide ores and rocks in the Early Proterozoic metavolcanic belt of northern Wisconsin. *Economic Geology*, 79(2), 338–353.

Black, L.P., 1977. A Rb–Sr geochronological study in the Proterozoic Tennant Creek Block, central Australia. *BMR Journal of Australian Geology & Geophysics*, 2, 111–122.

Black, L.P., 1980. Rb–Sr geochronology of the Jervois Range area in the eastern part of the Arunta Block, NT. *BMR Journal of Australian Geology & Geophysics*, 5, 265–270.

Black, L.P., 1984. U–Pb zircon ages and a revised chronology for the Tennant Creek Inlier, Northern Territory. *Australian Journal of Earth Sciences*, 31, 123–131.

Black, L.P. & Shaw, R.D., 1992. U–Pb zircon chronology of prograde Proterozoic events in the Central and Southern Provinces of the Arunta Block, central Australia. *Australian Journal of Earth Sciences*, 39, 153–171.

Black, L.P., Shaw, R.D. & Stewart, A.J., 1983. Rb–Sr geochronology of Proterozoic events in the Arunta Inlier, central Australia. *BMR Journal of Australian Geology & Geophysics*, 8, 129–137.

Blake, D.B. & Page, R.W., 1988. The Proterozoic Davenport province, central Australia: regional geology and geochronology. *Precambrian Research*, 40/41, 329–340.

Blake, D.B., Stewart, A.J., Sweet I.P. & Hone, I.G., 1987. Geology of the Davenport province, central Australia. *Bureau of Mineral Resources, Australia, Bulletin* 226.

Cooper, J.A., Mortimer, G.E. & James, P.R., 1988. Rate of Arunta Inlier evolution at the eastern margin of the Entia Dome, central Australia: implications for tectonic evolution. *Precambrian Research*, 40/41, 175–198.

Cumming, G.L. & Richards, J.R., 1975. Ore lead isotope ratios in a continuously changing Earth. *Earth Planetary Science Letters*, 28(2), 155–171.

Donnellan, N., Hussey, K.J. & Morrison, R.S., 1994. Flynn andTennant Creek, Northern Territory, 1:100 000 Geological Map Series. *Northern Territory Geological Survey, Explanatory Notes,* 5759 & 5758.

Freeman, M.J., 1986. Huckitta, Northern Territory, 1:250 000 Geological Map Series. *Northern Territory Geological Survey, Explanatory Notes,* SF53–11.

Gulson, B.L., Large, R.R. & Porritt, P.M., 1988. Gold exploration using lead isotopes at Tennant Creek, Australia. *Applied Geochemistry*, 3, 243–254.

Haines, P.W., Bagas, L., Wyche, S. Simons, B. & Morris, D.G., 1991. Barrow Creek, Northern Territory, 1:250 000 Geological Map Series. *Northern Territory Geological Survey, Explanatory Notes*, SF53–6.

Iyer, S.S., Woodford, P.J. & Wilson, A.F., 1976. Rb–Sr isotopic studies of a polymetamorphic granulite terrane, Strangways Range, central Australia. *Lithos*, 9, 211–224.

Main, J.V., Nicholson, P.M. & O'Neil, W.J., 1990. K44 ironstone copper–gold deposit, Gecko Mine. *In* Hughes, F.E. (Editor). Geology of the mineral deposits of Australia and Papua New Guinea. *Australasian Institute of Mining and Metallurgy, Monograph*, 14, 845–848.

Page, R.W., 1988. Geochronology of early to middle Proterozoic fold belts in northern Australia: a review. *Precambrian Research*, 40/41, 1–20.

Page, R.W. & Hancock, S.L., 1988. Geochronology of a rapid 1.85–1.86 Ga tectonic transition: Halls Creek orogen, northern Australia. *Precambrian Research*, 40/41, 447–468.

Shaw, R.D. & Wells, A.J., 1983. Alice Springs, Northern Territory, 1:250 000 Geological Map Series (second edition). *Bureau of Mineral Resources, Australia, Explanatory Notes*, SF 53/14.

Shaw, R.D., Warren, R.G., Offe, L.A., Freeman, M.J. & Horsfall, C.L., 1984a. Geology of the Arunta Block in the southern Huckitta 1:250 000 Sheet area, central Australia. Preliminary data, 1980 survey. *Bureau of Mineral Resources, Australia, Record*, 1984/3.

Shaw, R.D., Stewart, A.J. & Black, L.P., 1984b. The Arunta Inlier: a complex ensialic mobile belt in central Australia. Part 2: tectonic history. *Australian Journal of Earth Sciences*, 31, 457–484.

Sims, P.K., Van Schmus, W.R., Schulz, K.J. & Peterman, Z.E., 1989. Tectono-stratigraphic evolution of the Early Proterozoic Wisconsin magmatic terranes of the Penokean Orogen. *Canadian Journal of Earth Sciences*, 26(10), 2145–2158.

Sivell, W.J., 1988. Geochemistry of metatholeiites from the Harts Range, central Australia: implications for mantle source heterogeneity in a Proterozoic mobile belt. *Precambrian Research*, 40/41, 261–275.

Sullivan, C.J., 1953. The Home of Bullion Mine. *In* Edwards, A.B. (Editor). *Geology of Australian ore deposits.* 5th Empire Mining and Metallurgy Congress, Melbourne, 330–333.

Warren, R.G. & Shaw, R.D., 1985. Volcanogenic Cu–Pb–Zn bodies in granulites of the central Arunta Block, central Australia. *Journal of Metamorphic Geology*, 3, 481–499.

Watson, D.P., 1976. Attutra copper, lead and scheelite zone, Jervois Range. *In* Knight, C.L. (Editor). Economic Geology of Australia and Papua New Guinea 1 Metals. *Australasian Institute of Mining and Metallurgy, Monograph,* 5, 447–449.

Wedekind, M.R. & Love, R.J., 1990. Warrego gold-copper-bismuth deposit. *In* Hughes, F.E. (Editor). Geology of the mineral deposits of Australia and Papua New Guinea. *Australasian Institute of Mining and Metallurgy, Monograph*, 14, 839–843.

Wedekind, R., Large, R., Zaw, K. & Gulson, B., 1988. The composition and source of ore depositing fluids in the Tennant Creek goldfield. *In* Bicentennial Gold 88, Extended Abstracts, Poster Programme, Volume 2, *Geological Society of Australia, Abstracts,* 23, 492–494.

Williams, I.S., Collins, W.J. & Hand, M., 1992. The use of zircon U–Pb to provide a time base for the structural and metamorphic evolution of the northern Arunta Inlier, central Australia. *In* The application of geochronology to field related geological problems. Geological Society of Australia SGGMP Workshop, Alice Springs, July 5–11, 1992.

Young, D.N., Edgoose, C.J., Fanning, C.M. & Camacho, A., 1992. Ion-probe U-Pb zircon studies of the western Arunta Inlier, central Australia. *In* The application of geochronology to field related geological problems. Geological Society of Australia SGGMP Workshop, Alice Springs, July 5–11, 1992.

Zhao, J.-X., 1992. Proterozoic crust–mantle evolution in central Australia: geochemical and isotopic constraints. Ph.D. thesis, Australian National University (unpublished).

Zhao, J.-X & Cooper, J.A., 1992. The Atnarpa Igneous Complex, S.E. Arunta Inlier, central Australia: implications for subduction at an early-mid Proterozoic continental margin. *Precambrian Research*, 56, 227–253.

AGSO Journal of Australian Geology & Geophysics, 15(4), 511–517

Estimation of seismic quality factor Q for Victoria, Australia

J. Wilkie[1] & G. Gibson[2]

The effective quality factor Q for S wave attenuation in the Victorian lithosphere has been calculated using both the spectral ratio and coda Q methods. The frequency range studied was 2–20 Hz, and Q was found to be frequency dependent. A simple model has been adopted, with a low Q in the top 4 km of the crust that varies from 20 at a frequency of 1 Hz to 60 at 10 Hz. The lower crust has a higher Q that varies from 100 at 1 Hz to 700 at 10 Hz. Empirical formulae for Q determined by linear regression of logarithmic plots of amplitude versus frequency are

$Q = 20f^{0.5}$ for the 4 km thick upper crust, and

$Q = 100f^{0.85}$ for the lower crust, where f is frequency.

Introduction

The variation in seismic wave amplitudes about an earthquake is a fundamental study of seismology. This variation is due to the radiation pattern from the earthquake source, transmission path effects, including geometric spreading and many other disturbances of the wave field, and site effects due to near surface geology and topography. Seismic quality factor, Q, is a property of the material through which seismic waves pass. It summarises the characteristics that cause loss of amplitude with distance for reasons other than geometric spreading. A high Q (say over 500) means that amplitude does not decrease significantly with distance, while a low Q (say under 50) means there is considerable loss of amplitude with distance. Hard or cold rocks tend to have high Q, while soft or hot rocks tend to have low Q. It is usually found that Q increases with seismic wave frequency.

This study arose from the need for attenuation corrections to spectral amplitudes used to calculate the moments of earthquakes recorded by the Seismology Research Centre network, in Victoria. The local Richter magnitude of the earthquakes involved was normally less than M_L 3.0 with corner frequencies in the frequency range from 5 to 20 Hz.

The decrease in amplitude of a seismic wave with distance from the hypocentre can be represented by

$$A(f,R) = \frac{E(f)}{R^n} e^{-\gamma R} \qquad (1)$$

where R is the hypocentral distance, n is the geometrical spreading coefficient, f is frequency, E(f) is the earthquake source factor and g is the attenuation coefficient.

The quality factor Q is related to γ by

$$\gamma = \frac{\pi f}{uQ} \qquad (2)$$

where u is the propagation velocity. The exponent n is 1 for body waves propagating through a homogeneous medium and spreading spherically from a point source. Aki (1980) concluded that coda waves are primarily composed of backscattered S waves, so n = 1 is commonly used for coda. Investigating attenuation to improve estimates of Richter local magnitudes, Bakun & Joyner (1984) found n = 1.0 ± 0.1 in central California, and Greenhalgh & Singh (1986) determined n = 1.09 ± 0.07 in South Australia. It is unusual for surface waves to be associated with small Victorian earthquakes, except for very shallow events. The coda of local earthquakes is, therefore, substantially scattered S waves, and n = 1.0 was adopted in the Victoria region (Wilkie et al. 1993).

There is strong evidence from many sources (Aki & Chouet 1975; Singh & Herrman 1983; Woodgold 1990) that the value of Q varies with frequency. It combines the effect of anelastic properties of the medium, which may be frequency independent, and a frequency-dependent component due to scattering (Kvamme & Havskov 1989). The scattered energy depends on the distribution and size of crustal inhomogeneities and is, therefore, frequency dependent.

The common form of the relation between Q and frequency is a power law $Q = Qo\, f^{\eta}$, where Qo is a reference Q at a frequency of 1 Hz and η is a numerical constant (Singh & Herrman 1983; Kvamme & Havskov 1989; Ambeh & Fairhead 1989). Both Kvamme & Havskov (1989) for Norway and Ambeh & Fairhead (1989) for West Africa obtained values of η close to 1, i.e. a linear relationship between Q and frequency. Ibanez et al. (1990) found η to range between 0.81 and 0.89 in southern Spain. However, values of η as low as 0.3 for Eastern Canada (Woodgold, 1990) have been found and Lindley & Archuleta (1992) determined negative values of η in California, i.e. Q decreasing with frequency.

Methods of analysis

Spectral Ratio Method

Expression (1) can be rewritten

$$A(f,R) = \frac{E(f)}{R} e^{\frac{-\pi f t}{Q}} \qquad (3)$$

where t is the travel time of the wave and n = 1. This is a very simple model for attenuation about a point source in a homogeneous, isotropic, infinite space, so the following analysis clearly has limitations.

The spectral ratio for a particular frequency, f, is

$$\frac{A_1}{A_2} = \frac{R_2}{R_1} e^{\frac{\pi f(t_2 - t_1)}{Q}} \qquad (4)$$

where R_1, R_2 and t_1, t_2 are the hypocentral distances and travel times of P or S phases recorded at seismograph sites 1 and 2. A_1 and A_2 are the respective spectral amplitudes. Taking natural logarithms of both sides of expression (4) we obtain

[1] Department of Applied Physics, Victoria University of Technology, PO Box 14428 MMC, Melbourne, Victoria 3000, Australia

[2] Seismology Research Centre, Royal Melbourne Institute of Technology, Plenty Rd, Bundoora, Victoria 3083, Australia

$$\ln A_1 + \ln R_1 - \ln A_2 - \ln R_2 = \frac{\pi f(t_2 - t_1)}{Q} \quad (5)$$

which can be conveniently used to calculate Q. In this paper, log and ln refer to logarithms to the base 10 and e, respectively.

Singh et al. (1982) used data from aftershocks in the Imperial Valley of southern California and northern Mexico to determine spectral attenuation. Using real and synthetic SH-wave spectra, they found that the source factor E(f) derived from the analysis decayed too rapidly with frequency. They concluded that waves travelling nearly vertically through the upper crustal layers had a travel time and attenuation independent of R, and that their analysis could not distinguish between this and variations in the source spectrum. For sources deeper than 4 km, an expression of the form

$$A(f,R) = \frac{E(f)\, e^{-\pi f t^*}}{R}\, e^{\frac{-\pi f t}{Q}} \quad (6)$$

was introduced. They defined $t^* = {}^{t_s}/_{Q_s}$ where t_s is the vertical travel time in the upper 4 km of crust, t is the total travel time less t_s, while Q_s is the upper crust quality factor and Q is representative of the lower crust. The value of t^* is nearly independent of R, and can be constrained by the gradient of the spectral decay beyond the corner frequency. Reanalysis of their data using expression (6) gave consistent results.

A similar situation exists in Victoria, where the current lithospheric structure model shown in Figure 1 (after Wesson 1988) has an approximately 4 km thick low-velocity surface layer, through which the SH-waves would travel near normal to the surface.

The earthquakes used in this analysis were digitally recorded by the Seismology Research Centre network; the seismograph sites used are shown in Figure 2. The sampling rate was 100 samples per second, in most cases with an anti-alias filter at 25 Hz. An interval of 256 samples (2.56 seconds) of each S phase was Fourier transformed, passed through a 2 Hz high-pass filter and subjected to three iterations of three-point smoothing. Spectral amplitudes were then measured at 4, 5, 10, 15 and 20 Hz. The north–south and east–west components were combined to obtain a resultant amplitude.

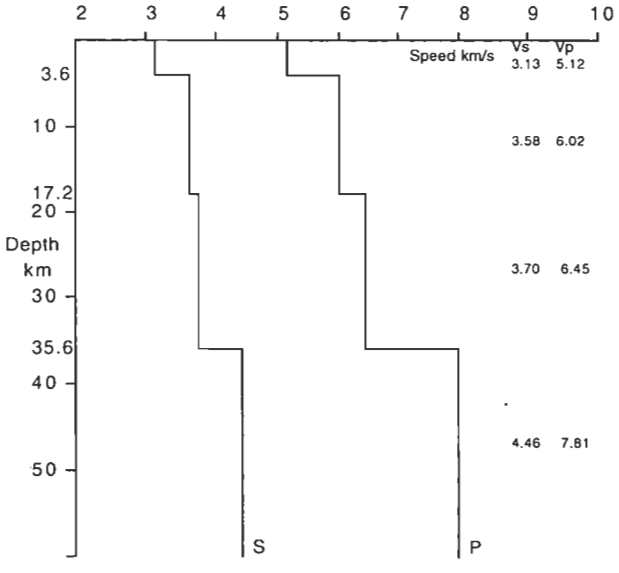

Figure 1. Victorian crustal structure (after Wesson 1988).

Local Richter magnitude seismograph site corrections for most of the network can be found in Wilkie et al. (1993). They represent the average difference between the magnitude computed for each site and the assigned magnitude for an earthquake. The assigned magnitude was the mean of magnitudes available from the Victorian network and neighbouring seismograph networks. Each spectral amplitude was multiplied by the exponential of the site correction to correct for amplification effects of local geology.

The data available for use in the analysis were from relatively small earthquakes, and no fault-plane information was available. Hence, the radiation patterns are unknown. A partial solution to this problem would be to use colinear epicentres and seismograph sites, but such favourable geometry proved to occur infrequently. It is assumed that the radiation patterns have a random effect. About 500 values of Q were calculated, where possible, for the events listed in Table 1.

Using a power-law relation between Q and frequency, $Q = Q_o f^{o\eta}$ and η can be determined using linear regression with the expression in the form

$$\log Q = \log Q_o + \eta \log f. \quad (7)$$

Figure 3 shows logQ versus logf for the S phase with the regression line of best fit. The regression line is:

$$\log Q = 2.0\ (\pm 0.2) + 0.8(\pm 0.2)\ \log f \quad (8)$$

The errors are calculated assuming a log-normal distribution.

To limit the influence of the excessively large values of Q due to the lack of correction for radiation patterns and focussing/defocussing on the analysis, the harmonic mean was calculated at each frequency and its logarithm is plotted against the logarithm of frequency in Figure 4. The line of best fit in this case gives the relation

$$\log Q = 1.78 + 0.85\ \log f \quad (9)$$

For the Bradford Hills series of earthquakes, the Upper Yarra seismograph group (POL, VPE, MCV) and the Thomson Reservoir seismograph group (SIN, MAL, TOD, MIC, PAT, TMD,ABE) are approximately in line with the epicentres. Values of Q were calculated for each earthquake using average amplitudes at the two seismograph groups. Log Q versus log f and the corresponding regression line are plotted in Figure 5. Q values are of the same order of magnitude but lower than those given by expressions (8) and (9). The value of η in this case is 1.0, i.e. a linear relation between Q and f: $Q = 27f$.

Coda Q Method

Aki (1969) and Aki & Chouet (1975) derived a formula for coda amplitude, assuming single or forward scattering. By determining the shape of the envelope of the coda for a particular frequency versus time, a value of Q can be obtained at that frequency. It is assumed that the coda consists of singly scattered waves from randomly distributed diverse scatterers in an isotropic medium and the earthquake source and seismograph are at the same location. Woodgold (1990) and Ambeh & Fairhead (1989) applied a correction for the separation of source and

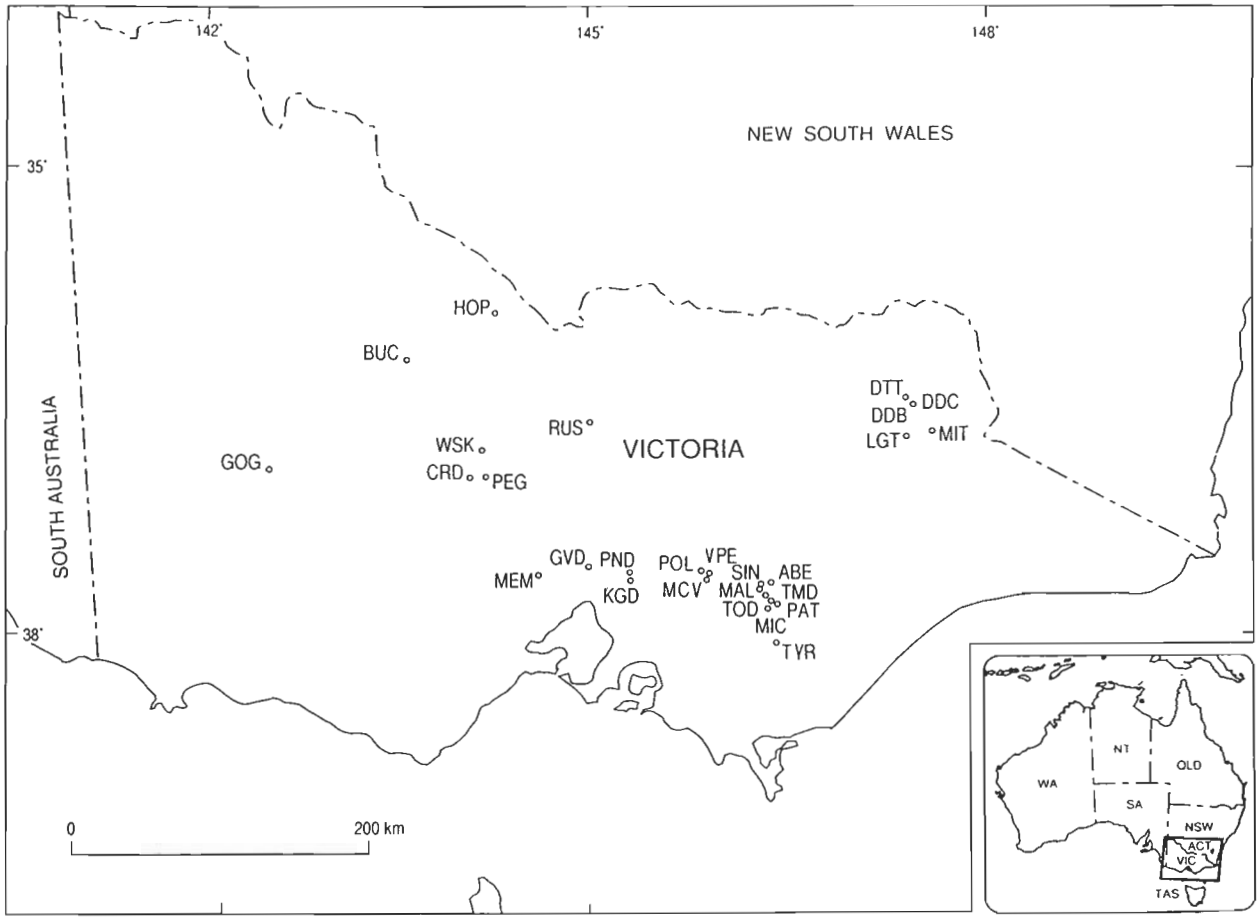

Figure 2. Seismology Research Centre network digital recording sites used in the determination of Q and moments.

receiver. However, the corrections in this study are small compared with errors in the estimation of the coda envelope and, consequently, are ignored.

The power spectral density for body waves at time t after the origin time (lapse time) can be written (Aki & Chouet 1975; Woodgold 1990) as:

$$P(\omega,t) = E(\omega)\, t^{-2} e^{\frac{-\omega t}{Q}} \qquad (10)$$

where $E(\omega)$ is a source spectrum. The amplitude spectrum is then

$$A = E_A(\omega)\, t^{-1} e^{\frac{-\omega t}{2Q}} \qquad (11)$$

where $E_A(\omega)$ is again a source term.

By taking the amplitude at different lapse times, t_1 and t_2, the amplitude ratio can be written

$$\frac{A1}{A2} = \frac{t2}{t1} e^{\frac{\pi f(t2-t1)}{Q}} \qquad (12)$$

Thus, by taking the amplitude of the coda envelope for a specified frequency at differing lapse times, Q can be determined at that frequency.

In practice, the digitised seismograph records were band-pass filtered, using zero-phase (acausal) filters in the bands : 3–7, 7.5–12.5, 12.5–17.5, 17.5–22.5 Hz, the bands being centred on 5,10,15 and 20 Hz. In each frequency band the coda envelope amplitude was estimated by eye and Q calculated using

$$\ln A_1 + \ln t_1 - \ln A_2 - \ln t_2 = \frac{\pi f(t_2 - t_1)}{Q} \qquad (13)$$

At short range (less than 17 km, mean 11.6 km), coda Q is significantly different from Q determined from the spectral ratio method. Using $Q = Q_0 f^{\eta}$ in the form of expression (7), Figure 6 was obtained with the corresponding regression expression

$$\log Q = 1.28 + 0.45 \log f. \qquad (14)$$

Assuming a log-normal distribution, the standard errors in the slope and intercept were calculated giving

$$\log Q = 1.28\ (\pm 0.15) + 0.45\ (\pm 0.14)\ \log f \qquad (15)$$

The standard deviation of the residual error in logQ was 0.25.

Evidence from source spectral analysis

The idealised spectrum of an earthquake consists of constant values at low frequencies, and above the corner frequency the spectral amplitude decreases as a power of frequency. The theoretical value of this power is –2 (Brune 1970, 1971) and the spectra of large earthquakes usually agree with that value (Wyss & Hanks 1972). However, for small earthquakes larger negative values often occur (Fletcher 1980).

Observed spectra—after corrections have been made for

Table 1. Seismic events used in the determination of Q.

Date	*UT*	*Place*	*ML*	*Longitude*	*Latitude*	*Depth*
1988-3-11	2253	Maldon	3.2	144.045	-37.043	10.8
1988-4-21	1645	Bunnaloo	3.2	144.463	-35.670	7.5
1988-5-20	1326	Rushworth	2.1	145.078	-36.608	6.0
1988-7-3	0823	Bunnaloo	4.0	144.496	-35.672	3.6
1989-7-15	0306	Bunnaloo	3.2	144.501	-35.730	8.6
1989-8-25	1500	Echuca	3.2	144.588	-36.184	21.4
1989-10-7	0045	Euroa	2.8	145.573	-36.815	8.5
1991-3-19	0109	Eildon	2.4	145.789	-37.169	13.0
1991-3-28	2126	Boolara South.	3.6	146.249	-38.525	20.6
1991-5-1	2239	Bradford Hills	2.8	144.086	-36.901	0.0
1991-5-2	0113	Bradford Hills	2.7	144.087	-36.893	0.0
1991-5-3	1728	Bradford Hills	3.5	144.086	-36.898	1.5
1991-6-8	1955	Bradford Hills	3.0	144.110	-36.888	0.8
1991-11-2	2056	Glenthompson	2.6	142.493	-37.608	1.2
1992-1-26	1454	Bradford Hills	2.6	144.093	-36.878	5.3
1992-2-9	1043	Mt Buller	2.5	146.527	-37.158	9.8

radiation pattern, geometrical spreading, attenuation, site amplification, and free surface—agree with the idealised shape and can be used to calculate the moment of the seismic source. If the correction for attenuation is accurate, then the spectral decay beyond the corner frequency will be independent of range R.

The spectral decay gradient of S wave spectra, corrected for attenuation, then plotted against range, was used as a check of η, the exponent giving the frequency dependence of Q. Three 1991 earthquakes (March 28, May 01 & May 02; Table 1) were used. The combined gradient versus range data are plotted in Figure 7(a–d) for respective values of η of 0.7, 0.8, 0.9, and 1.0. For all seismograms, 2.56 seconds of recording from the time from the S wave arrival were Fourier transformed and log spectral amplitude versus log frequency was plotted on a computer graphics display. The computer operator then manipulated lines representing a simplified source spectrum to determine the spectral amplitude at low frequency, the corner frequency, and the spectral decay gradient at higher frequencies. From Figure 7 the trend

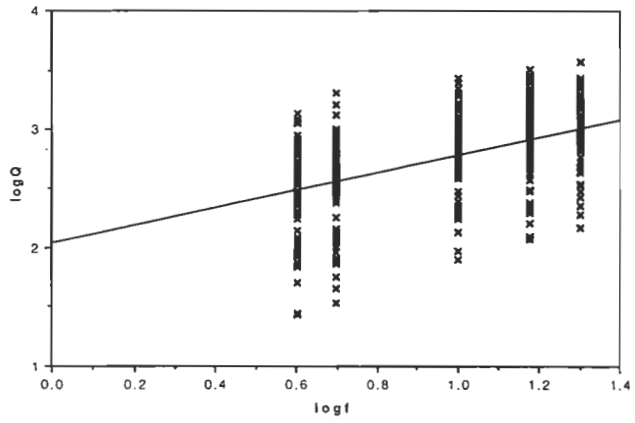

Figure 3. Plot of log Q against log frequency for the spectral ratio method.

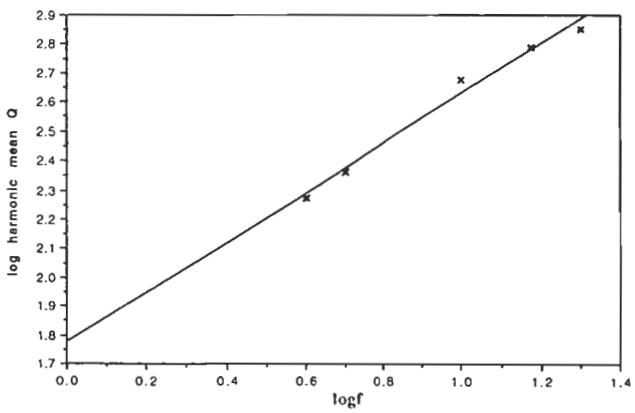

Figure 4. Plot of log of the harmonic mean of Q values determined using the spectral ratio method against log frequency.

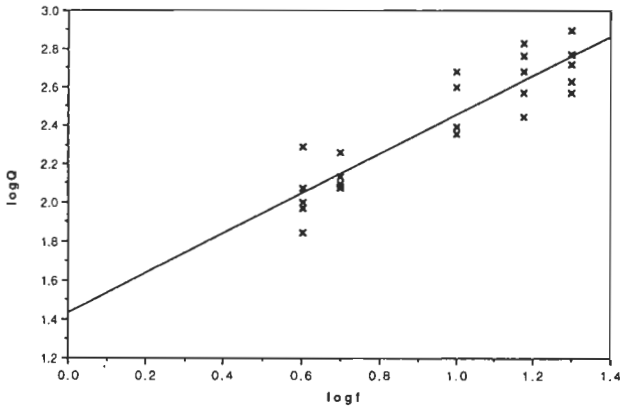

Figure 5. Log Q versus log frequency for Q values found using the spectral ratio method on S wave data from the Bradford hills events recorded at the Upper Yarra and Thomson Reservoir seismograph groups. The earthquakes and the seismograph groups are approximately colinear.

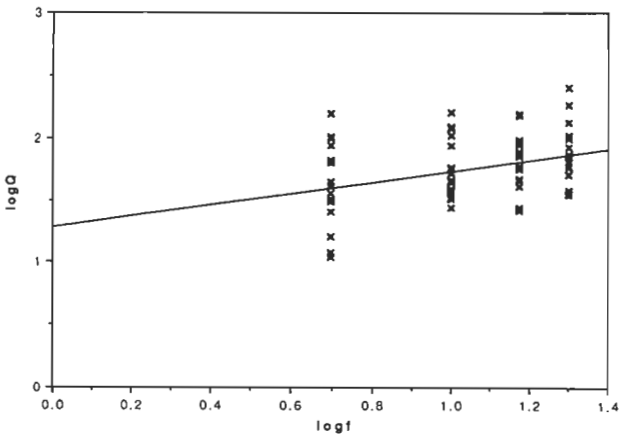

Figure 6. Plot of log Q versus log f for values of Q determined using the coda-Q method on short-range shallow events.

of the least squares regression lines indicates that for η = 0.9 there is minimum variation of spectral decay gradient with range. This value of η is close to that previously estimated from linear regression of harmonic-mean estimates of Q in Figure 4 and expression (9):

$$Q = Qo\ f^{\eta} = 60f^{0.85} \qquad (16)$$

The gradients in Figure 7 are not significantly different

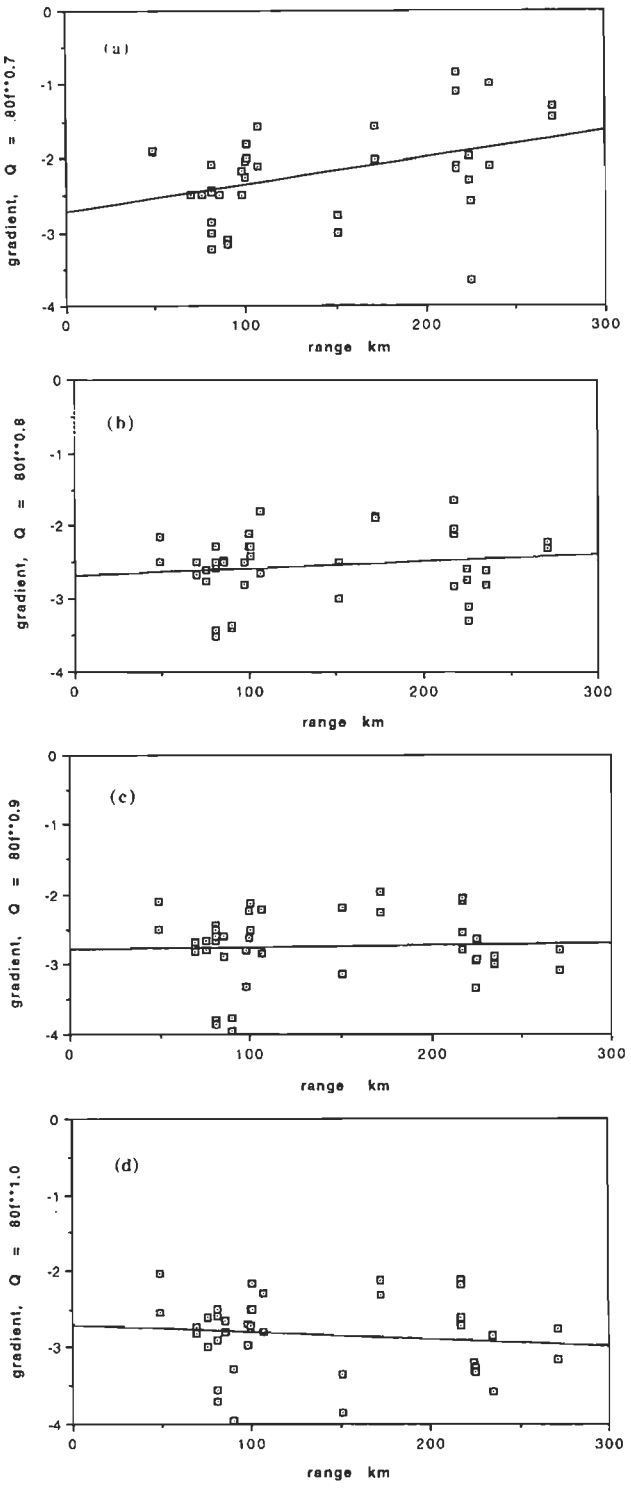

Figure 7. The gradient of log spectral amplitude against log frequency (above the corner frequency) plotted against range, with attenuation corrections using values of η of (a) 0.7, (b) 0.8, (c) 0.9, (d) 1.0.

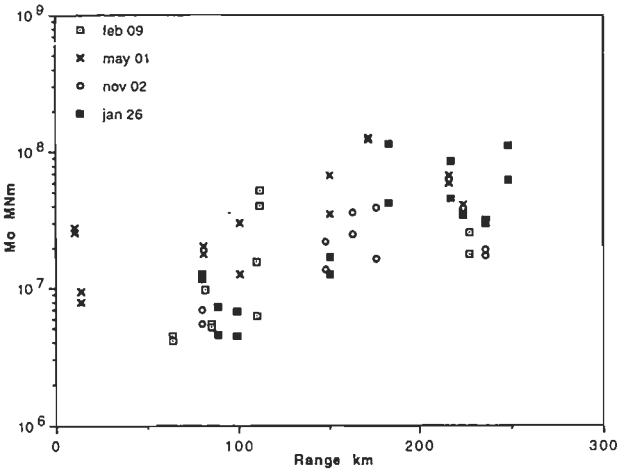

Figure 8. Superimposed plots of the moments of four earthquakes, calculated for each recording site using Q = 100f 0.9, against range. This shows a characteristic increase in range, which was also exhibited by all other analysed events.

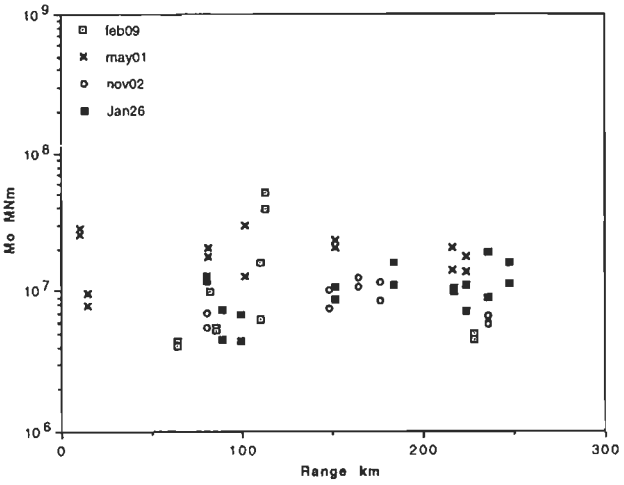

Figure 9. Superimposed plots of the moments of four earthquakes, calculated with Qo increasing over the range 100–200 km, against range.

from zero for η = 0.85 ± 0.1.

The spectral amplitude at low frequency can be used to estimate Mo, the moment of an earthquake, and stress drop (Brune 1970, 1971).

In Figure 8, moment estimates are shown from spectra at individual recording sites for four events (indicated in Figure 8 and listed in Table 1) with similar magnitude. The spectra have been corrected for attenuation using Q = $100f^{0.9}$. The moment estimate clearly increases with range between 100 and 150 km. A similar pattern is exhibited by other analysed events. This pattern could be explained by an increase of Q with range as waves travel at greater depth. Another explanation is in terms of phase arrivals. Remember that 2.56 seconds following the onset of the S arrival are used to estimate the spectrum. Up to a range of about 100 km, the S coda will be dominated by the Sg phase. According to Wesson's (1988) velocity model, reflections off the Moho (SmS) begin to arrive within 2.56 seconds of the Sg phase at a range of about 120 km. The extra energy contained in the SmS phase would contribute to the apparent increase of moment with range evident in Figure 8. It is likely that both phase arrival and variation of Q with depth contribute to the

moment pattern.

In Figure 9, the moments are again computed and corrected for attenuation, but this time allowing attenuation to increase with range (depth). Keeping η at 0.9, but varying Qo as follows:

Qo = 100 to a range of 120 km,

Qo = 100 + 1.25 (R – 120) for range R between 120 and 200 km, and

Qo = 200 beyond 200 km range.

There is no significant variation of the moment estimates with range. The scatter in Figure 9 can be attributed to the lack of accounting for the source radiation pattern and focussing/defocussing effects.

If the attenuation is correctly accounted for, then calculated values of Mo can be used to estimate magnitudes. Relations between magnitude and Mo that can be used include that given by the US Geological Survey, National Earthquake Information Centre:

$$\text{moment magnitude } Mw = (\tfrac{2}{3})\log Mo - 10.7 \qquad (17)$$

where Mo is expressed in dyne-cm (Hanks & Kanamori 1979), or

$$mb = \log Mo - 11.3 \qquad (18)$$

and $$1.4mb = \log Mo - 9.2 \qquad (19)$$

for western US earthquakes and eastern North American earthquakes respectively, where Mo is expressed in Nm, (Patton & Walter 1993).

Using Qo = 100 for the lower crust, the values of Mw, calculated using mean Mo values and expression (17), closely agree with the assigned Victorian local magnitude values (Table 2). The Mw scale was originally defined so that for smaller earthquakes the numerical values will be similar to those for the ML scale. Qo = 100 in the lower crust is consistent with estimates by the spectral ratio method. A mean stress drop of 1.8 MPa for the earthquakes used in the spectral amplitude analysis (Table 2) is consistent with values between 1 and 10 MPa expected for intraplate earthquakes (Nuttli 1983; Boatwright & Choy 1992).

Table 2. Comparison of ML assigned to the events with Mw calculated from the mean Mo values using expression (18)

Event	*Mo (MNm)*	*ML*	*Mw (exp.18)*	*Stress drop (MPa)*
May 01 1991	1.85×10^7	2.8	2.81	3.36
Jan 26 1992	1.20×10^7	2.6	2.68	1.42
Feb 09 1992	0.68×10^7	2.5	2.52	2.61
Nov 02 1991	1.17×10^7	2.6	2.67	0.53
Mar 19 1991	0.54×10^7	2.4	2.46	1.47

Discussion

The structure of the Victorian lithosphere is not known in detail; however, the surface structures have significantly different properties from the deeper lithosphere. Although there is considerable lateral variation with geological structures, the average depth of this low-velocity crustal region is 3.6 km in the model of the Victorian lithosphere, Wesson (1988). A simple two-layer model (Singh et al. 1982; Lindley & Archuleta 1992) can be adopted with a 3.6 km thick upper crust and a lower crust to an average depth of 36 km at the Mohorovicic discontinuity. Such a simple model is of sufficient accuracy for the methods used here to determine Q.

Q estimated from coda at close range is representative of the surface layer. The coda-Q method is, in theory, only applicable if earthquake and source are at the same location. However, by using events with an average range of 11.6 km and mean depth of 4.6 km, and using coda within a few seconds of the S phase arrival, the scattering volume was minimised and the values of Q obtained are representative of the higher attenuation, low Q, upper crustal region (Wennerberg1993). The coda-Q analysis found that the Qs in the upper crust were given by $Q = 20f^{0.5}$.

At greater distances (50–100 km) coda Q would be representative of a larger scattering volume and greater depth, and was found to be comparable with those obtained using the spectral ratio method.

The spectral ratio method can only determine Q in the region below the low-velocity upper crust (Singh et al. 1982). Two methods of data analysis were used: a linear least squares fit of individual Q estimates as a function of frequency in the log–log domain gave the relationship $Q = 100f^{0.75}$; and a linear least squares fit of log Q (harmonic means of Q at specific frequencies) and log f gave $Q = 60f^{0.85}$. Both methods, one taking the mean of logarithms and the other using harmonic means, reduce the contribution of extreme Q values in the analysis. Both are applicable to the lower crust. Considering also the results from the source spectrum analysis and earthquake moments, it is felt that $Q = 100f^{0.85}$ is representative of attenuation in the lower crust from depths of about 4 to 36 km.

The variation of seismic wave amplitudes with distance is very complex, and in this study we have not been able to resolve between increasing Q with depth and the effect of larger phase arrivals at particular distances, such as SmS reflections beyond 120 km. The original purpose of this study was to determine Q for moment computations, and it has been found that consistent moments can be determined if Q is increased for distances between 120 and 200 km.

The attenuation models used here are very crude. Future studies of Q could include more realistic attenuation functions that allow variation of Q between and within layers. Corrections could be included for source radiation pattern, travel path including amplitude variation with distance of different phases such as SmS, and spectral site effects. The analysis should include simultaneous inversion by least squares rather than step by step inversion.

Conclusions

Both the coda Q and spectral ratio methods show that Q increases with increasing frequency. A crude crustal attenuation model has been derived for the frequency range 2 Hz to 20 Hz with $Q = 20f^{0.5}$ in the 4 km thick upper crust, and $Q = 100f^{0.85}$ in the lower crust to a depth of about 36 km. This gives a low Q in the top

4 km of the crust that varies from 20 at a frequency of 1 Hz to 60 at 10 Hz, and a higher Q in the lower crust that varies from 100 at 1 Hz to 700 at 10 Hz.

Q in the lower Victorian crust is similar to estimates from central California by Aki & Chouet (1975), ranging from about 80 at 1 Hz to 500 at 10 Hz. From local magnitude studies, Wilkie et al. (1993) also found that the attenuation of seismic waves in the Victoria region is similar to that of central California.

Apparent variations of Q with range are likely to be the result of both mantle reflected and refracted phases and their presence within the first 2.56 seconds of S wave arrivals, and variation in Q with depth.

Accuracy considerations are complicated by the wide distribution of Q values determined for each frequency and the distortion resulting from data uncorrected for radiation patterns and focussing/defocussing effects. However in both upper and lower crust a clear dependence of Q upon frequency is evident. A progressive change in Q with depth in the lower crust probably exists, but has not been resolved by this initial study.

The close correspondence between local magnitude values, ML, and the values of Mw calculated from moments that were computed using these Q functions, and using the relationship adopted by the US Geological Survey, National Earthquake Information Centre, is encouraging. It implies that the local MI magnitudes computed for Victorian earthquakes are consistent with those in California. In future it will be possible to use a spectrally based magnitude for all local earthquakes.

Acknowledgments

The authors thank the referees for their detailed comments on the paper and considerable help with suggestions for presentation. J. Wilkie wishes to thank both the Victoria University of Technology for supporting the research with a grant of leave and the Director, G.Gibson, and staff of the Seismology Research Centre, RMIT, for access to resources and their generous cooperation.

References

Aki K., 1966. Generation and propagation of G waves from the Niigata earthquake of June 16, 1964, Part 2. Estimation of earthquake moment, released energy, and stress-strain drop from G-wave spectrum. *Bulletin, Earthquake Research Institute, Tokyo University,* 44, 73–88.

Aki, K., 1969. Analysis of seismic coda of local earthquakes as scattered waves. *Journal of Geophysical Research*, 74, 615–631.

Aki, K., 1980. Scattering and attenuation of shear waves in the lithosphere. *Journal of Geophysical Research*, 85(B11), 6496–6504.

Aki, K. & Chouet, B., 1975. Origin of coda waves: source, attenuation, and scattering effects. *Journal of Geophysical Research*, 80(23), 3322–3342.

Ambeh, W.B. & Fairhead, J.D., 1989. Coda Q estimates in the Mount Cameroon volcanic region, West Africa. *Bulletin of the Seismological Society of America*, 79(5), 1589–1600.

Bakun,W.H. & Joyner, W.B., 1984. The ML scale in Central California. *Bulletin of the Seismological Society of America*, 74(5), 1827–1843.

Boatwright, J. & Choy, G.L., 1992. Acceleration source spectra anticipated for large earthquakes in northeastern north america. *Bulletin of the Seismological Society of America*, 82(2), 660–682.

Brune J.N., 1970. Tectonic stress and the spectra of seismic shear waves from earthquakes. *Journal of Geophysical Research*, 75(26), 4997–5009.

Brune J.N., 1971. Correction. *Journal of Geophysical Research*, 76(20), 5002.

Fletcher J.B., 1980. Spectra from high-dynamic range digital recordings
of Oroville, California aftershocks and their source parameters. *Bulletin of the Seismological Society of America*, 70(3), 735–755.

Greenhalgh, S.A. & Singh, R., 1986. A revised magnitude scale for South Australian earthquakes. *Bulletin of the Seismological Society of America*, 76, no.3, 757–769.

Hanks, T. & Kanamori, H., 1979. A moment magnitude scale. *Journal of Geophysical Research*, 84(B5), 2348–2350.

Ibanez, J.M., Del Pezzo, E., De Miguel, F., Herraiz, M., Alguacil, G. & Morales, J., 1990. Depth dependent seismic attenuation in the Granada Zone (Southern Spain). *Bulletin of the Seismological Society of America,* 80(5), 1232–1244.

Kondorskaya N. V., Zakharova A.I. & Chepkunas L. S., 1989. The quantitative characteristics of earthquake sources as determined in the seismological practice of the U.S.S.R. *Tectonophysics,* 166, 45–52.

Kvamme, L.B.& Havskov, J., 1989. Q in southern Norway. *Bulletin of the Seismological Society of America*, 79(5), 1575–1588.

Lindley, G.T. & Archuleta, R.J., 1992. Earthquake source parameters and the frequency dependence of attenuation at Coalinga, Mammoth Lakes, and the Santa Cruz Mountains, California. *Journal of Geophysical Research,* 97(B10, 14),137–154.

Nuttli, O.W., 1983. Average seismic source-parameter relations for mid-plate earthquakes. *Bulletin of the Seismological Society of America*, 73(2), 519–535.

Patton, H.J. & Walter W.R., 1993. Regional moment: magnitude relations for earthquakes and explosions. *Geophysical Research Letters,* 20(4), 277–280.

Singh, S.K., Apsel, R.J., Fried, J. & Brune, J.N., 1982. Spectral attenuation of SH waves along the Imperial fault. *Bulletin of the Seismological Society of America,* 72(6), 2003–2016.

Singh, S. & Herrman, R.B., 1983. Regionalization of crustal Coda Q in the continental United States. *Journal of Geophysical Research*, 88, 527–538.

Wennerberg, L., 1993. Multiple-scattering interpretations of Coda-Q measurements. *Bulletin of the Seismological Society of America,* 83(1), 279–290.

Wesson, V., 1988. Seismic modelling of the Victorian lithosphere. MAppSc thesis, Phillip Institute of Technology, Victoria, Australia.

Wilkie, J., Gibson, G. & Wesson, V., 1993. Application and extension of the ML earthquake magnitude scale in the Victoria region. *AGSO Journal of Australian Geology & Geophysics*, 14(1), 35–46.

Woodgold, C.R.D., 1990. Estimation of Q in Eastern Canada using coda waves. *Bulletin of the Seismological Society of America*, 80(2), 411–429.

Wyss M. & Hanks T.C., 1972. The source parameters of the San Fernando earthquake inferred from teleseismic body waves. *Bulletin of the Seismological Society of America*, 62(2), 591–602.

AGSO Journal of Australian Geology & Geophysics, 15(4), 519–527

Upper crustal heterogeneities in Australian Precambrian provinces interpreted from deep seismic profiles and the Kola Superdeep Bore Hole

B.J. Drummond[2], A.G. Goncharov[1] & C.D.N. Collins[2]

Seismic reflection images of the upper crust of a large part of the Archaean Yilgarn Block in Western Australia contain very few reflections, implying that the upper crust is either compositionally homogeneous and largely unstructured or so completely folded and faulted that no laterally continuous surfaces remain to reflect seismic energy back to the surface. Seismic refraction data have, in the past, also been interpreted to show a homogeneous upper crust, at least at the broad reconnaissance scale sampled by previous experiments, which could not resolve structure or variations in composition over several kilometres or even tens of kilometres. Refraction data from the Pilbara Craton were similarly interpreted. However, in the light of more recent data with better spatial and temporal sampling from other shield areas, including the Kimberley Block and the Baltic Shield in Russia, the refraction data from the Yilgarn Block and Pilbara Cratons can be seen as consistent with a crust with more detail than was previously thought.

The long offset data from the Kimberley Block and Baltic Shield, although different in detail because of geological differences, have some important similarities. Both data sets contain bands of wide-angle reflections that are laterally continuous, but made up of several individual wavelets that have less lateral continuity and appear to constructively and destructively interfere with each other. This effect has been modelled for the Baltic Shield, using the variation of velocity with depth measured in basement penetrated in the Kola Superdeep Bore Hole, and is attributed to the effects of seismic energy refracted through and reflected off thin (200–500 m) layers of low-velocity (5.50 km.s^{-1}) to high-velocity (6.60 km.s^{-1}) rock interbedded in an upper crust with a median velocity less than 6.2 km.s^{-1}.

Thus, although the upper crust of the Kimberley and Yilgarn appears transparent to seismic reflection imaging, it is likely to contain heterogeneities comparable to the region of the Kola Superdeep Bore Hole, at least in terms of seismic velocity and density. The Pilbara Craton probably has similar heterogeneities. No estimate has been made of the relative distribution of vertical and horizontal heterogeneities. Despite the heterogeneities, original estimates of upper crustal seismic velocity are probably still a good indication of the average velocity in the Yilgarn Block and Pilbara Craton.

Introduction

Seismic reflection images in gneiss terranes of the Yilgarn Block of Western Australia show an upper crust almost devoid of reflections, overlying, at about 12 km, a lower crust with numerous, strong reflections (Figs 1a & 2). The non-reflective upper crust is interpreted as continuing farther east under greenstone supracrustals (Drummond et al. 1993); its western extent is not known. Published seismic sections from the western edge of the Yilgarn Block (Dentith et al. 1993) suggest that the upper crust there is not as reflective as the lower crust, although the weakly reflective upper crust may be thinner than farther east, consistent with the higher observed metamorphic grades and greater erosional denudation in the west (e.g., Gee 1979).

Several reasons can be put forward for the non-reflective nature of the upper crust:

(1) It is entirely homogeneous, which is unlikely, because the surface geology contains a range of rock types.

(2) Any geological boundaries that do offer seismic impedance contrasts* have limited lateral continuity, for example, because they are highly folded and faulted and, therefore, lack sufficient lateral continuity to be imaged with seismic waves.

(3) The upper crust may contain a range of rock types that have similar compositions, but different origins, in which case it will contain few if any geological boundaries with high seismic impedance contrasts.

Both the second and third explanations could apply in the Yilgarn Block. In the area of the seismic profile shown in Figure 2, granitoids and felsic gneisses predominate at the surface. These are not likely to provide laterally continuous, sub-horizontal geological boundaries, suitable for imaging with vertically travelling seismic waves. They also have similar seismic impedances, so geological boundaries are unlikely to reflect much energy.

Nor do seismic refraction data allow much scope for a range of rock types at depth likely to yield strong reflections. The variation of seismic velocity with depth through the crust (velocity/depth models) can be used to estimate crustal composition. Drummond (1982) estimated that Archaean crust has an average composition near that of diorite. Drummond & Collins (1986) developed an empirical relation between crustal thickness and the average seismic velocity in the crust. Durrheim & Mooney (1991) found similar variations in crustal velocity with depth in other continents. Drummond & Collins (1986) concluded that the lower crust, below 25–30 km depth, is likely to contain mafic material. This is consistent with evidence from lower crustal xenoliths (e.g. O'Reilly & Griffin 1985). Mafic material interlayered with more felsic rocks would provide compositional heterogeneities that are likely to be good reflectors of seismic energy.

Drummond (1988) and Drummond et al. (1993) matched seismic reflection data from the Yilgarn Block with velocity/depth models. After considering the effects of metamorphism on crustal velocity, Drummond (1988) suggested that the lower crust was most likely to comprise a mixture of felsic and mafic rocks, with the mafic component nowhere exceeding 20–35% of the total lower crustal volume. The mafic material probably exists as

* Seismic waves are reflected and refracted only at geological boundaries which have seismic impedance contrasts. Seismic impedance contrasts occur where the physical properties of rocks change across geological boundaries. The most important physical properties are density and the velocity at which seismic waves travel through the rock. Seismic velocity is a function of the bulk and shear moduli of the rock, as well as its density.

1 St. Petersburg Mining Institute, 2, 21 line, St Petersburg, 199026 Russia (present address as below)

2 Australian Geological Survey Organisation, GPO Box 378, Canberra ACT 2601, Australia

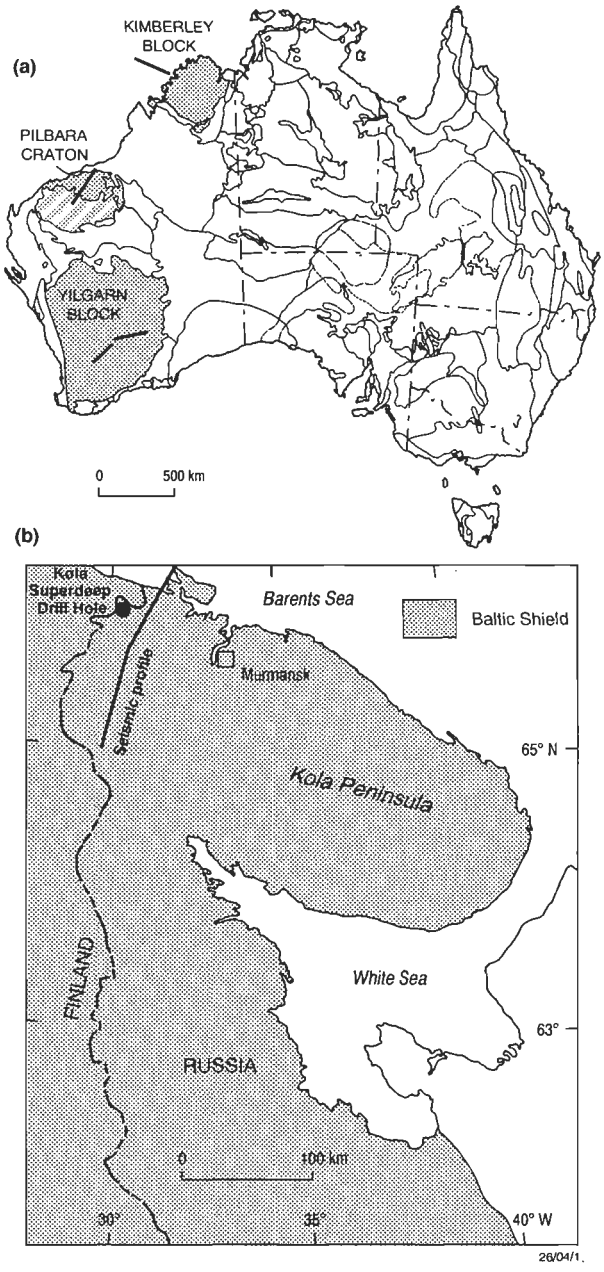

Figure 1. Location diagrams for the data presented in this paper. (a) Australian data sets; (b) Russian data and the location of the Kola Superdeep Drill Hole. The refraction data for the Yilgarn Block presented in Figure 2 are from the line on the left and the reflection data are from the western end of the line on the right.

sub-horizontal lenses. This is consistent with models of the lower crust derived from other studies (Fig. 3). The models in Figure 3a & b were derived by matching the principal features in observed seismic data with those in synthetic seismograms generated from theoretical models. The velocity/depth model of Hale & Thompson (1982) (Fig. 3c) is based on exposed rocks of supposed lower crustal origin.

However, in contrast with the lower crust, Drummond et al. (1993) concluded, on the basis of observed seismic velocity, that the upper crust in the Yilgarn Block was of felsic composition overall. The seismic velocities did not allow much scope for the inclusion of significant amounts of rock with a contrasting seismic impedance, such as mafic rocks.

The interpretation of seismic reflection images from the upper crust of the Yilgarn Block is therefore equivocal: the seismic data do not enable a clear choice of one interpretation from the several possible, which include completely homogeneous rocks, highly deformed rocks with varying seismic impedances, or juxtaposed rocks with similar composition but different geological histories, such as a felsic igneous rock and its gneissic equivalent. Other constraints on interpretation are needed for the full benefits to be realised from the seismic reflection images.

This paper presents the results from a study of the likely variation in velocity in the upper crust in shield regions, even in regions that appear to be homogeneous in seismic reflection data. It is based on a reassessment of existing data from the Yilgarn Block in the light of new data from the Kimberley Block, coupled with modelling based on variations of velocity with depth in the Kola Superdeep Bore Hole in the Baltic Shield.

The results are probably also applicable to the Pilbara Craton. The upper crust in provinces of other geological ages (e.g., Eromanga Basin—Finlayson & Leven 1987; Lachlan Fold Belt—Glen et al. 1994; continental shelf of NW Europe—Matthews & Cheadle 1986) is often also non-reflective. The results of this study, while directed principally at Australian shield areas, may also be relevant in those areas.

Constraints on estimates of seismic velocity

Seismic reflection data are usually a poor indicator of seismic velocity at depth. Velocity is therefore mostly mapped at depth in the crust using seismic refraction data. The best estimates of seismic velocity are made by matching both the theoretical travel times and amplitudes of seismic signals calculated for the model with those measured during refraction experiments.

The amount of detail that can be modelled in velocity/depth models depends to a large extent on the frequencies of the seismic signals used and the separation between the seismometers used to record the energy. Early estimates of seismic velocity in the Australian shield (Drummond 1983, 1988) used seismometer separations of 5–20 km and frequencies of 3–15 Hz (Fig. 4). The main indicator of seismic velocity in the upper crust was the time that the seismic energy took to travel to distances of about 100 km from the source. This indicated a velocity near 6.0 $km.s^{-1}$ at the surface. Modelling of both travel time and amplitude of the seismic arrivals showed that velocity increased to about 6.2 $km.s^{-1}$ at about 12 km depth (Figs 2, 5).

The velocity/depth models did not contain very much detail for the upper crust; that in Figure 5 is typical. However, the data (Fig. 4) do contain some indications that the crustal structure may be more complex. The main evidence for this is in the form of the seismic wavelets. For example, in Figure 4b, the first arrivals (marked with a '1') on the traces at 55, 62, 70, and 78 km are very similar, but they are different from those at 8, 17, 25 and 34 km. The first arrivals at the shortest and longest distances could be reinterpreted as several phases (e.g. '1' and '2') and, on the basis of the results presented below, this can be interpreted as due to either lateral or

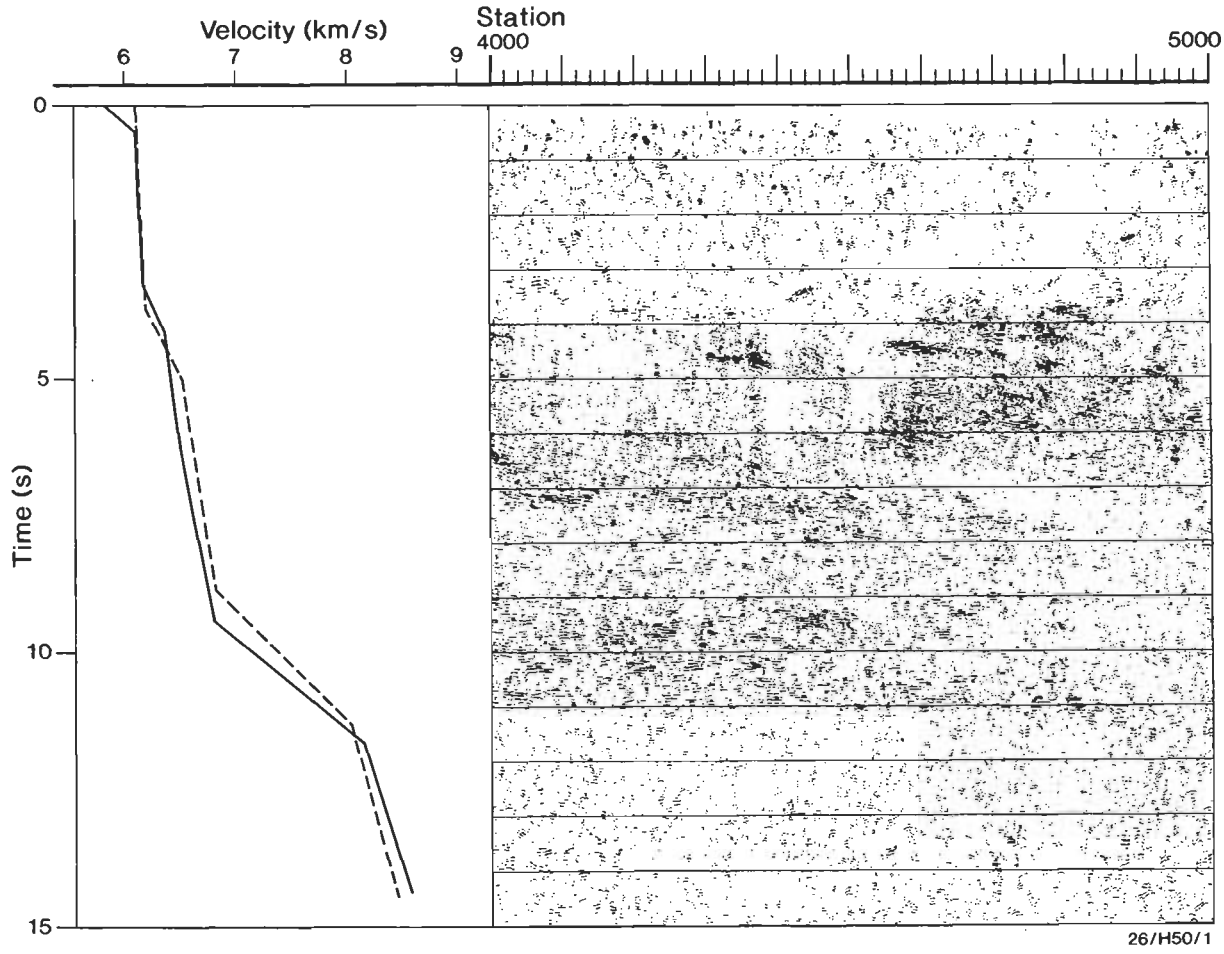

Figure 2. Portion of a seismic reflection image of the crust in the Yilgarn Block (on the right) juxtaposed against a graph showing the variation of seismic velocity with depth derived from a reversed refraction profile just off the end of the reflection section. The vertical scale is in seconds, recording the time seismic waves take to travel vertically into the Earth and reflect back to the surface. Time in the range 0–10 s can be converted to approximate depth with a multiplier of 3 km.s^{-1}. The upper crust (0–4 s, or 0–12 km) is almost devoid of reflections. The lower crust (5–11 s, or 15–33 km) contains numerous sub-horizontal reflections. The boundary between the non-reflective upper crust and the reflective lower crust correlates with an increase in seismic velocity in the range 4–5 s (12–15 km). (Modified from Drummond et al. 1993)

vertical variations in upper crustal structure.

The data in Figure 6 were collected across granite–gneiss terranes of the Baltic Shield in the Kola Peninsula in Russia. The trace spacing is 200 m and the length of the section is 4.6 km; i.e. the section covers about half the distance between any two traces in Figure 3b, whose first arrivals were just compared.

The first arrivals in Figure 6 (marked '1' on the trace) have a similar character on all traces. The decrease in amplitude (greatest at about 85.5 km, smallest at the right hand end) is typical for the Baltic Shield at these offsets. The velocity of the first arrivals is close to 6.2 km.s^{-1}.

A second wavelet ('2') occurs about 0.4 s after the first arrival. It is especially clear at the right hand end of the section, is less clear between 85.5 and 87 km because other wavelets interfere with it, and is clear on the trace on the left hand end, at 85 km. A third wavelet ('3') occurs on all traces about 0.3–0.4 after the second phase. These wavelets ('2' and '3') often become first arrivals at greater distances because of the decay in the amplitude of earlier phases ('1' and, subsequently, '2') between 80 and 120 km from the source. These effects, where (i) several wavelets occur within a few seconds of the first arrival, (ii) later wavelets extend to greater distances than earlier arrivals and then become first arrivals, and (iii) wavelets interfere with each other, seem ubiquitous across the Baltic Shield (Goncharov et al. in press).

The data in Figure 7 also have traces 200 m apart and are from a survey of the offshore Kimberley Block in northwest Australia. They extend over a greater distance than those in Figure 6. The detail of the data in Figure 7 is different from that in Figure 6, reflecting the different geological provinces, but one important similarity exists—the seismic arrivals in Figure 7 also form sub-parallel bands with varying lateral continuity. The data have several quite distinct phases; four are marked, and labelled as 'P1'—a first arrival set from near the source (at 0 km), 'P2', 'P3' and 'P4'. Phases P1 and P2 travelled through the upper crust; P3 penetrated more deeply; and P4 probably reflected off the crust–mantle boundary. Each phase can be traced for tens of kilometres, but each comprises a number of wavelets, many of which can only be traced for much shorter distances. Note that P1 marks the first recorded energy at any distance between 0 km and about 80 km, but it is defined by the end points of a number of phases, such as the one labelled 'P1a', which starts on the left above P1, but asymptotically approaches

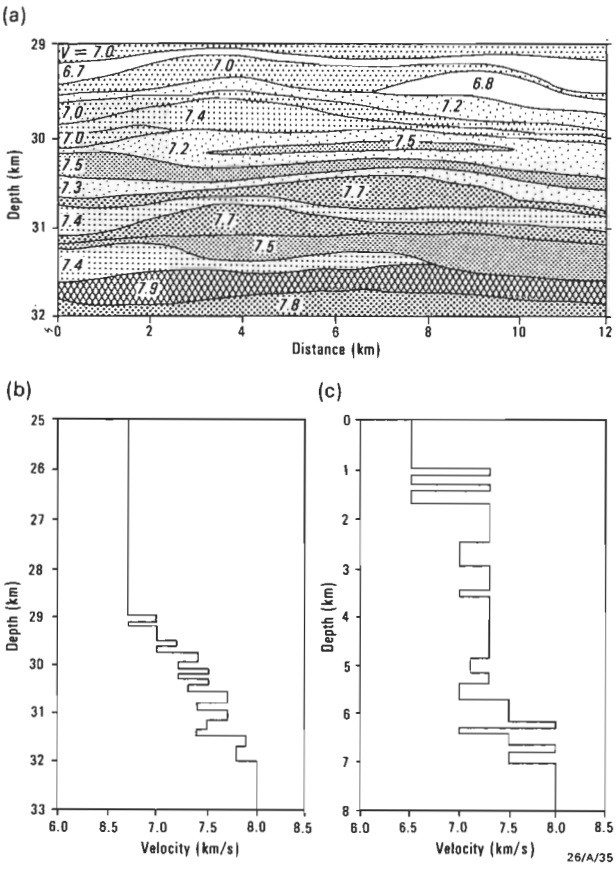

Figure 3. (a) Hypothetical velocity model of a Moho transition zone 3 km thick which satisfies many of the observed features of reflected and refracted seismic arrivals from the Moho (from Braile & Chiang 1986). (b) Representative velocity/depth model for this model at a position mid-way (6 km) along it. (c)Velocity/depth model derived from exposed section of the Ivrea-Verbano Zone (Hale & Thompson 1982) (From Collins 1991).

it at greater distances. Thus, the first energy to arrive at any distance across the seismic section is defined by the asymptotes to numerous wavelets P1, P2, P3 etc.

The seismic refraction data from the Kimberley Block are, therefore, similar in form to those from the Baltic Shield. Figure 8 shows seismic reflection data from the same profile as the data in Figures 7. The reflection data show an upper crust almost devoid of strong, reflections (between about 0.5 s and 2.7 s on the vertical axis), which Symonds et al. (1994) interpreted as the Proterozoic Kimberley Basin. However, the Kimberley Basin contains mainly mildly deformed sandstones and basalts, which might reasonably be expected to produce some reflections. It overlies a deeper crust with many, strong sub-horizontal and dipping reflections, interpreted as ?Archaean basement. Overall, these reflection data appear similar to those from the Southern Cross Province and sub-greenstone upper crust of the Eastern Goldfields Province of the Yilgarn Block.

The data from the Kimberley Block have the refraction character of the Baltic Shield and the reflection character of the Yilgarn Block. They therefore provide a useful link between the results from the Yilgarn Block and those from the Baltic Shield. Note, however, that the similarities are in the form of the style of the reflection and refraction data; the correlations are not being made on the basis of geological age.

Modelling upper crustal velocity variations

The Kola Superdeep Drill Hole (Kozlovsky 1984) was drilled through greenstone supracrustal rocks and ended in gneissic basement. A seismic reflection profile from south of the drill hole (Smythe et al. 1994) shows gneisses that are interpreted to have been thrust to the surface to be non-reflective, as in the Yilgarn Block. Whether these gneisses correlate in age and composition with those penetrated in the sub-greenstone basement in the well is uncertain.

Goncharov et al. (in press) generated simplified velocity and density logs from acoustic logs and vertical seismic profiles (VSPs), supplemented with physical measurements of core taken from the well.

The simplified velocity log, shown as the variation of velocity with depth, is illustrated in Figure 9. In the log, the upper 4.5 km through the supracrustal rocks have been replaced by a gradient from 5.8 km.s^{-1} at the surface to 6.2 km.s^{-1} at 4.5 km depth, similar to the velocity field in the uppermost crust outside the region of the supracrustal rocks, where the gneissic basement crops out. This was necessary because the volcanic supracrustal rocks in the area of the well form a high-velocity cover to the gneissic basement, preventing the surface return of refracted seismic energy from the upper crust immediately under the greenstones.

Below 4.5 km, basement comprises layers of high- and low-velocity rock, apparently randomly distributed throughout rocks with a velocity of 6.1 km.s^{-1}. Velocity falls as low as 5.50 km.s^{-1} in the low-velocity layers and reachs 6.6 km.s^{-1} in the high-velocity layers. In the simplified velocity log, the high- and low-velocity layers have varying thickness, from several hundred metres to over 500 m. In the original well logs, even finer laminations can be found.

Figure 10 is a synthetic seismic data set calculated for the model in Figure 9, using the algorithm of Ha (1984). The algorithm assumes that the model is one-dimensional; ie., layers in the model are laterally continuous. Consequently, the synthetic data can be used to study the general wave forms in the observed data and geological structures that persist over the length of the seismic profile, but features in the data resulting from lateral variations in the real Earth cannot be modelled with this algorithm.

In Figure 10, traces are shown every 200 m, and the maximum amplitude of every trace has been scaled to the same value. The significant feature of the synthetic data is that wavelets arriving at distances of about 45–100 km from the source are similar in form to those in the data from the Baltic Shield (Fig. 6) and the Kimberley Block (Fig. 7); i.e. energy propagating outwards from the source is made up of discrete arrivals, which interfere with each other, so that, although a band of first-arrival energy can be traced to distances of more than 100 km from the source, individual wavelets are not so continuous. The first energy to arrive between 45 and 100 km forms an envelope with an average velocity of 6.1 km.s^{-1}, equal to the average velocity in the model below 4.5 km depth. However, individual wavelets are

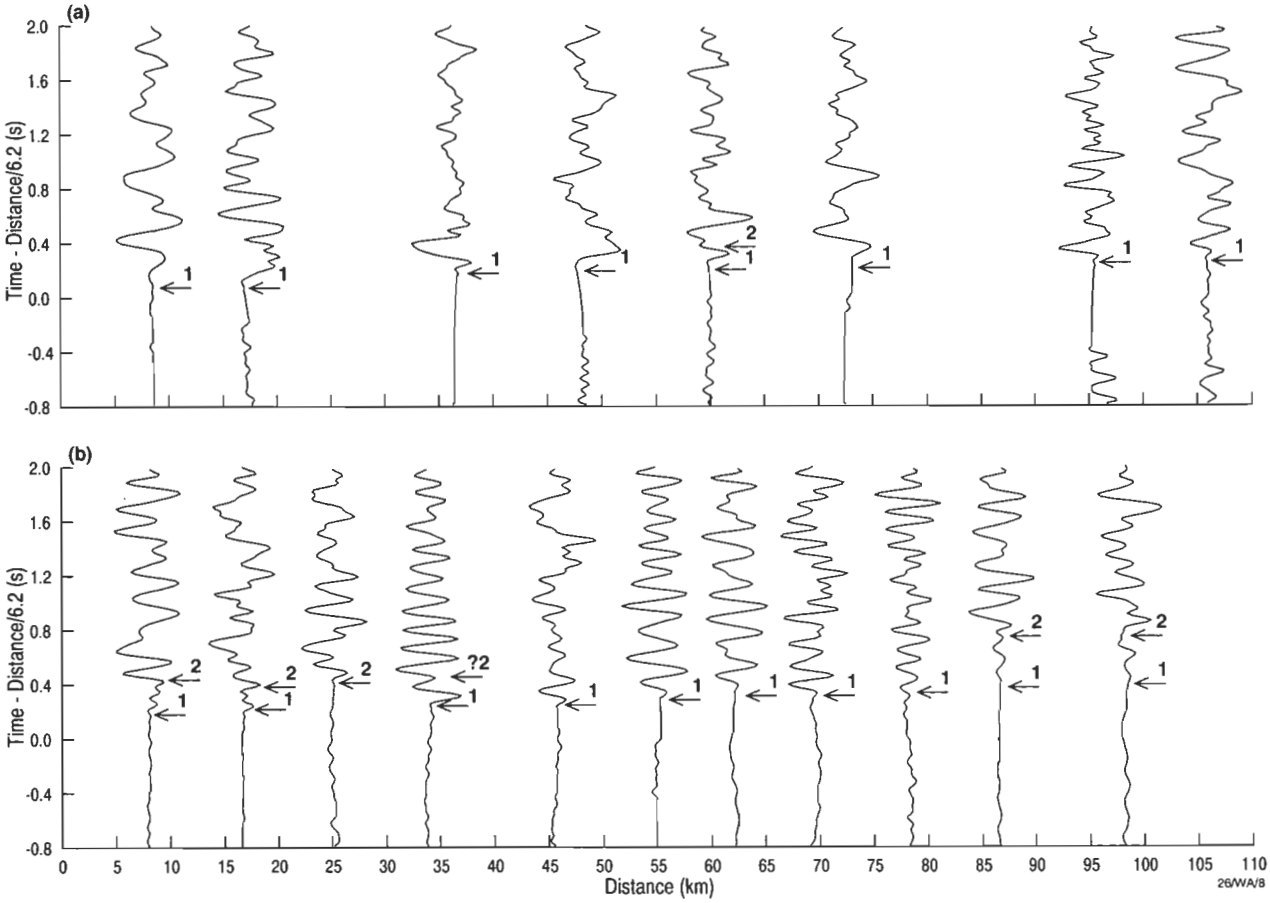

Figure 4. Seismic refraction record sections from (a) the Pilbara Craton (Drummond 1983) and (b) the Yilgarn Block (previously unpublished). The Pilbara data have an average trace spacing of about 20 km; those from the Yilgarn, about 8 km.

from sets of concave upwards phases that asymptotically approach a velocity of 6.2 km.s^{-1} at greater distances.

The individual wavelets represent energy that has not only refracted through some of the high-velocity layers in the model, but also formed primary and interbed multiple reflections off and between the thin high- and low-velocity layers. At distances less than the critical distance for any layer from which they were reflected, their slopes indicate apparent velocity higher than that in the layer, as would be expected with sub-critical reflections. At greater distances, their apparent velocity decreases and approaches the velocity in the highest-velocity cover above them; this represents energy with the lowest velocity that can escape back through the high-velocity cover.

Discussion

The results from the Kola Superdeep Bore Hole are from the upper crust in a region with a gneissic basement, similar to the Archaean Yilgarn Block and Pilbara Craton. The data can be used to generate synthetic seismograms similar in overall appearance to the refraction data recorded across the Kimberley Block. The upper portion of the Kimberley Block, probably correlating with the Kimberley Basin, is non-reflective, as is the upper crust in a large part of the Yilgarn Block.

The most significant similarity in all data sets is that seismic energy that propagates at non-vertical incidence through the upper crust of both the Baltic Shield and Kimberley Block comprises bundles of energy that can be traced for tens of kilometres, but it is made up of several wavelets, each of which has lateral continuity only for smaller distances. Modelling the variation of velocity with depth in the Kola Superdeep Bore Hole indicates that this is caused by constructive and destructive interference between energy refracted and reflected by many thin layers of high- and low-velocity material in a groundmass of velocity around 6.1 km.s^{-1}.

The synthetic seismograms in Figure 10 are based on the assumption that the velocity/depth model in Figure 9 is laterally continuous throughout the region. The likelihood that thin layers (200–500 m thick) will persist for large distances in the upper crust is low. Those in the Kola Superdeep Bore Hole can be variously attributed to variation in composition, shear zones and the presence of zones with high fluid content. The section penetrated by the well is more likely to represent the variability of the upper crust than a section through a laterally uniform, but vertically heterogeneous upper crust.

The results of this study are useful because they indicate that the degree of variation seen in the Kola Superdeep Bore Hole is likely to exist in the shield regions in Australia. The variations in seismic velocity are up to 6% from the average in zones with thicknesses of several hundreds of metres. This must be considered when interpreting seismic reflection data that appear devoid of reflections, such as those in the upper parts of Figures 2 and 8. However, these results give no indication of the relative importance of vertical and horizontal heteroge-

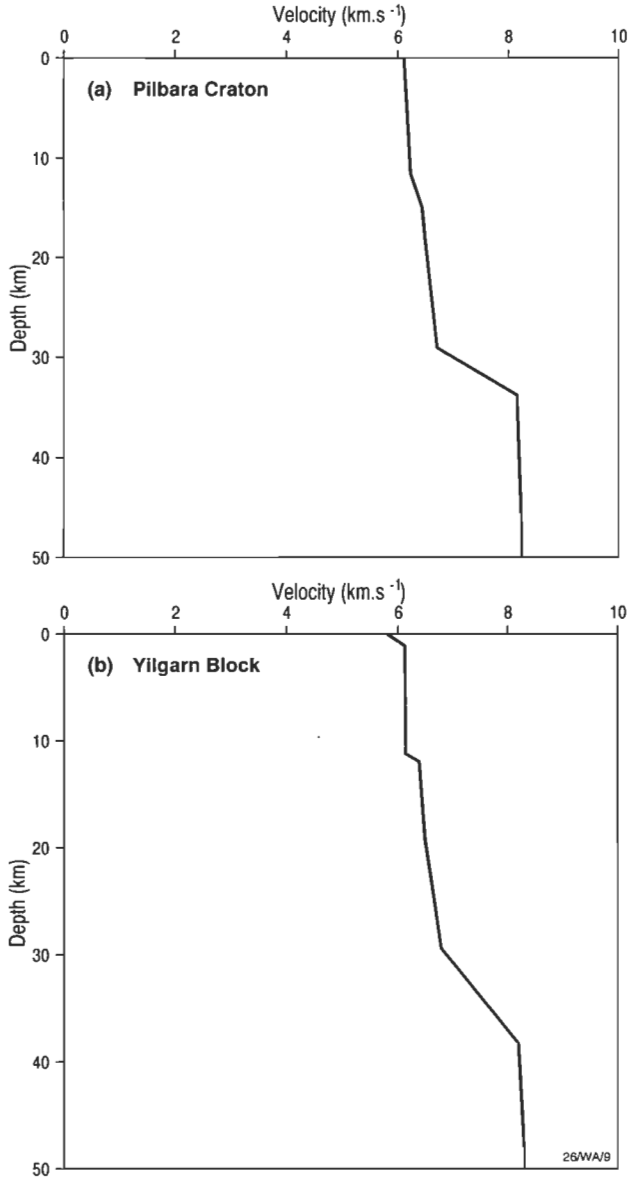

Figure 5. Velocity/depth models derived from the data shown in Figure 4 (Drummond 1983, 1988). Only the upper parts of the models, to about 10–12 km depth, were derived from the data shown in Figure 4. Deeper parts of the models were derived from more extensive data sets.

neity in generating the observed wavefields.

The other significant result is that even though the wide-angle, multiply reflected and refracted phases resulting from the high- and low-velocity layers in the velocity/depth model have high apparent velocities, the velocity of the envelope of first-arrival energy in the synthetic seismograms from the Kola Superdeep Bore Hole (Fig. 10) approaches that of the average crust, even though at different distances it represents energy from different sets of wavelets. This means that existing models of the upper crust in the Pilbara and Yilgarn Blocks are probably good estimates of the average velocity of the upper crust.

The same is probably also true for other regions with a non-reflective upper crust, such as the Lachlan Fold Belt and the Eromanga Basin in eastern Australia. On the basis of these results, non-reflective upper crust might reasonably be expected to contain velocity deviations of as much as 6% from the average in zones with thicknesses of a few hundred metres. Such zones might be caused by changes in composition, shear zones or by fluid-rich zones, as in the Kola Superdeep Bore Hole.

Acknowledgments

This study was supported by a grant from the Australian Department of Industry, Science and Technology that allowed Dr Alexey Goncharov to travel to Canberra in early 1994. The data in Figure 8 were provided by Phillip Symonds, and those in Figures 7 & 8 are part of a set compiled for the Continental Margins Program. Doug Finlayson and Phillip Symonds provided valuable criticism of an early version of the manuscript. Comments by Erwin Scheibner and two anonymous reviewers helped us focus the paper a little more closely on the Australian Precambrian.

References

Braile, L.W. & Chiang, C.S., 1986. The continental Mohorovicic discontinuity: results from near-vertical and wide-angle seismic reflection studies. *In* Barazangi, M. & Brown, L. (editors), Reflection seismology: a global perspective. *American Geophysical Union, Geodynamics Series*, 13, 257–272.

Collins, C.D.N., 1991. The nature of the crust-mantle boundary under Australia from seismic evidence. *In* Drummond, B.J. (editor), The Australian lithosphere. *Geological Society of Australia, Special Publication*, 17, 67–80.

Dentith, M.C., Bruner, I., Long, A., Middleton, M.F. & Scott, J., 1993. Structure of the eastern margin of the Perth Basin, Western Australia. *Exploration Geophysics*, 24, 455–462.

Drummond, B.J., 1982. Seismic constraints on the chemical composition of the crust of the Pilbara Craton, northwest Australia. *Revista Brasiliera Geosciencias*, 12, 113–120.

Drummond, B.J., 1983. Detailed seismic velocity/depth models of the upper lithosphere of the Pilbara Craton, northwest Australia. *BMR Journal of Australian Geology & Geophysics*, 8, 35–51.

Drummond, B.J., 1988. A review of crust/upper mantle structure in the Precambrian areas of Australia and implications for Precambrian crustal evolution. *Precambrian Research*, 40/41, 101–116.

Drummond, B.J. & Collins, C.D.N., 1986. Seismic evidence for underplating of the lower continental crust of Australia. *Earth and Planetary Science Letters*, 79, 361–372.

Drummond, B.J., Goleby, B.R., Swager, C.P. & Williams, P.R., 1993. Constraints on Archaean crustal composition and structure provided by deep seismic sounding in the Yilgarn Block. *Ore Geology Reviews*, 8, 117–124.

Durrheim, Raymond J. & Mooney, Walter D., 1991. Archaean and Proterozoic crustal evolution; evidence from crustal seismology. *Geology*, 19, 606–609.

Finlayson, D.M. & Leven, J.H., 1987. Lithospheric structures and possible processes in Phanerozoic eastern Australia from deep seismic investigations. *Tectonophysics*, 133, 199–215.

Gee, R.D., 1979. Structure and tectonic style of the Western Australian shield. *Tectonophysics*, 58, 327–369.

Glen, R.A., Drummond, B.J., Goleby, B.R., Palmer, D. & Wake-Dyster, K.D., 1994. Structure of the Cobar Basin, New South Wales, based on seismic reflection

profiling. *Australian Journal of Earth Sciences*, 41, 341–352.

Goncharov, A.G., Lizinsky, M.D., Kalnin, K.A., Platonenkova, L.N. & Fomina, T.N., in press. The nature of the upper crust seismic boundaries at the eastern part of the Baltic Shield from the Kola superdeep borehole data and wave field modelling. *In* Mooney, W. D. (editor), CCSS Meeting and Workshop, Moscow, 1993.

Ha, Joseph, 1984. Recurrence relations for computing complete P and SV seismograms. *Geophysical Journal of the Royal Astronomical Society*, 79, 863–873.

Hale, L.D & Thompson, G.A., 1982. The seismic reflection character of the continental Mohorovicic discontinuity. *Journal of Geophysical Research*, 87, 4625–4635.

Kozlovsky, Y.A., 1984. The world's deepest well. *Scientific American*, 251(6), 106–112.

Matthews, D.H. & Cheadle, M.J., 1986. Deep reflections from the Caledonides and Variscides west of Britain and comparison with the Himalayas. *In* Barazangi, M. & Brown, L. (editors), Reflection seismology: a global perspective. *American Geophysical Union Geodynamics Series*, 13, 5–19.

O'Reilly, S.Y & Griffin, W.L., 1985. A xenolith-derived geotherm for southeastern Australia and its geophysical implications. *Tectonophysics*, 111, 41–63.

Smythe, D.K., Smithson, S.B., Gillen G., Humphreys, C.,

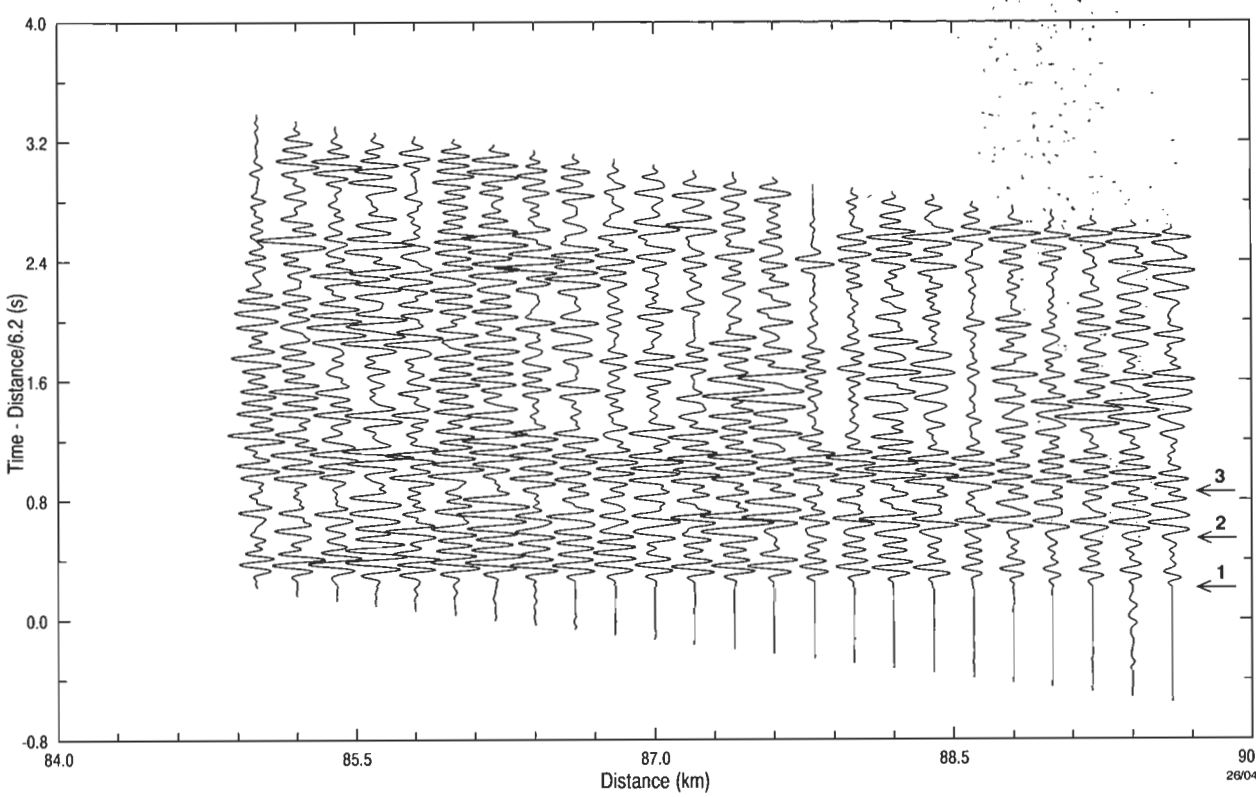

Figure 6. Seismic refraction data from granite/gneiss terrains in the Baltic Shield. Here the distance between traces is 200 m.

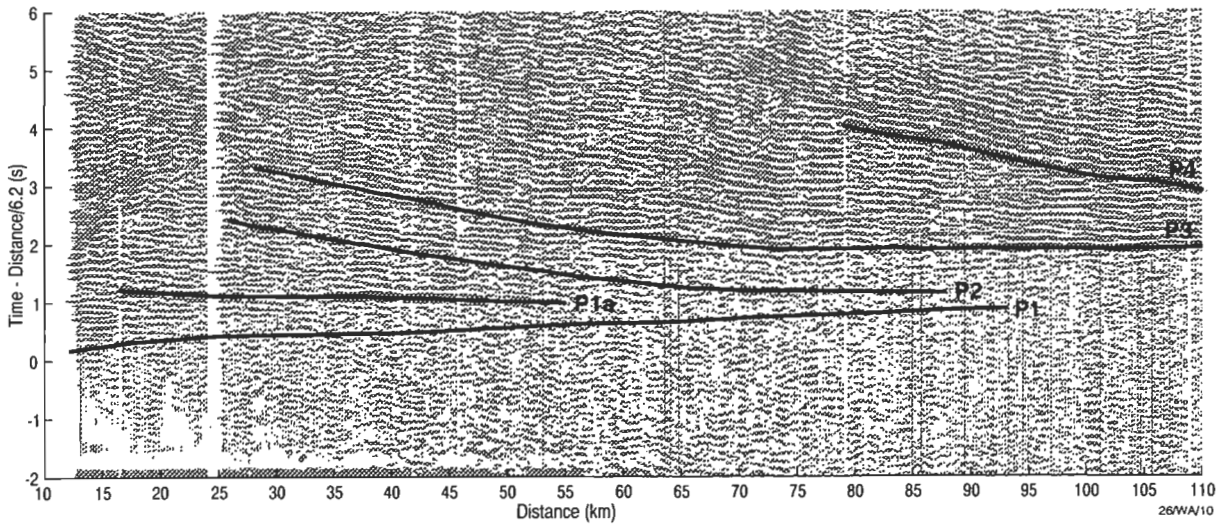

Figure 7. Seismic refraction data collected at sea across the submerged, offshore portion of the Kimberley Block in northwest Australia. Trace spacing is 200 m, as in Figure 6, but these traces were derived by performing an 11-trace running stack on data with a 50 m spacing.

Kristoffersen, Y., Karaev, N.A., Garipov, V.Z., Pavlenkova, N.I. and the Kola-92 Working Group, 1994. Project images crust, collects seismic data in world's largest borehole. *EOS, Transactions, American Geophysical Union*, 75(41), 473–476.

Symonds, P.A., Collins, C.D.N. & Bradshaw, J., 1994. Deep structure of the Browse Basin: implications for basin development and petroleum exploration. *In* Purcell, P.G. & Purcell, R.R. (editors), *The sedimentary basins of Western Australia.* Proceedings of the Western Australian Basins Symposium, Perth, Western Australia, 1994. Petroleum Exploration Society of Australia, 315–33.

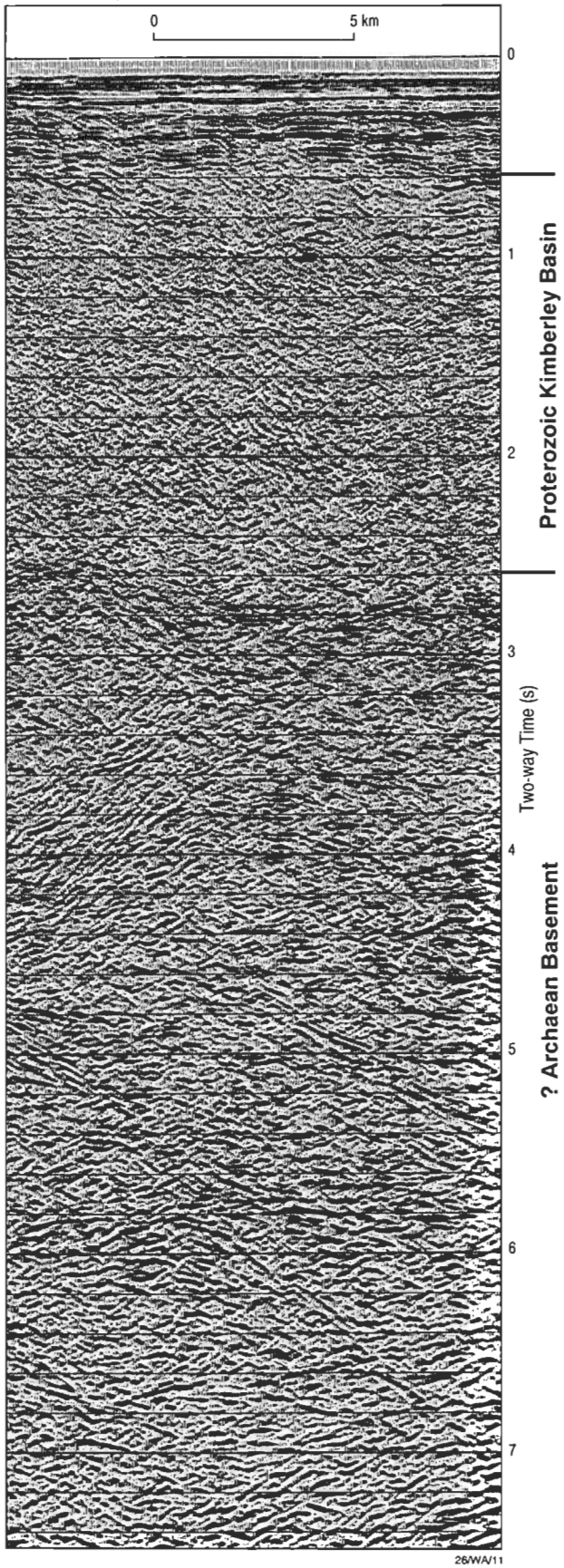

Figure 8. Seismic reflection profile collected at sea along a portion of the profile for which refraction data are presented in Figure 7. The upper crust (below about 0.5 s to about 2.7–2.8 s) is largely unreflective, and the deeper crust contains numerous, strong reflections.

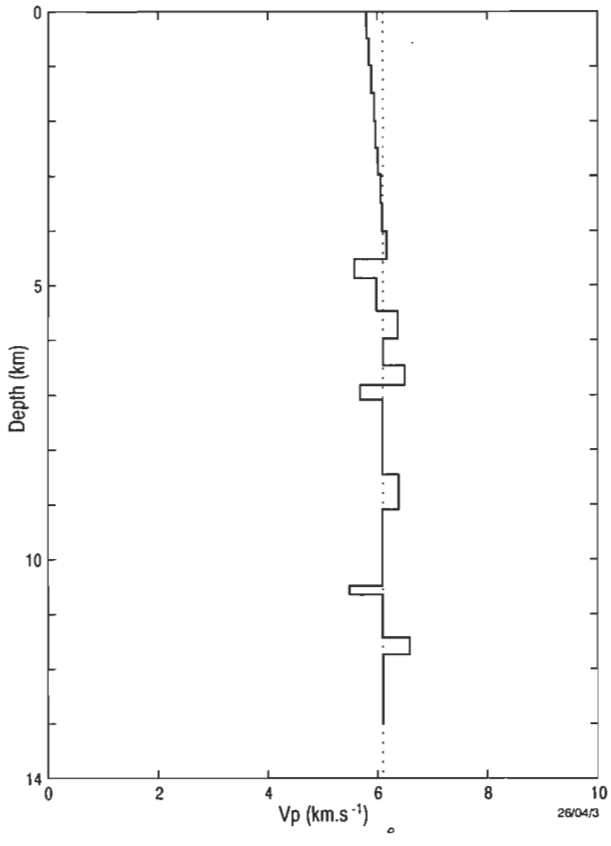

Figure 9. Velocity/depth model from the Baltic Shield, based on acoustic log and VSP measurements in the Kola Superdeep Bore Hole. In the upper 4.5 km of the model, the effects of volcanic supracrustals have been replaced by a uniform gradient. Dotted line represents a velocity of 6.1 km.s^{-1}.

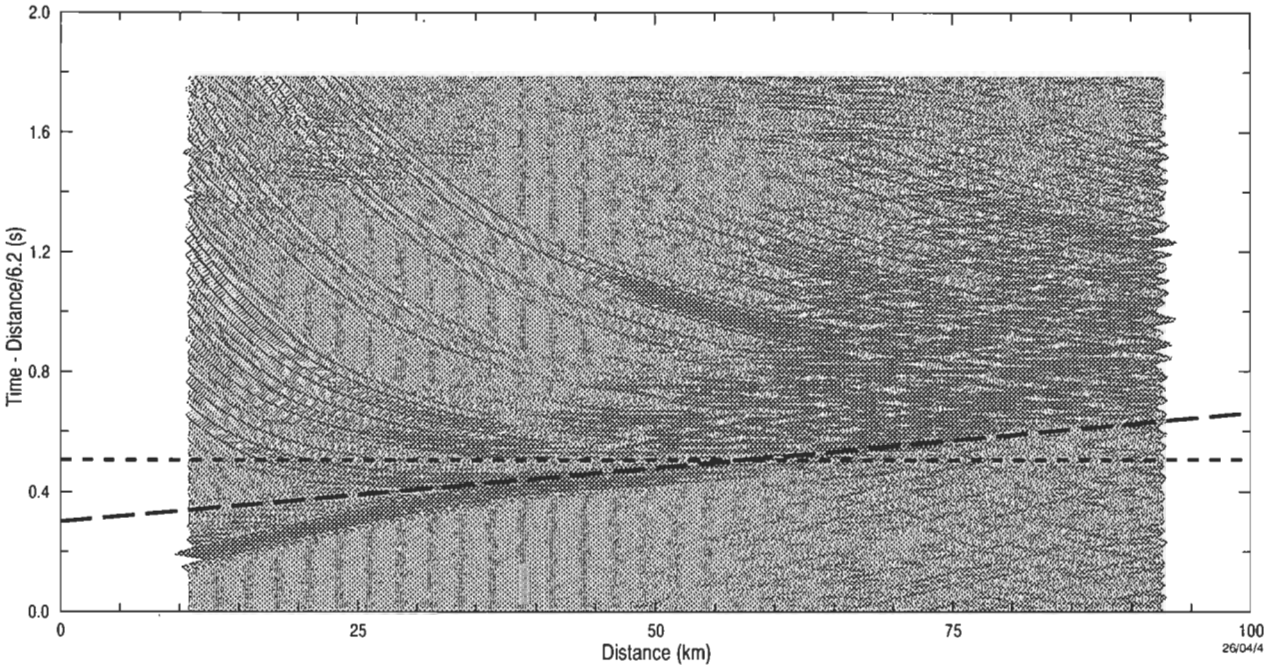

Figure 10. Synthetic seismograms calculated for the model in Figure 9 using the algorithm of Ha (1984). Trace spacing is 200 m. Slope of the dashed line represents 6.1 km.s^{-1}; Dotted line is 6.2 km.s^{-1}. Some numerical noise resulting from lack of computational precision occurs in the lower right hand corner and across the top of the figure and should be disregarded.

AGSO Journal of Australian Geology & Geophysics, 15(4), 529–537

Geological note: Igneous and sedimentary rocks dredged from the northern Macquarie Ridge, Southern Ocean

Nick Mortimer[1]

Altered basalt, dolerite and gabbro have been dredged from a previously unsampled portion of the Macquarie Ridge (47°–48° S), using the commercial fishing vessel *Amaltal Explorer*. These rocks are petrographically and geochemically similar to mafic–ultramafic volcanic and plutonic suites of MORB-like petrological affinity, collected along the ridge between 49° and 58° S by previous investigators. The northernmost part of the Macquarie Ridge (Puysegur Bank) is thus geologically related to the rest of the ridge, even though it is bathymetrically part of the New Zealand continental shelf. Sedimentary rocks dredged from 47°–48° S were derived from both 'oceanic' Macquarie Ridge and 'continental' New Zealand sources. There is no evidence of subduction-related magmatism along any part of the Macquarie Ridge.

Introduction

The Macquarie Ridge is a 1500 km long, complex bathymetric ridge in the Southern Ocean, lying along the Pacific–Australian plate boundary between latitudes 47° and 60° S (Fig. 1; Hayes & Talwani 1972; Williamson 1988). Only one part of the ridge, Macquarie Island, is above sea level, though in several places the ridge shoals to less than 500 m deep (Summerhayes 1969; Hayes & Talwani 1972). The Macquarie Ridge is bounded throughout much of its length by trenches and troughs to the east (Macquarie, Solander) and west (Puysegur, Hjort). North of about 47.5° S, the ridge shallows and joins the New Zealand continental shelf as the Puysegur Bank (Figs 1, 2). The main part of the Macquarie Ridge, between 49° and 60° S, has variously been interpreted as an island arc (Summerhayes 1969; Jakes & Gill 1970), a shear or fracture zone (Houtz et al. 1971) or uplifted oceanic crust (Varne & Rubenach 1972; Griffin & Varne 1980; Williamson 1988).

The purpose of this short paper is twofold: first, to present petrological data from rocks retrieved from commercial fishing trawls on the northern Macquarie Ridge (including Puysegur Bank) and second, by way of interpreting these data in a regional context, to summarise existing information on igneous rocks for the whole of the Macquarie Ridge. Such a summary is useful, given the intermittent reporting of previously collected samples from 1969 to 1983 and advances in interpretation of geochemical data since then. This contribution is timely in view of recently completed and ongoing marine geophysical and swath bathymetry studies aimed at increasing knowledge of the plate boundary tectonics of the Macquarie Ridge–New Zealand area (Delteil et al. 1993).

Previous work

The remoteness of the Macquarie Ridge has meant that, compared with other plate boundaries, its submarine portion is relatively little-studied. Figure 1 shows the 26 sites at which *in situ* material has been obtained previously. In contrast, geological mapping and interpretation of Macquarie Island have been extensive (Varne & Rubenach 1972; Griffin & Varne 1980; Duncan & Varne 1988; Varne & Thomson 1990). A useful recent summary of Macquarie Ridge geology and geophysics has been given by Williamson (1988).

The similarity of igneous material sampled from the Macquarie Ridge between 49° and 58° S, including Macquarie Island, was first noted first by Summerhayes (1969), who introduced the term 'Macquarie Tholeiite Province'. A variety of mafic and ultramafic igneous rocks has been described (Fig. 1), including low-K tholeiitic basalt, dolerite, ferrodiorite, gabbro, layered gabbro, troctolite, sodic gabbro, harzburgite, serpentinised peridotite and basaltic agglomerate. Apart from a granophyre reported by Matveyenkov & Baranov (1981), felsic igneous rocks are unknown. No granitoids or high-grade metamorphic rocks indicative of continental crust have thus far been found on the Macquarie Ridge.

Griffin & Varne (1980) interpreted Macquarie Island volcanic and plutonic rocks as a comagmatic ophiolite suite, formed at a mid-ocean ridge spreading centre. They noted that the Macquarie Island basalts and dolerites showed trace-element concentrations and ratios (e.g. Zr/Y, Zr/Nb) typical of mid-ocean ridge basalts (MORBs) from both geochemically normal and anomalous ridge segments, e.g. 36°–45° N on the mid-Atlantic ridge. Some Macquarie Island lavas and dolerites have more than 150 ppm Zr and 50 ppm Nb, values which, although more typical of ocean island basalts (OIBs), are also known from mid-oceanic ridges (Griffin & Varne 1980).

The ages of the igneous rocks of the Macquarie Ridge are poorly known. Pliocene and Lower Pliocene foraminifera have been reported in association with basaltic volcaniclastic detritus from Summerhayes' (1969) dredge sites 5 and 159, respectively (Fig. 1). The ages of the oldest sedimentary rocks overlying basalt at DSDP site 279 on the Macquarie Ridge are middle Early Miocene, and those at DSDP site 278, in the Emerald Basin, middle Oligocene (Ovenshine et al. 1975 and references therein). The age of some pillow lavas on Macquarie Island is Early or Middle Miocene (Quilty et al. 1973).

Solander Island lies to the east of the axis of the Puysegur Bank/Macquarie Ridge (Figs 1, 2) and consists of hornblende andesite flows of Late Pliocene to Early Pleistocene age (Bishop 1986). In contrast to the MORB-related Macquarie Ridge igneous rocks, Solander Island lavas show clear subduction-related affinities (Reay 1986). They are the only rocks known to have been generated by Cenozoic Pacific–Australian plate convergence south of New Zealand. Several possibly correlative Early Pliocene igneous bodies are located on the east side of the Puysegur Bank (Fig. 2; Turnbull et al. 1993, p. 50).

Sampling and analytical methods

Rock samples are commonly snagged by trawl nets during

[1] Institute of Geological & Nuclear Sciences, Private Bag 1930, Dunedin, New Zealand.

commercial fishing operations for orange roughy. Instead of throwing the rocks back in the sea, in 1991 and 1992, Chris Carey, then a first mate on the deep-sea trawler *Amaltal Explorer* from Nelson, New Zealand, forwarded fifteen samples (Fig. 2, Table 1) to staff at the Institute of Geological & Nuclear Sciences (formerly New Zealand Geological Survey) for cataloguing and study. On board, global positioning system satellite navigation was used to determine locations at the beginning and end of each trawl, and echo-sounders to determine water depth. The Puysegur Bank samples reported in this paper are the second set of New Zealand fishing industry samples to be thus described; an earlier paper (Carey et al. 1991) reported on volcanic and volcaniclastic samples recovered from the Challenger Plateau.

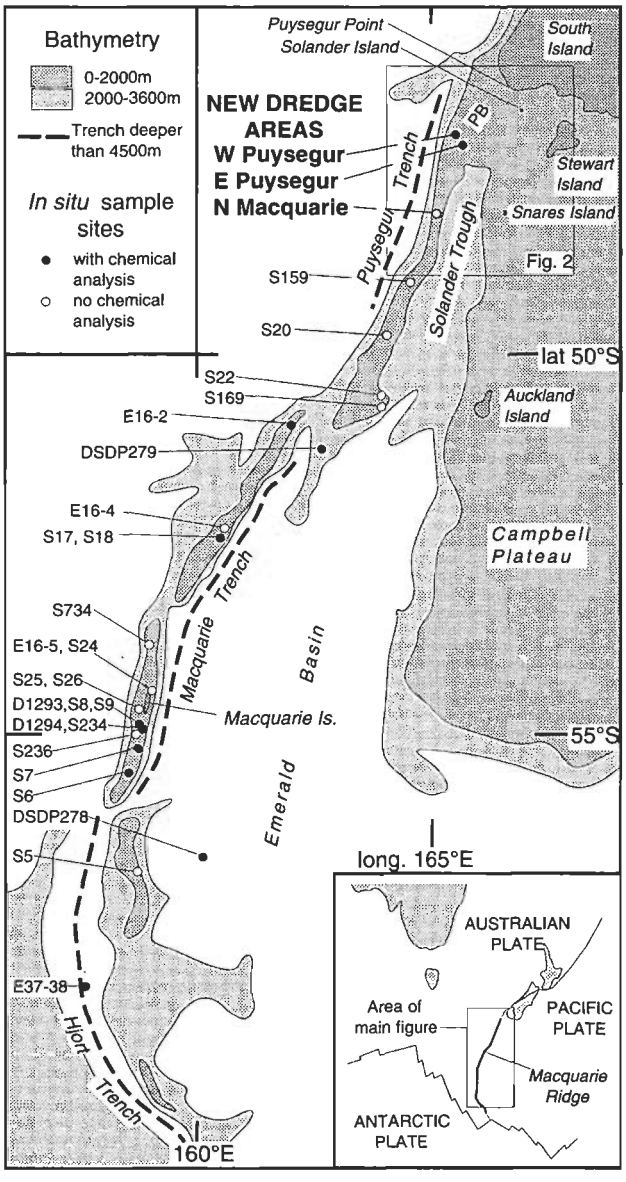

Figure 1. Location of *in situ* rock samples from the Macquarie Ridge and Puysegur Bank. Prefixes refer to different investigations as follows: S=HMNZS Endeavour dredges (Summerhayes, 1969), E = USNS Eltanin dredges (Watkins & Gunn 1971; Campsie et al. 1983), DSDP = Deep Sea Drilling Project sites (Ovenshine et al. 1975; Schilling & Ridley 1975), D = Dimitri Mendeleyev dredges (Matveyenkov & Baranov 1981). Studies of Macquarie Island rocks have been reported by Varne & Rubenach (1972), Matveyenkov & Baranov (1981) and Varne & Thomson (1990), and of Solander Island rocks by Reay (1986). The position of dredge 696 (Summerhayes, 1969), immediately east of Macquarie Island, has been omitted for clarity. PB = Puysegur Bank. Inset shows position of Macquarie Ridge at the Pacific–Australian plate boundary.

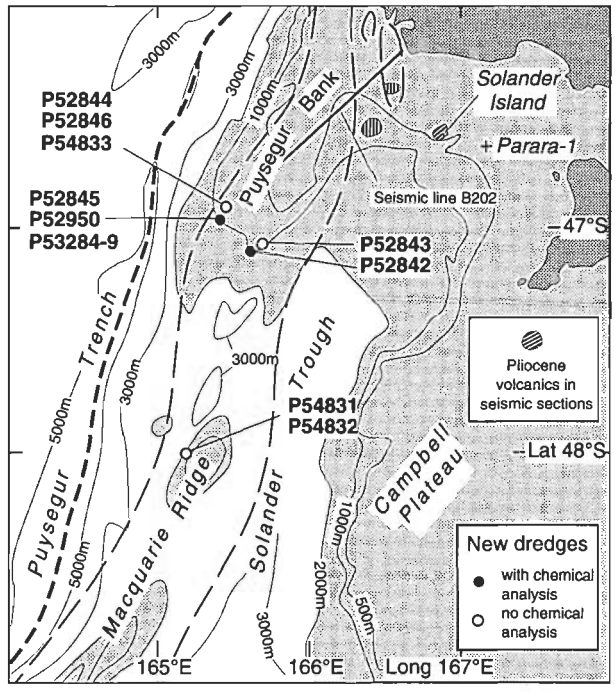

Figure 2. Generalised bathymetry of the North Macquarie Ridge–Puysegur Bank area, showing location of samples obtained from new dredge sites. P = petrological sample numbers of dredges from the present study. Dashed lines enclose regions of +700nT magnetic anomalies (Hatherton 1967; Woodward & Hatherton 1975). Location of Pliocene volcanics after Turnbull et al. (1993). Seismic line B202 is the southernmost industry seismic line in the area (Hunt International Petroleum Company 1976).

All submitted samples were archived in the National Petrology Reference Collection, Institute of Geological & Nuclear Sciences (to which sample numbers prefixed 'P' refer). Whole-rock samples for X-ray fluorescence (XRF) analysis were crushed to a powder, rinsed twice in deionised water, and dried. XRF and electron microprobe analyses were done at the Analytical Facility, Victoria University of Wellington, according to standard procedures described by Roser & Grapes (1990). Element concentrations for whole rocks are shown in Table 2; on all diagrams they have been recalculated to 100% loss-on-ignition free.

Sample description

Igneous rocks

Igneous rocks have been sampled in all three dredge areas (Figs 1 & 2). Summerhayes (1969) discussed at some length the criteria used to judge the in-place, redeposited, or ice-rafted nature of dredge samples in the New Zealand region. P52950 is the only unrounded sample, and, therefore, the only one that can reliably be interpreted as in place (Table 1).

P52842 is a medium-grained dolerite, consisting of about 50% plagioclase, 20% intersertal to subophitic clinopyroxene, 5% degraded opaque minerals, and 25% irregular mesostasis patches (now entirely altered to clay minerals). Pigeonite and hypersthene, often present in continental tholeiites, are absent. Some plagioclase grains are sieve-

Table 1. Sample site and hand specimen data for all igneous and sedimentary rocks retrieved by C. Carey on the *Amaltal Explorer* in 1991 and 1992. Archived material comprises hand specimen (H), thin section (T) and X-ray fluorescence analysis (X). *In situ* interpretation is based on degree of rounding of specimens.

P#	*Sample*	*Dredge area*	*Lat S (start–finish)*	*Long E (start–finish)*	*Depth m (s–f)*	*Size & shape*	*In situ?*	*Lithology*
Igneous rocks								
52842	HTX	E Puysegur Bank	47° 06.48′–47° 07.23′	165° 36.74′–165° 35.72′	760–1180	Rounded cobble	N	Friable dolerite
52950	HTX	W Puysegur Bank	46° 57.83′	165° 24.73′	947	Subangular block	Y	Amygdaloidal basalt
54831	HT	N Macquarie Ridge	~47° 59.98′	~165° 09.70′	~865	Rounded cobble 8x6cm	N	Altered basalt
54833	HT	W Puysegur Bank	~46° 54.38′	~165°27.00′	1050–1100	Subrounded cobble 9x6x3cm	N	Altered gabbro
Sedimentary rocks								
52843	HT	E Puysegur Bank	47° 05.33′–47° 04.32′	165° 41.36′–165° 43.03′	945–953	Wedge-shaped 25x12x5cm	Y?	Sandy siltstone
52844	H	W Puysegur Bank	46° 54.60′–46° 54.51′	165° 27.61′–165° 28.11′	1050–1082	Small bag	?	Stiff green clay
52845	H	W Puysegur Bank	46° 56.73′–46° 55.83′	165° 26.00′–165° 26.51′	1000–1040	Small bag	?	Stiff green clay
52846	H	W Puysegur Bank	46° 56.11′–46° 55.26′	165° 27.55′–165° 28.04′	1130–1290	Small bag	?	Stiff green clay
53284	HT	W Puysegur Bank	46° 55.77′–46° 57.51′	165° 24.46′	1200–990	Angular fist-size	Y	Foraminiferal siltstone
53285	HT	W Puysegur Bank	46° 57.51′	~165° 24.46′	990	30x20x12cm bored block	Y?	Foraminiferal shelly siltstone
53286	HT	W Puysegur Bank	46° 56.87′–46° 57.64′	165° 24.95′–165° 25.21′	970–950	25x20x10cm bored block	Y?	Foraminiferal shelly fine sandstone
53287	HT	W Puysegur Bank	46° 57.63′–46° 55.75′	165° 22.18′–165° 22.42′	1070–1080	50x25x15cm bored block	Y?	Fine-medium sandstone
53288	HW	Puysegur Bank	46° 57.88′–46° 57.65′	165° 28.61′–165° 28.32′	990–952	Large fist size block	Y?	Muddy sandstone
53289	HT	W Puysegur Bank	–46° 57.83′	~165° 24.73′	106–947	Piece of large boulder	Y?	Silty clay
54832	HT	N Macquarie Ridge	–47° 59.98′	~165° 09.70′	~865	Rounded cobble 4x3cm	N	Medium sandstone

Table 2. Whole-rock X-ray fluorescence analyses of two Macquarie Ridge igneous rocks. CIPW norms and Mg numbers calculated assuming Fe_2O_3/FeO = 0.15 and with P52950 apatite-free.

	P52842 Dolerite	*P52950 Basalt*
SiO_2 (wt%)	48.55	38.45
TiO_2	1.89	2.40
Al_2O_3	16.00	13.23
Fe_2O_3 (tot.)	10.43	12.83
MnO	0.22	0.09
MgO	5.72	3.28
CaO	10.40	14.49
Na_2O	3.16	3.30
K_2O	0.49	1.22
P_2O_5	0.34	4.60
LOI	2.80	5.98
total	**100.00**	**99.87**
Sc (ppm)	28	22
V	311	288
Cr	173	264
Ba	230	263
La	16	27
Ce	40	64
Ni	57	76
Cu	73	27
Zn	122	153
Zr	127	166
Nb	19	32
Ga	21	18
Pb	6	7
Rb	14	18
Sr	290	795
Th	2.8	3.7
U	10	3
Y	30	27
As	27	30
norm (wt%)		
Q	0.0	0.0
Or	3.0	8.6
Ab	27.7	17.7
An	29.1	21.6
Ne	0.0	8.7
Di	18.1	25.0
Hy	11.0	0.0
Ol	3.4	9.4
Mt	3.1	3.4
Il	3.7	5.5
Ap	0.8	0.0
Mg#	**56**	**37**

textured, oscillatory zoned, and up to 5 mm long; a more typical grain size is 1 mm.

P52950 is an amygdaloidal basalt with a microcrystalline groundmass. Phenocrysts comprise about 10% ?olivine (now completely replaced by clay and oxide alteration products), 15% plagioclase, and 10% clinopyroxene (sometimes glomeroporphyritic), and no opaques. There are about 20% irregularly shaped amygdules, all rimmed by the zeolite mineral phillipsite. About a third of all amygdules are also partly to totally filled by green sandy clay with a detrital grain population similar to other Puysegur Bank samples described below. This geopetal sediment infilling occurred after coating of the vesicles by zeolites and took place by infiltration along pervasive cracks, which are also filled with clay.

P54831 is an extremely altered aphyric variolitic basalt with about 5% calcite amygdules. Intersertal mafic minerals have been completely replaced by chlorite. Intergranular opaques are the only relict igneous phase remaining, but have not been analysed. The sample is cut by calcite veinlets.

P54833 is a highly altered medium–coarse gabbro. All mafic minerals have been completely replaced by chlorite + calcite assemblages, and all plagioclase is saussuritised. Subhedral opaques remain unaltered. Secondary euhedral quartz grains are scattered throughout the specimen. Both olivine and pyroxene may have originally been present in the gabbro; relict semi-curving fractures and fine-grained secondary opaques are present in some chlorite patches, but are conspicuously absent from others.

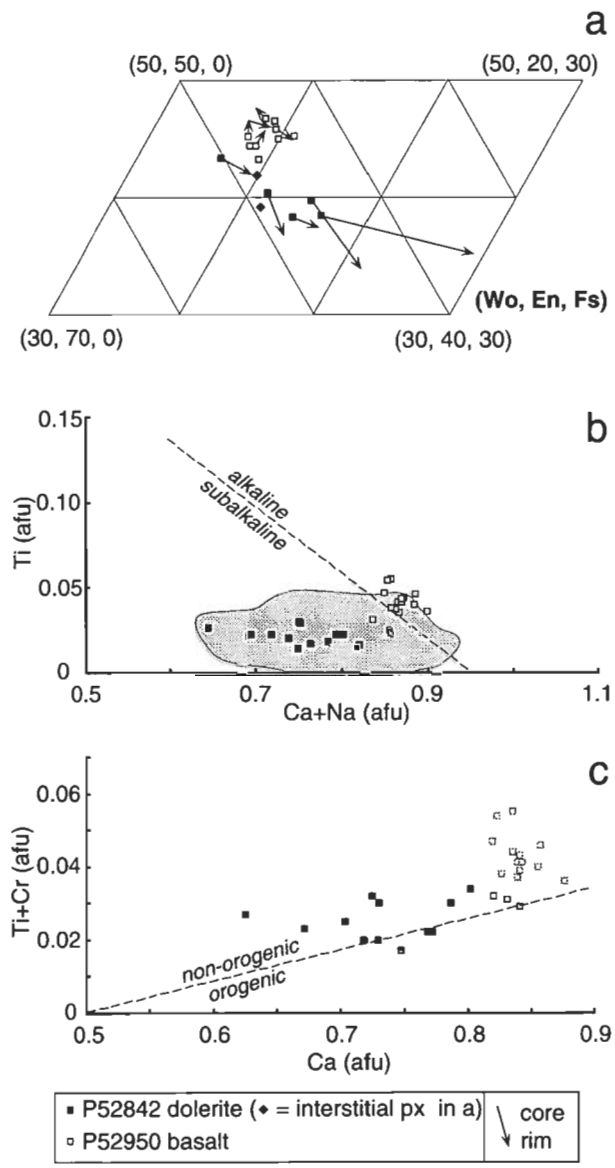

Figure 3. Pyroxenes from samples P52950 and P52842. a—pyroxene quadrilateral showing zoning trends; b & c—diagrams of Leterrier et al. (1982), showing magmatic affinity. Shaded area in b encloses 95% of subalkaline basalt pyroxenes analysed by Leterrier et al. (1982). Most of P52950 pyroxenes plot above the alkaline–subalkaline line in b and should not strictly be plotted in c (grey symbols). afu = atomic formula units.

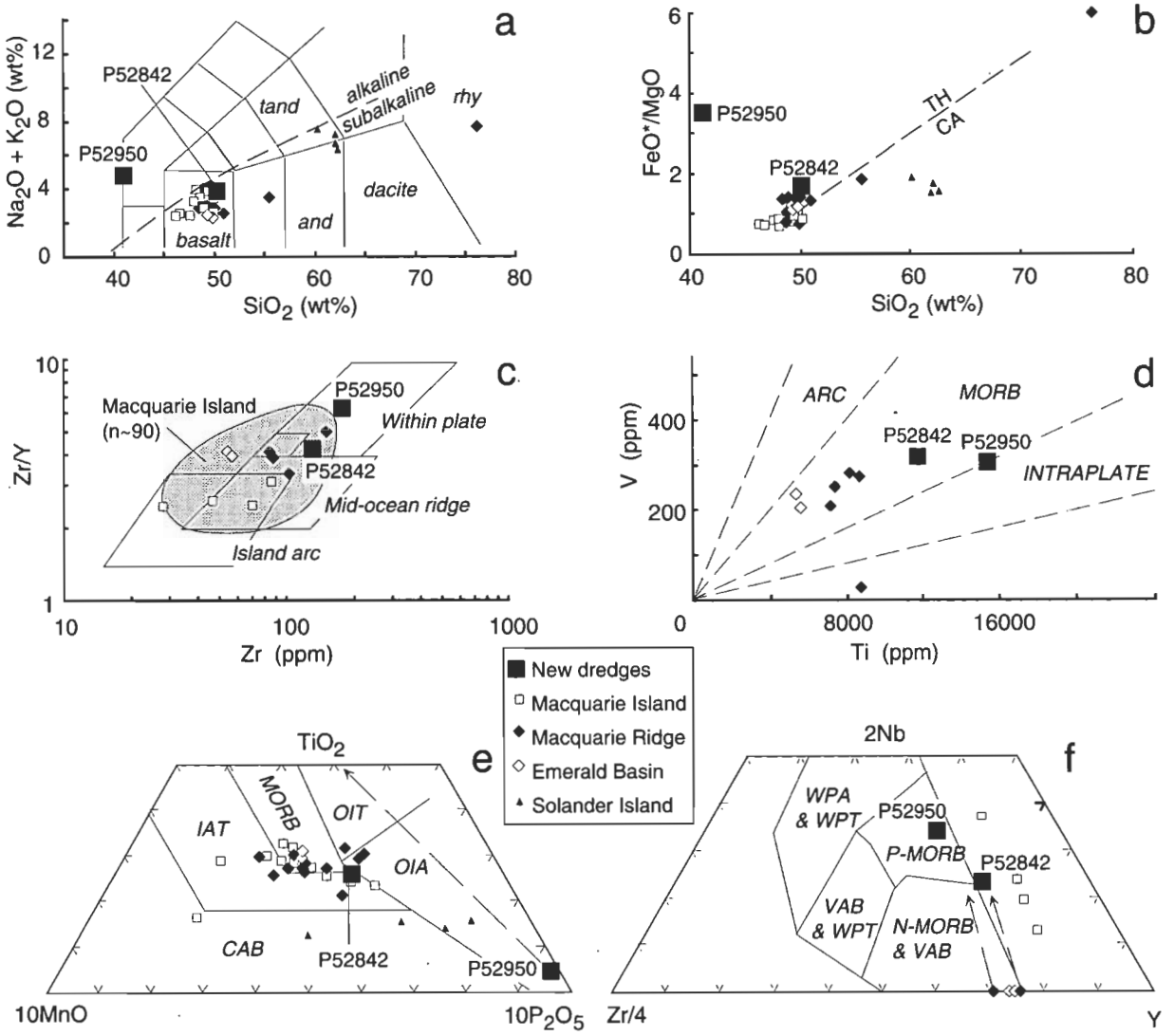

Figure 4. Analyses of Macquarie Ridge region rocks plotted on geochemical diagrams. See text for data sources. a—silica versus total alkalies (LeMaitre 1989; Irvine & Baragar 1971). and = andesite, tand = trachyandesite, rhy = rhyolite; b—silica versus FeO*/MgO (Miyashiro, 1975). TH = tholeiitic, CA = calcalkaline; c—Zr versus Zr/Y (Pearce & Norry 1979); field of Macquarie Island analyses from Griffin & Varne (1980); d—Ti versus V (Shervais 1982); e—TiO_2 versus MnO versus P_2O_5 (Mullen 1983); IAT = island arc tholeiite, OIT = ocean island tholeiite, MORB = mid-ocean ridge basalt, OIA = ocean island alkalic, CAB=calc-alkaline basalt; f—Nb versus Zr versus Y (Meschede 1986); WPA = within plate alkalic, WPT = within plate tholeiitic, vab = volcanic arc basalt, N-MORB = normal mid-ocean ridge basalt, P-MORB = plume type mid-ocean ridge basalt.

Sedimentary rocks

Despite the wide range in grain size and type of bioclastic material, all the sectioned sedimentary rocks have the same mineral and lithic components. Different proportions of detrital quartz (which dominates—some grains are polycrystalline and strained), plagioclase, alkali feldspar, biotite, muscovite, tourmaline, epidote, green–straw pleochroic amphibole, and brown altered volcanic rock can be seen in thin section. The volcanic rock fragments tentatively date the clastic rocks as syn- to post-Macquarie Ridge volcanics.

From a provenance point of view, the most informative rock is the coarsest sandstone (P54832). This is moderately well sorted, subangular, and medium-grained; and has approximate modal components (visual estimates) of quartz 40%, feldspar 15%, basaltic volcanic lithics 10%, fine sedimentary lithics 15%, individual mineral grains 5%, and unrecrystallised muddy matrix 15%. Obvious authigenic zeolites or other metamorphic minerals are absent. As P54832 is a rounded cobble, an ice-rafted origin cannot be entirely dismissed, though previous ice-rafted dredges from the Macquarie Ridge have been dominated by plutonic and high-grade metamorphic rocks (Summerhayes 1969; Watkins & Gunn 1971). Assuming a non-ice-rafted origin, P54832 must have been derived locally, as it was dredged from near the top of a prominent submarine edifice (Fig. 2).

Chemistry of igneous rocks

Minerals

Relict pyroxenes in P52842 and P52950 are 'quad' pyroxenes and fall within the augite and diopside compositional fields of Morimoto (1988) (Fig. 3a). Pyroxene analyses from basalt P52950 show a restricted range of composition and negligible radial compositional zoning; Mg# is between 87 and 80 (Fig. 3a). Pyroxene analyses

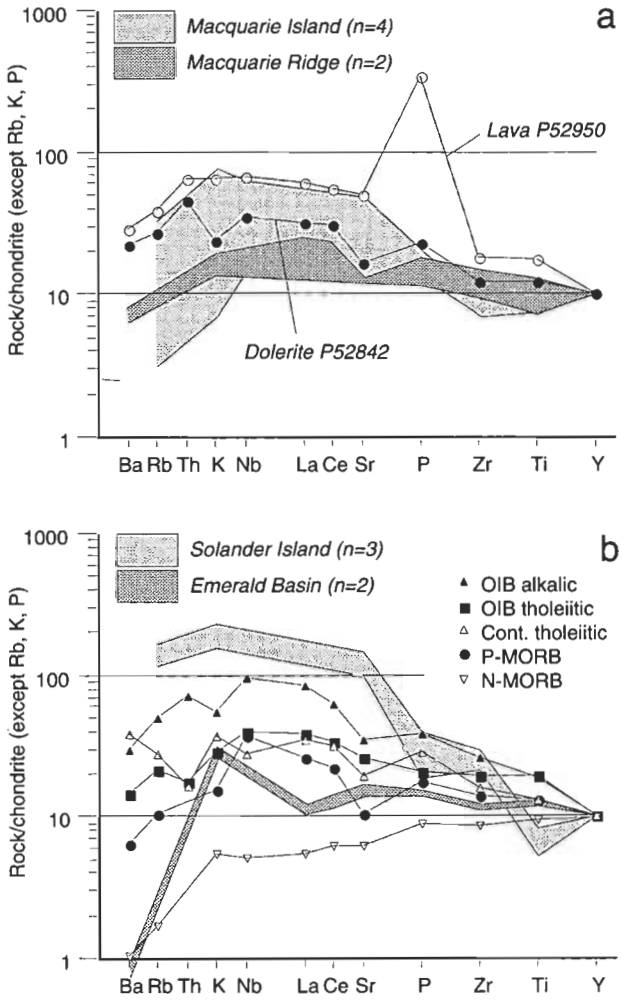

Figure 5. Normalised multielement diagrams (spidergrams) after Thompson et al. (1984), double normalised to Y_n = 10. See text for data sources. cont = continental. See Figure 4 for other abbreviations. a—new samples and previously analysed samples from the Macquarie Ridge and Macquarie Island; b—Solander Island (strictly, double normalisation is for basalts only), Emerald Basin and various oceanic reference suites.

from dolerite P52842 show a wider range of composition and significant radial zoning; the most magnesian core has Mg# = 90 and the most iron-rich rim (adjacent to a mesostasis patch) Mg# = 67 (Fig. 3a). The lack of overlap in pyroxene core–rim compositions between the two samples suggests that the main control on chemistry was magma composition rather than crystal chemistry. The M2 site occupancy and Ti concentrations suggest that the two samples crystallised from magmas belonging to different lineages (Leterrier et al. 1982). Specifically, whereas the dolerite is clearly subalkaline, the basalt is less easy to classify, as the analyses straddle the best-fit alkaline–subalkaline dividing line, but are still largely within the range of 95% of subalkaline pyroxenes of Leterrier et al. (1982) (Fig. 3b). Pyroxenes from both samples indicate a non-orogenic affinity (Fig. 3c).

Plagioclases from P52950 and P52842 likewise show restricted and broad compositional ranges, respectively. In P52950, the phenocrysts are labradorite, An_{64-56} (mol%), and $Or_{1.2-1.9}$ with no significant core–rim zoning within that range. All analysed plagioclases in dolerite P52842 are normally zoned from bytownite to andesine compositions; the ranges for six analysed core–rim pairs being An_{59-38}, An_{61-42}, An_{58-50}, An_{74-52}, An_{55-46} and An_{77-43}. The alkali feldspar component ranges from $Or_{0.5}$ to $Or_{1.5}$. Oscillatory zoning is visible in thin section, but no detailed microprobe traverses were made to explore this variation.

Opaque Fe–Ti oxide grains in P52842 are considerably degraded, in part to titanite. Analyses have poor totals with non-stoichiometric ferric–ferrous iron ratios and appreciable amounts of Si, Ca and Al, but no Cr. TiO_2 contents of analysed spots are 20–41wt%, indicating that ulvospinel–magnetite and/or ilmenite compositions may have originally been present. Exsolution features have not been investigated.

Whole rocks

The two least altered samples, basalt P52950 and dolerite P52842, were analysed for major and 19 trace elements (Table 2). The secondary alteration in both (see above) means that element concentrations, particularly of alkali and alkaline earth elements, are probably not primary and must be treated with caution, as must the CIPW norms.

In general, dolerite P52842 shows element concentrations similar to a subalkaline tholeiitic basalt (Table 2, Fig. 4a, b). In terms of element ratios thought to be characteristic of certain tectonic settings (e.g. Zr/Y, Ti/V, Zr/Nb; Fig. 4c–f), the dolerite plots in or close to fields of normal- to plume-type mid-ocean ridge basalt (N-MORB & P-MORB). Normalised multielement concentrations of P52842 (Fig. 5 after Thompson et al. 1984) also reveal a broad igneous coherence to the trace-element concentrations, and a similarity with P-MORB.

Lava P52950 has lower SiO_2 and MgO, and much higher P_2O_5 and LOI than typical basalts, which result in its plotting away from typical basic igneous compositions in Figure 4. These features may be at least partially explained by the presence of infiltrated secondary clay (presumably phosphate-rich), along with precipitated phillipsite in the amygdules (removal of all P_2O_5, and some CaO and LOI, as hydroxyapatite results in an anhydrous normalised SiO_2 concentration of 46.9 wt%, cf. Fig. 4a, b).

Despite the obvious gains and losses of the above elements, many other element concentrations and ratios in P52950 approximate to sensible mafic igneous values (e.g. Fig. 4c–f, Fig. 5). P52950 has trace element ratios that would indicate a different mantle source region to P52842, generally more enriched in incompatible elements, and similar to that found beneath modern day intraplate oceanic islands. The rock is possibly an alkali rather than tholeiitic basalt, as suggested by the vesicularity (implying high primary volatile contents), lack of Ca-poor pyroxene, relict Ca-rich pyroxene composition, overall concentrations of incompatible elements, which are as high as mildly nepheline-normative OIBs (Fig. 5), and presence of nepheline in the apatite-corrected CIPW norm (Table 2). Lavas containing secondary analcime, and of presumed primary alkaline affinity, constituted a minor part of Summerhayes' (1969) 'Macquarie Tholeiite Province'. However, extreme alteration, and intimate addition of sedimentary material to P52950 mean that an alkaline and/or OIB affinity cannot be established with any certainty.

Discussion

Significance of igneous rocks

Although sampling is sparse, and many chemical analyses are old or incomplete, the compositions of all basalts and dolerites from the Macquarie Ridge and Macquarie Island, including the new dredges, show many common features; generally mafic rock types and trace and minor element ratios within or near the range of MORB and, possibly, OIB (Figs. 3–5). The petrological unity of Macquarie Ridge rocks south of 49° S noted by Summerhayes (1969) and Matveyenkov & Baranov (1981) is thus reconfirmed by the present study and is shown to encompass the igneous rocks from as far north as 47° S. The data support the general interpretation of the ridge by Hayes & Talwani (1972), Varne & Rubenach (1972), Griffin & Varne (1980) and Williamson (1988) as tectonically uplifted oceanic crust.

Although P52950 is at the upper end of the range of enrichment of Macquarie Ridge samples (e.g. Zr/Y, Fig. 4c), and may be mildly alkaline, it is still distinct from the strongly alkaline and commonly differentiated Late Cenozoic lavas that are widespread throughout the South Island and on the Campbell Plateau (e.g. Weaver & Smith 1989). Secondary alteration notwithstanding, the impressively wide range in Zr/Y ratio in mafic rocks of Macquarie Island and the Macquarie Ridge would seem to suggest geochemically complex N-MORB and P-MORB (and possibly OIB) mantle reservoirs along the ridge.

Constraints imposed from ocean magnetic lineations indicate that transpressional underthrusting has occurred along the entire length of the Macquarie Ridge at the Puysegur, Macquarie and Hjort trenches (Davey & Smith 1983; Williamson 1988 and references therein). However, no subducting slab has apparently reached depths of ~100 km beneath the Macquarie Ridge, at which slab-related melts with their characteristic Nb- and Ti-depleted chemistry have been generated. The Plio-Pleistocene andesites of Solander Island, which lie east of the axis of the Macquarie Ridge, remain the only Cenozoic subduction-related rocks known in the entire area of Figure 1. Solander Island is located at the zone of maximum total Cenozoic Pacific–Australian plate convergence (Davey & Smith 1983).

Significance of sedimentary rocks

The petrographically identified detrital components of all seven sectioned sedimentary rocks are consistent with two distinct sources (1) basaltic igneous rocks of the Macquarie Ridge and (2) Paleozoic–Mesozoic continental basement rocks of Fiordland (SW South Island, Fig. 1), which are also exposed on Stewart Island, at the bottom of oil exploration well Parara-1 and beneath the Campbell Plateau (Fig. 2; Beggs et al. 1990).

A continental provenance might be expected for the samples at the northern (Puysegur Bank) dredge sites (Fig. 2), as these are only 120 km across a smooth continental shelf from Fiordland. However, a continental provenance is unusual for sandstone P54832, from the southern dredge site. This was sampled from near the top of an isolated submarine edifice (Fig. 2) and must, therefore, have undergone post-depositional isolation from its continental source. This source may have been either the Campbell Plateau prior to opening of the Solander Trough or, perhaps more likely, the west coast of the South Island prior to the approximately 400 km post-Middle Miocene northward displacement of western New Zealand along the Pacific–Australian plate boundary (Fig. 1 inset; Davey & Smith 1983). A western source has also been inferred for the thick Cretaceous–Cenozoic sequences seen in seismic sections beneath the northern Puysegur Bank (Norris & Carter 1980; Turnbull et al. 1993).

P54832 is the southernmost known sedimentary rock of continental provenance on the Macquarie Ridge; sedimentary rocks from the ridge further south comprise only foraminiferal oozes and volcaniclastic rocks (Summerhayes 1969; Ovenshine et al. 1975 and references therein; Varne & Rubenach 1972; Quilty et al. 1973; Duncan & Varne 1988).

Continent–ocean transition

Hatherton (1967) and Woodward & Hatherton (1975) have identified a large positive regional magnetic anomaly associated with the Macquarie Ridge, as well as two smaller ones offshore of Puysegur Point (Fig. 2). The Macquarie magnetic anomaly does not continue into Fiordland (Woodward & Hatherton 1975) and Watkins & Gunn (1971) have correlated it with the occurrence of dredged ultramafic rocks. Although ultramafic rocks have not been sampled north of 49° 40′ S (Fig. 1; Summerhayes 1969, station 20), the newly dredged gabbro and dolerite cobbles from the Puysegur Bank (P54833 and 54842), support the geological continuity of the ridge north to at least 47° S, in agreement with the inferred magnetic continuity outlined by Hatherton (1967). Although the Macquarie magnetic anomaly clearly continues north of 47° S (Fig. 2), volcanic or plutonic rocks are puzzlingly absent from seismic line B202 on the crest of the Puysegur Bank and from lines to the north of it (Norris & Carter 1980; Turnbull et al. 1993).

The newly dredged igneous rocks do not show the weak negative Nb anomalies typical of many continental igneous rocks (compare Fig. 5). However, this can only be taken as tentative evidence that P52950 and P52842 have not erupted through crust of continental character or thickness, as some continental basalts are chemically indistinguishable from oceanic basalts (Thompson et al. 1984).

In summary, the transition from tectonically uplifted Cenozoic oceanic crust of the Macquarie Ridge to Paleozoic–Mesozoic continental crust of the South Island cannot, at this stage, be satisfactorily defined by bathymetric, reflection seismic, magnetic, geochemical or sedimentary provenance data. The local occurrence of subduction-related andesites on Solander Island, possibly coeval with some Macquarie Ridge magmatism, further attests to the tectonomagmatic complexity of this remote southwestern edge of the Pacific Plate.

Summary & conclusions

Gabbro, dolerite, basalt and a variety of clastic sedimentary rocks have been sampled from between 47° and 48° S on the northern part of the Macquarie Ridge (including Puysegur Bank). Despite extensive alteration, the igneous rocks appear petrographically and geochemically similar to the dominantly tholeiitic plutonic and volcanic suites sampled on the ridge between 49° and 58° S by previous workers. This study thus reaffirms the petrological simi-

larity of all Macquarie Ridge igneous rocks (Summerhayes 1969) and further shows that these similarities can now be extended as far north as 47° S. The mainly MORB-like Macquarie Ridge igneous rocks are distinctly different from widespread Late Cenozoic alkalic intraplate lavas of the Campbell Plateau and South Island, as well as Pliocene subduction-related andesites of Solander Island.

The sampling of Macquarie Ridge-type oceanic igneous rocks on the New Zealand continental shelf (Puysegur Bank), is significant and indicates a complex intrusive and/or tectonic transition from uplifted Cenozoic oceanic crust of the Macquarie Ridge to Paleozoic–Mesozoic continental crust of New Zealand. Continent-derived sandstone of presumed Late Cenozoic age has been identified on the Macquarie Ridge as far south as 48° S.

Acknowledgements

Funded by the Foundation for Research, Science & Technology. I thank Chris Carey for providing the samples that made this study possible. I also thank Chris Uruski for passing on the samples, Ken Palmer for XRF analyses and assistance with electron microprobe analyses, Ray Soong for XRD analyses, Neville Orr for thin sections, and Stewart Bush for crushing rocks. Earlier versions of the manuscript were improved by comments from Fred Davey, Steve Weaver, Andy Tulloch, Ian Smith and Rick Varne. Institute of Geological & Nuclear Sciences contribution number 384.

References

Beggs, J.M., Challis, G.A. & Cook, R.A., 1990. Basement geology of the Campbell Plateau: implications for correlation of the Campbell Magnetic Anomaly System. *New Zealand Journal of Geology and Geophysics*, 33, 401–404.

Bishop, D.G., 1986. Sheet B46—Puysegur. *Geological map of New Zealand 1:50000.* Map (1 sheet) and notes (36 pp.). Department of Scientific and Industrial Research, Wellington, New Zealand.

Campsie, J., Neumann, E.R. & Johnson, L., 1983. Dredged volcanic rocks from the southern oceans: the Eltanin collection. *New Zealand Journal of Geology and Geophysics*, 26, 31–45.

Carey, C., Mortimer, N., Uruski, C.I. & Wood, R.A., 1991. Fire and brimstone on the western Challenger Plateau: further evidence from Mount Spong and Megabrick. *New Zealand Geological Survey Record*, 43, 123–128.

Davey, F.J. & Smith, E.G.C., 1983. The tectonic setting of the Fiordland region, south-west New Zealand. *Geophysical Journal of the Royal Astronomical Society*, 72, 23–38.

Delteil, J., Collot, J.-Y., Wood, R.A., Herzer, R.H. & shipboard party, 1993. More than a peek at a plate boundary: what the butler saw on the Puysegur leg. *Geological Society of New Zealand Miscellaneous Publication*, 79A, 61.

Duncan, R.A. & Varne, R. 1988. The age and distribution of the igneous rocks of Macquarie Island. *Papers and Proceedings of the Royal Society of Tasmania*, 122, 45–50.

Griffin, B.J. & Varne, R., 1980. The Macquarie Island ophiolite complex: mid-Tertiary oceanic lithosphere from a major ocean basin. *Chemical Geology*, 30, 285–308.

Hatherton, T., 1967. Total magnetic force measurements over the north Macquarie Ridge and Solander Trough. *New Zealand Journal of Geology and Geophysics*, 10, 1204–1211.

Hayes, D.E. & Talwani, M., 1972. Geophysical investigations of the Macquarie Ridge complex. *In* Hayes, D.E. (Editor). Antarctic Oceanology II—the Australian–New Zealand sector. *American Geophysical Union, Antarctic Research Series* 19, 211–234.

Houtz, R., Ewing, J. & Embley, R., 1971. Profiler data from the Macquarie Ridge area. *In* Reid, J.L. (Editor). Antarctic Oceanology I. *American Geophysical Union, Antarctic Research Series* 15, 239–245.

Hunt International Petroleum Company, 1976. Well completion report Parara-1. Institute of Geological & Nuclear Sciences unpublished Open File Petroleum Report 673.

Irvine, T.N. & Baragar, W.R.A., 1971. A guide to the chemical classification of the common volcanic rocks. *Canadian Journal of Earth Sciences*, 8, 523–548.

Jakes, P. & Gill. J.B. 1970. Rare earth elements and the island arc tholeiitic series. *Earth and Planetary Science Letters*, 9, 17–28.

LeMaitre, R.W., (editor) 1989. *A classification of igneous rocks and glossary of terms.* Blackwell Scientific Publications, Oxford.

Leterrier, J., Maury, R.C., Thonon, P., Girard, D. & Marchal, M., 1982. Clinopyroxene composition as a method of identification of the magmatic affinities of paleo-volcanic series. *Earth and Planetary Science Letters*, 59, 139–154.

Matveyenkov, V.V. & Baranov, B.V., 1981. Magmatic rocks of the Macquarie Ridge (southwest part of the Pacific Ocean). *International Geology Review*, 23, 417–425.

Meschede, M., 1986. A method of discriminating between different types of mid-ocean ridge basalts and continental tholeiites with the Nb–Zr–Y diagram. *Chemical Geology*, 56, 207–218.

Miyashiro, A., 1975. Classification, characteristics, and origin of ophiolites. *Journal of Geology*, 83, 249–281.

Morimoto, N., 1988. Nomenclature of pyroxenes. *Fortschritte der Mineralogie*, 66, 237–252.

Mullen, E.D., 1983. $MnO/TiO_2/P_2O_5$: a minor element discriminant for basaltic rocks of oceanic environments and its implications for petrogenesis. *Earth and Planetary Science Letters*, 62, 53–62.

Norris, R.J. & Carter, R.M., 1980. Offshore sedimentary basins at the southern end of the Alpine Fault, New Zealand. *Special Publication of the International Association of Sedimentologists*, 4, 237–265.

Ovenshine, A.T., Winkler, G.R., Andrews, P.B. & Gostin, V.A., 1975. Chemical analyses and minor element composition of Leg 29 basalts. *Initial Reports of the Deep Sea Drilling Project*, 29, 1097–1102.

Pearce, J.A. & Norry, M.J., 1979. Petrogenetic implications of Ti, Zr, Y and Nb variations in volcanic rocks. *Contributions to Mineralogy and Petrology*, 69, 33–47.

Quilty, P.G., Rubenach, M. & Wilcoxon, J.A., 1973. Miocene ooze from Macquarie Island. *Search*, 4, 163–164.

Reay, A., 1986. Andesites from Solander Island. *Royal Society of New Zealand Bulletin*, 23, 337–343.

Roser, B.P. & Grapes, R.H., 1990. Whole-rock and mineral analyses of volcanic, pelagic and turbidite lithologies from Red Rocks, Wellington. *Victoria University of Wellington, Research School of Earth Sciences, Geology Board of Studies Publication* 6.

Schilling, J-G. & Ridley, W.I., 1975. Volcanic rocks from DSDP Leg 29: petrography and rare-earth abundances.

Initial Reports of the Deep Sea Drilling Project, 29, 1117–1121.

Shervais, J.W., 1982. Ti–V plots and the petrogenesis of modern and ophiolitic lavas. *Earth & Planetary Science Letters*, 59, 101–118.

Summerhayes, C.P., 1969. Marine geology of the New Zealand subantarctic sea floor. *New Zealand Department of Scientific and Industrial Research Bulletin* 190.

Thompson, R.N., Morrison, M.A., Hendry, G.L. & Parry, S.J., 1984. An assessment of the relative roles of crust and mantle in magma genesis: an elemental approach. *Philosophical Transactions of the Royal Society of London*, A310, 549–590.

Turnbull, I.M., Uruski, C.I. et al., 1993. Cretaceous and Cenozoic sedimentary basins of Western Southland, South Island, New Zealand. *Institute of Geological and Nuclear Sciences Monograph* 1.

Varne, R. & Rubenach, M.J., 1972. Geology of Macquarie Island and its relationship to oceanic crust. *In* Hayes, D.E. (editor). Antarctic Oceanology II—the Australian–New Zealand sector. *American Geophysical Union, Antarctic Research Series* 19, 251–266.

Varne, R. & Thomson, J.W., 1990. Macquarie Island. *In* LeMasurier, W.E. & Thomson, J.W. (editors). Volcanoes of the Antarctic Plate and Southern Oceans. *American Geophysical Union, Antarctic Research Series*, 48, 476–479.

Watkins, N.D. & Gunn, B.M., 1971. Petrology, geochemistry, and magnetic properties of some rocks dredged from the Macquarie Ridge. *New Zealand Journal of Geology and Geophysics*, 14, 153–168.

Weaver, S.D. & Smith, I.E.M., 1989. New Zealand intraplate volcanism. *In* Johnson, R.W., Knutson, J. & Taylor, S.R. (editors). *Intraplate volcanism in eastern Australia and New Zealand.* Cambridge University Press. 157–188.

Williamson, P.E., 1988. Origin, structure and tectonic history of the Macquarie Island region. *Papers and Proceedings of the Royal Society of Tasmania*, 122, 27–43.

Woodward, D.J. & Hatherton, T., 1975. Magnetic anomalies over southern New Zealand. *New Zealand Journal of Geology and Geophysics*, 18, 65–82.

CORRECTION

D.W. Durney & H.J Kisch—A field classification and intensity scale for first-generation cleavages

Volume 15, Number 3, 257–295

p. 269, par. 4, l. 5 should read	in Foster & Hudleston (1986, fig. 4D) are clearly joint-
p. 270, Fig. 3c, the figure should include	a 'c' spacing as shown by 'Sb' in Fig. A1A
p. 280, last line should read	mica content (silt-size flakes of clear white mica set in
p. 286, section (4), equation should read	$c/b = A\ (i/b)^B$
p. 293, eqn. (A1), second line:	replace with $f_b = 1/\ s_b$,
eqn. (A4), first line:	replace with $c \equiv s_b$,
eqn. (A5), first line:	replace with $c/b = R_{cb} = s_b\ /\ s_c = l_c\ /\ l_b$,
eqn. (A5), third line:	replace with $i/c = R_{bi} = s_i\ /\ s_b = l_i\ /\ l_c \sin \beta$.
p. 294, Table 2, $R(S_0)$ n values should be:	for Wimborne, (4); Tamworth Council Quarry: (1).

ISSN 0028–8306

New Zealand Journal of Geology and Geophysics

- An international journal of the Earth Sciences of the Pacific and Antarctic regions
- Includes papers on geology, geophysics, geomorphology, soil science and the atmospheric sciences
- Accepts papers from authors worldwide. Every paper is internationally refereed and distributed
- Welcomes review articles, letters to the editor, book reviews and preliminary notes
- Has regular special issues of topical thematic importance
- Is published quarterly in large A4 format, about 500 pages per year
- Has an established international reputation of over 35 years

Abstracted in: Aquatic Sciences & Fisheries Abstracts; Bibliography & Index of Geology; Signaletique; Chemical Abstracts; Current Contents; Geo Archive; GeoRef; Geological Abstracts; INIS Atomindex; Meteorological & Geoastrophysical Abstracts; Mineralogical Abstracts; Oceanic Abstracts; Pollution Abstracts; Research Alert; Science Citation Index; Scisearch; SIRIS/STIX.

Editor Mr R. P. Lynch

Manuscripts, advertising, enquiries, and requests for "Information for authors" should be addressed to:

Editor
New Zealand Journal of Geology and Geophysics
SIR Publishing
P.O. Box 399, Wellington, New Zealand
International phone +64 - 4 - 472 7421
International fax +64 - 4 - 473 1841

Subscriptions for 1994

Institutional:	New Zealand and Australia, NZ$220
	Other countries, US$190
Individual:	New Zealand and Australia, NZ$132
	Other countries, US$47.50
Authors:	New Zealand and Australia, NZ$77
	Other countries, US$38
Scientific Society members:	
	New Zealand and Australia only, NZ$77

All prices include postage and packing, and GST within New Zealand

REVIEWERS OF MANUSCRIPTS — EDITOR'S NOTE

The quality, success and continuance of any journal depends on the cooperation of many individuals, among whom the reviewers of manuscripts submitted for publication also play a vital role. Their task is difficult and time-consuming; yet frequently their unselfish contribution is not acknowledged.

The Editorial Board of the *AGSO Journal of Australian Geology & Geophysics* sincerely appreciates, on behalf of the readers, the contributions made for volume 15 by the following reviewers in their efforts to maintain the *Journal's* standard and in selecting papers for publication.

Karl H. Wolf
Senior Editor

V. Anfiloff
L. Anglin (Canada)
M. Apthorpe
N.W. Archbold
J. Backhouse
P. Baillie
B.E. Balme
P.M. Barber
T.H. Bell
S.M. Bergström (USA)
K.P. Black
D.H. Blake
P.R. Bowen (UK)
P. Brenkle (USA)
M. Brown
P.E. Brown (USA)
R.T. Buffler (USA)
G.C.H. Chaproniere
A.E. Cockbain
M.F. Coffin (USA)
J.B. Colwell
P. Conaghan
D. Cooke
J. Cosgrove
K.W.A. Crook (Hawaii, USA)
H.L. Davies
J. Deane
D. Denham
M. Dentith
M.E. Dettmann
B. Dickson
M. Duggan
S.M. Eggins
R.L. Ethington (USA)
G. Ewers
N.F. Exon
B.A. Gaull
G. Gibson
J. Gorter
R.L. Grasty (Canada)
S.A. Greenhalgh
O. Gudmundson
P.J. Hamilton
M.J. Hawladder
R.C. Haydon
D.T. Heggie
R.J. Helby
M.J. Jackson
D. Johnson
R.W. Johnson
P.J. Jones
J. Kellett
B. Kennett
R. Kerrich (Canada)
G.E. Lau
K. Lidmar-Bergström (Sweden)
A.R. Lord (UK)
M.K. Macphail
M. Mattauer (France)
C.K. Mawer
K. McNamara
A.D. McCracken (Canada)
P. McFadden
K.G. McQueen
C.A. McRoberts (USA)
R. Meissner (Germany)
T.P. Mernagh
E. Mikucki
J.F. Miller (USA)
G. Morrison
G.C. Nanson
R.S. Nicoll
G.S. Nowlan (Canada)
P.E. O'Brien
N. Oliver
M.J. Orchard (Canada)
B.S.Oversby
C.W. Passchier (Germany)
A.D. Partridge
J.P. Petit (France)
S. Planke
I. Premoli-Silva (Italy)
C.V. Reeves (The Netherlands)
J.P. Rexilius
C.B. Rexroad (USA)
M.J. Rickard
B. Roberts
A.L. Robertson
I. Scheibner
R.W. Schön
N.J. Sheard
J.H. Shergold
K. Simpson
I. Smith (New Zealand)
N.D. Smith (USA)
P. Snepp
A.J. Stewart
D.L.Strusz
P. Stuart-Smith
S-S. Sun
F.L. Sutherland
I.P. Sweet
J.A. Talent
G. Taylor
D. Tucker
R. Varne
J.J. Veevers
R.H. Vernon
J.K. Volkman
C. von der Borch
G.P. Wahlman (USA)
M. Wallace
B.D. Webby
P. Wellman
J.B. Willcox
S.A. Wilde
G.E. Wilford
P.R. Williams
G.D. Wood (USA)
Six *Anonymous*

AGSO JOURNAL
OF AUSTRALIAN GEOLOGY & GEOPHYSICS

VOLUME 15
1994

AUSTRALIAN GEOLOGICAL SURVEY ORGANISATION
CANBERRA

AGSO Journal of Australian Geology & Geophysics

Editor: Karl H. Wolf, Corporate Publications, AGSO

Editorial Board

Policy

The *AGSO Journal of Australian Geology & Geophysics* is a quarterly journal of geoscientific research results relating to the program and interests of the Australian Geological Survey Organisation (AGSO). It complements other earth science journals by focusing on Australia, and includes papers covering the broader Australasian and SW Pacific region.

The *Journal*'s target audience is the world-wide geoscientific community, catering for the interests of the resource, exploration and environmental industries, as well as those of researchers in universities and State and Federal agencies.

The Editorial Board is responsible for the scientific policies and standards of the *Journal*, which will publish papers on fundamental research, applied research and review topics. Contributions are invited from anyone. Scientific excellence and relevance to the broad aims of AGSO are the main criteria for acceptance of manuscripts for publication. Peer review and editorial and production standards are similar to those of leading international journals.

ISSN 1320–1271

Subscriptions to the AGSO Journal are available through the Australian Geological Survey Organisation (GPO Box 378, Canberra ACT 2601; tel. 06 249 9642; fax 06 249 9982).

Other matters concerning the Journal should be sent to the Editor, AGSO Journal

VOLUME 15, NUMBER 1

Thematic issue: Geology of the outer North West Shelf, Australia*

---

* This issue should be referred to as:

Exon, N.F. (Ass. Editor), 1994. Thematic issue: Geology of the outer North West Shelf, Australia. *AGSO Journal of Australian Geology & Geophysics*, 15(1), 1–190.

VOLUME 15, NUMBER 2

VOLUME 15, NUMBER 3

VOLUME 15, NUMBER 4

Burst, J.F., 1965. Subaqueously formed shrinkage cracks in clay. *Journal of Sedimentary Petrology*, 35, 348–353.

Davies, G.R., 1970. Algal-laminated sediments, Gladstone Embayment, Shark Bay, Western Australia. *In* Logan, B.W., Davies, G.R., Read, J.F. & Cebulski, D.E. (editors). Carbonate sedimentation and environments, Shark Bay, Western Australia. *American Association of Petroleum Geologists, Memoir* 13, 169–205.

Friedman, G.M. & Sanders, J.E., 1978. *Principles of Sedimentology*. Wiley, New York.

Wellman, P. & McDougall, I., 1974. Cainozoic igneous activity in Eastern Australia. *Tectonophysics*, 23, 49–65.

Illustrations

Line diagrams or maps should be professionally drafted. (AGSO can provide a full professional drafting service to *Journal* standards at competitive rates. See advertisement below.) Figures should be designed for reproduction at either single column (80 mm) or double column (165 mm) width. Final versions of line drawings should be supplied as high-contrast photographic prints, but photocopies of draft figures may be submitted initially (see **Submissions** above).

All illustrations, both line drawings and photographs, are referred to as figures.

Figures should be numbered consecutively, in the order in which they are referred to in the text, with parts of an individual figure identified, if necessary, by upper case letter.

Do not draft figure titles on the figure. Captions are typeset and should be listed on a separate sheet.

Photographs should be good quality glossy prints. Scale in photographs should be indicated by either a recognisable object or a plain bar scale whose length is given in the figure caption.

Figures are reproduced in black and white unless special arrangements for use of colour have been made with the editor.

Tables

Tables should be set out on separate sheets. When preparing tables, if possible, please use the Tables function of your wordprocessor rather than use tabs to align columns.

Providing a disk version

When your manuscript has been accepted, you will be asked to provide a copy on disk.

The disk can be either 3.5 or 5.25 inch MS-DOS or Apple Macintosh format. The *Journal* is edited using WordPerfect 5.2 for Windows, which can convert from most other word-processing programs. If you are using WordPerfect for DOS version 6, please save your file as WordPerfect 5.1/5.2. Please check with the editor if you have any doubts, and send an ASCII file as backup.

Proofs

Authors will receive one proof of their manuscript, in its final formatted version, but without illustrations, to check before it goes for printing. Authors may be charged for the cost of major changes.

Reprints

The author(s) will receive a total of 50 free reprints of their paper.

Authors may buy extra reprints, which should be ordered when proofs are returned. The cost for 50 additional reprints is $100; special rates apply if more are required.

Please address all correspondence to

The Editor,
AGSO Journal of Australian Geology & Geophysics
Australian Geological Survey Organisation
GPO Box 378
ACT 2601

Tel. (06) 249 9114
Fax (06) 249 9987

AGSO
AUSTRALIAN GEOLOGICAL SURVEY ORGANISATION

AGSO Journal of Australian Geology & Geophysics

Volume 15, Number 4, 1994

CONTENTS